Examining the effects of anti-cancer combination therapy on tumour cell proliferation, migration and chemoresistance: Targeting Autophagy and Other Novel Pathways

Yomna Saleh

A thesis submitted to fulfil requirments for the degree of:

Doctor of Philosophy (Medicine)

Faculty of Medicine and Health

The University of Sydney

2023

Statement of Authentication

I certify that the work presented in this thesis is an original research work carried out during my candidature as PhD candidate in Faculty of Medicine and Health, University of Sydney. This research work has been carried out in Bill Walsh Cancer Research Laboratory within Kolling Institute of Medical Research. This thesis has not been submitted for any degree in University of Sydney or any other institution.

I certify that all intellectual content and experimental work is the product of my own work and that all assistance received in preparing this thesis and sources has been acknowledged

Yomna Saleh

June 2023

Acknowledgment

All thanks and deepest praise to ALLAH who bestows me guidance, aid, and prosperity throughout my life, as well as in this work.

This thesis owes its existence to the help, support, and inspiration of several people. Firstly, I would like to express my sincere appreciation and gratitude to my supervisor, Dr. Sumit Sahni who has promoted me throughout my thesis with his patience, understanding and knowledge. His guidance, persistent help and inspiring suggestions have been precious for the development of this thesis content.

I am also indebted my profound gratitude to my auxiliary supervisor, Dr. Patric Jansson who has been a constant source of encouragement and enthusiasm, not only during this thesis but also during all the years of my candidature. You will always be my mentor not only in the scientific field but also in general life.

Also, I would like to express my grateful thanks to the rest of Bill Walsh lab members: Dr. Emily Colvin for her training and assistance in cell migration experiments, Shihani Stoner for contributing her time and effort in planning and performing the animal experiments, Taymin du Toit-Thompson for always giving a hand whenever needed especially in the animal experiments, Elizabeth Millar for her training and guidance in IHC experiments, Hasanthi De Silva and Dr. Madiha Yunus for their help in imaging with microscope and troubleshooting problems in the experiments, Dr. Saurabh Satija for his assistance with the experiments, Dr. Matthew Mckay for his help in mass spectrometry analysis and Lionel, Sooin, Advaitha and Josef for all joyful time we spent together.

I would like also to express my gratitude appreciation for Prof. Anthony Gill, A/Prof. Angela Chou, Dr. Betty McDowell, Ms. Loretta Sioson, and MS Amy Sheen from the Anatomical

Pathology Department at the Royal North Shore Hospital for their help in getting the specimens and IHC scoring. Also, I would like to extend my appreciation to the Australian Breast Cancer Tumour Bank (ABCTB) for their help in providing breast cancer specimens and associated data.

Last but not the least, I would like to extend my gratitude and love to all my family: Mum, Dad and my brother for their valuable guidance and support during this journey even though they are far away. Also, my backbone, Taha (my husband) and my children: Hamza, Karma, and Selim, I know how difficult this 4 year was, but finally I did it and without your support and love, I believe I would not be able to reach this moment. Thanks for being my family.

Finally, I would like to dedicate this work to my lovely aunt (May Allah bless her soul) whom I consider my second mum. I was not able to say Goodbye before you go, but you will always be in my mind and heart. May Allah grant you heaven In Shaa allah.

Authorship Attribution Statement

The content in chapter 1 of this thesis has been published as an original three review articles:

Emerging role of autophagy in the development and progression of oral squamous cell carcinoma. YS Abd El-Aziz, LYW Leck, PJ Jansson, S Sahni. Cancers 13 (24), 6152.

Autophagy: A promising target for triple negative breast cancers. YS Abd El-Aziz, J Gillson, PJ Jansson, S Sahni. Pharmacological Research 175, 106006.

Role of ABCB1 in mediating chemoresistance of triple-negative breast cancers (2021). YS Abd El-Aziz, AJ Spillane, PJ Jansson, S Sahni. *Bioscience Reports* 41 (2), BSR20204092.

I am the primary author of this publication who did all the research, drafting, and writing the original manuscripts. LYW Leck, PJ Jansson, J Gillson, AJ Spillane and S.Sahni helped in editing and reviewing the manuscripts.

Yomna Saleh
26/06/2023

As I am the primary supervisor for the candidture upon which this thesis is based, I certify that authorship attribution statement above is correct.

Dr. Sumit Sahni
26/06/2023

List of Publications

Autophagy: A promising target for triple negative breast cancers (2022). **YS Abd El-Aziz**, J Gillson, PJ Jansson, S Sahni. Pharmacological Research 175, 106006.

Emerging role of autophagy in the development and progression of oral squamous cell carcinoma (2021). **YS Abd El-Aziz**, LYW Leck, PJ Jansson, S Sahni. Cancers 13 (24), 6152.

Role of ABCB1 in Mediating Chemo-resistance of Triple Negative Breast Cancers (2021). **YS Abd El-Aziz**, Andrew J. Spillane, Patric J. Jansson and Sumit Sahni. Bioscience Reports 2021;41:2.

Autophagy: A key player in pancreatic cancer progression and a potential drug target (2022). J Gillson, **YS Abd El-Aziz**, LYW Leck, PJ Jansson, N Pavlakis, JS Samra, A Mittal, S Sahni. Cancers 14 (14), 3528.

List of Presentations

YS Abd El-Aziz, PJ Jansson, S Sahni. Development of Novel Autophagy Inhibitors Based Anti-Cancer Combination Therapy. **Cancer Research Network HDR Student Symposium**, November 2022. **Oral Speaker**

YS Abd El-Aziz, PJ Jansson, S Sahni. Development of Novel Autophagy Inhibitors Based Anti-Cancer Combination Therapy. **Sydney Vital ECR Symposium**, March 2021. **Oral Speaker**

YS Abd El-Aziz, PJ Jansson, S Sahni. Development of Novel Autophagy Inhibitors Based Anti-Cancer Combination Therapy. **LORNE Cancer**, February 2021. **Poster presentation**.

YS Abd El-Aziz, PJ Jansson, S Sahni. Development of Novel Autophagy Inhibitors Based Anti-Cancer Combination Therapy. **Eradicate Cancer**, December 2020. **Poster presentation**

YS Abd El-Aziz, PJ Jansson, S Sahni. Development of Novel Autophagy Inhibitors Based Anti-Cancer Combination Therapy. **Cancer Research Network, Postgraduate and ECR Cancer Research Symposium**, November 2020. **Oral Speaker**.

YS Abd El-Aziz, PJ Jansson, S Sahni. Development of Novel Autophagy Inhibitors Based Anti-Cancer Combination Therapy. **Sydney Catalyst Postgraduate and Early Career Researcher Symposium**, October 2020. **Poster presentation**

List of Awards

RNSH Scientific Staff Council Virtual Travel Award (2021)

Postgraduate Research Support Scheme Award (2021) (Awarded $716.85)

2020 Sydney Catalyst Travel and Education Award (2021) (Awarded $500)

Cancer Research Network 2020 Postgraduate and ECR Conferences and Education Awards (2020) (Awarded $1375)

Postgraduate Research Support Scheme Award (2020) (Awarded $716.85)

Fully Funded Scholarship from Higher Education Ministry, Egypt (2019) ($ 25,000 p.a.)

Research Training Program Scholarship (Fee offset) USYD (2019)

Abstract

Autophagy is a degradation process in which damaged proteins and organelles are being recycled by the cell in response to any type of stress such as energy or nutrient deprivation. At the basal level, autophagy helps to maintain normal homeostasis. It is considered as a survival mechanism by which cells can survive under different types of stressors. It is well established that solid tumours are subjected to various microenviromental stressors such as hypoxia, energy and nutrient deprivation. These stressful microenviroment could lead to activation of pro-survival autophagy in tumour cells to aid in its survival under these condition and result in cancer progression. Also, autophagy has been linked to different aspects of cancer such as tumour growth, metastasis and chemoresistance, which makes it a promising target in cancer treatment. Currently, clinicaly available autophagy inhibitors (*e.g.,* chloroquine) only provide modest inhibitory activity with adverse side effects. Hence, development of novel strategies to potently inihibt autophagy to resensitise cancer cells toward conventional chemotherapy is warranted.

Oral squamous cell carcinoma (OSCC) represents about 90% of oral cancer cases. It has a poor prognosis due to late diagnosis, early metastasis, and recurrence, which is often resistant to chemotherapy. Autophagy has been previously indicated to be associated with aggressive behaviour of OSCC. Thus, targeting autophagy in OSCC may lead to development of a new treatment strategy in OSCC.

Triple negative breast cancer (TNBC) constitutes 15% of all breast cancer types. It is characterised by lack of estrogen, progesteron and huma epidermal growth factor receptor 2 (HER2) expression which make the endocrine or HER2 targeted therapy ineffective in these cancers. Also, 30-40% of TNBC patient experience resistant to conventional chemotherapy. Aggressive clinicopathological features in TNBC were previously shown to be associated with autophagy. Therefore, targeting autophagy may open up new venues in TNBC treatment. Taken together, this thesis aimed to examine the effect of novel autophagy inhibitors on OSCC and TNBC proliferation, migration and resensitisation to conventional chemotherapy and identify the novel molecular targets that may contribute to chemoresistance.

Chapter 3 demonstrated the effect of tumour microenvironmental stressors (*i.e.,* serum and glucose starvation) on levels of autophagic marker LC3-II in OSCC and TNBC *via* immunoblotting and immunofluresence. It had been shown that serum and glucose starvation induced increased autophagic flux in OSCC and TNBC cellular models. Then, effect of combinations between standard chemotherapy and specific autophagy inihibtors was tested *via* MTT cellular proliferation assay. Cellular proliferation assay exhibited synergistic effect between standard chemotherapy (*e.g.,* Cisplatin or Paclitaxel) and Beclin-1 inhibitor (SAR405) in both OSCC and TNBC cell models. Also, combination of different autophay inhibitors was tested which showed a syergistic effect between Beclin-1 inhibitor (SAR405) and ULK-1 inhibitor (MRT68921). The effect of these combinations on tumour cell migration was also examined in both OSCC and TNBC cel models *via* scratch-wound assay. It revealed that combination of standard chemotherapy (*e.g.,* Cisplatin or Paclitaxel) and Beclin-1 inhibitor (SAR405) impaired tumour cell migration in both OSCC and TNBC cell models. Finally, combination between Paclitaxel and different

autophagy inhibitors was tested *in vivo* in an orthotopic TNBC xenograft model. The animal study demonstrated that Paclitaxel-SAR405-MRT68921 combination significantly reduced TNBC tumour volume and weight compared to the control. These data demonstrate the utility of autophagy inhibitors as novel anti-cancer agents and warrants further investigation into development of a novel autophagy targeting anti-cancer therapy.

In **chapter 4,** to further validate the role of autophagy in OSCC and TNBC cancer models, the expression of autophagic marker (LC3 and P62) was examined in OSCC and TNBC specimens via immunohistochemistry (IHC) and relation between their expression and clinicopathological variables and survival data was evaluated. Positive LC3 expression was shown to be associated with low histologic grade of OSCC. On the other hand, positive LC3 and P62 expression in TNBC was associated with high histologic grade of TNBC. Notably, better overall survival of TNBC pateints was associated with positive LC3 expression.

In **chapter 5,** we focused our work on chemotherapy resistant models of OSCC and TNBC. Initially, resistant OSCC and TNBC cell models were developed, which was performed by treating the parent cells with increasing concentration of standard chemotherapy for each cell model. The resistant phenotype was futher confirmed by cellular proliferation assay and colony formation assay which indicated markedly higher IC_{50} for chemotherapy in resistant cell lines compared to the parent cells. To futher elucidate the role of autophagy in chemoresistance, some effective combinations from parent cell lines were tested on the resistant OSCC and TNBC cell models. Both resistant cell models showed a synergistic effect on SAR405-MRT68921 combination. While only

OSCC resistant cell model exhibited synergistic effect on Cisplatin-SAR405-MRT68921 combination that was unlike the parent cells which showed antagonistic effect with the same combination. This can be explained by activation of autophagy in resistant OSCC cell lines that was found after untargeted proteomic analysis of these cell lines. Moreover, a proteome-wide approach was utilised to identify the novel molecular pathways and upstream activated or inhibited in OSCC and TNBC chemoresistant cell models. This analysis demonstrated TGM2 as being activated upstream mediator of chemoresistance in boh OSCC and TNBC resistant cell models. The role of TGM2 in chemoresistance was evaluated by assessing IC_{50} of standard chemotherapy after *TGM2* silencing *via* MTT cellular proliferation assay. The assay showed that there was a reduction of 20-25% of IC_{50} for Cisplatin and Paclitaxel in OSCC and TNBC resistant cell model respectively after *TGM2* silencing, which indicates TGM2 role in chemoresistance. Furthermore, combination of standard chemotherapy (*e.g.,* Cisplatin or Paclitaxel) and TGM2 inhibitor (GK921) was assessed by cellular proliferation assay which showed synergistic effect in both cell models. These data indicate that TGM2 could be another promising target to resensitise tumour cells to conventional chemotherapy.

Collectively, this study for the first time confirms the efficacy of autophagy inhibition *via* novel autophagy inhibitors in OSCC and TNBC models, which may help in developing new strategies in treating these cancers. Further, novel pathways and molecules were also identified in resistant OSCC and TNBC cell models, which could be developed as promising targets for cancer treatment in future.

Table of Contents

Abbreviations

μM	Micromolar
3-MA	3-methyladenine
ADCD	Autophagy dependent cell death
AMPK	AMP activated protein kinase
ATP	Adenosine triphosphate
Baf A1	Bafilomycin A1
BLIA	Basal like immune activated
BLIS	Basal like immune suppressed
BNIP3	Bcl2 interacting protein 3
CAFs	Cancer associated fibroblast
CQ	Chloroquine
CT	Chemotherapy
CTLs	Cytotoxic T-lymphocytes
DAPK	Death associated protein kinase
DMEM	Dulbecco's Modified Eagle Medium
DNA-PK	DNA-defendant protein kinase
ECM	Extracellular matrix
EGF	Epidermal growth factor
EMT	Epithelial to mesenchymal transition
ER	Endoplasmic reticulum
ER	Estrogen receptor
h	Hour
HCQ	Hydroxychloroquine
HER2	Human epidermal growth factor receptor2
HIF-1 α	Hypoxia inducible factor-1α

HMGB1	High mobility group box 1
IF	Immunoflurosence
IHC	Immunohictochemistry
IM	Immunomodulatory
IPA	Ingenuity Pathway Analysis
JNK-1	C- jun N terminal protein kinase
Kg	Kilogram
LAR	Luminal androgen receptor
LC3	Microtubule-associated protein 1 light chain 3
M	Mesenchymal
MAPK	Mitogen associated protein kinases
mg	Milligram
MHC-1	Major histocompatibility complex-1
mm	Millimetre
MMPs	Matrix metalloproteinases
MSC	Mesenchymal stem cell
mTORC1	Mammalian target of rapamycin complex 1
MTT	3-(4,5-dimethylthiazol-2-yl)-5-(3-carboxymethoxyphenyl)-2-(4-sulfophenyl)-2H-tetrazolium
NFκB	Nuclear factor κB
nM	Nanomolar
NSCLC	Non-small cell lung cancer
OS	Overall survival
OSCC	Oral squamous cell carcinoma
PBS	Phosphate buffered solution
PDGFR β	Platelet derived growth factor receptor β

PDK1	Phosphoinositide-dependent protein kinase 1
PE	Phosphatidylethanolamine
PI3K	Phosphoinositide 3-kinase
PI3P	Phosphatidylinositol 3- phosphate
PR	Progesterone receptor
PVDF	Polyvinylidene difluoride
ROS	Reactive oxygen species
RT	Radiotherapy
RUBICON	Run domain protein as Beclin-1 interacting and cysteine-rich containing
SDS	Sodium dodecyl sulfate
SEM	Standard error of mean
TAMs	Tumour associated macrophages
TCA	Tri-carboxylic acid
TCEB	Tris(2-carboxyethyl)phosphine
TEAB	Triethylammonium bicarbonate
TGF- β	Tumour growth factor-β
TICs	Tumour initiating cells
TILs	Tumour infiltrating lymphocytes
TAMs	Tissue microarrays
TME	Tumour microenvironment
TNBC	Triple negative breast cancer
TSC	Tuberous sclerosis complex
ULK-1	Unc-51 like autophagy activating kinase 1
UVRAG	UV radiation resistance-associated gene
VEGF	Vascular endothelial growth factor

WB	Wetern Blot
WIPI2	WD-repeat PtdIns(3)P effector protein I2

List of Figures

List of Tables

Chapter 1

Introduction

Portions of this chapter have been reproduced, in whole or in part, from the original publications:

Emerging role of autophagy in the development and progression of oral squamous cell carcinoma (2021). YS Abd El-Aziz, LYW Leck, PJ Jansson, S Sahni. *Cancers* 13 (24), 6152.

Autophagy: A promising target for triple negative breast cancers (2022). YS Abd El-Aziz, J Gillson, PJ Jansson, S Sahni. *Pharmacological Research* 175, 106006.

Role of ABCB1 in mediating chemoresistance of triple-negative breast cancers (2021). YS Abd El-Aziz, AJ Spillane, PJ Jansson, S Sahni. *Bioscience Reports* 41 (2), BSR20204092.

1. Autophagy

Autophagy, which literally means “eating self”, is a cellular catabolic process used to recycle damaged cytoplasmic organelles and misfolded proteins via lysosome mediated degradation in response to stress conditions or certain signals [1]. The autophagic process is considered to be an internal defensive mechanism against stressful conditions such as hypoxia and nutrient deprivation, which allow the cell to survive by breaking down cytoplasmic constituents into primitive components needed for survival [2]. Beside the pro-survival effect, it is also involved in pro-death mechanism called autophagic cell death where large scale sequestration of part of the cytoplasm within autophagososme occurs, giving the cell vacuolated appearance [3]. Autophagy plays an important role in maintaining normal cellular homeostasis and development [4]. Notably, autophagy has been shown to be involved in inflammatory disorders (*e.g.,* Crohn’s disease), neurodegenerative disorders and cancer [5].

1.1. Types of Autophagy

Three types of autophagy has been described, namely, macroautophagy, microautophagy and chaperon mediated autophagy (**Figure 1.1)**. Macroautophagy is the most well-known type and will be referred as autophagy in this thesis. It involves engulfment of any damaged organelles or proteins in double membrane vesicle, called autophagosome which subsequently fuses with the lysosomes to facilitate degradation of encapsulated cargo. After degradation of the engulfed material components such as amino acids and fatty acids are released back into the cytoplasm and reused by the cell [6]. Recently, there are growing evidences that autophagy can be selective by targeting certain organelles such as macropexophagy (peroxisomes) and mitophagy (mitochondria) [7].

Microautophagy involves invagination in the lysosomal membrane to envelop cytoplasmic components for degradation [7]. On the other hand, in chaperone mediated autophagy, proteins with KFERQ motif are being recognised by heat shock protein 70 (HSP 70) and shuttled into the lysosome via lysosome associated membrane protein 2A (LAMP2A) for degradation [8].

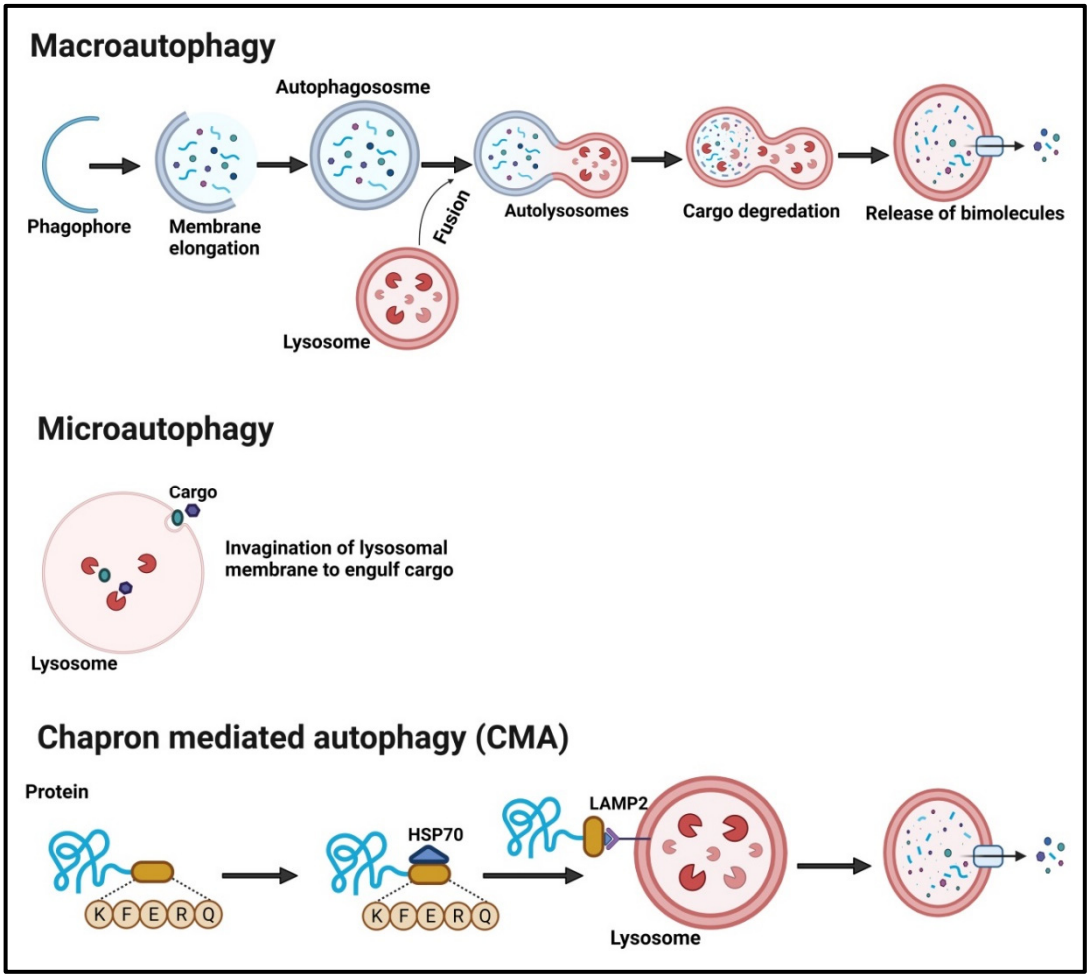

Figure 1.1. Different types of autophagy: Macroautophagy, microautophagy and chaperon mediated autophagy (CMA). Macroautophagy involves formation of double membrane vesicle called autophagosome that engulf cargo and deliver it to lysosome for degradation. Microautophagy is invagination in the lysosomal membrane to engulf foreign material. CMA is delivery of proteins with KFERQ motif to lysosome via heat chock protein (HSP) and LAMP2. Created with BioRender.com

1.2. Mechanism and molecules involved in autophagy

Autophagy is a multistep process that includes a series of molecules for its initiation and completion (**Figure 1.2**). One of these series is proteins encoded by the autophagy related genes (*ATGs*). Eighteen of the ATG proteins (ATG1 to ATG10, ATG12 to ATG14, ATG16 to ATG18, ATG29, and ATG31) control the autophagic process [9]. Autophagy consists of three steps: **(1)** nucleation and induction of autophagy-isolation membrane; **(2)** isolation membrane elongation and completion of autophagosome; and **(3)** lysosomal fusion and cargo degradation.

(i) Induction of autophagy-isolation membrane and nucleation: The autophagic process begins when there is nutrient or energy stress that is mediated by AMP activated protein kinase (AMPK). Activation of the AMPK pathway in turn activates Unc-51 like autophagy activating kinase 1 (ULK-1) either by direct phosphorylation of ULK-1 at Ser317 and Ser777 or inhibition of mammalian target of rapamycin complex 1 (mTORC1) to relieve inhibitory phosphorylation of ULK-1 at Ser757 [10]. mTORC1 is a serin/threonine kinase that detects presence or absence of nutrients [10]. In case enough nutrients are available, mTORC1 inhibits ULK-1 by its phosphorylation at Ser 757, thus, inhibiting autophagy [10]. After ULK-1 activation, the next step is assembly of ULK-1 complex that consists of ULK-1, ATG13, ATG101 and FIP200 [11]. This is followed by induction and assembly of the class III phosphoinositide 3-kinase (PI3K) complex, which comprise Vps34, p150, Beclin-1, Atg14L and Autophagy and Beclin1 Regulator 1 (AMBRA1), by the effect of ULK-1 complex [12]. Then, both ULK-1 and class III PI3K complexes translocate to the nucleation site where they stimulate the formation of isolation membrane called phagophore from membrane integration of various organelles such as golgi apparatus and mitochondria [13].

(ii) Isolation membrane elongation and completion of autophagosome: Nucleation is followed by elongation of the isolation membrane which involves 2 conjugation systems *i.e.,* ATG12-ATG5 conjugation and microtubule-associated protein 1 light chain 3 (LC3) processing [11]. The conjugation is mediated by E1 and E2 ligases, ATG7 and ATG10 [14]. In the first conjugation system, two molecules of ATG12-ATG5 conjugate combines with ATG16L forming a complex which is incorporated into the isolation membrane and stimulates phagophore membrane elongation. The localisation of the ATG12-ATG5-ATG16L complex to the autophagosomal membrane is achieved by the effect of protein family called WD-repeat PtdIns(3)P effector protein I2 (WIPI2) [15, 16]. The ATG12-ATG5-ATG16L conjugate dissociates from the completed autophagosome membrane [17].

The second conjugation system involves LC3 proteins and its homologues. In the cytoplasm, LC3 is present as an immature precursor called pro-LC3 which is cleaved, in the presence of ATG4, to give rise to LC3-I with C-terminal-exposed glycine residue [18]. Conjugation of phosphatidylethanolamine (PE) to the exposed glycine, in the presence of ATG3 and ATG7, leads to generation of a lipidated form of LC3, *i.e.,* LC3-II. This lipidated LC3 is then inserted into the autophagosomal membrane [19]. In contrast to ATG12-ATG5-ATG16L conjugate, LC3-II remains on the autophagosome membrane, and thus, it is considered as a classical autophagosomal marker [20].

At the end of this stage, the phagophore membrane is closed to form a double membrane autophagosome [20]. This is achieved by the effect of mammalian ATG8 homologues which consists of LC3 and GABARAP families [21]. Both LC3 and GABARAP are essential in autophagosome biogenesis. It was suggested that LC3 is important for autophagic membrane elongation, whereas, GABARAP mediates the membrane closure [22]. This

concept was supported by *in vivo* study that revealed accumulation of immature phagophore in cells expressing mutant LC3/GABARAP [22].

(iii) Lysosomal fusion and cargo degradation: Once autophagosome formation is completed, it undergoes a series of membrane trafficking events to fuse with lysosomes. Transport of autophagosome to the endo-lysosome is achieved along the microtubule system [23]. The C-terminal part of LC3 combines to the autophagosomal membrane, while its amino terminal end connects to the microtubule [24]. This is followed by binding of autophagosome to early endosomes, late endosomes and multivesicular bodies, forming amphisomes prior to fusion with lysosomes [25]. Finally, amphisomes are converted into autolysosomes by fusion with lysosomes [23]. The Vps34-Beclin-1 complex mediates autophagosomal fusion with endo-lysosomes based on its binding to co-regulatory proteins (**Figure 1.3**). UV radiation resistance-associated gene (UVRAG) competes with ATG14 to combine with Vps34-Beclin-1 complex [26]. After UVRAG bound to the Beclin-1 complex, it induces the fusion between autophagosome and endo-lysosomes via Rab7 [27]. Another regulatory protein is Run domain protein as Beclin-1 interacting and cysteine-rich containing (RUBICON), which act as negative regulator for the fusion events when bound to UVRAG-Vps34-Beclin-1 complex [28]. The last step in autophagy involves degradation of inner autophagosomal membrane and the entrapped cargo by lysosomal enzymes such as cathepsins, followed by the release of biomolecules into the cytosol for reuse [29]. After cargo degradation, the inner portion of LC3-II are broken down within the autolysosome, a process by which the autophagic flux is measured [30]. On the other hand, LC3-II located on the outer autophagosomal membrane is reconverted into LC3-I [30]. Moreover, the release of biomolecules in the cytoplasm recruits mTORC1 to the autolysosomes and leads to autophagy attenuation with lysosomal reformation from autolysosomes [31].

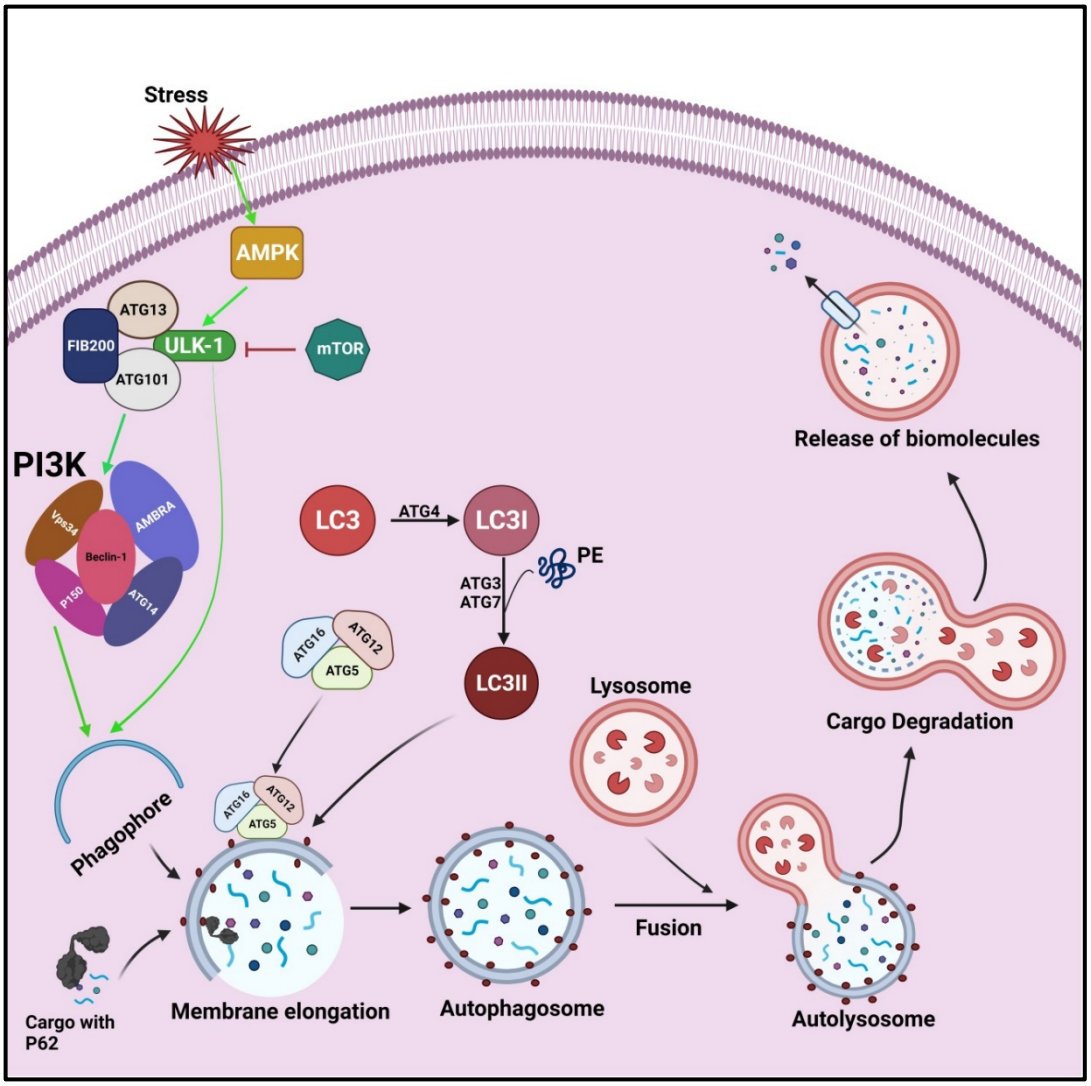

Figure 1.2. Autophagy Pathway: Autophagy starts with activation of serial cascades of major molecules as the cell is subjected to stress, followed by phagophore formation. This is followed by further membrane elongation leading to formation of a double membrane vesicle called autophagosome. Autophagosomes fuses with lysosomes to form autolysosomes that results in cargo degradation and release of biomolecules. Green arrow indicates activation and red arrow indicates inhibition. Created with BioRender.com

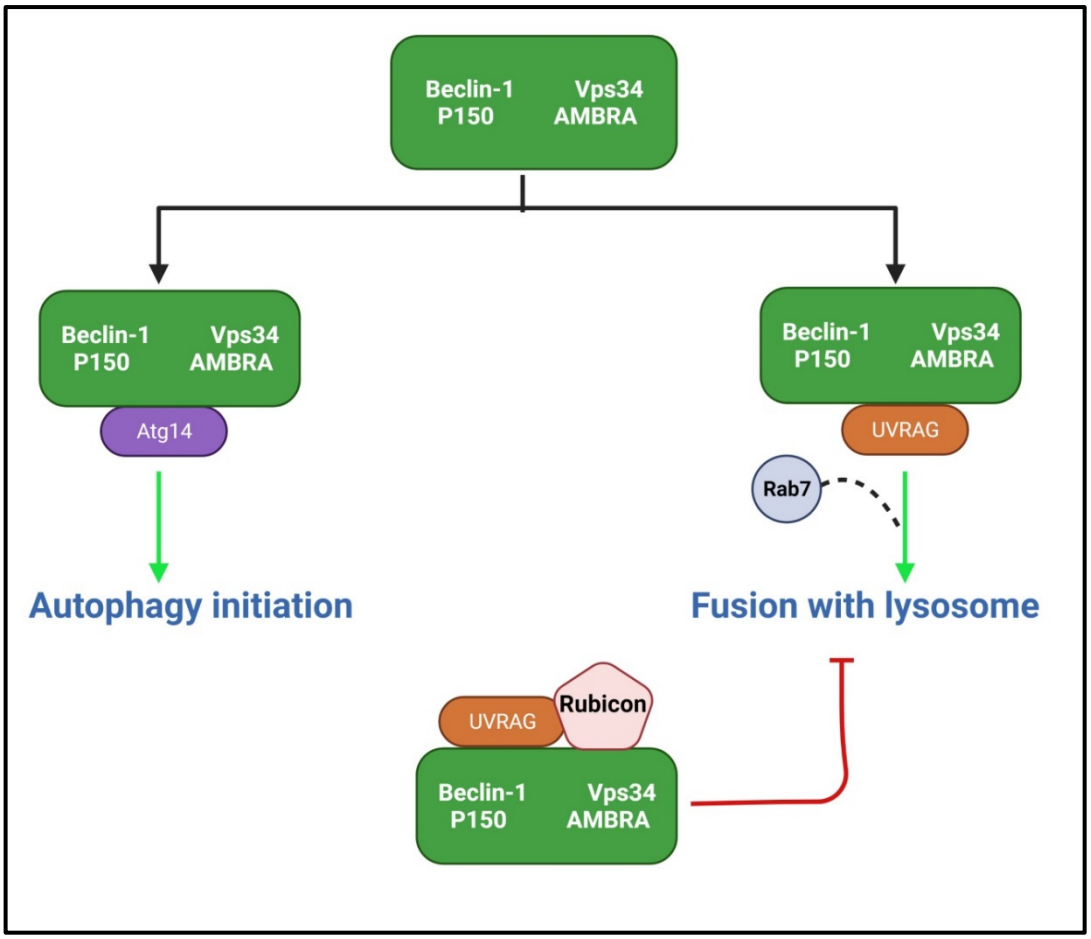

Figure 1.3. Role of Beclin-1/Vps34 complex in autophagic pathway: At the initiation step, Beclin-1/Vps34 complex bind to ATG14 to induce autophagy initiation. After that, Beclin-1/Vps34 complex binds to UVRAG to induce fusion between autophagosome and lysosome. This step can be inhibited by attachment of Rubicon to UVRAG. Green arrow indicates activation and red arrow indicates inhibition. Created with BioRender.com

1.3. Cargo Recognition and Targeting

The view that autophagy involves random degradation of cellular components via lysosomes has now changed. Autophagy is recognized to selectively degrade certain proteins, protein aggregates, intra cellular pathogens or cellular organelles [32]. This has been supported by data obtained from quantitative mass spectrometry which demonstrated activated autophagy against cytosolic protein rather than organellar proteins under amino acid starvation [33].

Lately, the discovery of autophagy receptors, that deliver specific cargo to the autophagosome for lysosomal degradation, has formed a better understanding for the mechanism of cargo specific targeting. Two categories of autophagy receptors have been identified based on how they recognise cargo: ubiquitin dependent and ubiquitin independent recognition [34].

(i) Ubiquitin dependent cargo recognition*:* p62/SQSTM1 is an example for ubiquitin dependent receptors. p62 contains an LC3 interacting region (LIR) which binds to the ATG8 homologues surface and a C-terminal ubiquitin-associated (UBA) domain that attaches to mono- and poly ubiquitinated proteins [35]. This dual recognition site provides, p62 and other ubiquitinated autophagy receptors an ability to physically link ubiquitin-tagged cargo to the autophagosome for further lysosomal degradation [36]. p62 is also involved in autophagy of intracellular bacteria such as Salmonella enterica [37]. Hence, p62 is a multifunctional autophagy receptor that is involved in aggrephagy (selective autophagy of aggregated proteins) and xenophagy (selective autophagy of intracellular bacteria or virus).

(ii) Ubiquitin independent cargo recognition*:* This category includes autophagy receptors that identify different proteins, lipids and sugars. NCOA4 is an example for these receptors. NCOA4 mediates ferritinophagy which is important for cellular iron homeostasis. Several studies indicated that NCOA4 is crucial for ferritin delivery to autophagosome for subsequent lysosomal degradation in case of low intracellular iron level [38]. C-terminal residue of NCOA4 interacts with ferritin heavy chain subunit and mutations at these binding sites abrogate ferritinophagy [39].

1.4. Control of autophagy induction

Autophagy initiation is being regulated by the effect of upstream regulators (*i.e.,* Class I PI3K/AKT/mTORC1 and AMPK) and regulators within the core autophagic machinery (*i.e.,* ULK1.ATG13.FIP200 complex and Class III PI3K/Vps34-Beclin-1 complex).

(i) Upstream regulators*:* (a) Class I PI3K.AKT.mTORC1: mTOR is serine/threonine kinase which acts as cellular sensor of nutrient, growth factors availability, stress signals and energy levels and it is the downstream target of class I PI3K [32]. mTOR is involved in formation of two different protein complexes (mTORC1 and mTORC2). mTORC1 is positive regulator of anabolism and negative regulator of catabolism (*i.e.,* autophagy) [40]. Under nutrient rich condition, class I PI3K catalyses the formation of phosphatidylinositol 3- phosphate (PI3P) at the plasma membrane which subsequently leads to recruitment of AKT and its activator phosphoinositide-dependent protein kinase 1 (PDK1) [30]. Once AKT is activated, it phosphorylates to inhibit tuberous sclerosis complex 1/2 (TSC) that in turn, diminish the suppression of Rheb which is mTOR activator [30]. As mTORC1 is activated, it inhibits ULK-1 via phosphorylation at Ser-757 and blocks the autophagic pathway (**Figure 1.4**) [40].

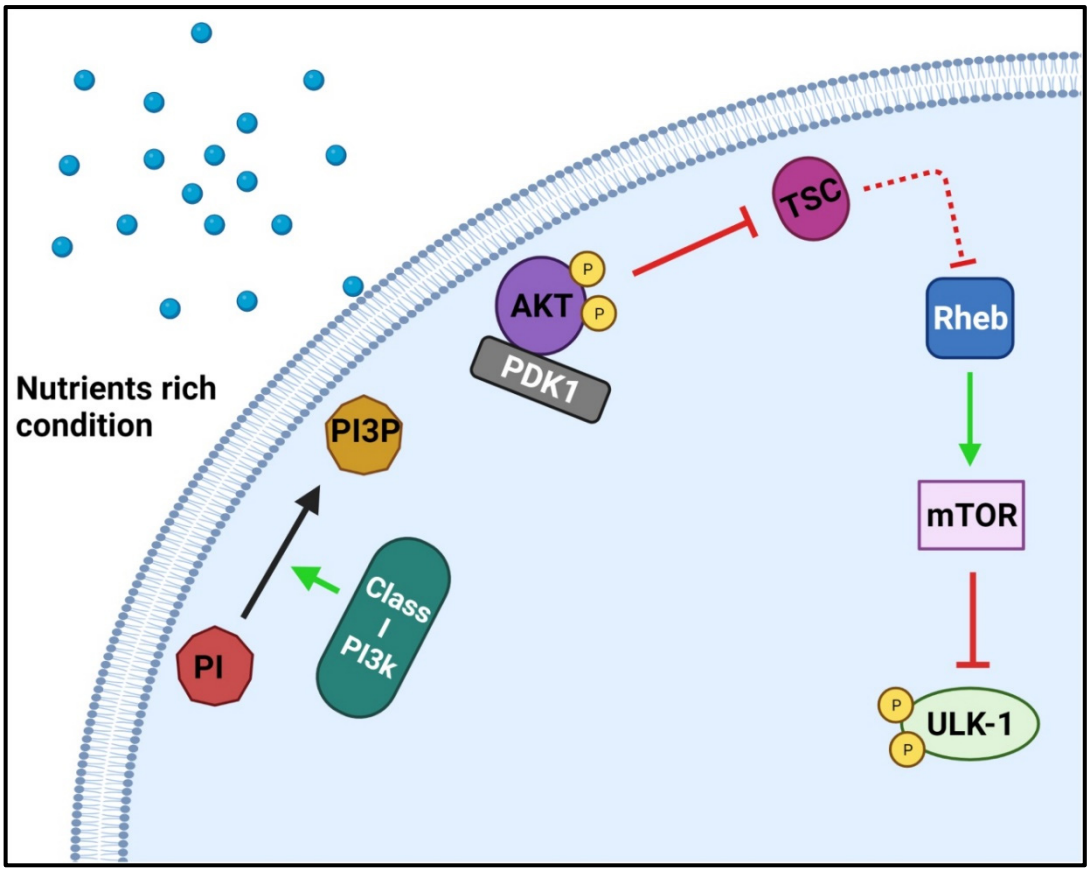

Figure 1.4. Role of Class I PI3K/AKT/mTORC1 in regulating the autophagic pathway: Under nutrient rich conditions, phosphatidylinositol(PI) is converted to phosphatidylinositol 3- phosphate (PI3P) by the effect of Class I PI3K that leads to recruitment of AKT and its activation via phosphorylation. AKT activation inhibits TSC which results in activation of Rheb, which is mTOR activator. mTOR activation inhibits ULK-1 via phosphorylation and lead to autophagy inhibition. Created with BioRender.com

(b) AMPK: AMPK is a serine/threonine kinase which is a cellular energy sensor [41]. Under low ATP/AMP conditions, AMPK is activated which in turn activate ULK-1 via direct phosphorylation at Ser-317 and Ser-777 [42] or via inhibiting mTORC1, which in turn leads to dephosphorylation of ULK-1 (Ser-757). Activation of ULK-1 results in autophagy initiation [40].

(ii) Regulators within the autophagic pathway*:* (a) ULK-1.ATG13.FIP200: The activated ULK-1 begins to form a complex with ATG13, ATG101 and FIP200 which then

localises to the nucleation site of the isolation membrane, which leads to the induction of autophagic pathway [10].

(b) Class III PI3K/Vps34-Beclin-1 complex: This complex is formed by assembly of five proteins which are Vps34, Beclin-1, ATG14, P150 and Ambra [12]. Under normal condition, Ambra connects inactive Beclin-1/Vps34 complex to microtubule via its binding to Dyanin [43]. As autophagic pathway is induced, ULK-1 phosphorylates Ambra resulting in its dissociation from microtubule and it translocates with Beclin-1/Vps34 complex to the endoplasmic reticulum to initiate autophagic nucleation (**Figure 1.5**) [43].

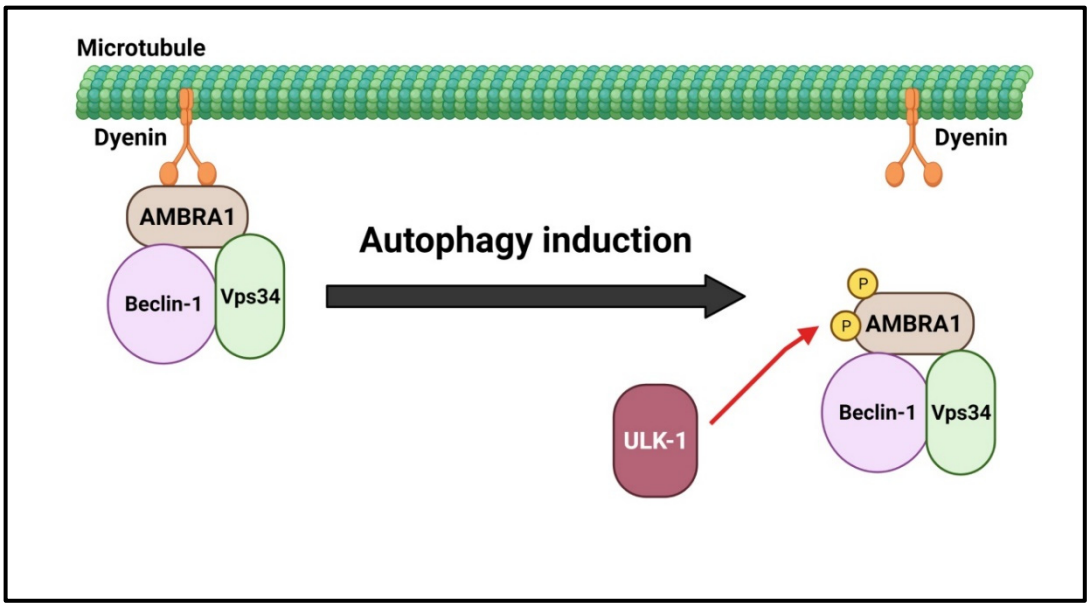

Figure 1.5. Role of Class III PI3K in the autophagic pathway: Under normal conditions, class III PI3K is attached to microtubule through Ambra and Dyanin. Upon autophagy induction, ULK-1 phosphorylates Ambra resulting to its detachment from microtubule and its recruitment to the nucleation site. Created with BioRender.com

1.5. Autophagy-Apoptosis regulation via Bcl2-Beclin-1 complex

The B-cell lymphoma 2 (Bcl2) family is a family of proteins which contains BH region. This family is divided into 3 subfamilies; **(1)** anti-apoptotic proteins (Bcl2, Bcl-xL) that have four BH domains; **(2)** pro- apoptotic proteins (Bax, Bak) which contain three BH domains; and **(3)** pro apoptotic BH3-only proteins [44]. The Bcl2 subfamily has a cleft called BH3 binding groove where a BH3 domain from pro-apoptotic proteins (*e.g.,* Bax, Bak) can attach [44]. The Bcl2 protein normally localises at the mitochondrial membrane to protect mitochondria from the effect of pro-apoptotic proteins (Bax, Bak) [45]. It exerts its anti-apoptotic effect by antagonizing Bak and Bax and preventing their translocation to the mitochondria [46].

Beclin-1, a Bcl2 homology 3 (BH3) domain only protein, is an essential protein for autophagy induction through recruitment of autophagic proteins to form Class III PI3K/Vps34-Beclin-1 complex, leading to initiation of phagophore [47]. Under normal conditions, BH3 domain of Beclin-1 binds to BH3 groove of Bcl2, hindering Beclin-1 from initiating phagophore structure which results in inhibition of autophagy. Thus, Bcl2 has an inhibitory effect on both apoptosis and autophagy [48]. This effect has been demonstrated by a study in which over-expression or silencing of Bcl2 results in inhibition or increased the level of autophagy, respectively [49].

The interaction between Bcl2 and Beclin-1 can be controlled by different factors such as cellular localisation, binding partners and phosphorylation of both proteins [50]. Originally, it has been demonstrated that Bcl2-Beclin-1 interaction is localised to both endoplasmic reticulum (ER) and mitochondria [49]. However, later studies have demonstrated that only interactions at ER are capable of inhibiting autophagy [51].

Binding proteins such as High mobility group box 1 (HMGB1) and Bcl2 interacting protein 3 (BNIP3) can disrupt Bcl2-Beclin-1 interaction. HMGB1 is a chromatin associated nuclear protein that competes with Bcl2 for binding to Beclin-1 and stimulates autophagy [52].

BNIP3 has a BH3 domain through which it can attach to Bcl2, and thus, disrupting the binding between Bcl2 and Beclin-1, leading to induction of autophagy [53]. Hence, competitive proteins are considered to be another mechanism to regulate the autophagy by affecting the Bcl2-Beclin-1 interaction.

Further, phosphorylation of either Beclin-1 or Bcl2 affects their interaction with one another. Bcl2 phosphorylation by stress activated C- jun N terminal protein kinase (JNK1) results in dissociation of Bcl2 from Beclin-1, leading to induction of autophagy [54]. In a similar manner, Beclin-1 can be phosphorylated at its BH3 domain by Death associated protein kinase (DAPK) which causes dissociation of the complex which allows autophagy to proceed [55].

On the other hand, apoptosis can induce the cleavage of essential autophagic proteins such as Beclin-1 and ATG5. Beclin-1 is cleaved by the effect of caspase 8 rendering it non-functional, which results in inhibition of autophagy [56]. Upon Beclin-1 cleavage, C-terminus of cleaved Beclin-1 acquires a proapoptotic function and translocate from cytosol to mitochondria to induce apoptosis [57]. Moreover, ATG5 is also cleaved by calpain, a calcium dependent protease, producing fragment (*i.e.,* tATG5) that translocate to the mitochondria to trigger the release of cytochrome c and caspases activation [58]. Moreover, tATG5 binds to Bcl-xL and disrupt Bcl-xL-Bax complex resulting in release of Bax and induction of apoptosis [58].

1.6. Pathophysiological role of autophagy

At physiological levels, autophagy is considered as cellular recycling machinery that helps to maintain the normal cellular homeostasis by turnover of damaged organelles, long lived or misfolded proteins and protein aggregates [59]. Upon exposure to cellular stresses such as nutrient deficiency, hypoxia, infection or oxidative stress, autophagy is induced to supply the cell with metabolic building blocks that allow the cell to overcome this stress. Therefore, autophagy is essential for preservation of normal homeostasis and cell survival at both basal and stress-induced levels, respectively [60].

In case of nutrient starvation, autophagy degrades damaged proteins and organelles to release essential building blocks such as amino acids, sugars and fatty acids to be used for Adenosine triphosphate (ATP) production or de novo synthesis of biomolecules [61]. During hypoxic conditions, hypoxia inducible factor-1α (HIF-1α), which is a transcription factor activated by low oxygen level, increases the expression of BNIP3 which induce the autophagic process via release of Beclin1 from BCL2/ Beclin-1 complex [53].

Autophagy is also important in capturing intracellular invading pathogens and presenting it to the lysosome for degradation [62]. Furthermore, in case of oxidative stress, reactive oxygen species (ROS) levels are increased which activate one of mitogen associated protein kinases (MAPK), *i.e.,* JNK1,[63] that in turn induce phosphorylation of Bcl2, which result in release of Beclin-1 from Beclin-1/Bcl2 complex. Thus, Beclin-1 can participate in VPS34 complex that is essential for autophagy induction [64].

In addition to its role in cell survival, it was found that autophagy also may play a role in inducing cell death. Some studies indicated that excessive autophagy stimulates cell death in a phenomenon called autophagy dependent cell death (ADCD) [65]. In ADCD,

the lethality comes from extreme levels of autophagy flux that lead to over consumption of cellular organelles and cytoplasmic content, as well as usage of cellular membrane to support autophagosome formation to a degree that result in disruption of cellular membrane homeostasis [66]. It was suggested that ADCD occurs due to: **(1)** hyperactivation of induction signals including AMPK, ULK1, Vps34-Beclin-1 complex or modulation of Bcl2-Beclin-1 complex via DAPK or BNIP3; **(2)** unrestrained activation of downstream components; **(3)** presence of second signal such as GCase-generated ceramide that develop sustained lethal levels of autophagy; **(4)** mis-regulated termination due to inhibition of proteasome degradation of ULK1, Beclin-1 and Vps34 [65]. Hence, autophagy is considered to have a dual role in both cell survival and cell death mechanisms.

2. Autophagy and cancer

Autophagy plays a complex, dual and paradoxical role in cancer. At early carcinogenesis, autophagy exerts a tumour suppressor function as it limits the DNA damage and genomic instability through induction of senescence, thus, limiting tumour growth. However, in advanced cancers, autophagy also contributes to tumour progression by supporting metabolic reprogramming of cancer cells to survive under different stressful conditions [67]. In addition, autophagy is known to be regulated by some tumour suppressors (*e.g.,* p53) and oncogenes (*e.g.*, RAS) [68].

2.1 Regulation of autophagy by oncogenes and tumour suppressors

(i) p53: The tumour suppressor, p53, is known as the guardian of the genome as its main function is to activate cell cycle arrest or cell senescence in response to DNA damage. It

is considered to be a tumour suppressor as it eliminates cells with mutated DNA from the cell cycle and stimulate apoptotic genes. This function allows p53 to maintain cellular homeostasis and prevents processes that lead to tumour transformation [69]. However, more than 50% of human cancer encounters p53 loss of function [70] due to its direct mutation or mutation in kinases responsible for its activation [71]. Recently, p53 was found to not only act as a transcription factor that control cell cycle [72] and pro-apoptotic effects [73], but also regulate autophagy.

p53 has a dual role on autophagy according to its cellular localisation [74]. In the nucleus, p53 acts as pro-autophagic factor as it stimulates the autophagy via transactivation of many genes responsible for autophagy activation. Nuclear p53 induces the activation of AMPK, which is upstream regulator of autophagy [75]. Also, it activates DAPK-1 that in turn phosphorylates Beclin-1 and liberates it from Bcl2/Beclin-1 complex, resulting in activation of autophagic initiation [55]. p53 also triggers ULK-1 and ULK-2 transcription leading to elevated levels of autophagy [76].

In contrast, cytoplasmic p53 tends to repress the autophagic machinery. One of p53 targets is TP53-induced glycolysis and apoptosis regulator (TIGAR), which inhibits intracellular levels of reactive oxygen species (ROS). This inhibition of ROS leads to suppression of the autophagic process [69]. Furthermore, *Morselli et al.* [77] showed that cytoplasmic p53 could inhibit autophagy through its interaction with FIP200, which is one of major molecules in autophagy initiation. Taken together, the dual function of p53 is in line with the paradoxical role of autophagy in cancer and it depends on subcellular localisation of p53. Thus, future studies should put this into consideration to determine whether p53 has pro- or anti-autophagic role under certain settings.

(ii) *RAS*: *RAS* is an oncogene that is activated in cancer cells. It is responsible for regulation of cell survival and growth [78]. Recently, several studies had linked *RAS* with autophagy, where autophagy could either enhance or suppress the oncogenic effect of *RAS* [79-81]. When *RAS* expression was acutely induced, which mimic the early stage carcinogenesis, this resulted in induction of autophagic cell death via upregulation of Beclin-1 [79]. Also, another study showed that in response to *RAS* activation, autophagy induces tumour cells to acquire a senescent state so as to limit the tumour cell proliferation [82].

In other experiments, stable exogenous over-expression of *RAS* resembles a phenotype corresponding to later stages of cancer progression [80, 10, 83]. In this context, autophagy is induced to allow metabolic reprogramming of cancer cells to deal with metabolic stresses, which promotes tumour cell survival [80]. As *RAS* hinders Acetyl CoA production from pyruvate, which is the main substrate of mitochondrial tri-carboxylic acid (TCA) cycle, autophagy provides substrates as amino acids to recharge the mitochondrial cycle [84]. Additionally, *RAS* induced autophagy has been shown to remove damaged mitochondria from the cytosol and thus, preserves the cellular homeostasis [68]. Moreover, studies have also demonstrated that inhibition of autophagy in *RAS* expressing cancer cells resulted in accumulation of damaged mitochondria with impairment of oxidative phosphorylation and reduced tumourgenicity of *RAS* mutant cells [80, 85]. Taken together, *RAS* induced autophagy has a binary effect on tumourigenic process according to the context and tumour stage.

(iii) *MYC*: *MYC* is one of the oncogenes that is activated and contributes to many aspects of human cancer [86]. High levels of MYC induce proliferation of tumour cells and stimulate the transcription of genes involved in mitochondria biogenesis and glycolysis, thus

promoting metabolic reprograming of cancer cells [87]. Therefore, *MYC* knockdown enhanced growth arrest and apoptosis in tumour cells both *in vivo* and *in vitro* [88, 89]**.** Notably, It was demonstrated that MYC inhibited the autophagic pathway in human MYC driven B-cell lymphoma through suppressing the transcription of genes responsible of autophagy [90]. Similar results were observed in Hela human cell line [91]. In contrast, *Toh et al*. [92] demonstrated that *MYC* knockdown in Hela cells had an inhibitory effect on autophagy via regulating JNK-1 activity and phosphorylation of Bcl2. In the same context, *Dey et al.* [93] found that MYC induced endoplasmic reticulum stress mediated autophagy in human lymphoma cells. These data indicate a dual effect of MYC on autophagy, which needs further investigations and may unveil as a new therapeutic approach for MYC driven cancers.

2.2 Autophagy as a tumour suppression pathway

Autophagy has been connected to tumour suppression via discovery of monoallelic loss of autophagy gene *BECN1* in several types of human cancers such as breast and ovarian cancers [94]. In addition, *BECN1* heterozygous deletion leads to increased malignancies in mice [95], with decreased tumour growth in mice when *BECN1* expression is restored [96]. Moreover, mutation of other autophagy related genes such as *ATG5*, *ATG9* and *ATG12* have been observed in gastric and colorectal cancers [97]. These data suggest that autophagy repress tumour initiation.

Autophagy is involved in tumour suppression through several pathways. The main function of autophagy is to maintain cellular hemostasis through degradation of damaged organelles and protein aggregates [98]. Thus, autophagy helps to protect the cells against DNA damage and genomic instability caused by elevated levels of ROS. This damage and instability result in increased risk of tumour initiation [99]. Another mechanism via which

autophagy mediates its tumour suppressor function is through induction of senescence. Senescence is a prolonged growth arrest process in which the cell is metabolically active, but cannot undergo further division or re-enter the cell cycle [100]. Autophagy prevents the proliferation of transformed cells via oncogene induced senescence [100]. Depletion of autophagy genes leads to escape of abnormal cells from senescence [82]. This indicates that autophagy exerts a role in acquiring senescent phenotype upon oncogene activation, leading to the elimination of abnormal cells from cell cycle.

Moreover, autophagy can inhibit tumour development by controlling the cellular levels of p62. The main function of p62 is to deliver ubiquinated proteins to autophagosomes for degradation and subsequently p62 is being degraded in this process [101]. p62 tends to be involved in pro-tumourigenic signaling and has been overexpressed in human cancers [101]. It was found that p62 depletion decreased the tumour size in *ATG7* deficient mice [102] and eradicated RAS-induced lung carcinoma [103]. p62 is also considered as a regulator of NRF2, which is a transcriptional factor responsible for upregulation of antioxidant genes under oxidative stress. Normally, NRF2 binds to KEAP1 for its polyubiquitination and proteasomal degradation [104]. Under autophagy deficient conditions, p62 accumulates in the cytoplasm and binds to KEAP1 at NRF2 binding site, which leads to NRF2 activation that allows cancer cells to survive under oxidative stress [84].

Another potential mechanism by which autophagy may contribute to tumour suppression is through prevention of necrotic cell death and subsequent inflammation that may drive tumour growth. Under apoptotic and autophagy deficiencies in tumour xenograft model, necrosis and subsequent inflammation were increased, which resulted in accelerated tumourigenesis by the effect of pro-tumourigenic inflammatory microenvironment [105].

Therefore, the anti-inflammatory activity of autophagy helps to eliminate apoptotic cells, which could limit the inflammation that may contribute to tumour growth [106].

2.3. Autophagy as a tumour promoting mechanism

Beside its tumour suppressive role, autophagy has also been shown not only to promote malignant transformation into cancer cells, but, also, support the survival of cancer cells. Deletion of autophagic genes such as *FIP200 or ATG5 or ATG7* abolishes tumour growth in mouse models [81, 107]. Similarly, shRNA induced knockdown of *ATG5* hinders pancreatic adenocarcinoma in a mouse model [81]. Moreover, *Yang et al*. [81] demonstrated that pancreatic cancer cells had elevated basal autophagy levels, which were required for sustained tumour growth. This group also showed that autophagy inhibition using chloroquine or RNAi led to impairment of tumour growth both *in vitro* and *in vivo* [85]. These studies reflect the vital role of autophagy in tumour maintenance and progression.

Autophagy can serve as pro-tumourigenic factor via different potential mechanisms. It is well known that cancer cells are metabolically stressed due to their rapid tumour growth and poor blood supply, which results in lack of nutrients and oxygen availability. As a compensatory mechanism, cancer cells up-regulate autophagy to provide themselves with the required nutrients for survival [108]. Autophagy induction in hypoxic regions is regulated by HIF-1, which stimulates BNIP3 that in turn disrupt the association between Beclin-1 and Bcl2 that consequently leads to release of Beclin-1 and induction of autophagy [109].

Furthermore, autophagy contributes to cell dormancy, which is a state in which cells stop their division and motility to preserve energy [100]. Dormancy is also known to play a

crucial role in tumour recurrence [100]. Under microenvironmental stress, autophagy can sustain cell survival by supplying the required nutrients during the dormant state. When the microenvironment improves, cancer cells can reenter the cell cycle and start proliferation again [110]. This phenomenon allows cancer cells to utilise autophagy to cope under metabolic stresses, which later can result in tumour recurrence.

Conversion of normal cell to a malignant cell phenotype is associated with cascade of molecular and biological changes that result in cancer initiation and progression [111, 112]. These series of events were defined as “Hallmarks of cancer” and were first reported by Hanahan et al. [111]. Recently, pro-survival autophagy had been linked to hallmarks of cancers as a positive regulator.

(i) Self-sufficiency of growth signals - sustained proliferation: One of the major hallmarks of cancer is the autonomy of growth signals to sustain their proliferative ability [112]. To achieve this, cancers utilise autophagy to provide themselves with the building blocks and ATP required for various functions by recycling damaged organelles and nutrients [108]. Also, elevated oncogenes expression result in increased levels of basal autophagy, that helps in tumour longevity under various stress conditions [113]. Thus, tumour cells highly depend on autophagy for their survival and growth, which has been described as “autophagy addiction” [114]. As an example of this phenomenon, pancreatic ductal adenocarcinoma with *KRAS* mutation shows higher basal autophagy levels, which promote tumour growth and contributes to gemcitabine resistance in pancreatic cell lines [115]. Also, autophagy inhibition in pancreatic cancer cells led to tumour regression [113]. In a similar manner, *ATG7* deletion in a lung cancer model inhibited tumour growth [116]. Moreover, autophagy is important for non-small cell lung cancer (NSCLC) growth by

decreasing ROS levels [117]. These data indicates that autophagy is essential for continued growth of cancer cells.

(ii) Evasion of apoptosis: Apoptosis is the programmed cell death cascade in multicellular organisms [118]. In case of cancer, tumour cells have deficient apoptotic machinery which contributes to sustained proliferation of cancer cells even after DNA damage and oncogene activation [112]. It has been well established that p53, which induces apoptosis when DNA damage occurs beyond repair, is lost in different types of cancer. The loss of p53 confers cancer cells to resist apoptosis [111].

Autophagy and apoptosis are closely related to one another and a crosstalk exists between these two cellular machineries as they have many common core mediators and upstream regulators [119]. As autophagy has been shown to have a dual role in cancer, it can resist or enhance the apoptosis according to the intensity of the stimulus and the threshold of each response [120]. For instance, *Abedin et al*. [121] demonstrated that Beclin-1 and ATG7 mediated autophagy suppress apoptosis after DNA damage and extend the survival of breast cancer cells. In line with the previous data, knockdown of *ATG7* resulted in enhanced apoptosis in melanoma cell lines [122]. Of note, mitochondrial autophagy was found to have a protective role against heat shock induced apoptosis via inhibiting the release of cytochrome C and caspase 3 [123].

On the other hand, autophagy may also be implicated in cell death, namely “autophagic cell death”. It is a form of cell death that is caspase independent and happens due to excessive autophagy [124]. Autophagic cell death can be induced by the effect of certain chemotherapy regimens as in case of glioblastoma where it was demonstrated that chemotherapy led to autophagic cell death and tumour regression [125]. Collectively,

these finding reflect a potential role of autophagy in regulation of apoptosis during tumour progression.

(iii) Angiogenesis: Angiogenesis means the ability of tumour to form a new vasculature. Tumour cells cannot grow more than few millimeters due to lack of blood supply. That is why cancer cells begin to switch from avascularised state to vascularised state, often called “angiogenic switch”[126]. Cancer cells stimulate themselves, or stimulate other cells to, secrete vascular endothelial growth factor (VEGF) to facilitate endothelial cells to form new blood vessels [127]. Autophagy has been implicated to play a role in angiogenesis. *Du. et al.* [128] demonstrated that ATG5 modulate angiogenesis in endothelial cells via AKT activation under hypoxia and starvation. Moreover, high mobility group box protein (HMGB) is a nuclear protein that has sequence homolog with Beclin-1, stimulates autophagy [129]. HMGB1 acts as an inflammatory cytokine that induce angiogenesis both *in vivo* and *in vitro* [130]. These findings indicate a role of autophagy in angiogenesis but more research is needed to elucidate the regulatory mechanism exerted by autophagy in regard to angiogenesis.

(iv) Invasion and Metastasis: One of the properties that cancers gain during their malignant transformation is the ability to invade surrounding tissues and settle down away from the primary site, which is known as “metastasis” [111]. It is a multistep process that involves: (1) Local invasion of the surrounding tissues; (2) Intravasation in the circulation; (3) Survival of cancer cells in the circulation; (4) Extravasation at secondary site; (5) Cancer cells survival at the secondary site; and (6) Tumour development at the secondary site [111].

It has been shown that autophagy has an integral role in metastasis, as autophagy mediates an important role in epithelial to mesenchymal transition (EMT) [131]. Autophagy

is also involved in persistence of dormant cancer cells in the circulation and at the secondary site [132]. Various studies have linked autophagy to invasion and metastasis as a positive regulator. Silencing of *ATG12* and *SQSTM1* decreased invasion and metastasis of glioma cells in 3D cell culture model [133] and glioblastoma stem cells [134] *in vitro,* respectively. In addition, starvation induced autophagy increases invasion and metastasis of hepatocellular carcinoma (HCC) via TGF-β/SMAD3 signaling [135]. A similar connection was observed in colon cancer where SMAD3 suppression via microRNA resulted in interrupted autophagy and reduction in invasiveness capability [136]. Moreover, autophagy inhibition via chloroquine or siRNA against ATG3 or ATG7 in HCC resulted in repression of EMT [135]. Taken together, autophagy is involved in every step of metastasis, which could be utilised as a therapeutic approach.

(v) Anoikis resistance: Anoikis is programmed cell death that occurs due to loss of detachment with the extracellular matrix (ECM). Normal cells have integrins on their surface, which help to maintain their anchorage to the ECM and preserve tissue homeostasis [137] . In contrast, cancer cells are characterised by loss of integrins, which lead to their detachment, EMT transition and migratory ability by way of anoikis resistance [138]. Autophagy had been involved in anoikis resistance as cancer cells tends to upregulate autophagy to promote their survival under ECM detachment stress [138]. *Avivar-Valderase et al.* [139] demonstrated that autophagy is responsible for the survival of ECM detached mammary epithelial cells via activation of AMPK. Autophagy inhibition is also shown to reduce pulmonary metastasis in mouse model of hepatocellular carcinoma via impairing anoikis resistance [140]. Moreover, BNIP3 induced autophagy contributes to anoikis resistance in hepatocellular carcinoma [141]. Similarly, induction of autophagy by rapamycin enhances spheroid formation and survival in peritoneal carcinomas and sarcomas by boosting anoikis resistance and apoptosis inhibition [142].

In summary, autophagy is essential for survival of detached cancer cells, which represents the first step in invasion and metastatic process.

(vi) Avoidance of immune destruction: Evasion of immune system is one of the major hallmarks in cancer [112]. Cancer cells tend to avoid immune destruction to allow their survival within the circulation until their extravasation and settlement at secondary site [112]. Over the last few years, autophagy has been identified as one of the mechanisms in tumour immune surveillance. It was suggested that inhibition of tumour immune surveillance is induced by pro-survival autophagy in different types of cancers [143]. For example, lysis of MCF7 breast cancer cells by cytotoxic T-lymphocytes (CTL) was suppressed when they were induced to undergo EMT with concurrent induction of autophagy [143]. Autophagy inhibition in MCF7 cancer cells, through silencing of *BECN1*, restored the CTL lysis capability in the same model [143]. Also, impairment of CTL lysis in melanoma cells was attributed to autophagy through degradation of Connexin 43 [144]. In the same manner, *FIP200* null cancer cells showed enhanced entrance of CTL within the tumour via elevated levels of CXCL10, which resulted in decreased primary tumour growth [107]. Notably, pancreatic cancer cells have reduced surface expression of major histocompatibility complex-1 (MHC-1) as it is lysosomally degraded via autophagy dependent mechanism [145]. Furthermore, inhibition of autophagy boosted the destruction of renal cell carcinoma by natural killer cells [146]. Overall, autophagy seems to modulate tumour immune surveillance to allow the survival of disseminated tumour cells.

(vii) Metabolic reprogramming: Metabolic reprogramming is considered to be one of the hallmarks of cancer and is known as “Warburg effect”[112]. Once cells have committed to malignant transformation, they seem to depend mostly on aerobic glycolysis for energy production and reduce the oxidative phosphorylation via mitochondrial electron transport

chain [147]. This metabolic shift is induced by oncogenes such as *RAS* [148] and *MYC* [149]. As mentioned before, *RAS* transformation impairs production of acetyl-CoA from decarboxylation of pyruvate and induces the uptake of both glucose and glutamine [84]. *RAS* induced autophagy plays a crucial role in this shift by providing essential building blocks that fuels the reprogramming [83]. Although there is a dependence of cancer cells on aerobic glycolysis for energy production, they still rely on functional mitochondria for their growth. Autophagy provides amino acids, from degradation of proteins, which are required to replenish TCA cycle [84]. Consistent with these data, some studies exhibited that autophagy inhibition leads to impairment in glycolysis [83, 107]. It has been reported that autophagy promoted glycolysis that is cardinal for RAS mediated oncogenic transformation [83]. Similarly, sustained glycolysis was observed in chronic myeloid leukemia with ATG7 mediated autophagy [150]. Taken together, these studies indicate the pivotal role of autophagy in metabolic reprogramming of cancer cells that needs to be further investigated to fully understand the underlying mechanisms and how it can be used as a therapeutic approach.

Overall, autophagy plays a major role in acquiring different properties of cancer cells which enable tumour growth and progression. Thus, autophagy is a good candidate for therapeutic targeting.

3. Autophagy in oral cancer

The role of autophagic pathway had been studied in many type of cancer *e.g.,* breast, pancreatic, prostate and ovarian cancer [95]. Recently, there has been emerging evidence of the critical role played by autophagy in progression of oral cancer. This might open up

new avenues for the treatment which could potentially culminate into better outcomes for oral cancer patients.

3.1 Oral Squamous Cell Carcinoma (OSCC)

Oral cancer is considered to be the sixth most prevalent malignancies worldwide [151] with about 377,713 new cases diagnosed and 177,757 deaths annually [152]. It has been prevalent in South Asia with one third of oral cancer burden in India and Sri Lanka [152]. In Australia, cancer of oral cavity represents the ninth most common cancer among men with incidence rate of 8.8 [153]. It constitutes about 2.9% of total cancer burden and 1.6% of all cancer related deaths [154]. At least 3 cases of oral cancer are diagnosed daily in Australia that represents about 3% of total cancer cases detected [155].

Oral squamous cell carcinoma (OSCC) represents about 90% of all oral cancer cases [156]. Tongue is the most common site for OSCC followed by the lips [157]. Major risk factors for OSCC are tobacco and alcohol consumption [158]. Products arising from smoked/smokless tobacco are carcinogenic and able to interact with DNA [159]. Also, risk of OSCC seems to be linked to overall alcohol use [160]. Viral infection with human papilloma virus (HPV) has been associated with increased risk of OSCC [161]. Also, ultraviolet (UV) radiation has been identified as additional risk factor especially for lip cancer [158]. Australia is known to have high levels of UV due to its geographical position close to the equator [162]. Patients with oral cancer suffer from high morbidity and mortality rates and poor 5 year survival rates even after surgical excision. This is due to late detection, early local lymph node metastasis at time of diagnosis and local recurrence [163]. The 5-year survival rate for OSCC pateints without lymphnode metastasis at time of diagnosis is 80%, which drop to less than 40% with lymphnode metastasis [164].

Surgical excision with safety margins is the most prevalent method for treatment of OSCC, but it can be combined with radiotherapy (RT) or chemotherapy (CT) before or after the surgery as in case of operable tumours, while treatment involves RT or CT alone when the tumour is inoperable [165]. Cisplatin is the gold standard chemotherapeutic agent used for treatment of OSCC [166]. It exerts its cytotoxic effect by forming adducts with DNA, resulting in DNA damage, cell cycle arrest and eventually cell death [167]. Administration of chemotherapeutic agents, *e.g.,* Cisplatin, results in shrinkage of tumour size that facilitate RT feasibility and decrease the disfigurement associated with surgery [168]. However, these conventional therapeutic strategies have not increased the overall survival (OS) in the past two decades [169]. This is usually due to development of chemo-resistance that reduces the efficacy of CT toward cancer cells [170]. Initial response towards the platinum based chemotherapies is satisfactory in OSCC patients, but 70% of the patients show cancer relapse due to drug resistance [171]. Thus, OSCC still have a poor prognosis due to abrupt deterioration of oral health from surgery or RT and development of drug resistance with the anti-cancer agents [172]. Hence a better understanding of OSCC biology is required so that effective therapeutic targeting can be achieved to improve the survival rates and quality of life for patients.

3.2 Stressful OSCC microenvironment

Previous research in OSCC had majorly focused on the cancer cells itself, their genetic alteration and how this affects its behavior and patient's prognosis. However, there are increasing evidence about the inter-relation between cancer cells and surrounding tumour microenvironment (TME) components. TME contains different type of cells (*e.g.,* cancer associated fibroblasts (CAFs), immune cells and endothelial cells) and extracellular matrix (ECM) that consists of collagen fibers, growth factors, cytokines and chemokines [173].

Thus, TME is considered as a part of the cancerous tissue, which contributes to the behavior and prognosis of tumours [174].

(i) Cancer associated fibroblast (CAFs): CAFs are non-immune, infiltrative cells that harbor in tumour microenvironment [175]. The exact origin of CAFs is still debated. It is thought that they arise from normal resident fibroblast, cancer cells itself or bone marrow derived mesenchymal stem cells [176]. The trans-differentiation of normal fibroblast into CAFs seems to be regulated by molecules released from OSCC cells. An *in vitro* study revealed that OSCC cells produce tumour growth factor-β (TGF-β) that induce trans-differentiation of normal fibroblast into CAFs, which in turn secret growth factors that result in OSCC proliferation and invasion [177]. Further, it was demonstrated that increased expression of IL-1β in OSCC results in activation of nuclear factor κB (NFκB) in normal fibroblast that subsequently release CXCL1 from fibroblast [178]. CXCL1 creates an autocrine mechanism that causes transformation of normal fibroblast into CAFs [179]. CAFs are characterised by expression of α-smooth muscle actin (α-SMA) which not found in normal fibroblast [180].

Clinico-pathological studies showed that high stromal CAFs existence is associated with poor prognosis in oral cancer [180, 181]. CAFs are involved in multiple tumour activities such as sustained proliferation of tumour cells, angiogenesis, invasion and metastasis and actin cytoskeleton remodeling, which favors migratory properties through reciprocal crosstalk between cancer cells and CAFs [176]. *Wong et al*. [182] reported that increased expression of platelet derived growth factor receptor β (PDGFRβ) in CAFs led to activation of JAK2/STAT3 pathway and release of epidermal growth factor (EGF) from CAFs to promote EMT. In the same context, it was demonstrated that OSCC cells release IL-1β, which stimulate the release of CCL7 from CAFs. The latter binds to CCR1-3, on the

surface of OSCC, increasing cell migration *in vitro* [183]. These data indicate the role played by CAFs in acquisition of migratory properties of OSCC cells.

Beside CAFs' role in metastasis, they also exert an immunosuppressive role. It was shown that CAFs liberate anti-inflammatory mediators such as TGFβ and IL-10 that hinder T cell proliferation and increase infiltration of CD163 tumour associated macrophages (TAMs) [184]. CD163 M2 macrophages are usually expressed in the resolution stage of inflammation, indicating that their infiltration in TME activate an immunosuppressive environment [185].

Autophagy is known to play an important role in the mechanisms via which CAFs are known to promote tumour progression in a variety of cancers, such as pancreatic cancer [186, 187]. Notably, *Tan ML et al.* [188] showed that autophagy induction via TGF-β1 in normal oral fibroblast results in fibroblast activation and senescence, which are known to be associated with more aggressive tumours [189] and enhanced OSCC migration [188]. However, the exact role of autophagy in CAFs mediated OSCC progression is currently elusive and is an important area for future research.

(ii) Tumour associated macrophages (TAMs): The main role of immune cells in TME is to help cancer cells evade immune destruction by secreting cytokines that blocks cytotoxic T-lymphocytes (CTLs), which result in immune tolerance [190]. TAMs are one of the main immune cells in TME. CD163 M2 phenotype is the predominant type of TAMs within TME [191]. TAMs are involved in many aspects of OSCC behavior. They can promote angiogenesis via secretion of angiogenic factors such as VEGF [192]. They also induce proliferation of OSCC cells through EGF secretion [193]. Moreover, TAMs are involved in invasion and metastasis process as NF-κB expressed by TAMs leads to

upregulation of matrix metalloproteinases (MMPs), which remodel ECM in a way that permit an invasive and metastatic behavior [190]. It has been demonstrated that expression of CD163 TAMs is associated with poor prognosis and lymph node metastasis [194].

Interestingly, autophagy has been shown to play an important role in polarisation of macrophages to M2 phenotype in colon and liver cancer cells [195-197]. This polarisation provides TME conditions conducive to tumour growth and progression, highlighting an essential role played by autophagy in TME.

(iii) Hypoxia and angiogenesis: As OSCC grows and reaches size of few millimeters, some tumour cells are not directly exposed to blood vessels to obtain nutrition, resulting in hypoxic microenvironment [198]. Hypoxia is the main triggering event that stimulates angiogenesis through upregulation of HIF-1α, which in turn induce expression of angiogenic factors such as VEGF [199]. It was found that HIF-1α is responsible for expression of multiple downstream targets that regulate different OSCC activities. Beside its role in angiogenesis, HIF-1α is also involved in proteolytic modification of ECM via stimulating the expression of proteolytic enzymes such as MMP-2 and cathepsin D, which are crucial for invasion and metastasis [200, 201]. Moreover, HIF-1α facilitates EMT by inducing SNAIL and TWIST pathways that repress E-cadherin, which result in tumour metastasis [201, 202].

It is well known that hypoxia is one of the conditions that trigger autophagy [53]. Under hypoxic conditions, activation of HIF-1α led to activation of BNIP3 that binds to Bcl2 and allow its release from Bcl2-Beclin1 complex resulting in liberation of Beclin-1 and autophagy induction [203]**.** *HIF-1α* knockout have been shown to result in decreased

levels of autophagic marker such as LC3 and Beclin-1 [204]. Also, another study revealed via gene expression data that hypoxia induced autophagy in tumour initiating cells (TICs) of patient derived colorectal cancer culture [205]. In the same context, *Yang et al.* [206] demonstrated that activated autophagy in bladder cancer cells under hypoxic conditions significantly increase gemcitabine cytotoxicity when combined with autophagy inhibitor (3-methyladenine). These data indicate that autophagy can be utilised by tumour cells in order to cope with a hypoxic TME.

(iv) ECM: Collagen fibers are the main component of the ECM part of TME [207]. Modification of ECM occurs during different stages of the tumour. It was found that ECM of OSCC is characterised by increased stiffness due to collagen deposition by either cancer cells or stromal cells [208]. Increased ECM deposition was associated with poor prognosis and metastasis [209]. At the invasive front of OSCC, increased turnover of ECM was prominent, indicating increased EMT and high levels of crosstalk between cancer cells and stromal cells [210]. Also, increased expression of tenascin-1 and type I collagen were observed in OSCC specimens with lymph node metastasis [211]. Importantly, recent studies have shown that autophagy is regulated by stiff microenvironmental conditions in breast cancer cells [212]. The effect of stiff OSCC microenvironment on autophagy is still elusive and requires further investigations.

In summary, OSCC cells are subjected to different types of microenvironmental stressors which affect OSCC behavior. As autophagy is a stress response pathway, it appears to play a crucial role in the crosstalk between tumour and different TME components in OSCC.

3.3 Role of autophagy in OSCC progression

OSCC, like any other type of cancers, develops in a multistep process that results from interaction between genetic and environmental factors, which eventually lead to oncogenesis and cancer progression [213]. Autophagy is one of the mechanisms that may contribute towards initiation and growth of the cancer cells, as seen in other types of cancers. Hence, autophagy could be an attractive target for the development of effective therapeutic strategy against OSCC [67].

Several studies had shed light on the possible role of autophagy in OSCC, which may contribute to tumour progression and prognosis. *De et al.* [214] reported a significant increase in levels of autophagy in OSCC specimens, through quantification of LC3 immuno-positive cells by immunohistochemistry (IHC), in comparison to normal mucosa and premalignant lesions *e.g.,* leukoplakia. Similarly, LC3 expression by IHC was correlated with unfavorable prognosis in OSCC specimens [215]. The same group demonstrated that ATG9A overexpression was associated with poor overall survival and earlier relapse [215]. Another study showed that ATG16L1 upregulation is related to shorter overall survival and a more aggressive phenotype [216]. In the same manner, *Liu et al.* [217] observed increased LC3 expression is linked to aggressive clinicopathological features. However, it should be noted that LC3-II, not LC3, is a marker for autophagosome. Furthermore, the levels of autophagosomes in the cells are balance between autophagic initiation and lysosome mediated degradation. Hence, future studies examining simultaneous expression of multiple molecules in autophagic machinery are necessary to further delineate the role of autophagy in OSCC progression.

Interestingly, overall survival rate of OSCC patients with high p62 expression post chemotherapy was lower than those with low p62 expression [218]. Although p62 is

involved in shuttling cargo, it degrades with the cargo when autophagosomes fuses with lysosomes. Therefore, evaluation of p62 levels needs to be assessed at both mRNA and protein levels. *Liu et al.* [217] demonstrated that high *SQSTM1* (*i.e.,* gene encoding p62) mRNA expression correlated with high p62 protein expression in the cytoplasm, which was associated with aggressive clinicopathologic features and unfavorable prognosis.

Additionally, autophagy is suggested to be involved in protection of OSCC cells from apoptosis and allow their survival under different microenvironmental stresses. *Park et al.* [219] showed that fisetin, a natural flavonoid that has anti-oxidant activity, induced apoptosis of OSCC cells through inhibition of autophagy. Furthermore, *Lin et al.* [220] showed that ursolic acid induced autophagy in OSCC cell line (Ca922) and autophagy inhibition by chloroquine increased ursolic acid induced apoptosis. This latter study provides further evidence of the protective role played by autophagy in OSCC.

It was observed that circCDR1 enhanced the viability of OSCC cells under hypoxic conditions through autophagy induction [221]. Likewise, clusterin induced autophagy in oral cancer cell lines that resulted in cell survival and protection from serum starvation induced apoptosis [222].

Autophagy also seems to play a role in chemotherapy resistance and cancer stemness. *Naik et al.* [223] showed that cisplatin resistant cell lines had higher levels of stemness markers and more autophagic flux than parental OSCC cells. When autophagy is inhibited, reduction in stemness was observed [223]. Likewise, high levels of autophagic flux had been observed in cisplatin- resistant OSCC which was manifested by increasing the autophagosomes' number by electron microscopy, increase conversion of LC3 I into LC3 II and decrease P62 expression [224]. Furthermore, cisplatin sensitivity in OSCC was

found to be reduced by induction of autophagy [225]. In the same context, autophagy inhibition decreased resistance in tongue squamous cell carcinoma [226].

On the other hand, low expression of *BECN1* in OSCC specimens has been reported by multiple studies [227-229] and is associated with poor prognosis [227] and enhanced proliferation, invasion and metastasis [229]. Moreover, *BECN1* silencing was found to induce proliferation, migration and invasion of OSCC, while repressing apoptosis and restoring chemo-sensitivity to cisplatin [230]. These latter findings are in direct alignment with tumour suppressor role of *BECN1* [231]. Importantly, *Kong et al.* [232] demonstrated that autophagy inhibited the invasive potential of OSCC via regulation of the NF-κB pathway. Furthermore, a study unveiled that curcumin induce apoptosis in OSCC cells via induction of autophagy, indicating that autophagy act as pro-death signal [233]. Another study also exhibited that tanshinon IIA induced autophagic cell death in OSCC cell line (SCC9) via induction of Beclin1/ Atg7/ Atg12-Atg5 pathway [234]. Similarly, curcuminoids decreased cell viability in oral cancer cells by induction of autophagic cell death [235].

Taken together, there is increasing evidence about the crucial role of autophagy in OSCC progression, suggesting that autophagy has great potential as a future therapeutic target.

4. Autophagy in Triple negative breast cancer

4.1 Triple Negative Breast Cancers

Breast cancer is the most commonly diagnosed cancer worldwide which represents 11.7% of total cases with 2,261,419 new cases diagnosed annually [152]. It is also considered to be the major cause of cancer related death in women with 684,996 deaths per annum

[152]. In Australia, breast cancer is identified as the most common cancer in women with one in eight women is affected by the disease [236]. Further, it is the second most common cause of cancer related death between women in Australia [236]. Due to early detection and advances in treatment modalities, the 5-year survival rate has improved from 72% in 1980s to 90% over the recent years [236]. However, a progressive increase in the number of new cases over the same time has been observed [236] and mortality rates still remains high [237].

Breast cancer is a heterogeneous disease which is categorsed into 4 main types according to expression of four main proteins, *i.e.,* estrogen receptor (ER), progesterone receptor (PR), human epidermal growth factor receptor 2 (HER2) and Ki67 which is a proliferation marker [237]. The four types of breast cancers based on the expression of these proteins are: 1) Luminal A which are positive for ER and PR and negative for Ki67 and HER2 (ER^+ or PR^+, $Ki67^-$, $HER2^-$); 2) Luminal B which are positive for ER, PR, Ki67 and HER2 (ER^+,PR^+, $Ki67^+$ and $HER2^+$); 3) HER2 which are positive for HER2 and ER negative (ER^-, $HER2^+$); and 4) Triple negative breast cancers (TNBCs) which are negative for ER, PR and HER2 (ER^-, PR^- and $HER2^-$) [237]. TNBCs are further divided into 6 subtypes: 1) basal like immune activated (BLIA); 2) basal like immune suppressed (BLIS); 3) luminal androgen receptor (LAR); 4) mesenchymal stem cell (MES); 5) immunomodulatory (IM); and 6) mesenchymal (M) [238, 239].

TNBCs account for 15% of all types of breast cancers [240] and has the lowest survival rate of all breast cancer types [241]. Due to its specific molecular pattern, endocrine or HER-2 targeted therapies are ineffective toward TNBCs [240]. The commonly used strategy of curative-intent treatment of TNBCs is combination of surgery and chemotherapy [242]. The most commonly used chemotherapeutic agents are

anthracyclines such as taxanes and doxorubicin and they are used as neo-adjuvant chemotherapy to reduce the size of the tumour before surgery or as adjuvant chemotherapy [243]. A study showed that addition of capecitabine in combination with standard anthracycline regime is associated with better disease fre survival (DFS) [244] . Likewise, another study revealed that addition of platinum based agents to anthracyclin regime is associated with higher 5 years DFS relative to standard regime only, but it did not address the role of platinum agents addition to the regime [245]. Another meta-analysis study for nine randomised clinical trial exhibited that there was 10-15% increase in pathological complete response (PCR) when platinum based agents were addded, but there was no link between increase PCR and prolongation of event free survival [246]. However, 30-40% of TNBC patients experience metastatic relapse, which is often resistant to chemotherapy, leading to poor patient prognosis [247].Recently, immunotherapy had been used as neoadjuvant therapy in TNBC. Prembolizumab exhibited a higher PCR when combined with standard chemotherapy in comparison to satndrd chemotherapy alone in phase III clinical trial of TNBC [248]. Thus, understanding the molecular profile of TNBC is imperative to identify the critical pathways, so that they can be targeted for the development of an effective therapeutic approach.

4.2 Stressful Tumour Microenvironment in TNBCs

Over the last decade, there is increasing evidence about the role of tumour microenvironment (TME) in tumour progression. TME consists of different types of cells (immune cells, cancer associated fibroblast CAFs), extracellular matrix and cytokines [249]. It was demonstrated that reciprocal crosstalk occurs between cancer cells and TME in a way that contribute to tumour progression [250]. A growing number of studies have focused on exploring TME to identify new biomarkers and therapeutic targets in an attempt to guide cancer therapy and develop novel therapies, respectively [251, 252]. As TNBCs

are an aggressive type of breast cancers, TME is believed to play a critical role in TNBC progression.

(i) Tumour infiltrating lymphocytes (TILs): TILs are one of the cellular components of TME. It consists mainly of T lymphocytes, with CD8 cytotoxic T cells and CD4 helper T cells being the main subtypes that harbor TME [253]. Due to TNBC aggressive behavior, it is highly infiltrated by TILs [254] because of emergence of new antigens as a result of continuous mutations that attract immune cells [255] It was demonstrated that increased TILs infiltration was associated with reduced recurrence free survival and overall survival in case of neoadjuvant chemotherapy of TNBC [256].

Li et al.[257] observed that tenascin C, which is highly expressed in malignant tumours and involved in modulation of cell migration, is inversely correlated with CD8 T lymphocytes in TNBC tissue samples. This study further demonstrated that tenascin C inhibition in autophagy impaired TNBC cells restored T-cell mediated tumour killing. In the same context, autophagy inhibition via *BECN1* silencing in breast carcinoma restored cytotoxic T lymphocytes mediated lysis [143].

(ii) Tumour associated macrophages (TAMs): TAMs originate from blood monocytes and they are recruited to tumour by the effect of chemokines such as CCL2 secreted by the tumour cells themselves or the stroma [258]. There are two distinct phenotypes of TAMs; M1 and M2 [259]. M2 is the most predominant type in TME [259] and M2 differentiation is associated with immunosuppression, enhanced tumour cell invasion, metastasis, angiogenesis and matrix remodeling [260]. Also, it was found that breast cancer cells secret cytokines such as IL4 and TGF- β which drives M2 differentiation of TAMs [261]. This effect was more pronounced in TNBC cell line (MDA-M231) [262].

Moreover, more aggressive behavior of TAMs was noticed upon co-culture of macrophages with TNBC with elevated levels of cytokines such as CCL2 and changes in their morphology in comparison to HR^+ breast cancer cell line (T27D) [263]. Further studies are needed to correlate TAMs presence and their location within TNBC with the clinical prognosis.

(iii) Cancer associated fibroblasts(CAFs): CAFs are one of the most critical component of TME [264]. The origin of CAFs is not clear. It may arise from mesenchymal stem cells, haemopoietic stem cell, resident fibroblast and epithelial cells via EMT [265]. CAFs are characterised by expression of α-smooth muscle actin (α-SMA) which is not found in normal fibroblast [265]. They are involved in series of pro-tumourigenic events such as invasion and metastasis, ECM remodeling and angiogenesis [266]. It was proposed that CAFs are involved in crosstalk with cancer cells that stimulated the secretion of interleukins and chemokines such IL-6 and CXCL3 [267]. CAFs allowed TNBC progression via tumour growth factor-β (TGF-β) activation [268]. They are known to promote TNBC metastasis through upregulation of matrix metalloproteinase 9 (MMP9), that result in ECM degradation, promoting cancer cell migration [269]. Moreover, co-culture of TNBC cell line (MDA-MB231) with fibroblast revealed a sharp increase in α-SMA expression, in comparison to MCF-7 cell line, which indicates acquisition of myofibroblast phenotype [270]. In the same context, TNBC cell line showed increased migration when co-cultured with fibroblast via upregulation of EMT pathways [267]. This interaction may be characteristic for TME of TNBC and affects the prognosis of TNBC patients [267]. Notably, TNBC cells proliferation, migration and invasion were significantly enhanced when co-cultured with CAFs-conditioned media in comparison to the control group [271]. Thus, CAFs may aid in clinical prognosis of TNBC patient, therefore, further research is

warranted to detect CAFs unique markers that might provide better insights about TNBC prognosis.

(iv) Hypoxia*:* As TNBCs are rapidly proliferating tumours, hypoxia develops as oxygen and nutrients that cannot be provided with the existing vasculature [272]. Hypoxia stabilises HIF-1α which is a critical transcription factor. HIF-1α in turn activates genes responsible for angiogenesis, tumour growth, invasion and metastasis [273]. VEGF is one of the crucial pro-angiogenic factors that has been dysregulated in TNBC [274]. VEGF stimulates neovascularisation within TME [274]. Also, it has been shown both *in vivo and in vitro* that TNBC cells could transdifferentiate into endothelial cells via acquiring endothelial phenotype that form blood lacunae surrounded by tumour cells [275].

Hypoxia is also one of the stressors that stimulate autophagy within cancer cells which allows survival under stressful microenvironmental condition [276]. HIF-1α activation not only induces the transcription of genes responsible of autophagy,[277] but also, promotes BNIP3 activation which compete with Beclin-1 to bind to Bcl2 [53]. Thereby, Beclin-1 is liberated from Beclin-1-Bcl2 complex and induction of autophagy occurs [53]. It was shown that hypoxia induce autophagy and drug resistance in TNBC in a xenograft model [278]. Also, *He et al.*[279] demonstrated activation of autophagy in breast cancer cells under hypoxic conditions and autophagy activation was also associated with increased radio-resistance of tumour cells. Indeed, autophagy inhibition resulted in enhanced radiosensitivity [279]. This designates that autophagy is a mechanism applied by cancer cells to deal with different TME stressors.

(v) Extracellular matrix (ECM): ECM consists of structural proteins (*e.g.,* collagen), glycoproteins (*e.g.,* fibronectin) and proteoglycans [280]. Collagen is the main component

of ECM and is responsible for cancer cell strength and resilience [281]. Glycoproteins are important for cell to ECM adhesion, whereas, proteoglycans control passage of growth factors and cytokines between the cells [282]. Collagen accumulation is observed in TNBC within ECM which results in stiffness [268]. Importantly, collagen and stiffness are associated with increased aggressiveness of TNBC and TAMs infiltration [283-285].

Taken together, TNBC cells are exposed to a complex and stressful TME, which is intricately involved in tumour progression. As autophagy is a stress response pathway, there is an emerging evidence of the induction of autophagy in tumour cells as well as associated microenvironment that could facilitate tumour progression, which is discussed in next section.

4.3 Role of Autophagy in TNBC

Many recent studies have linked the autophagic pathway to TNBC progression. *Abdelbary et al.*[286] showed that high LC3 and cytoplasmic p62 expression were significantly correlated with lymph node metastasis in TNBC tumour specimens. Similarly, *Bornik et al*.[287] demonstrated that increased LC3 and GABARAP expression are correlated with poor prognosis and a more aggressive phenotype of breast cancer including TNBC. Notably, it was observed that LC3 expression levels were independent prognostic factor in residual tumour for TNBC patients who received neoadjuvant chemotherapy [288]. Hence, this indicates that autophagy is a good candidate for cancer therapy against cancer progression and metastasis.

In the same context, *Hamurcu et al*.[289] demonstrated that inhibition of autophagy, via *MAP1LC3* and *BECN1* knockdown, in TNBC cell line (MDA-MB231) resulted in suppression of cell proliferation, colony formation, invasion and migration with induction of apoptosis and inhibition of proto-oncogenic pathways such as cyclinD1. Further, autophagy was found to promote TNBC metastasis *in vitro* through stimulation of yes-associated protein (YAP) nuclear translocation [290]. In addition, *Li et al.*[291] reported that autophagy inhibition, via cantharidin, inhibited TNBC cell proliferation and induced tumour cells apoptosis both *in vivo* (in nude mice) and *in vitro* (MDA-MB231 cell line). Similar results were observed by *Wang et al*.[292] who demonstrated that combination of autophagy inhibition, via chloroquine (CQ) with Wnt signaling inhibitors, *in vitro*, resulted in reduction of stemness genes expression which in turn led to inhibition of TNBC cell migration and self-renewal ability. The role of autophagy in TNBC progression has not been only limited to tumour cells, but has been extended to include cells in the tumour microenvironment such as cancer associated fibroblast (CAFs). Indeed, increased autophagy in CAFs can enhance TNBC cell proliferation, invasion, metastasis and EMT [271].

Autophagy has also been shown to play an essential role in promoting drug resistance. Indeed, paclitaxel resistant TNBC cell lines had higher levels of autophagy than the parental cell lines when exposed to starvation [288]. Also, there was a significant reduction in cell viability, growth and invasion in drug-resistant cells compared to the parental cell line when treated with autophagy inhibitor (chloroquine) [288]. Moreover, autophagy inhibition via 3-methyladenine (3-MA) sensitised TNBC to gefitinib (epidermal growth factor receptor (EGFR) inhibitor) both *in vivo* and *in vitro* through activation of mitochondrial dependent apoptosis [293]. Similar results were also observed in other studies where autophagy inhibition restored sensitivity to chemotherapeutic agents in

TNBC cells [294-296]. Furthermore, autophagy could also play a critical role in maintaining an immunosuppressive TME in TNBCs. Of interest, a recent study by *Li etal.*[297] demonstrated that aerobic glycolysis in TNBCs controlled AMPK-induced autophagy, leading to maintenance of the immunosuppressive phenotype of the TME.

Studies have also observed an inhibitory effect of autophagy on TNBC tumour progression. Higher ATG7 expression levels were found to inhibit cell proliferation, migration and invasion, while inducing apoptosis in TNBC that is significantly associated with better prognosis and favorable clinicopathological outcomes in TNBC patients [298]. Moreover, *Li et al.*[299] indicated that autophagy deficiency in TNBC suppress T-cell mediated cytotoxicity in *vivo* and in *vitro* via blockade of Tenascin C degradation. Notably, autophagy was found to be induced through anti-CD73 monoclonal antibody which resulted in inhibition of TNBC cell migration and invasion in vitro [300].
Hence, autophagy seems to be a promising target for TNBC but more studies are still required to facilitate this therapeutic approach in TNBC patients.

5. Targeting autophagy as a therapeutic approach

Autophagy seems to play a pivotal role affecting all major hallmarks of cancer progression. Therefore, autophagic machinery can be targeted using different compounds that can inhibit the autophagic process at different stages of this complex pathway (**Figure 1.6**).

5.1. Chloroquine and its derivatives

Lysosomes are essential organelles in the autophagic pathway. Lysosomes fuses with the autophagosome leading to degradation of autophagosome content via their hydrolytic

enzymes [29]. The function of lysosomal hydrolytic enzymes is dependent on the acidic environment within lysosomes (pH range 4.5 to 5) [301]. Over the last decades, many compounds have been developed to target the lysosome, which consequently also targets autophagy. Chloroquine (CQ) has been found to inhibit autophagy [302]. It is an antimalarial drug [303], which is also used in some autoimmune diseases such as rheumatoid arthritis [304] and lupus erythrematosus [305]. CQ becomes entrapped and protonated within the lysosome, which result in increased lysosomal pH that consequently renders lysosomal hydrolytic enzymes inactive [303]. Hence, it blocks autophagy at its late stage [85]. Although, CQ is being well tolerated in humans, it causes retinal toxicity [306]. A CQ analogue, Hydroxychloroquine (HCQ), has been developed by adding a hydroxyl group to CQ. This addition of hydroxyl group limits CQs capability to cross the blood-retinal barrier, thereby decreasing the retinal toxicity associated with CQ [307].

Over the last few years, CQ and HCQ have been used in preclinical studies as a combination therapy together with the conventional therapies. CQ/HCQ increase sensitivity of glioma cancer cells to radiation therapy and temozolomide treatment [308-310]. Likewise, the efficacy of mTOR inhibitor (*e.g.*. everolimus), tyrosine kinase inhibitor (*e.g.,* MK2206) and gefitinib is enhanced when co-administered with CQ/HCQ [311-313]. CQ is also shown to resensitise endometrial cancer cells to cisplatin [314] and overcame resistance to different chemotherapeutic agent such as cyclophosphamide [315], vorinostat [316], and saracatinib [315]. Further, HCQ enhances T cells/NK cells cytotoxicity in murine model [317].

However, it had been found that CQ/HCQ may cause kidney impairment, neurodegenerative and cardiovascular disease when administrated in high doses [318, 319]. Despite this, several clinical trials have been performed to determine the efficacy of

CQ/HCQ in combination with various standard chemotherapeutic agents against different types of cancer [320-326]. However, none of these trials have reached phase III, suggesting the necessity for development of more selective compounds to inhibit autophagy.

As CQ/HCQ may not be able to potently inhibit autophagy at a tolerable clinical dose, new derivatives have been developed [327]. Lys05 is a new derivative of CQ/HCQ that accumulates more readily in the lysosome, and has been demonstrated to increase the lysosomal pH and blocks autophagy at late stage [328]. Lys05 exhibited 10 folds potency to block autophagy compared to HCQ [328]. Also, Lys05 displayed anti-tumour activity in mice without causing any non-specific toxic side effects [327]. Since, Lys05 has shown promising results in the preclinical studies, clinical trial of this agent would be of a great interest.

5.2. Specific autophagy inhibitors directed toward major molecules in autophagic machinery

Recently, many autophagic inhibitors have been developed against major molecules or pathways involved in the early stage of autophagy. Most of these compounds are still at the preclinical stage and need further investigations to validate their potential under clinical settings [329].

(i) PI3K inhibitors: Due to its pivotal implication in autophagy, PI3K has become an interesting target for autophagy inhibition. PI3K are divided into three groups Class I, Class II, and Class III. Class III PI3K corresponds to Vps34 and is responsible for autophagy induction, whilst, Class I PI3K triggers mTOR, which in turn inhibits autophagy [330].

Agents that have been developed to inhibit PI3K include, 3-MA, Wortmannin and LY294002 [327]. 3-MA was first discovered from isolated hepatocytes of starved rats [331]. It is directed toward Vps34 of Class III PI3K, which results in autophagy inhibition [332]. However, prolonged administration of 3-MA can also inhibit Class I PI3K even in nutrient rich conditions. Hence, 3-MA appears to have a dual role on autophagy [333]. Despite this, high concentration of 3-MA is needed to inhibit autophagy *in vitro,* which results in inhibition of other kinases such as MAPK, mTOR and DNA-defendant protein kinase (DNA-PK) [334]. Moreover, beside lack of specificity and off-target activities, 3-MA also has poor solubility [327]. As a result, the clinical application of 3-MA is limited.

Wortmannin, derived from fungal metabolites [335], is another PI3K inhibitor that has anti-inflammatory activity [336]. Wortmannin is a highly potent inhibitor that inhibits Class III PI3K permanently, with transient inhibition of Class I PI3K and has an inhibitory effect on other kinases [333]. Similarly, the PI3K inhibitor, LY294002 has a low potency against Class I and III PI3K, but affects more mTOR and DNA-PK pathways [337]. Hence, these three inhibitors have a lot of limitations, including off-target activities, limited potency, and solubility, which contribute to their limited clinical application.

Thus, various inhibitors have been designed to actively target Vps34 either directly (*e.g.,* SAR405) or indirectly (*e.g.,* Spautin-1). Vps34 is a member of phosphoinositide 3 kinase (PI3K) protein family and a major molecule in autophagy induction. Vps34 converts phosphatidylinositol into PI3P, via its lipid kinase activity, which is essential for autophagosome biogenesis [330].

Spautin-1 is quinazolin derivative of 4-[[3,4-(methylenedioxy)benzyl]amino]-6-chloroquinazoline (MBCQ) [338], which inhibit two ubiquitin specific peptidases USP10 and USP13[339]. These enzymes deubiquitinate Beclin-1 [339]. Under nutrient deficient

conditions, treatment with Spautin-1 led to Beclin-1 ubiquitination and its proteasomal degradation, which in turn resulted in destabilisation and degradation of Vps34 and that consequently resulted in autophagy inhibition [339]. Thus, Spautin-1 indirectly inhibits Vps34 activity through Beclin-1 degradation. In preclinical studies, Spautin-1 shows synergism with Imatinib in chronic myeloid leukemia. Furthermore, Spautin-1 promotes cancer cell death under nutrient deficient conditions [340].

SAR405, is a potent and highly selective Vps34 inhibitor that directly affect the catalytic activity of Vps34 [341]. SAR405 suppressed autophagy under nutrient starvation[341] when combined with the mTOR inhibitor (*e.g.,* AZD8055) [342]. Interestingly, synergism is also observed between SAR405 and other chemotherapeutic agents in different cancer models [343-345].

PIK-III is a bisaminopyrimidine that is designed to selectively inhibit Vps34 by direct binding to the hydrophobic pocket at the ATP binding site of Vps34 [346]. PIK-III showed 100 fold better potency in Vps34 inhibition than Class I PI3K [346]. Despite the emergence of these Vps34 inhibitors, more preclinical studies are required to evaluate the potential of these inhibitors as clinical useful drugs.

(ii) ULK-1/2 inhibitors: ULK-1 is a key autophagy regulator, that upon phosphorylation results in activation of multiple autophagy initiating proteins including Beclin-1 [347]. ULK-1 is subjected to negative and positive phosphorylation by mTOR and AMPK respectively [348]. Various inhibitors, such as MRT68921 and SBI0206965, have been designed to target ULK-1 and lead to suppression of autophagy. MRT68921 is a potent highly specific ULK-1/2 inhibitor that acts via competitive ATP binding [349]. It exhibited some off-target

effect on kinases such as AMPK, but studies had demonstrated that MRT68921 reduced the autophagic flux via inhibition of ULK-1 specifically [349].

SBI-0206965 is a small molecule inhibitor of ULK-1/2 that acts through blocking the Vps34 phosphorylation by ULK-1 [350]. This agent suppressed autophagy induced by mTOR inhibitor AZD8055, resulting in apoptotic cell death [350]. Also, SBI-0206965 activates apoptotic pathway through destabilisation of pro-survival proteins Bcl2 and BCLXL [351]. Recently, SBI-0206965 has also been identified as AMPK inhibitor [352, 353]. These findings indicate that ULK-1 is a promising therapeutic target to inhibit autophagy.

Collectively, the new era in autophagy modulation, by using specific inhibitors directed toward major molecules of autophagic machinery, needs more preclinical investigations to validate these inhibitors as clinical useful agents.

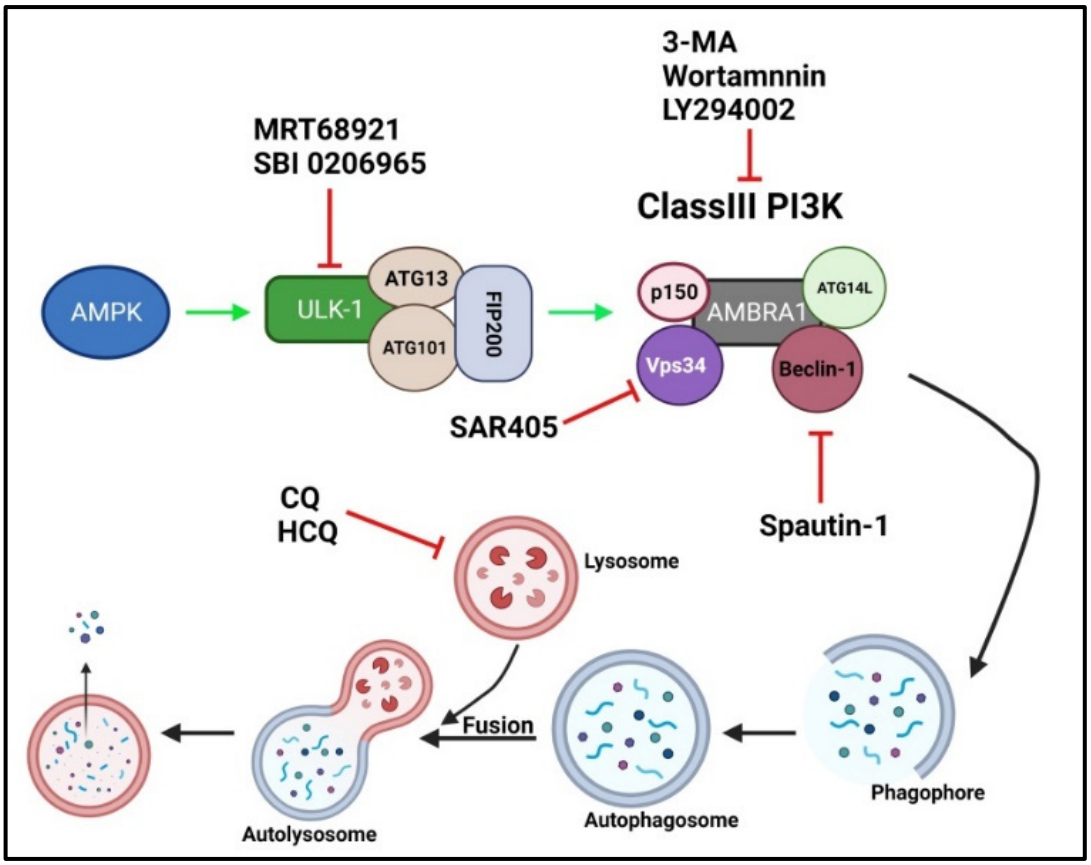

Figure 1.6. Autophagy Inhibitors and their site of action in autophagic machinery. MRT68921 and SBI-0206965 are ULK-1 inhibitors. 3-MA, Wortmannin and LY294002 are Class III PI3K inhibitors. Spautin-1 is Beclin-1 inhibitor and SAR405 is Vps34 inhibitor. Chloroquine (CQ) and hydroxyl chloroquine (HCQ) are late autophagy inhibitors which target lysosomal pH rendering the fusion between autophagosome and lysosome. Green arrow indicates activation and red arrow indicates inhibition. Created with BioRender.com

6. Autophagy inhibitors in OSCC

Some studies had been performed to evaluate the effect of autophagy inhibition in OSCC progression. These autophagy inhibitors target the major molecules in the autophagic machinery either in the early or late stage of the autophagic process.

In regard to late stage autophagy blockage, autophagy inhibition by chloroquine showed a synergism with interferon- gamma with induction of apoptosis in OSCC cell lines and

xenograft [354]. Also, *Ahn et al.* [355] observed enhanced cytotoxicity of Apicidin, a histone deacytlases inhibitor, in OSCC cells when combined with late stage autophagy inhibitor chloroquine. Similarly, chloroquine suppressed OSCC cells proliferation and colony formation ability, arrested the cell cycle *in vitro* and inhibited tumour growth *in vivo* [356]. In the same context, *Magnano et al.* [357] observed significant increase in the rate of apoptosis upon combination treatment of cisplatin and chloroquine compared to cisplatin alone *in vitro,* indicating that chloroquine facilitates re-sensitisation of OSCC cells to cisplatin induced apoptosis. Additionally, blocking autophagy via bafilomycin-A1 enhanced the effect of baicalein, which is a phytochemical with inhibitory effect on cancer cells, induced apoptosis. This latter study suggests a protective role of autophagy in OSCC [358].

In regards to early stage autophagy inhibitors, 3-MA was found to enhance apoptosis induced by nutrient depletion [359] and IL-24 [360]. Moreover, LY294002 loaded hyperbranched polyacylhydrazone conjugated doxorubicin (LY-HPAH-DOX) micelles potentiated the inhibitory effect on proliferation of OSCC cells compared to HPAH-DOX or DOX alone [361]. Interestingly, co-administration of an early autophagy inhibitor SAR405 with cisplatin resulted in significant lower rates of apoptosis compared to cisplatin alone in OSCC cell lines, whilst, combined treatment of cisplatin with late autophagy inhibitor CQ showed enhanced cisplatin induced cell death. This discrepancy may be due to specificity of each inhibitor and may suggest that targeting autophagy at different stages may result in different cellular response [357]. Notably, autophagy inhibition via SAR405 induced normal oral fibroblast activation into myofibroblast [188].

Altogether, more pre-clinical research is still needed to elucidate if inhibiting autophagy is a viable therapeutic approach for OSCC treatment.

7. Autophagy inhibitors in TNBC

Recently, autophagy inhibition has been the focus of many studies and is suggested to be a new approach in cancer therapeutics. As described previously, autophagy is a multistep process that can be inhibited at different stages. Thus, autophagy inhibitors are divided into early- and late-stage inhibitors.

7.1. Late-stage autophagy inhibitors (Chloroquine and its derivatives): as mentioned before, CQ is originally used as anti-malarial drug[303], but it can also be used to inhibit autophagy (at a late stage). It is the only autophagy inhibitor which is currently used in clinical trials [362]. CQ is shown to reduce TNBC's capability to metastasise both *in vitro* and *in vivo* (xenograft model) [363]. Moreover, co-administration of CQ with carboplatin inhibited autophagy, diminished expression of DNA repair proteins and reduced the tumour growth *in vitro* [364]. *Abdel-Mohsen et al.*[365] demonstrated that CQ co-administration with Doxorubicin (DOX) enhanced the growth inhibitory effect of DOX *in vivo*. Autophagy inhibition by CQ led to suppression of mamosphere formation *in vitro* and increased the survival of xenografted mice [366]. Further, HCQ and CQ resulted in growth reduction of chemo-resistant TNBC cell lines [288, 367]. In the same context, CQ increased the effectiveness of Osimertinib via upregulation of apoptosis related proteins[368] and re-sensitised TNBC to paclitaxel in both preclinical and clinical settings [369].

As CQ and its derivative HCQ have shown promising results in inhibiting autophagy in preclinical studies, they have been used in a number of clinical trials to test their efficacy in combination with standard chemotherapeutic agents as summarised in **Table 1.1**. Despite the clinical trials, the clinical application of CQ as an anti-cancer therapeutic has

been limited due to the high dose requirement to effectively inhibit autophagy [370]. The high dose requirement often result in kidney impairment and cardiovascular diseases [318].

Table 1.1 : Clinical trial that use chloroquine or hydroxychloroquine for the treatment of breast cancers. (Source: clinicaltrial.gov)

Type of Breast Cancer	Study design	Drug and Dose	Status	Serial No.
Invasive breast cancer	Phase 2, Randomised, Double-blind, Placebo controlled	CQ 500mg/day untill the day of surgery	Unknown	NCT02333890
Advanced or metastatic breast cancer	Phase 2, Non-randomised, open label	CQ 250mg/day+taxanes every 3weeks	Completed	NCT01446016
Intraductal carcinoma or Ductal carcinoma in situ	Phase 1, Phase 2 Non-randomised, open label,	CQ 5oomg/day or 250mg/day for 1 month before surgery	Completed	NCT01023477
Metastatic breast cancer	Phase 1, Phase 2, open label	HCQ 200mg/day or 200mg twice a day + Ixabepilone	Terminated (slow accrual)	NCT00765765
Invasive breast cancer	Phase 2 Randomised, open label	HCQ 600mg twice a day+ Abemaciclib	Not yet recruiting	NCT04523857
Breast cancer stageIIB	Phase 2 pilot randomised	HCQ alone or with Everolimus	Recruiting	NCT03032406
Breast cancer	Phase 2 pilot, open label	HCQ 800mg once then 400mg/ day	Unknown	NCT01292408
Recurrent breast cancer	Phase1, Phase2, Randomised	HCQ 600 mg twice a day alone or with Gedatolisib	Withdrawn due to business decision about study drug	NCT03400254
Breast cancer	Phase 2, Randomised, open label	HCQ 600 mg twice a day alone or with Palbociclib	Recruiting	NCT04841148

7.2. Early-stage autophagy inhibitors

One of the essential molecules in the autophagic machinery is Class III PI3K which is important for induction of autophagy [330]. Therefore, different compounds have been developed to target Class III PI3K such as 3-MA, Wortmannin and LY294002. Autophagy inhibition via 3-MA was found to have an anti-proliferative effect in TNBC, indicating the cytoprotective role of autophagy [371]. Also, high concentration of 3-MA was needed to inhibit autophagy in vivo [334]. Due to limited potency and off-target effects, clinical application of 3-MA has been hampered.

Moreover, *Chen et al.*[372] demonstrated that blockage of autophagy with Spautin-1 (Beclin-1 inhibitor) induced cell apoptosis in MDA-MB231 cell lines. Importantly, inhibition of autophagy with Spautin-1 augmented paclitaxel induced cell death in resistant MDA-MB231 [373]. SAR405 (Beclin-1 inhibitor) demonstrated good synergism with different chemotherapeutic agents in various cancer types (*e.g.,* breast and bladder cancer) *in vitro*, however further studies focusing on TNBCs are still required [343, 374, 344]. Moreover, SBI-0206965 was found to effectively suppress AMPK activity [352, 353]. Interestingly, both MRT68921 and SBI-0206965 demonstrates promising results in suppressing tumour proliferation *in vitro* in lung cancer cell lines [350, 351] which indicate their effectiveness in autophagy inhibition and autophagy's impact on cancer progression. Future studies examining these agents in TNBC models are warranted.

These initial preclinical studies demonstrate the potential of these next generation autophagy inhibitors and could perhaps overcome the potential high dose toxicity associated with CQ. Future studies utilizing these next generation early-stage autophagy inhibitors will be vital to establish if autophagy can serve as a novel anti-cancer strategy in the clinic.

Chapter 2

Material and Methods

This chapter provides details of the materials and methods used in the following chapters.

2.1. Materials

List of materials used are mentioned in the following tables: **Table 2.1** enlists the equipment used in this thesis. **Table 2.2** provides details of antibodies and siRNAs used. Details of biological reagents used is provided in **Table 2.3, while** chemicals and drugs used are listed in **Table 2.4**. The list of buffers used in this study are provided in **Table 2.5**.

Table 2.1. List of equipment used in this study.

Equipment	Manufacturer
Type II Biosafety Cabinet (sterile)	Not Applicable
Tissue culture incubator (5% CO_2, 37˚C)	Thermo Fisher Scientific, USA
DMi1 Inverted Microscope	Leica GmbH, Wetzlar, Germany
Guava® Muse® Cell Analyser	Luminex, USA
Bench top, temperature regulated Centrifuge	Eppendorf South Pacific, Australia
ChemiDoc XRS+ Imaging System	Bio-rad, Australia
Mini Trans-Blot® Cell and Criterion™ Blotter	Bio-rad
Cup-horn Sonicator	Sonics and Materials, USA
FLUOstar® Omega Microplate Reader	BMG Labtech, Australia
Incucyte® 96-well Wound Maker Tool	Sartorius AG, Germany
Incucyte® S3 Live Cell Analysis System	Sartorius AG
Q-Exactive HFX mass spectrometer (MS)	Thermo Fisher Scientific
SP5 II Confocal Microscope	Leica GmbH

Table 2.2. List of antibodies and siRNAs used in this study. (WB=western Blot, IF=Immunoflurosence, Immunohistochemistry= IHC)

Primary Antibodies	Supplier	Dilution
LC3 (Rabbit, PM036)	MBL International, Woburn, Massachusetts, USA	WB: 1:1000 IF: 1:200
β-Actin (Mouse, A1978)	Sigma Aldrich, VIC, Australia	WB: 1:5000
LAMP2 (Mouse, ab25631)	Abcam, VIC, Australia	IF: 1:100
LC3B (Mouse, E5Q2K)	Cell Signaling Technology, WA, Australia	IHC: 1:100
P62 (Mouse, 56416)	Abcam	IHC: 1:200
Negative Control Mouse IgG2a	Agilent Technologies, VIC Australia	IHC: (1:200-1:100)
Secondary Antibodies	**Supplier**	**Dilution**
Anti-rabbit IgG antibody (7074S)	Cell Signaling Technology	WB: 1:10000
Anti-Mouse IgG (A4416)	Sigma Aldrich	WB: 1:10000
Anti-rabbit IgG (H+L) Alexa Fluor® 488 (4412S)	Cell Signaling Technology	IF: 1:1000
Anti-mouse IgG (H+L) Alexa Fluor® 594 (8890S)	Cell Signaling Technology	IF: 1:1000
Dako EnVision +System – HRP Labelled Polymer Anti-mouse	Agilent Technologies	IHC: 1:100
Silencers	**Supplier**	**Concentration**
TGM2 siRNA (S14087)	Thermo Fisher Scientific	60 nM for resistant SCC9, resistant HCC1806 and resistant MDA-MB231 80 nM for resistant HN6
Negative Control siRNA	Thermo Fisher Scientific	

Table 2.3. List of biological reagents used in this study.

Reagent	Manufacturer
Dulbecco's Modified Eagle Medium (DMEM)	Thermo Fisher Scientific, Australia
RPMI Medium	Thermo Fisher Scientific
DMEM/F-12, GlutaMAX™ supplement	Thermo Fisher Scientific
Opti-MEM™ Reduced Serum Medium	Thermo Fisher Scientific
DMEM, no glucose	Thermo Fisher Scientific
Trypsin-EDTA (0.5%), 10X no phenol red	Life Technologies, Australia
Foetal Calf Serum	Fisher Biotech, Australia
Insulin	Sigma Aldrich
Penicillin/Streptomycin	Sigma Aldrich
HEPS	Sigma Aldrich
Matrigel® Basement Membrane Matrix	Eppendorf South Pacific
Lipofectamine® RNAiMAX Reagent	Thermo Fisher Scientific
Bovin Serum Albumin (BSA)	Sigma Aldrich

Table 2.4. List of chemicals and drugs used in this study.

Chemical/ Drug	Manufacturer
Paclitaxel (10461)	Cayman Chemical, Michigan, USA
Cisplatin (13119)	Cayman Chemical
SAR405 (S7682)	Selleck chemical, Houston, USA
MRT68921 (S7949)	Selleck chemical
Spautin-1 (17769)	Cayman Chemical

SBI-0206965 (18477)	Cayman Chemical
GK921(S6417)	Selleck chemical
Ethanol (Absolute)	POCD, Australia
Methanol, 100% AR Grade	POCD
Sodium dodecyl sulphate (SDS)	Sigma Aldrich
Triton X-100	Sigma Aldrich
Tween-20	Sigma Aldrich
Protease Inhibitor Cocktail	Sigma Aldrich
Phosphate Inhibitor Cocktail	Sigma Aldrich
N-Ethylmaleimide	Sigma Aldrich
β- mercapto-ethanol	Bio-rad
Kaleidoscope Precision plus™ protein standard	Bio-rad
Glycine	Sigma Aldrich
Trizma® Base	Sigma Aldrich
Sodium Chloride	Sigma Aldrich
Ammonium persulfate	Sigma Aldrich
30% Acrylamide	Bio-rad
Tetramethylethylenediamine (TEMED)	Sigma Aldrich
Digitonin	Sigma Aldrich
Prolong™ Antifade Gold Mounting reagent with DAPI nuclear stain	Thermo Fisher Scientific
Dako Target Retrieval Solution (Ph 6) (10x)	Aligent Technologies
0.3% Hydrogen peroxide	Chem-supply, Australia
Xylene	POCD
ImmPACT® NovaRED® Substrate Kit, Peroxidase (SK-4805)	Vector Laboratories, USA
EnVision FLEX WASH BUFFER (20x)	Agilent Technologies

Table 2.5. List of buffers used in this study and their composition.

Buffer	Composition
Trypsin stock solution	1 mg/mL resuspended in 50 mM triethylammonium bicarbonate (TEAB)
1x lysis buffer (immunobloting)	10 mM Tris buffer (pH 6.8), 150 mM NaCl, 0.5% SDS, 1% Triton X-100, 1 mM EDTA, 0.04 mM NaF, protease inhibitor cocktail, phosphatase inhibitor and 20 mM *N*-ethylmaleimide
1X lysis buffer (mass spectrometry)	5% sodium dodecyl sulfate (SDS) with MΩ water
Reductant buffer	120 mM Tris(2-carboxyethyl)phosphine (TCEP) in water
Alkylating buffer	500 mM iodoacetamide in isopropanol
Acidifier	27.5% (v/v) phosphoric acid, dissolved in water
Binding/wash buffer	100mM TEAB, dissolved in 90% methanol
Digestion buffer	50 mM TEAB
Elution buffer 1	50 mM TEAB in water
Elution buffer 2	0.2% formic acid in water
Elution buffer 3	50% acetonitrile in water
10x SDS running buffer	30 g Tris, 144 g Glycine and10 g SDS with MΩ water to 1L (pH 8.3)
10x Transfer buffer	30 g Tris and 144 g Glycine with MΩ water to 1L
Resolving gel buffer	90.8 g Tris and 2 g SDS with MΩ water to 1L (pH 8.8)
Stacking gel buffer	30.3 g Tris and 2 g SDS with MΩ water to 1L (pH 6.8)
5x Tris-buffered saline (TBS)	12.1 g Tris and 40 g NaCl with MΩ water to 1L (pH 7.6)
Loading Dye	25 ml 1M Tris-HCl (pH 6.8), 10 g SDS, 30ml glycerol, bromophenol blue and 5 ml B-mercaptoehtanol
4% paraformaldyhyde	4 g paraformaldehyde with 100ml phosphate buffered solution (PBS) (pH 7.4)

2.2. Methods

2.2.1. Cell Culture Maintenance

In this thesis, four cell lines were used, two for triple negative breast cancer (TNBC) and two for oral squamous cell carcinoma (OSCC). TNBC cell lines (HCC1806 and MDA-MB231) were a gift from Professor Robert Baxter (The University of Sydney, NSW, Australia). Both TNBC cell lines were grown in RPMI media. HCC1806 was further supplied by 5% fetal bovin serum (FBS), 1% penicillin/streptomycin, 1% Insulin and 1.5% HEPES. Whereas, MDA-MB231 was complemented by 10% FBS and 1% penicillin/streptomycin.

OSCC cell lines (SCC25 and SCC9) were a gift from Dr. Naisana Seyedasli (The University of Sydney, NSW, Australia) and HN6 was a gift from Professor Guy Lyons (The University of Sydney,NSW, Australia). SCC25 and HN6 were cultured in DMEM media supplemented by 10% FBS, 1% penicillin/streptomycin, while, SCC9 were grown in DMEM/F12 Glutamax media with 10% FBS, 1% penicillin/streptomycin and 1.5% HEPES.

All cell lines were maintained in humdified incubator under 5% CO_2 and 37˚C temperature. Periodic mycoplasma screening every 6 months were performed for all cell lines using a commercial testing kit (Catalog code: rep-mys-10, InvivoGen).

Cellular growth, viability and confluency were assessed by phase contrast microscopy. All cells are sub-cultured when reaches 80% confluency. Cell counting was performed via Guava® Muse® Cell Analyser according to manufacturer's protocol. For long term storage, cells were suspended in 10% DMSO in FBS, in a cryogenic vials, then stored in Cool-Cell at -80°C overnight and next day, it was moved to liquid nitrogen vapour phase

tank. For microenviromental stresses studies, DMEM or RPMI with no glucose medium were used.

2.2.2. Development of chemoresistant cell lines

Chemoresistance was developed by treating the parent cell line with gradient concentrations of standard chemotherapeutic agent. Treatments started with IC_{30} of standard chemotherapeutics for 3 days, then, cells were transferred into drug free media and left for 3 days to revive again. Once the cells were confluent, they were split and concentration was increased by two fold. This process was repeated until cells were able to grow under high concentration where cellular proliferation assay were performed to determine IC_{50} of generated resistant cell line in comparison to the corresponding parent cells.

2.2.3. siRNA Transfection

Cells were seeded in either 6 well plate (15×10^4 for resistant HN6 and MDA-MB231, 2×10^5 for resistant SCC9 and 35×10^4 for resistant HCC1806) or 96 well plate (1×10^4 for resistant HCC1806 and SCC9 and 4500-5000 for resistant HN6 and MDA-MB231, respectively). At this density cells were 30-50% confluent for 96 well or 6 well plate, respectively, on the next day. Directly after seeding, siRNA (*TGM2* or negative control) was added to each well, after being pre-incubated with Lipofectamine® RNAiMAX Reagent for 20 min. The siRNA concentration varies according to cell line used (**Table 2.2**). After that, plates were shaked on orbital shaker for 5 min and then allowed to grow overnight in the incubator. Silencing was done for two time periods 24 h or 72 h, then protein extraction were performed. In case of 96 well plate, next day of silencing, cells were treated with standard chemotherapeutics for 72 h and cellular proliferation assay was carried out.

2.2.4. Drug treatments

Seven drugs were used in this thesis, namely, Paclitaxel, Cisplatin, SAR405, MRT68921, Spautin-1, SBI-0206965 and GK921. Both Paclitaxel and Cisplatin were always prepared fresh on the same day of treatment by dissolving in DMSO at concentration of 10 mM. Autophagy inhibitors (SAR405, MRT68921, Spautin-1 and SBI-0206965) were prepared in advance at concentrations of 198 mM, 23.01 mM, 180 mM, and 100 mM, respectively, in DMSO and stored in small aliquots at -20˚C. Similarly, TGM2 inhibitor (GK921) was prepared at concentration of 25 mM in DMSO and stored at -20°C as small aliquots. Repeated freez-thaw of frozen drugs was avoided. All treatments were diluted in respective cell culture medium and applied to cells at 37˚C for indicated lengths of time. Final DMSO concentration was <5% under all conditions.

2.2.5. Protein extraction and Immunoblotting

First, cells were seeded in 6 well plate at density of 3×10^5 for SCC25 and MDA-MB231, 35×10^4 for SCC9 and 4×10^5 to achieve 80% confluency next day. After this, cells were either incubated with serum or glucose free media for 0.5-4.0 h or pre-incubated with late-stage autophagy inhibitor (Bafilomycin A1; 100 nM) for 2 h and then, incubated with serum or glucose free media for 1 h. Protein extraction was performed following incubation of cells under different stressors.

Protein extraction

Briefly, after indicated treatment, cells were lysed using lysis buffer (**Table 2.5**). The use of *N*-ethylmaleimide was to inhibit the activity of Atg4 which is responsible for conversion of LC3-I into LC3-II, so, preserve the stability of LC3-II. Cell lysates were collected, sonicated for 1 min with cup horn sonicator, centrifuged for 40 min at 14000 rpm at 4°C and supernatant were collected.

Protein concentration was measured in every sample using BCA protein assay according to manufacturer's manual. Briefly, BCA reagent mix was prepared by mixing reagent A and B at ratio of 50:1, then 200 µL of BCA reagent mix were added to 2 µL of sample and 8 µL of water in 96 well plate. Along with the samples, standards were also prepared as serial dilution of BSA solution in SDS at concentration of 2 mg/mL. After addition of BCA reagent mix, all samples and standards were incubated at 37°C for 30 min. After 30 min, plates were read by FLUOstar® plate reader at 562nm.

Sodium Dodecyl Sulphate and polyacrylamide gel electrophoresis (SDS-PAGE) and immunoblotting

Proteins were separated using SDS-PAGE gel and transferred to a polyvinylidene difluoride (PVDF) membrane by trans-Blot cell with wire electrode system (Bio-Rad). The upper part of electrophoresis consisted of 4% stacking gel to condense the proteins in one band and the lower part was 10 or 12% seperation (resolving) gel that separate proteins according to size and charge. A 10 or 12% separation gel and 4% stacking gel were used for all western blot experiments. A 1ˣrunning buffer was utilised during the electrophoresis which was prepared from 10x stock running buffer solution. All samples were prepared at 30 µg/µl protein concentration with 5% of loading dye and β-mercapto-ethanol. A total 25 µl volume were prepared and heated at 95°C on a dry heat block for 2 min. Kaleidoscope Precision plus™ protein standard was used as a ladder control. Electropheresis was carried out at 80 volt for the first 30 min, then, changed to 120 volt for about 90 min. Once proteins were separated, they were electro-blotted on PVDF membrane using 1ˣtransfer buffer, which prepared from 10ˣtransfer stock buffer, and added to it 20% methanol and 70% water. Transfer was accomplished at 30 volt for 16 h at 4°C.

Once transfer is completed, PVDF membrane is soaked in methanol for 1 min and left to dry at room temperature for 10 min. After that, membrane was blocked using a mixture of 5% milk in tris-buffered saline with 0.1% Tween 20 (TBST) buffer for 1 h at room temperature, then, incubated with the primary antibodies (**Table 2.2**) which were diluted in a solution of 0.1% BSA in TBST, at 4°C overnight. This was followed by a series of washing (5× 10min) with TBST at room temperature on orbital shaker, then, secondary antibodies; anti –Rabbit IgG (1:10000) and anti-Mouse IgG (1:10000) were applied for 1 h at room temperature. The final step was doing a last round of washes with TBST (5× 3 min). Detection of immunoblots were performed using ChemiDoc XRS+ System and image lab software and the Luminata Forte or Cresendo Western HRP substrate. After applying the substrate, the membranes were exposed to U.V light for specific time interval and multiple images were obtained.

All bands were measured by densitometry analysis where volume of each band was determined by drawing square around and Image lab software automatically measured its volume with substracting the background. Normalisation to β-actin was carried out by dividing the band volume of intreseted protein over volume of β-actin band, then normalisation to the control was done by dividing the value of each treatment band over the control.

2.2.6. Immunofluorescence

Cells were grown, at 30× 10^3 cells/well for SCC25 and SSCC9, 35 × 10^3 cells/well for HCC1806 and 70 × 10^3 cells/well for MDA-MB23, on a coverslips in 24 well plate and left overnight to adhere. The next day, cells were incubated with either glucose or serum free media for 1 h, with or without pre-incubation (2 h) with a late stage autophagy inhibitor,

Bafilomycin A1 (100 nM). After that, the media is discarded and cells were quickly washed with ice cold PBS 3 times, then, cells were fixed using 4% paraformaldehyde for 10 min at room temperature, followed by series of washing with ice cold PBS (3× 5min).

Next, coverslips were incubated with digitonin for permeabalisation 10 min at room temperature before another series of washing with ice cold PBS (3× 5min). Notably, digitonin was used as a mild detergent to preserve the lysosomal integrity by avoiding dissolution of lysosome's membrane. Afterwards, blocking was performed using 5% BSA for 1 h on an orbital shaker at room temperature. During blocking time, humidity chamber was prepared by placing a layer of wet filter paper in 35mm cell culture dish and covered by another layer of parafilm.

Primary antibody; anti LC3 antibody (1:250) and anti LAMP2 (1:100); diluted in 1% BSA dissolved in ice cold PBS were prepared and 12 µl of antibody mixture were added as droplet on the parafilm layer of the humid chamber. After that, the coverslip is picked up from 24 well plate using a forceps, allowed to drain excess blocking agent on a paper towel and flipped over the antibody droplet where the cells were facing the antibody without any air bubbles. The humid chamber was then covered and sealed with parafilm to prevent moisture loss and incubated overnight at 4°C.

Next day, coverslips were removed from the humid chamber, placed again in 24 well plate and washed with ice cold PBS (3×10min), followed by application of secondary antibody which was anti-rabbit IgG Alexa Fluora 488 for anti-LC3 Ab and anti-mouse IgG Alexa Fluora 594 (1:1000) for 1 h at room temperature on orbital shaker placed in a dark place. Following that, a final round of washing with ice cold PBS were done (4×10min). Coverslips

were mounted on slides using Prolong™ Antifade Gold Mounting reagent with DAPI nuclear stain and left overnight in dark place for the mounting reagent to harden.

Stained samples were examined and imaged using Leica TCS SPF5 confocal microscope. Three lasers with varying wave length (DAPI-405nm blue-diode, 594 helium-neon and 488 argon lasers) were used to visualise cell nuclei, LC3 and LAMP2 antibodies, respectively. All scan parameters (pinhole, gain and offset) remain fixed during acquisition of all images. Three separate fields were selected in each sample assessed with no selection criteria applied. Analysis of the images was performed using Image J.

Image J analysis was performed using Gaussian Blur filter and difference of Gaussians for counting puncta where LUT was changed to gray first, then, two copies of each image was created before application of Gaussian Blur filter for the two images. The difference of Gaussian between the two images was then calculated by the software and the brightness of resultant image was adjusted. The threshold of resultant image was adjusted as the original image , then, analysis was performed where number of puncta was obtained. Also, JACOP plugin was used for measuring Pearson's coefficient of colocalisation where threshold was adjusted for each image, then the coefficient was automatically calculated by the software. Colocalisation plot was done using colocalisation finder plugin.

2.2.7. Cellular proliferation Assay

Cellular proliferation were investigated using 3-(4,5-dimethylthiazol-2-yl)-5-(3-carboxymethoxyphenyl)-2-(4-sulfophenyl)-2H-tetrazolium (MTT) assay where dehydrogenase enzymes' activity in metabolically active cells are measured via their ability to reduce yellow MTT salt into purple formazan crystals. Cells were seeded in 96

well plate at cell density of 4×10^3 cells/well for SCC25, 10^4 cells/well for both HCC1806 and SCC9 and 10^3 cells/well for MDA-MB231, then, left to attach overnight at 37°C.

The next day, cells were treated with agents at series of two fold dilutions with highest concentration for each agent being: Spautin-1 (360 µM), SAR405 (99 µM), MRT68921 (23 µM), SBI0206965 (250 µM), GK921 (25 µM), Cisplatin (100 µM) and Paclitaxel (40 nM). To study the effect of microenviromenntal stressors, cells were pre-incubated with glucose or serum free media for 1 h before incubation with agents in nutrient replete medium. After treatment, cells were further incubated for 72 hrs at 37°C. After that, 25 µl of MTT (2.5 mg/ml) in PBS were added to each well and incubated for 2 h at 37°C. The crystals formed were then dissolved by adding 70 µl of DMSO/well and plates were put on a shaker for 10 min. Following these, plates were read at 570 nm using FLUOstar® Omega Microplate Reader. All treatment wells were normalised to the control well and cell viability were calculated using the following equation:

Cell viability= $\frac{Well\ value\ per\ treatment\ concentration}{Well\ value\ for\ no\ treatment\ control} \times 100$

A linear line graph is plotted between concentration of agent and cell viability. Then, IC_{50} was calculated using intercept and slope functions in Microsoft Excel, using the following equation:

$IC_{50} = \frac{50 - Intercept}{Slope}$

All IC_{50} values are mean ± SEM, n=3.

For combinations studies, *Chou-Talaly* method was used where cells were seeded as in cellular proliferation assay. The next day, cells were treated with gradient concentrations

(0.125x, 0.25x, 0.5x, 1x, 2x, 4x, 8x IC_{50}) of two drugs, one vertically and the other is horizontally for 72 h, then same steps were done as for cellular proliferation assay. Only wells with constant combination ratio (1:1) were considered. All treatment wells were normalised to the control well, then, CompuSyn.exe software was used to analyse the data and calculate the combination index for each drug combination. After that, GraphPad Prism 9 Software (Version 9.3.1, San Diego, CA, USA) was used to plot the dose-response curve. All values are mean ± SEM, n=3.

2.2.8. Incucyte® Cell Migration (Wound Healing) Assay

This assay was performed using Incucyte® 96-well Woundmaker tool which allowed formation of clean and precise scratches in each well of the 96 well plate. SCC25, SCC9, HCC1806 and MDA-MB231 were seeded as 24,000, 30,000, 32,000 and 23,000 cells in 100µL/well in 96 well plate to ensure 100% confluency after 24 h. After 24 h, 96 well plate was placed into Wound maker base plate holder and Woundmaker tool is positioned carefully over the 96 well plate as each pin in the woundmaker tool should be inside each well. Then, the black lever at the base plate was pressed to produce the scratches. After that, the wound maker tool is removed from the 96 well plate and placed into wash boat to start washing procedure according to the manufacturer's instructions. The washing process involved successive washing with 0.5% Alconox, 1% Virikon, sterile water and 70% ethanol for 5 min/each.

Following wound production, cells were washed with PBS 2-5 times, according to cell line used, to wash out any debris from the scratching procedure and ensure formation of clean scratches. After PBS washing, 100 µL of media was placed in each well and treatments were administered. First, cells were treated with gradient concentrations of each drug to

determine which concentration will be used for combination studies. To make sure that the resultant effect was from inhibition of cellular migration not as a result of their effect on cellular proliferation, cells were treated with the same concentrations and tested using cellular proliferation assay which demonstrated minimal inhibition of cell proliferation at the different concentrations during the incubation time for this assay. A dose which had a minimal effect on cellular proliferation but had a significant effect on cell migration was selected for each drug for combination studies.

Following this, combination studies were carried out by treating each row of cells with different drugs and or their fixed dose combination. After adding treatments, plates were placed in Incucyte® Live-Cell Analysis system which gave about 30 min for cells to warm up before any scanning. Scan time was set to every 3 h and continued for a period of 18 h in SCC25 and HCC1806, 24 h in SCC9 and 28 h in MDA-MB231 at which the wound in the control group had been closed. Relative wound denisty was calculated using Incucyte ®Scratch Wound Analysis Software which analyse the data based on 2 factors, wound width and confluency. The data obtained from wound analysis software was transferred to GraphPad where statistical analysis and graphs were created.

2.2.9. *In vivo* studies

This *in vivo* study was carried out in Kearns Facility at the Kolling Institute of medical Research. All animal procedures were conducted with approval from the Northern Sydney Local Health District (NSLHD) Animal Ethics committee (Ref# RESP_20_084). Briefly, female Bulb C/nude mice (6-8 weeks) were used in this study. First, dose escalation study was carried out by injecting mice intraperitoneally with two different doses of SAR405 and MRT68921 to determine a maximum tolerated dose with no observable adverse effects. The mice were treated twice week for 3 weeks.

After completion of dose escalation, the orthotopic xenograft were established by injecting the mice with MDA-MB231 tumour cells ($5^{x}\ 10^{6}$ cells) in the 2^{nd} mammary gland subcutaneosly. At day of injection, tumour cells were prepared in 1:1 mixture of Matrigel® and cold PBS. After tumour cells implantation, tumours were allowed to expand *in vivo*. During this period, mice were monitored twice /week for their weight. Tumour size was measured using digital venier calipers. Tumour volume was calculated using the following formula :

$$\text{Tumour volume} = \text{Length} \times \text{Width}^2 / 2$$

Once tumour size nearly reached $100mm^3$, mice were randomly allocated to 8 groups (8 mice/ group) and treatments started. Each group was treated with either, PBS as a control vechicle, SAR405 (20 mg/kg), MRT68921 (20 mg/Kg), SAR405 and MRT68921, Paclitaxel (5 mg/Kg), Paclitaxel and SAR405, Paclitaxel and MRT68921 or Paclitaxel, SAR405 and MRT68921. Treatments were applied twice a week with monitoring the mice twice a week for weight and tumour size. Treatments continued for 21 days as most of tumours reached tumour size of 1000 mm^3 that is considered as the border line at which mice needs to be culled. At this point, experiment was terminated and tumours were harvested along with all major organs such as spleen, kidney, brain and heart. Tumours were wighed after harvesting them. Further, all organs and tumours were kept in neutral buffer formalin (10 %) for 24 h, then transferred into 70% ethanol.

2.2.10. Immunohistochemistry staining (IHC)

All studies involving human specimens were done after obtaining approval from the NSLHD Human Research Ethics Committee (Ref# 2020/ETH02372). OSCC tumour sections were obtained from the Anatomical Pathology Department at the Royal North Shore Hospital, Sydney, Australia. In regards to TNBC tissue microarray (TMA) sections, 3 sections of TMAs were obtained from the Australian Breast Cancer Tissue Bank, Westmead Institute for Medical Research, Sydney, Australia and 4 TMA sections were from the Anatomical Pathology Department at the Royal North Shore Hospital, Sydney, Australia.

OSCC tumour sections and TNBC TMAs were cut as 5 µm sections with 3 slides for each case, 2 sections were placed on a positive charged slides for IHC staining and the 3rd section was on an ordinary glass slide for Hematoxylen and Eosin staining. Immunohistochemistry staining procedure was carried out following the standard procedure [375]. Briefly, tissue sections were left overnight in 40°C oven to remove any excess wax. Next day, deparafinisation step are done through sequential incubation in 2 different sets of Xylene (10 min/ each), followed by rehydration with water using gradient concentration of Ethanol, 2 sets of 100% Ethanol (5 min/ each), 2 sets of 95% Ethanol (5min/ each), 70% Ethanol (5min) and 50% Ethanol (5min).

After that, tissue sections were washed under running water for 2 min, followed by incubation of the tissue sections in antigen retrieval solution (pH 6) at 99.5°C for 20 minutes. Notably, antigen retrieval solution was pre-heated to 99.5°C before adding the slides. After 20 min, slides were taken out from the water bath and left to cool down at room temperature for about 20-25 min. Following this, slides were washed under running water for 2 min, followed by incubation with 0.3% hydrogen peroxide (H_2O_2) for 5 min to

block any endogenous peroxidase. Again, slides were washed under running water for 2 min, then, slides were loaded in squenzas and topped with wash buffer and left to run down for 6 min to make sure that squenzas were not leaking. Then, 100 µL of primary antibodies were added (either LC3B or P62; **Table 2.2**) to each squenza and incubated at 4°C for 18 h.

After 18 h, tissue sections were washed with wash buffer (room temperature) for 6 min. This was followed by addition of 100 µL of HRP Labelled Polymer Anti-mouse secondary antibody for 30 min at room temperature. Anti-mouse secondary antibody (room temperature) was used for both LC3B and P62. During this time, ImmPACT® NovaRED® Substrate Kit was prepared according to the manufacturer's instructions. After 30 min, another 2 rounds of washing with wash buffer was performed (5 min/ each). Next, slides were removed from squenzas and placed in the staining tray after wiping down its bed and the corners. At that time, 200 µL of ImmPACT® NovaRED® Substrate Kit was added to each slide enough to cover the tissue section for 15 min. After 15 min, slides were immediately dipped in water to stop the reaction, placed in slide holder and washed for 2 min under running water.

Afterwards, counter staining with hematoxylin was proceeded by dipping the slides in hematoxylin stain for 2 min, followed by washing under running water for 2 min, dipping in Scott's blue for 30 sec and final washing under running water for 2 min. Last step was sequential incubation with 4 different sets of 100% Ethanol, followed by 3 different sets of Xylene and finally, mounting on the coverslips using mounting media with caution to remove any air bubbles.

Assesment of immunohistochemical staining was performed by an expert pathologist, without knowledge of clinicopathological data. LC3 staining was scored as negative or positive according to absence or presence of the staining. In case of P62 staining (cytoplasmic and nuclear) in OSCC, it was scored according to the precentage of positively stained cells (0-100%) and cases were further categorised into ≤50% and >50%. For P62 staining in TNBC, it was recorded as positive or negative according to presence or absence of the staining.

2.2.11. Mass spectrometry analysis

Parent and resistant cell lines were analysed for untargeted proteomic using LC-MS/MS quantitative technique. All samples preparations were done by the candidate. LC-MS/MS acquisition and quantification *via* the MaxQuant Software were carried out by Dr. Matthew Mckay (Sydney Mass Spectrometry Core Research Facility, Kolling Institute, The University of Sydney).

Briefly, triplicates of each parent and resistant cell line were grown at 10^6 cell density, trypsinised, centrifuged at 1400 rpm for 3 min and resuspended in PBS. This step was repeated 3 times and at the last time, supernatant was discarded and then, cell pellets were kept in -80°C for further preparations for LC-MS/MS technique. S-Trap™ micro-MS sample spin-columns (PROTIFI; Cat# C02-micro-80) were used for protein trapping according to the manufacturer's procedure. First, the pelleted cells were solubilised in 23 µL of 1x lysis buffer, then, vortex to lysis the sample and dissolve proteins. Also, Benzonase was added to sheer DNA. After that, samples were centrifuged for 8 min at 13000 xg to clarify samples from debris.

Following centrifugation, 1 µL of reductant buffer was added to each sample and samples were incubated at 55°C in dry heat block for 15 min. Next, 1 µL of alkaylating buffer were added to each sample and incubated for 10 min at room temperature. Afterwards, 2.5 µL of acidifier was added to each sample to denature the proteins and trap them efficiently. Notably, care was taken to adjust pH≤ 1. At this point, 165 µL of binding / wash buffer was added to each sample and mixed. Meanwhile, Individual S-Trap™ columns were prepared by placing it into 2 mL microcentrifuge tube and samples were loaded in the S-Trap™ columns, and then centrifuged at 4000 xg for 3 min. This step was repeated 3 times and every time, care was taken to visualise that the entire sample passed through the column, flow was discarded through and 150 µL of binding/ wash buffer was added again. Last round of centrifugation was done at 4000 xg for 1 min to make sure that binding/wash buffer was fully removed. Then, S-Trap™ columns were transferred into a clean 2 mL microcentrifuge tube for protein digestion.

Protein digestion was performed by dissolving trypsin in digestion buffer at weight to weight ratio of 1:10, so, 5 µg of trypsin was dissolved in 15 µL of digestion buffer and 20 µL of digestion buffer containing trypsin was added to each column and incubated at 37°C overnight. Caution was taken that columns' caps were loose to limit evaporative loss. The next day, elution of peptides was carried out by adding 40 µL of elution buffer 1, then centrifuged at 4000 xg for 1 min and follow through was collected. After that, 40 µL of elution buffer 2 was added to the columns, centrifuged again at 4000 xg for 1 min and follow through was also collected with first follow-through. Lastly, 40 µL of elution buffer 3 was added to the columns, centrifuged for 1 min at 4000 xg and follow through was again collected with the other follow- throughs.

Afterwards, the eluted peptides were lyophilised using SpeedVac™ for 1 h and resuspended in 0.1% formic acid and protein concentration in each sample was measured using NanoDrop™ ND-1000 spectrometer (Thermo Fisher Scientific). Now, the samples are ready for LC-MS/MS acquisition. The samples were injected in reverse-phase analytical column on a nanoultra- pressure-liquid chromatography system (Thermo Fisher Scientific) coupled to a tandem mass spectrometer (QExactive HF-X, Thermo Fisher Scientific) with a nanospray source operating in positive mode. . The temperature of the column was maintained at 60˚C.The peptides were seperated using a stepped gradient of actonitrile (2 -95 %) over 120 min after which the column was adjusted to 2% in 15 min at a flow rate of 300 nL/min. Data-dependant acquisition (DDA) mode was used for tandem mass spectrometry analysis with higher energy collisional dissociation (HCD) fragmentation of the top 15 most abundant ions per cycle across the LC gradient. The settings were adjusted to 6×10^4 resolution, 3×10^6 AGC target and 350-1650 m/z scan range for MS1 spectra. For MS2 spectraresolution of 1.5×10^4 , 2.9×10^3 AGC and 200 – 2000 m/z scan range were used.

The raw files obtained from MS analysis were analysed using default setting for library free searches using DIA-NN software where false discovery rate (FDR) of 1% was adjusted to identify peptides and proteins, mass accuracy was set 0.0 ppm and 1 missed cleavage was permitted for trypsin. The data obtained from the analysis were transformed to log squared (log2) and the missing values were excluded. The *p-values* were generated by Graphpad Prism 9 using mutiple student's t-test, and the (log2) values with *p-values* ≤ 0.05 and $q<0.1$ were considered significant for further analysis. Inguinty Pathway Analysis software (IPA; Qiagen) was used for indentification of affected diseases, canonical pathways and molecules that has been altered in our samples. IPA categorises pathways and regulators according to *p*-value of overlap and z-score. *p*-value of overlap determines

if there is a significance of overlap between your dataset and a gene dataset for a pathway, regulator or function that is established by IPA. z-score indicates either activation or inhibition based on relationship of proteins/genes in your dataset compared to the known relationship in literature.

2.3. Software and statistics

Software

Several softwares had been used across this thesis. Image Lab software was used for dentistometric analysis of immunoblots. LAS X and Image J software (Gaussian Blur filter, JACOP and colocalisation finder plugins) were utilised for adjusting and analysis of immunoflurosence images. Incucyte® Live-Cell Analysis software was used for analysis of wound denisty. Ingenuity Pathway Analysis (IPA) was utilised for analysis of data obtained from mass spectrometry and identifying canonical pathways and regulators in the samples. All graphs in this thesis were plotted using GraphPad Prism 9. All Diagrams were created using Biorender.com

Statistics

All statistical analysis across the thesis was carried out using Graphpad Prism 9 and SPSS. Student's *t*-test and multiple *t*-test were used to calculate the statistical significance in the experiments. Chi-square test was used to compare categorical variables. Also, Kaplien-Miere (Log-rank test) and univariable and multivariable Cox regression analysis in SPSS software were used for analysis of survival data. Unless specified otherwise, data was shown as mean ± S.E.M and *p*-value of <0.05 was considered statistically significant. Asterisks were utilised to express level of statistical significance as follow, *$p<0.05$, ** $p<0.01$, *** $p<0.001$ and **** $p<0.0001$

Chapter 3

Development of Novel Autophagy Inhibitors-Based Anti-Cancer Combination Therapy

3.1. Introduction

Autophagy is a dynamic process by which damaged organelles and misfolded proteins are engulfed by a double membrane vesicle, termed the autophagosome, that eventually fuses with lysosome forming autolysosomes and result in breakdown of the unwanted material and release of primary biomolecules into the cytosol [1]. It is considered a survival process utilised by cells under metabolically stressful conditions such as hypoxia or nutrient starvation [2]. The autophagic pathway is a complex pathway which starts when the cell is subjected to stress, activating a signaling cascade of autophagic regulators (*e.g.,* ULK-1 and Beclin-1) [376]. These regulators activate the formation of double membrane vesicles called autophagosomes which is characterised by the presence of a well-known autophagic marker LC3-II on its membrane [376]. The autophagosome, in turn, fuses with lysosomes and lysosomal enzymes are responsible for the degradation of unwanted material. This is followed by the degradation of autophagosomes [376]. In the basal physiological conditions, there is an equilibrium between autophagy induction and degradation [59].

Autophagy has been implicated in many pathologies including cancer. It has a dual role in cancer with both pro- and anti-tumourigenic effects [67]. In early carcinogenesis, it exerts a tumour suppressor role by limiting the DNA damage and as the tumour progresses; this role is converted to a tumour promoter role where it allows the tumour cells to survive under stressful microenvironmental conditions [67]. It is well known that tumours are subjected to stressful microenvironment such as nutrient deprivation, hypoxia, and also, exogenously induced stress by chemotherapy [377]. Tumour cells try to upregulate autophagy to overcome these stressful microenvironmental conditions [378]. Notably,

autophagy is known to be involved in tumour growth, metastasis and chemoresistance development [378]. Hence, targeting the autophagic pathway could be a potential strategy for inhibition of cancer progression.

Chloroquine and hydroxy-chloroquine are conventional autophagy inhibitors that act via inhibition of the fusion between autophagosomes and lysosomes, and thus, block the autophagic pathway at the degradation stage [85]. Although these inhibitors have entered clinical trials as a combination therapy with the standard chemotherapeutic agents, they showed a moderate inhibitory effect with serious side effects (*e.g.,* kidney impairment) [379]. Thus, development of novel autophagy inhibitors is warranted.

Notably, autophagy had been associated with aggressive clinicopathological features and malignant prognosis of both triple negative breast cancer (TNBC) [380] and oral squamous cell carcinoma (OSCC) [217]. TNBC do not respond to endocrine or HER2 targeted therapies and use of conventional chemotherapy is not effective in all patients [240]. Similarly, OSCC has a poor prognosis due to metastasis, recurrence and poor chemosensitivity [163]. Therefore, targeting autophagy via novel autophagic inhibitors could be an effective strategy to inhibit TNBC and OSCC progression, and re-sensitise TNBC and OSCC to the standard chemotherapeutic agents.

The aims of this chapter are:

1) To evaluate the effect of different metabolic stressors (*i.e.*, nutrient and energy deprivation) on the autophagic pathway in TNBC and OSCC cell models.

2) To assess the effect of novel autophagy inhibitors on tumour cell proliferation and migration in cellular models of TNBC and OSCC.
3) To determine the effect of combination between standard chemotherapy and autophagy inhibitors *in vivo*.

3.2. Results

3.2.1. Effect of microenvironmental stressors on the autophagic marker LC3-II and lysosomal marker LAMP2 in both OSCC and TNBC cell models

It is well known that the tumour cells are subjected to different types of microenvironmental stressors such as serum and glucose starvation and autophagy might play a role to allow survival of tumour cells under these stressful conditions. To investigate effect of autophagy in response to different tumour microenvironmental stressors, OSCC (SCC25 and SCC9) and TNBC (HCC1806 and MDA-MB231) cell lines were incubated in either serum or glucose free media for increasing length of time (0.5-4.0 h). Autophagosome levels were determined by the assessment of LC3-II levels, which are present on the membrane of this organelle and is a classical marker to measure its levels in the cell [20]. Protein lysates were harvested from the cells, and immunoblotting was performed to determine the levels of LC3-II under different microenvironmental stressors. In immunoblotting, LC3 appeared as two separate bands, corresponding two forms of LC3 (LC3-I and LC3-II) with molecular weight of 16 and 18 KDa, respectively. Although LC3 II has a higher molecular weight (18 KDa), it is known to resolve as a lower band due to lipidation. Also, lysosomes levels were determined by assessing LAMP2 levels, which is a classical marker for lysosomes [381].

Under serum starvation conditions, LC3-II levels were significantly increased (p<0.0001-0.05) in SCC25 cell line after 0.5-2 h incubation with serum free media. Also, LAMP2 levels in the same cell line were significantly decreased (p<0.05) at 0.5 h and 4 h when incubated under same condition **(Figure 3.1 A-C)**. Moreover, SCC9 showed a significant increase (p<0.05) in both LC3-II and LAMP2 levels upon treatment with the serum depleted media for 0.5-1 h, respectively **(Figure 3.1 D-F)**.

In HCC1806, LC3-II was significantly upregulated (p<0.05) following 1 h treatment with serum free media with no detectable changes in LAMP2 levels were observed **(Figure 3.1. G-I).** In contrast, no significant upregulation of LC3-II levels was observed in MDA-MB231 when treated with the same conditions as HCC1806. However, LAMP2 levels were significantly increased (p<0.05) upon 1 h serum starvation in MDA-MB231 **(Figure 3.1.J-L).**

Next, we examined the effect of glucose starvation on LC3-II and LAMP2 levels. In SCC25 cells, 1-4 h glucose starvation resulted in a significant increase (p<0.0001-0.05) in LC3-II levels, while no significant increase in LAMP2 levels was observed **(Figure 3.2 A-C)**. Likewise, in SCC9 cells, there was a significant upregulation (p<0.001-0.05) of LC3-II levels after 0.5-1 h treatment with glucose depleted media, with no significant change observed in LAMP2 levels **(Figure 3.2 D-F)**.

In HCC1806, a significant increase (p<0.01) of LC3-II levels were observed upon glucose starvation for 2 h, with no significant increase in LAMP2 levels under any incubation conditions **(Figure 3.2. G-I)**. On the contrary, no significant increase in both LC3-II and LAMP2 levels was observed in MDA-MB231 cells when incubated with glucose free media **(Figure 3.2.J-L)**. These results indicate increased autophagosome levels under certain incubation conditions in the TNBC and OSCC cell lines examined. As 1 h incubation with serum or glucose depleted media led to increase in LC3-II under majority of conditions, this time point was chosen for further studies.

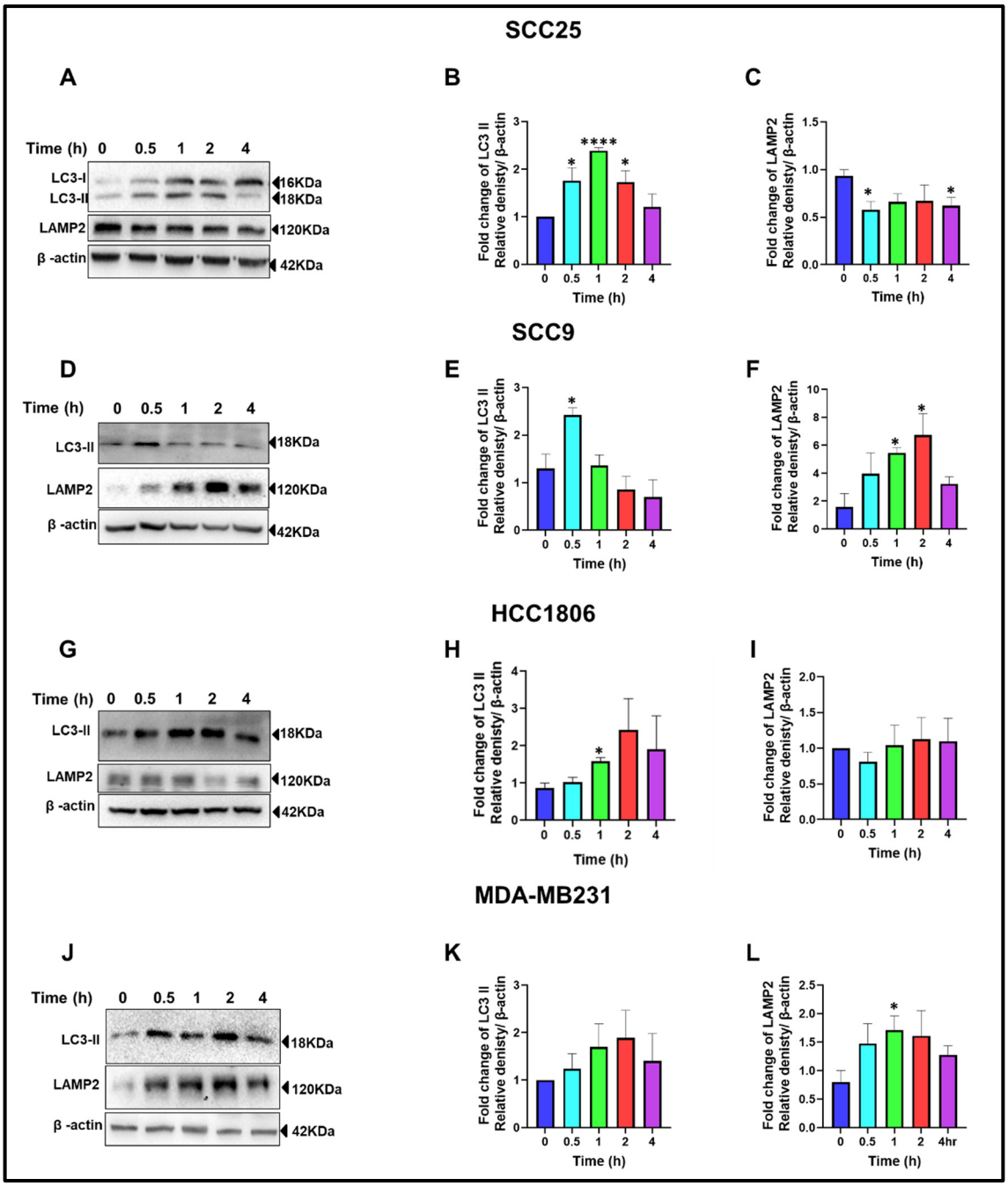

Figure 3.1. Effect of serum starvation on the levels of LC3-II and LAMP2 in all cell lines used. (A,D,G,J) Western blotting was performed to investigate LC3-II and LAMP2 levels in SCC25, SCC9, HCC1806 and MDA-MB231, respectively. Cells were incubated under serum free medium for increasing lengths of time (0-4 h). Blots shown are typical of 3 experiments. **(B,E,H,K)** Densitometric analysis of LC3-II results shown in **A,D,G,J,** respectively. **(C,F,I,L)** Densitometric analysis of LAMP2 results shown in **A,D,G,J,** respectively. Densitometric analysis are mean ± SEM (n = 3) normalised to β-actin. *p<0.05, ****p<0.0001 versus the Control.

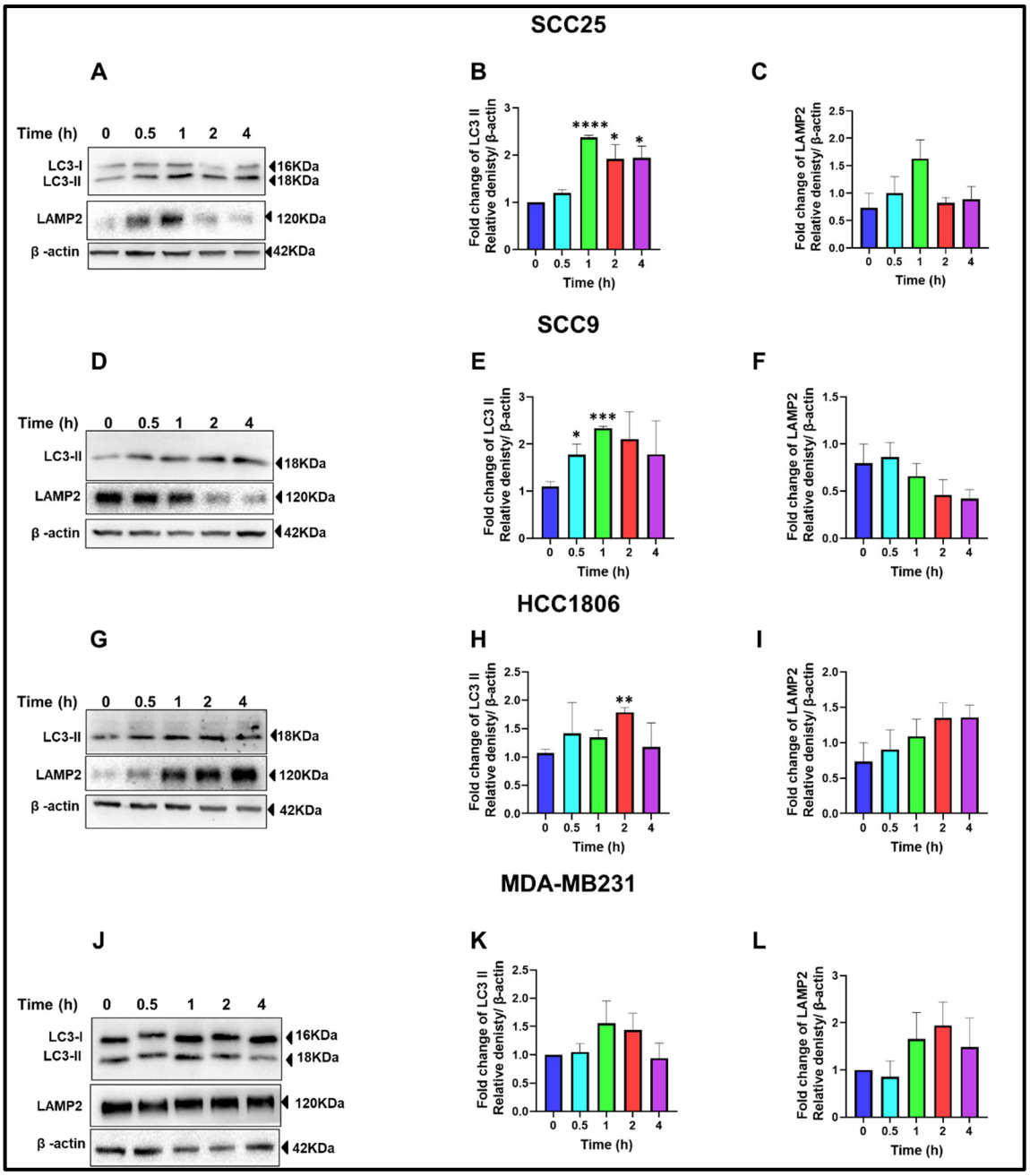

Figure 3.2. Effect of glucose starvation on the levels of LC3-II and LAMP2 in all cell lines used. (A,D,G,J) Western blotting was performed to investigate LC3-II and LAMP2 levels in SCC25, SCC9, HCC1806 and MDA-MB231, respectively. Cells were incubated under glucose free medium for increasing lengths of time (0-4 h). Blots shown are typical of 3 experiments. **(B,E,H,K)** Densitometric analysis of LC3-II results shown in **A,D,G,J,** respectively. **(C,F,I,L)** Densitometric analysis of LAMP2 results shown in **A,D,G,J,** respectively. Densitometric analysis are mean ± SEM (n = 3) normalised to β-actin. *p<0.05, **p<0.01, ***p<0.001, ****p<0.0001 versus the Control.

3.2.2. Effect of microenvironmental stressors on the autophagic initiation in both OSCC and TNBC cell models

As mentioned in chapter 1, autophagy is a dynamic process which involves both formation and degradation of autophagosomes. As LC3-II is a marker for autophagosome, LC3-II levels are correlated to autophagosome abundance. Thus, increase in LC3-II levels could be due to either increase in autophagy induction or decreased degradation **(Figure 3.3)**. To determine if the upregulated LC3-II levels observed after serum or glucose starvation was due to increased autophagy induction or decreased degradation, cells were pre-treated with Bafilomycin A1 (100 nM) for 2 h. Baf A1 blocks the autophagosome degradation and prevents the fusion between lysosomes and autophagosomes, therefore, the extent of autophagosome formation upon serum or glucose starvation can be determined.

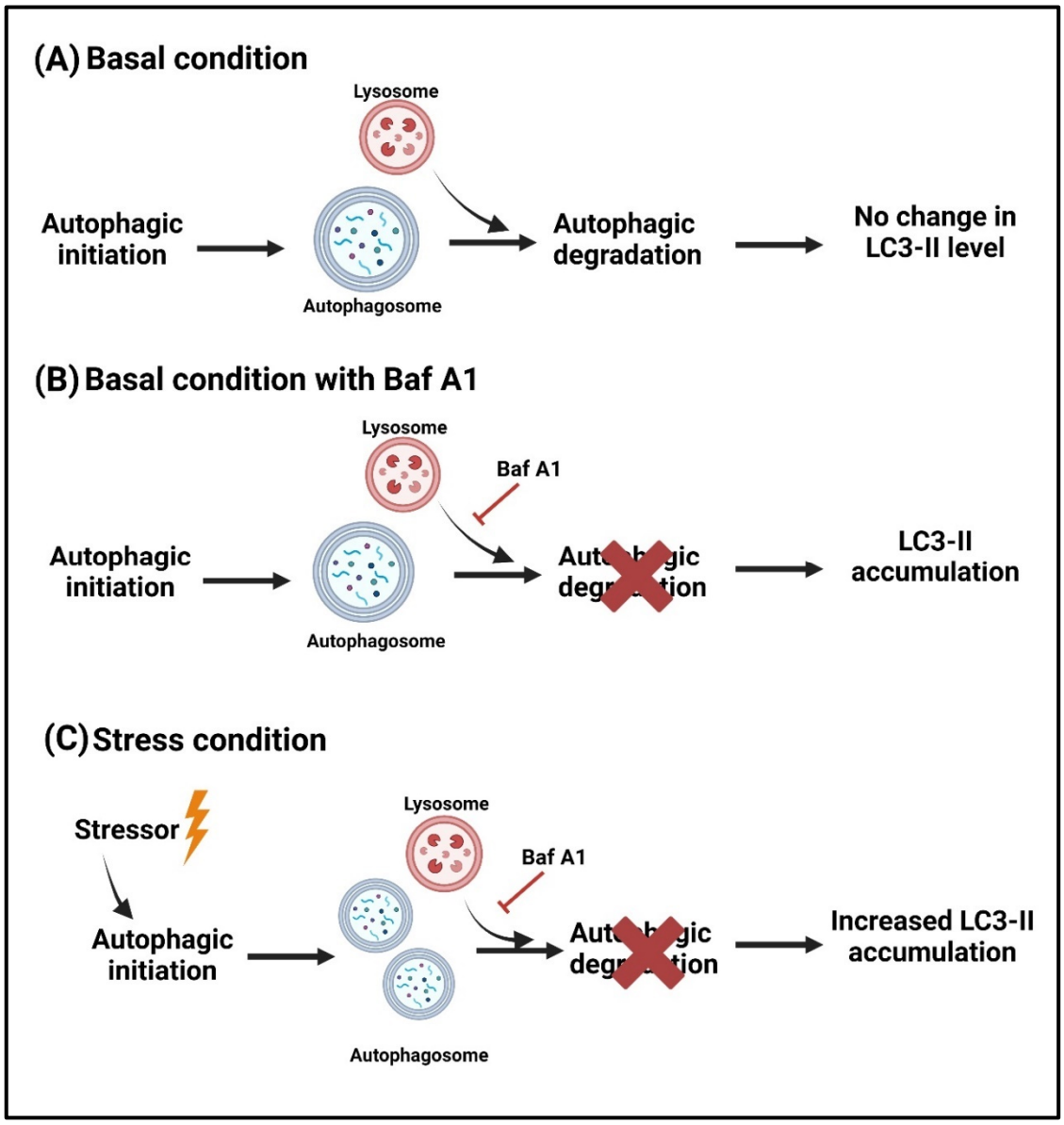

Figure 3.3. Diagram illustrates that LC3-II levels are either due to increased synthesis or decreased degradation of autophagosomes. (A) At basal condition, autophagosome are being degraded after fusion with lysosomes resulting in unchanged LC3-II levels. **(B)** In presence of Baf A1, fusion between autophagosomes and lysosomes is blocked with subsequent blockade of autophagy degradation, resulting in LC3-II accumulation that reflects the extent of autophagosome formation. **(C)** Under stress condition in presence of Baf A1, autophagosome synthesis is increased compared to basal state, resulting in increased LC3-II accumulation.

OSCC and TNBC cell lines were pre-incubated with Baf A1 for 2 h followed by treatment with serum and glucose free media for 1 h. Under control conditions, Baf A1 induced an increase in LC3-II levels in comparison to control cells without Baf A1 treatment in all four cell lines used. Moreover, significant upregulation of LC3-II ($p<0.05$) *was* observed following co-incubation of Baf A1 with serum free media in OSCC cell lines which indicates increased autophagy induction by serum starvation. The same results were observed in SCC25 cell line when treated with glucose free media in presence of Baf A1 compared to control cells incubated with Baf A1 only, but not in SCC9 cells **(Figure 3.4**).

In TNBC cell model, incubation with serum free media in presence of Baf A1 increased LC3-II levels in comparison to control condition incubated with Baf A1 only, but it was not significant (**Figure 3.5**). In contrast, co-incubation of Baf A1 with glucose free media significantly increased LC3-II levels ($p<0.05$) in comparison to control cell treated with Baf A1 only in both TNBC cell lines. These results indicate that the increase in LC3-II levels upon serum starvation for 1 h in OSCC cell model is due to increased autophagy induction. In addition, 1 h glucose starvation increased autophagy induction in all cell lines except SCC9, explaining the observed increase in LC3-II levels under these conditions.

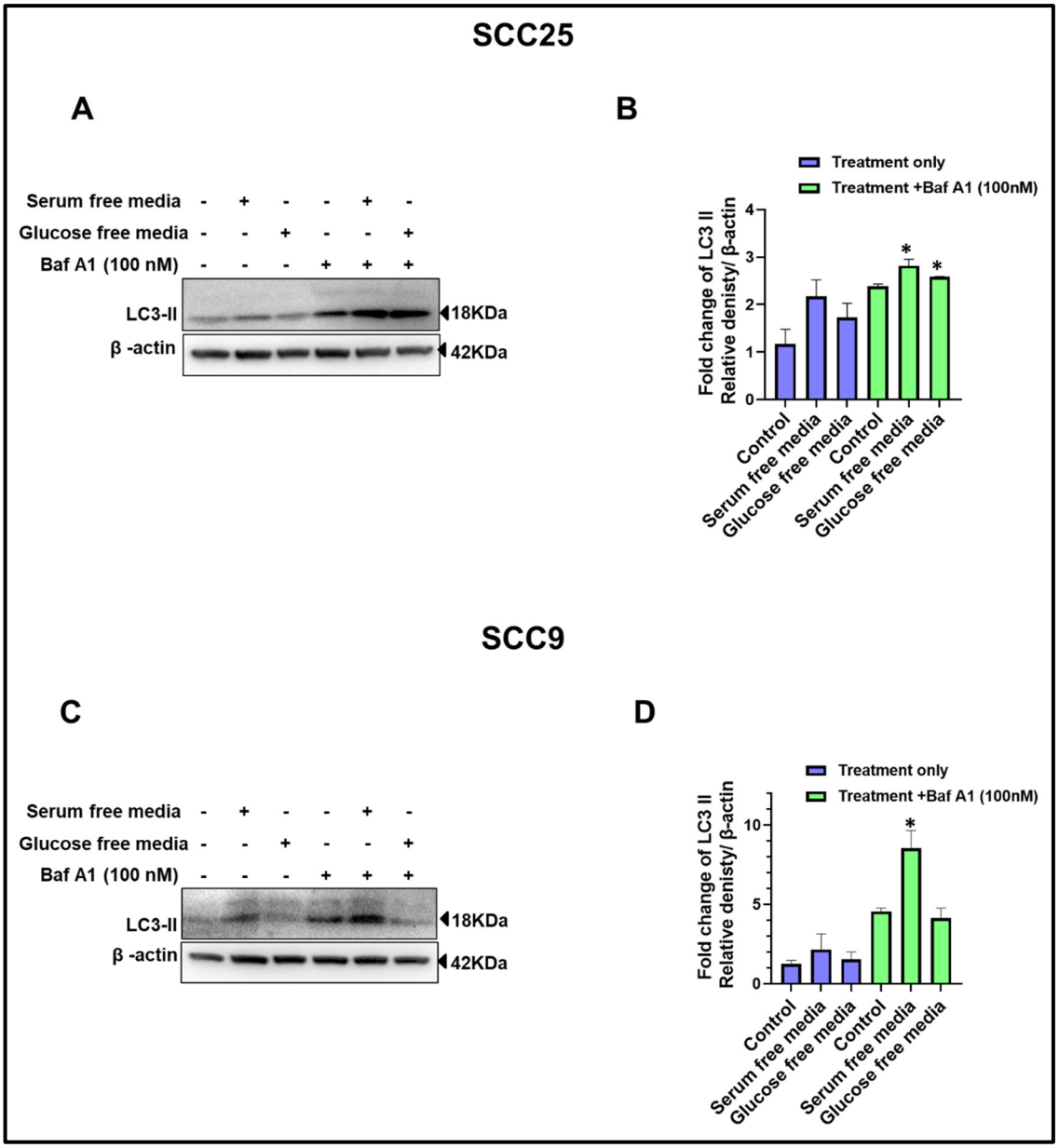

Figure 3.4. Effect of 1 h serum and glucose starvation with 2 h Baf A1 pre-incubation on autophagosome synthesis in OSCC cell lines. (A,C) SCC25 and SCC9 were pre-incubated with control media or media containing Baf A1(100nM) for 2 h/37°C,then treated with either control media, serum, or glucose free media for 1 h/37°C respectively. **(B,D)** Densitometric analysis of the results shown in **(A,C)** respectively. Blots shown in **(A,C)** are typical of 3 experiments. Densitometric analysis in **(B,D)** are mean ± SEM (n = 3) normalised to β-actin. **p*<0.05 versus Baf A1 treatment only.

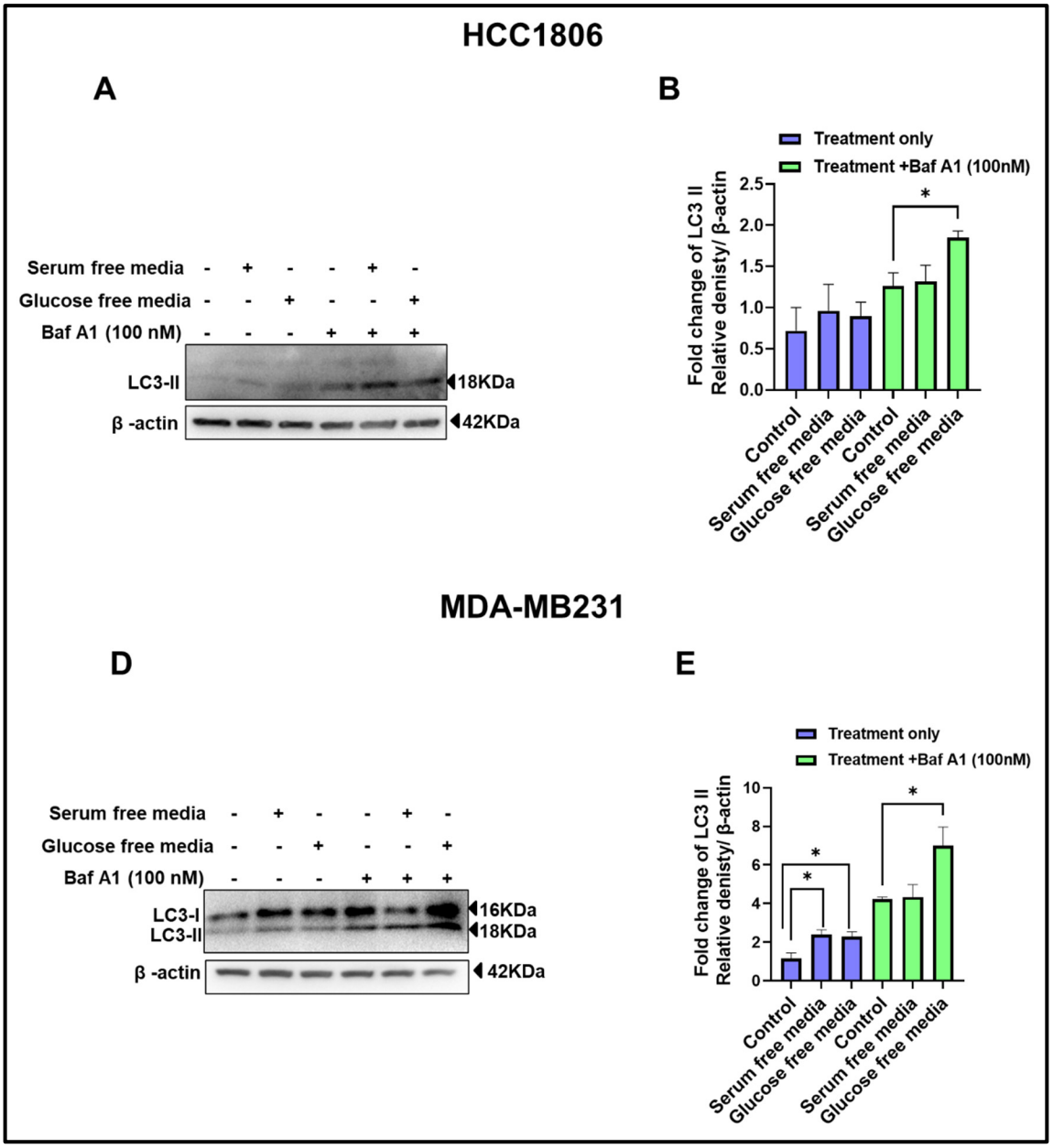

Figure 3.5. Effect of 1 h serum and glucose starvation with 2 h Baf A1 pre-incubation on autophagosome synthesis in TNBC cell lines. (A,C) HCC1806 and MDA-MB231 were pre-incubated with control media or media containing Baf A1(100nM) for 2 h/37°C, then treated with either control media, serum, or glucose free media for 1 h/37°C respectively. **(B,D)** Densitometric analysis of the results shown in **(A,C)** respectively. Blots shown in **(A,C)** are typical of 3 experiments. Densitometric analysis in **(B,D)** are mean ± SEM (n = 3) normalised to β-actin. *p<0.05 compared to the treatment shown in the figure.

3.2.3. Effect of microenvironmental stressors on LC3 punctate via confocal microscopy and co-localisation between LC3 and LAMP2 in both OSCC and TNBC cell models

In order to validate the results from immunoblotting, LC3-II levels were further examined using confocal microscopy by which a punctate pattern in the cytoplasm is visualised. As mentioned before, LC3-II levels are correlated to number of autophagosomes as LC3-II is present on the autophagosome membrane throughout its lifecycle. Thus, an increase in the number of detected punctate indicates a rise in autophagosomes abundance. All cell lines used were pre-incubated with Baf A1 for 2 h, followed by incubation with serum or glucose free media for 1 h. After that, cells were processed and examined by confocal microscopy.

Our results showed that there was a significant increase (p<0.05) in number of LC3-II punctate upon 1 h serum or glucose starvation in all cell lines used **(Figure 3.6, 3.8, 3.9)** except SCC9 in which no significant increase was observed when treated with the same conditions **(Figure 3.7)**.

As previously mentioned, any increase in LC3-II levels implies either increased autophagy initiation or decreased degradation (**Figure 3.3**). Thus, upon pre-incubation with Baf A1, a significant increase (p<0.05) in LC3-II punctate was identified in SCC25 cells when incubated with serum or glucose deprived media compared to Baf A1 treatment only **(Figure 3.6)**. Likewise, SCC9 displayed a significant increase (p<0.01-0.05) in LC3-II punctate upon incubation with serum or glucose free media with Baf A1, compared to standalone Baf A1 treatment **(Figure 3.7)**. Furthermore, the same trend was seen in HCC1806 which demonstrated a significant rise (p<0.001-0.05) in LC3-II punctate

following 1 h serum or glucose starvation with Baf A1 in comparison to Baf A1 treatment only **(Figure 3.8)**. In addition, MDA-MB231 demonstrated significant increase (p<0.01) in LC3-II puncta upon 1 h glucose starvation combined with Baf A1 treatment when compared to Baf A1 treatment only. In contrast, treatment with serum free media and Baf A1 resulted in no significant increase in LC3-II puncta in MDA-MB231 compared to Baf A1 treatment alone **(Figure 3.9)**. These results are consistent with results from immunoblotting which indicates that glucose starvation induced autophagy induction in SCC25, HCC1806 and MDA-MB231, whilst serum starvation increased autophagy induction only in OSCC cell model.

It is well known that the fusion between autophagosomes and lysosomes is a crucial step in the autophagic pathway [25]. Therefore, the association between autophagosomes and lysosomes was examined using immunofluorescence via detecting the co-localisation between LAMP2 and LC3 which are well-established lysosomal and autophagic markers that is expressed on the membrane of lysosomes and autophagosome, respectively [381, 20]. Co-localisation of LC3 (green stain) and LAMP2 (red stain) results in a yellow staining. This co-localisation was analysed using Pearson's coefficient (R) which provides statistical information about the objects' position with their relative intensities. This suggests the close proximity between autophagosomes and lysosomes to form autolysosomes.

In SCC25 cell line, a marked overlap between LC3 and LAMP2 with increase in (R) value were seen in case of 1 h serum (R=0.682) or glucose starvation (R=0.736) compared to control condition (R=0.509), respectively **(Figure 3.6.C)**. The same trend was observed in SCC9 upon serum starvation (R=0.69), or glucose starvation (R=0.594), compared to

control cells (*R*=0.461) **(Figure 3.7.C)**. Similarly, HCC1806 demonstrated a marked overlap in the merged image upon 1 h serum starvation (*R*=0.773) or glucose starvation (*R*=0.*787*), when compared to control (*R*=0.681) **(Figure 3.8.C)**. Marked increase in overlap was also observed in MDA-MB231 in case of 1 h incubation with serum free (*R*=0.837) or glucose free (*R*=0.838) media, in comparison to control (*R*=0.655) **(Figure 3.9.C)**. Again, these findings are consistent with the previous results from immunoblotting and number of LC3 puncta which altogether demonstrates that serum and glucose starvation results in increased autophagic flux.

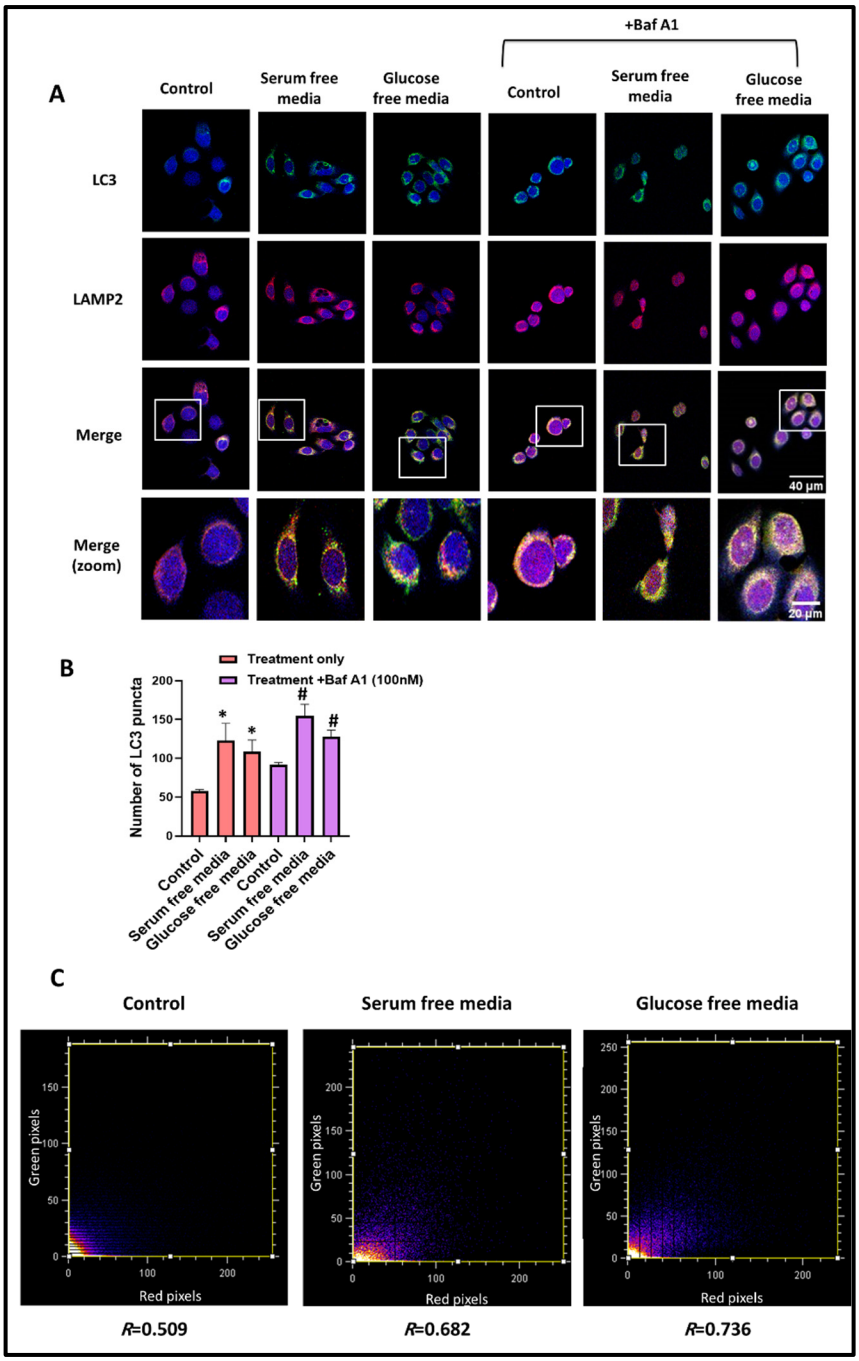

Figure 3.6. Serum and glucose starvation for 1 h with Baf A1 pre-incubation for 2 h enhances LC3 punctate with marked overlap between LC3 and LAMP2 in SCC25 cell line. (A) SCC25 were pre-incubated with control media or media containing Baf A1(100 nM) for 2 h/37°C, then treated with either control media, serum-free, or glucose-free media for 1 h/37°C. Immunofluorescence studies assessed LC3 punctate staining and LC3 and LAMP2 co-localisation. Representative images shown are typical of 3 experiments. Scale bar: 40 µm except for zoomed image: 20 µm **(B)** Statistical analysis of the results shown in **(A)** and represented as mean ± SEM (n = 3). *p<0.05 versus control, #p<0.05 versus Baf A1 treatment only. **(C)** Pearson's coefficient for LC3 and LAMP2 co-localisation was calculated using Image J.

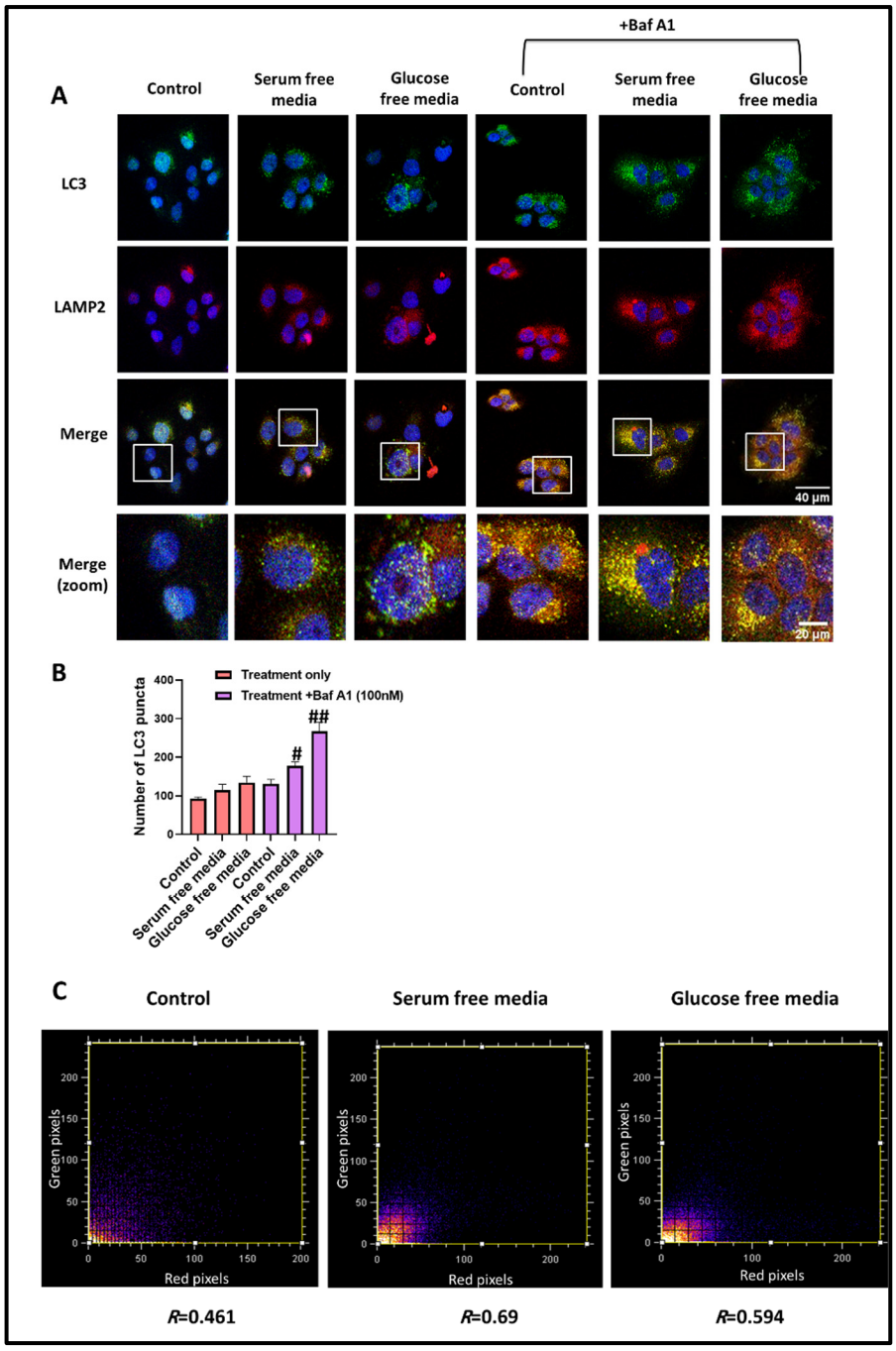

Figure 3.7. Serum and glucose starvation for 1 h with Baf A1 pre-incubation for 2 h enhances LC3 punctate with marked overlap between LC3 and LAMP2 in SCC9 cell line. (A) SCC9 were pre-incubated with control media or media containing Baf A1(100 nM) for 2 h/37°C, then treated with either control media, serum-free, or glucose-free media for 1 h/37°C. Immunofluorescence studies assessed LC3 punctate staining and LC3 and LAMP2 co-localisation. Representative images shown are typical of 3 experiments. Scale bar: 40 µm except for zoomed image: 20 µm **(B)** Statistical analysis of the results shown in **(A)** and represented as mean ± SEM (n = 3). $^{\#}p<0.05$, $^{\#\#}p<0.01$ versus Baf A1 treatment only. **(C)** Pearson's coefficient for LC3 and LAMP2 co-localisation was calculated using Image J.

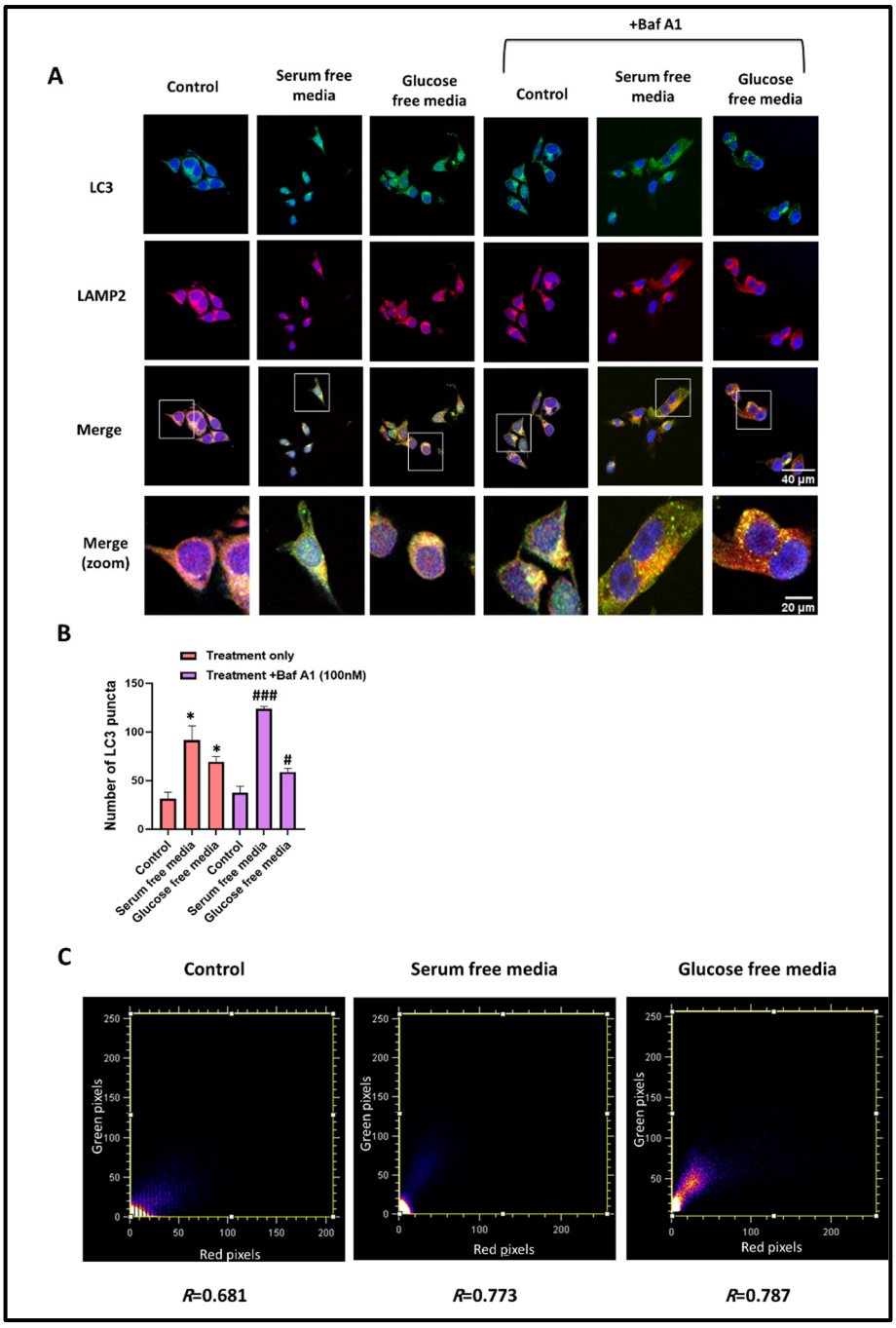

Figure 3.8. Serum and glucose starvation for 1 h with Baf A1 pre-incubation for 2 h enhances LC3 punctate with marked overlap between LC3 and LAMP2 in HCC1806 cell line. (A) HCC1806 were pre-incubated with control media or media containing Baf A1(100 nM) for 2 h/37°C, then treated with either control media, serum-free, or glucose-free media for 1 h/37°C. Immunofluorescence studies assessed LC3 punctate staining and LC3 and LAMP2 co-localisation. Representative images shown are typical of 3 experiments. Scale bar: 40 µm except for zoomed image: 20 µm. **(B)** Statistical analysis of the results shown in **(A)** and represented as mean ± SEM (n = 3). *p<0.05 versus the control, #p<0.05, ###p<0.001 versus Baf A1 treatment only. **(C)** Pearson's coefficient for LC3 and LAMP2 co-localisation was calculated using Image J.

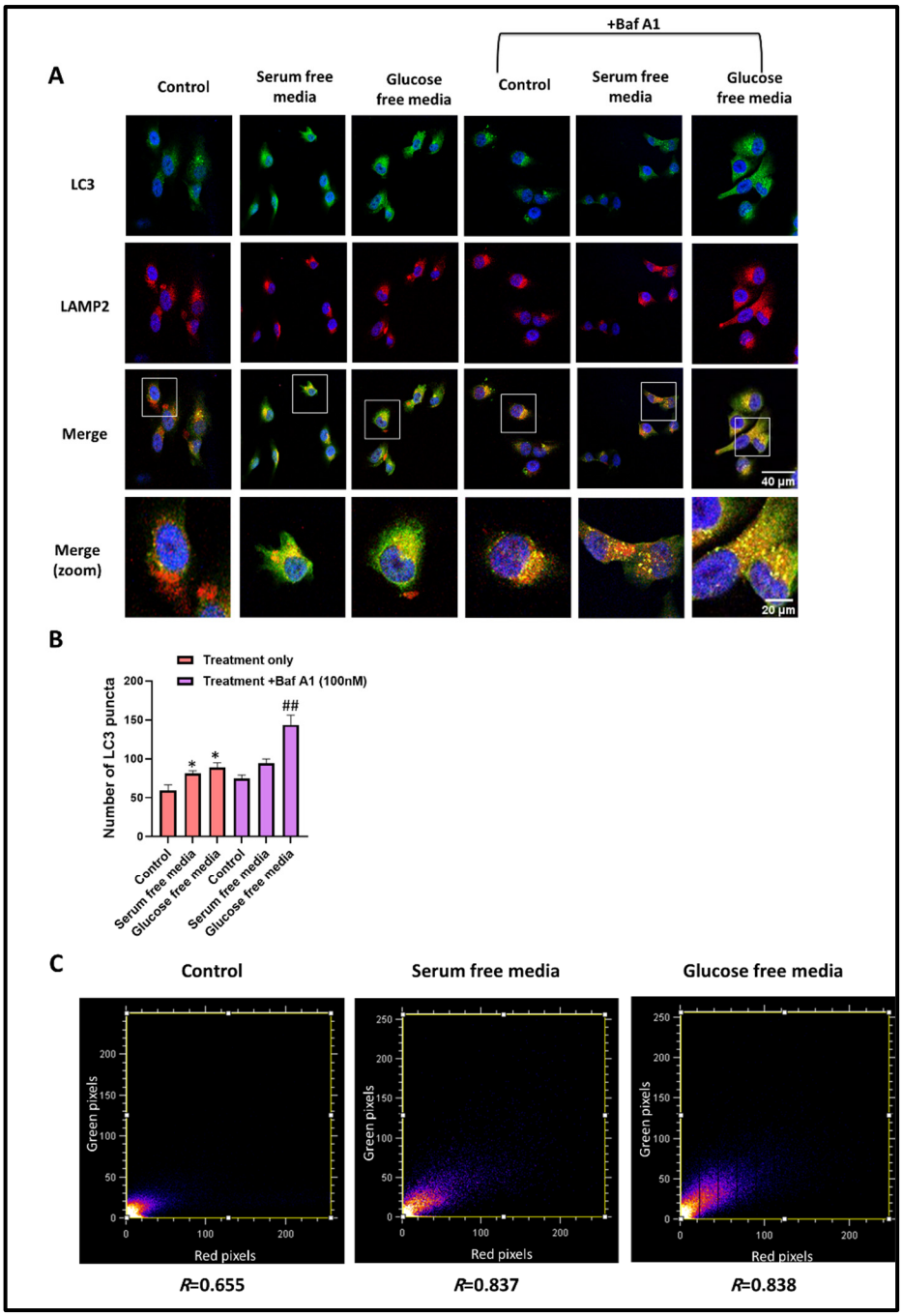

Figure 3.9. Serum and glucose starvation for 1 h with Baf A1 pre-incubation for 2 h enhances LC3 punctate with marked overlap between LC3 and LAMP2 in MDA-MB231 cell line. (A) MDA-MB231 were pre-incubated with control media or media containing Baf A1(100 nM) for 2 h/37°C, then treated with either control media, serum-free, or glucose-free media for 1 h/37°C. Immunofluorescence studies assessed LC3 punctate staining and LC3 and LAMP2 co-localisation. Representative images shown are typical of 3 experiments. Scale bar: 40 µm except for zoomed image: 20 µm **(B)** Statistical analysis of the results shown in **(A)** and represented as mean ± SEM (n = 3). *p<0.05 versus the control, ##p<0.01 versus Baf A1 treatment only. **(C)** Pearson's coefficient for LC3 and LAMP2 co-localisation was calculated using Image J.

3.2.4. Combination of standard chemotherapeutics with specific autophagy inhibitors directed toward major autophagic molecules has marked anti-proliferative activity in both OSCC and TNBC cell models

We examined the anti-proliferative effect of autophagy inhibitors directed towards two major autophagy regulatory complexes (*i.e.,* ULK-1 complex inhibitors and Beclin-1 complex inhibitors). Further, synergy between autophagy inhibitors and standard chemotherapy (Cisplatin for OSCC and Paclitaxel for TNBC) was also assessed. Considering increased levels of autophagy upon 1 h serum or glucose starvation, these studies were also performed after activation of autophagy by pre-incubation of cells with serum or glucose depleted medium (1 h), followed by proliferation assay under serum replete conditions for 72 h.

First, IC_{50} (*i.e.*, concentration at which 50% decrease in viability was observed) for ULK-1 complex inhibitors (*i.e.,* MRT68921 and SBI-0206965), Beclin-1 complex inhibitors (*i.e.,* SAR405 and Spautin-1), Paclitaxel and Cisplatin were determined by incubating the cells under varying concentrations of the drugs for 72 h. IC_{50} values of different agents for SCC25, SCC9, HCC1806 and MDA-MB231 cell lines under nutrient replete medium are shown in **Table 3.1 and 3.2**. IC_{50} values for different agents after 1 h pre-incubation with serum or glucose depleted media for OSCC and TNBC cell lines are shown in **Table 3.3-3.6.** SCC25 showed increased IC_{50} for Cisplatin and decreased IC_{50} for autophagy inhibitors after 1 h serum starvation in comparison to nutrient replete condition. After 1 h glucose starvation, only decreased IC_{50} of MRT68921 and SBI-0206965 was observed compared to nutrient replete condition. Similarly, IC_{50} of Cisplatin was increased after either 1 h serum or glucose starvation in SCC9 cell line compared to nutrient replete

condition. Decreased Spautin-1 IC_{50} was also noted in SCC9 cells after 1 h serum or glucose starvation when compared to nutrient replete condition.

HCC1806 showed decreased IC_{50} for Spautin-1, SAR405 and SBI-0206965 after 1 h serum or glucose starvation in comparison to nutrient replete condition. MDA-MB231 demonstrated increase of Paclitaxel's IC_{50} after 1 h serum starvation and decrease of IC_{50} for both Spautin-1 and SAR405 after 1 h glucose starvation when compared to nutrient replete condition. Altogether, these results indicate that autophagy induction by tumour microenvironmental stressors (*i.e.,* serum or glucose starvation) could lead to development of resistance to standard chemotherapy and sensitisation of tumour cells towards autophagy inhibitors.

Table 3.1. Summary of IC_{50} values for OSCC cell lines obtained from cellular proliferation assay at 72 h time-point in nutrient replete medium. Results are mean ± SEM (n = 3)

	Cisplatin (μM)	Spautin-1 (μM)	SAR405 (μM)	MRT68921 (μM)	SBI-0206965 (μM)
SCC25	2.9 ± 0.4	17.1 ± 5.5	15.8 ± 6.9	1.2 ± 0.5	9.9 ± 1.5
SCC9	17.5 ± 3.7	14.6 ± 0.8	11 ± 1.1	1.9 ± 0.5	7.2 ± 1.2

Table 3.2. Summary of IC_{50} values for TNBC cell lines obtained from cellular proliferation assay at 72 h time-point with nutrient repletion. Results are mean ± SEM (n = 3).

	Paclitaxel (nM)	Spautin-1 (μM)	SAR405 (μM)	MRT68921 (μM)	SBI-0206965 (μM)
HCC1806	3.2 ± 0.6	34.3 ± 15.7	15.9 ± 3.3	1.5 ± 0.4	12.4 ± 4.9
MDA-MB231	0.99 ± 0.2	63.8 ± 22.9	5.9 ± 0.9	0.56 ± 0.07	4.7 ± 0.8

Table 3.3. Summary of IC_{50} values for OSCC cell lines obtained from cellular proliferation assay at 72 h time-point after 1 h serum starvation. Results are mean ± SEM (n = 3).

	Cisplatin (μM)	Spautin-1 (μM)	SAR405 (μM)	MRT68921 (μM)	SBI-0206965 (μM)
SCC25	3.2 ± 0.7	7.6 ± 1.2	13.9 ± 1.8	1.0 ± 0.6	7.8 ± 0.08
SCC9	31.3 ± 1.7	9.6 ± 2.4	48.9 ± 5.5	3.4 ± 0.7	41.7 ± 4.3

Table 3.4. Summary of IC_{50} values for TNBC cell lines obtained from cellular proliferation assay at 72 h time-point after 1 h serum starvation. Results are mean ± SEM (n = 3).

	Paclitaxel (nM)	Spautin-1 (μM)	SAR405 (μM)	MRT68921 (μM)	SBI-0206965 (μM)
HCC1806	1.7 ± 0.3	26.9 ± 6.5	8.3 ± 0.8	2.8 ± 0.4	10.3 ± 1.8
MDA-MB231	1.3 ± 0.3	150.3 ± 16.7	6.1 ± 0.5	1.3 ± 0.1	4.4 ± 0.5

Table 3.5. Summary of IC_{50} values for OSCC cell lines obtained from cellular proliferation assay at 72 h time-point upon 1 h glucose starvation. Results are mean ± SEM (n = 3).

	Cisplatin (μM)	Spautin-1 (μM)	SAR405 (μM)	MRT68921 (μM)	SBI-0206965 (μM)
SCC25	2.1 ± 0.2	5.6 ± 0.7	14.1 ± 0.3	0.34 ± 0.05	5.9 ± 0.4
SCC9	22.4 ± 2.6	12.9 ± 3.5	17.3 ± 0.3	2.9 ± 0.4	35.3 ± 3.4

Table 3.6. Summary of IC_{50} values for TNBC cell lines obtained from cellular proliferation assay at 72hr time-point upon 1 h glucose starvation. Results are mean ± SEM (n = 3).

	Paclitaxel (nM)	Spautin-1 (μM)	SAR405 (μM)	MRT68921 (μM)	SBI-0206965 (μM)
HCC1806	1.3 ± 0.2	5.7 ± 1.8	9.5 ± 0.8	1.9 ± 0.1	7.8 ± 0.6
MDA-MB231	0.45 ± 0.04	53.8 ± 16	4.5 ± 0.6	0.92 ± 0.04	4.7 ± 0.8

Next, combination between standard chemotherapy (*i.e.,* Cisplatin or Paclitaxel) and different autophagy inhibitors was examined for their anti-proliferative potential. These studies were performed either under nutrient replete conditions or after incubation of cells with serum or glucose starved medium for 1 h. These combination studies were performed using Chou-Talalay method at 72 h time point where cells were treated with fixed dose combination of IC_{50} (0.125-8x IC_{50}) for each drug either alone or in combination. The combination index (CI) values were calculated which demonstrates the degree of synergism between two drugs **(Table 3.7)**. Values of CI were determined at concentrations which produce 50% and 75% effect (*i.e.,* ED_{50} and ED_{75}). Moreover, a concentration

response curve was established to show the effect of each drug combination on cell survival across all 4 cell lines used.

Table 3.7. Detailed description of Combination Index (CI) used in combination studies.

Range of CI	Description
<0.1	Very strong synergism
0.1-0.29	Strong synergism
0.3-0.69	Synergism
0.7-0.84	Moderate synergism
0.85-0.89	Slight synergism
0.9-1.09	Nearly additive
1.10-1.19	Slight antagonism
1.2-1.44	Moderate antagonism
1.45-3.29	Antagonism
3.3-10	Strong Antagonism
>10	Very strong antagonism

i. Cisplatin and Beclin-1 complex inhibitors (Spautin-1 and SAR405) combination

- **Cisplatin and SAR405**

In SCC25, combination of Cisplatin with SAR405 under nutrient replete conditions demonstrated a moderate synergism at ED_{50} with significant reduction of cell survival at concentration of 2x IC_{50} in comparison to Cisplatin (p<0.01) and SAR405 (p<0.01) treatment alone. In contrast, same combination showed slight to moderate antagonism at ED_{50} in case where cells were pre-incubated with medium depleted of serum or glucose for 1 h respectively **(Figure 3.10)**.

In SCC9, slight synergism at ED_{50} under nutrient replete media, with a significant (p<0.0001) reduction in cell survival at 1x IC_{50} concentration of combination in comparison to SAR405 treatment was observed (**Figure 3.10**). After pre-incubation of SCC9 cells with either serum or glucose depleted media, there was a synergism to strong synergism observed at ED_{50} between combination of cisplatin and SAR405. Under these latter incubation conditions, there was a significant (p<0.0001-0.01) decrease in cell survival at 1x IC50 concentration of combination compared to either cisplatin or SAR405 alone (**Figure 3.10**).

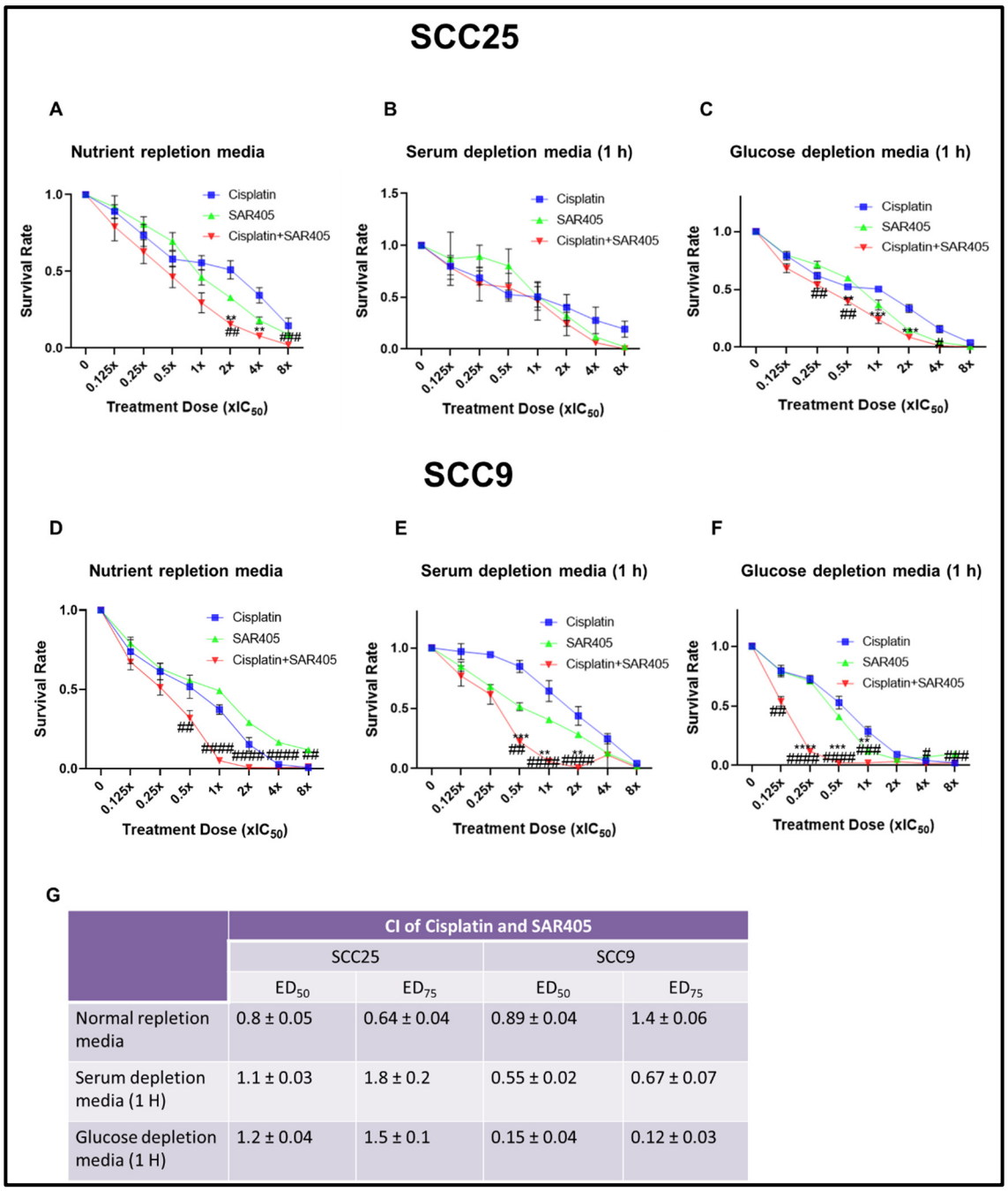

G

	CI of Cisplatin and SAR405			
	SCC25		SCC9	
	ED_{50}	ED_{75}	ED_{50}	ED_{75}
Normal repletion media	0.8 ± 0.05	0.64 ± 0.04	0.89 ± 0.04	1.4 ± 0.06
Serum depletion media (1 H)	1.1 ± 0.03	1.8 ± 0.2	0.55 ± 0.02	0.67 ± 0.07
Glucose depletion media (1 H)	1.2 ± 0.04	1.5 ± 0.1	0.15 ± 0.04	0.12 ± 0.03

Figure 3.10. Dose response curves and CI for Cisplatin and SAR405 in SCC25 and SCC9 cell lines under nutrient replete, serum deplete, and glucose deplete conditions. (A-C) Dose response curve of Cisplatin and SAR405 in SCC25 under nutrient replete, serum deplete, and glucose deplete conditions, respectively. **(D-F)** Dose response curve of Cisplatin and SAR405 in SCC9 under nutrient replete, serum deplete, and glucose deplete conditions, respectively. **(G)** Table is showing combination index (CI) of Cisplatin and SAR405 in SCC25 and SCC9 under nutrient replete, serum deplete, and glucose deplete conditions at ED_{50} and ED_{75}. *p<0.05, **p<0.01, ***p<0.001, ****p<0.0001 versus Cisplatin. #p<0.05, ##p<0.01, ###p<0.001, ####p<0.0001 versus SAR405. Graphs and CI values are mean ± SEM, n=3.

- **Cisplatin and Spautin-1**

Additive effect at ED_{50} was seen in SCC25 when Cisplatin was co-administrated with Spautin-1 under nutrient replete condition, while slight to moderate antagonism was detected after 1 h serum or glucose starvation **(Figure 3.11)**.

At the same time, Cisplatin showed strong synergism with Spautin-1 at ED_{50} in nutrient replete media in SCC9, associated with significant reduction in cell survival at concentrations of 0.25-2.0x IC_{50} compared to either Cisplatin alone (p<0.001) or Spautin-1 alone (p<0.01). Upon 1 h serum starvation, same combination at ED_{50} demonstrated slight antagonism, while moderate synergism was observed after 1 h glucose starvation **(Figure 3.11)**.

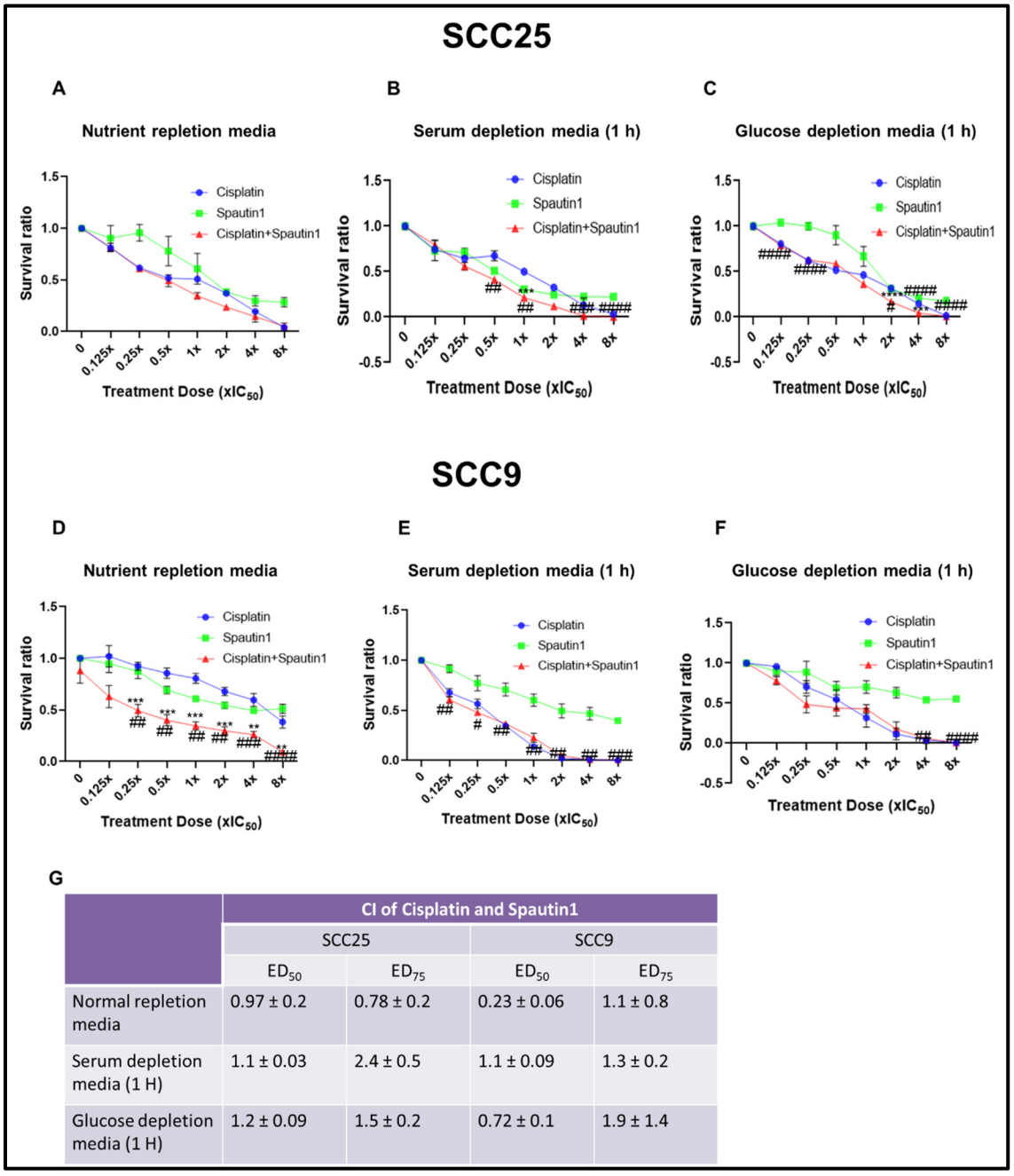

G

	CI of Cisplatin and Spautin1			
	SCC25		SCC9	
	ED_{50}	ED_{75}	ED_{50}	ED_{75}
Normal repletion media	0.97 ± 0.2	0.78 ± 0.2	0.23 ± 0.06	1.1 ± 0.8
Serum depletion media (1 H)	1.1 ± 0.03	2.4 ± 0.5	1.1 ± 0.09	1.3 ± 0.2
Glucose depletion media (1 H)	1.2 ± 0.09	1.5 ± 0.2	0.72 ± 0.1	1.9 ± 1.4

Figure 3.11. Dose response curves and CI for Cisplatin and Spautin-1 in SCC25 and SCC9 cell lines under nutrient replete, serum deplete, and glucose deplete conditions. (A-C) Dose response curve of Cisplatin and Spautin-1 in SCC25 under nutrient replete, serum deplete, and glucose deplete conditions respectively. **(D-F)** Dose response curve of Cisplatin and Spautin-1 in SCC9 under nutrient replete, serum deplete, and glucose deplete conditions respectively. **(G)** Table is showing combination index (CI) of Cisplatin and Spautin-1 in SCC25 and SCC9 under nutrient replete, serum deplete, and glucose deplete conditions at ED_{50} and ED_{75}. **p<0.01, ***p<0.001, ****p<0.0001 versus Cisplatin. #p<0.05, ##p<0.01, ###p<0.001, ####p<0.0001 versus Spautin-1. Graphs and CI values are mean ± SEM, n=3.

ii. Cisplatin and ULK-1 complex inhibitors (MRT68921 and SBI-0206965) combination

- **Cisplatin and MRT68921**

In SCC25, Cisplatin exhibited moderate antagonism at ED_{50} in combination with MRT68921 when cells were incubated under nutrient replete media or pre-incubated with serum- or glucose-depleted media (1 h). Again, in SCC9, slight antagonism and antagonism were seen on combination of Cisplatin with MRT68921 in nutrient replete and glucose deplete (1 h pre-incubation) conditions. On the contrary, after 1 h serum starvation, moderate synergism was observed with significant reduction of cell survival in comparison to Cisplatin treatment alone (p<0.001) at 1-2x IC_{50} concentrations (p<0.01) **(Figure 3.12)**.

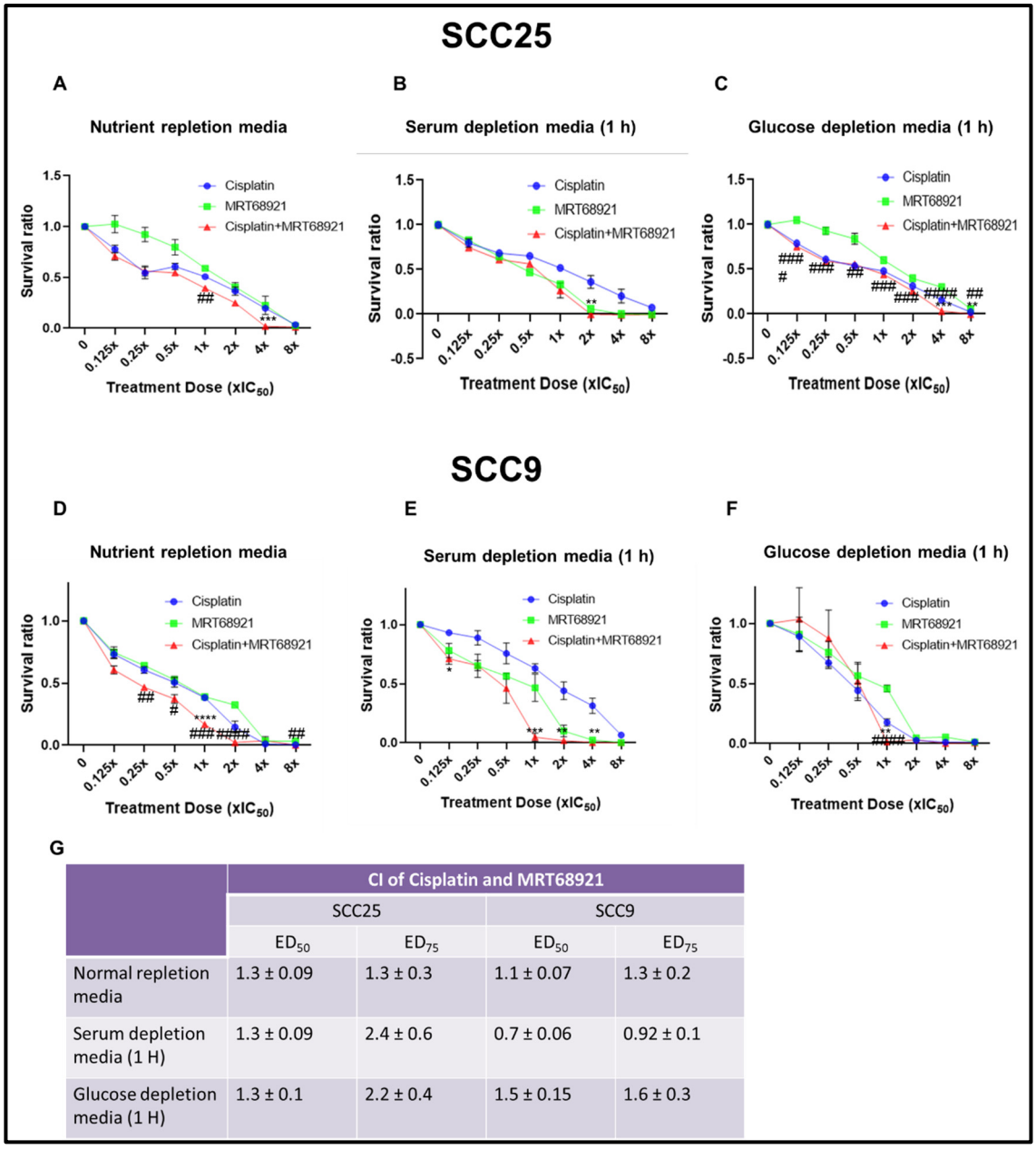

	CI of Cisplatin and MRT68921			
	SCC25		SCC9	
	ED_{50}	ED_{75}	ED_{50}	ED_{75}
Normal repletion media	1.3 ± 0.09	1.3 ± 0.3	1.1 ± 0.07	1.3 ± 0.2
Serum depletion media (1 H)	1.3 ± 0.09	2.4 ± 0.6	0.7 ± 0.06	0.92 ± 0.1
Glucose depletion media (1 H)	1.3 ± 0.1	2.2 ± 0.4	1.5 ± 0.15	1.6 ± 0.3

Figure 3.12. Dose response curves and CI for Cisplatin and MRT68921 in SCC25 and SCC9 cell lines under nutrient replete, serum deplete, and glucose deplete conditions. (A-C) Dose response curve of Cisplatin and MRT68921 in SCC25 under nutrient replete, serum deplete, and glucose deplete conditions respectively. **(D-F)** Dose response curve of Cisplatin and MRT68921 in SCC9 under nutrient replete, serum deplete, and glucose deplete conditions respectively. **(G)** Table is showing combination index (CI) of Cisplatin and MRT68921 in SCC25 and SCC9 under nutrient replete, serum deplete, and glucose deplete conditions at ED_{50} and ED_{75}. **p<0.01, ***p<0.001, ****p<0.0001 versus Cisplatin. #p<0.05, ##p<0.01, ###p<0.001, ####p<0.0001 versus MRT68921. Graphs and CI values are mean ± SEM, n=3.

- **Cisplatin and SBI-0206965**

Cisplatin was antagonistic in combination with SBI-0206965 in SCC25 under nutrient repletion and glucose depletion (1 h pre-incubation) conditions, with nearly additive effect after 1 h serum starvation. Moreover, the same combination showed moderate antagonism in SCC9 after 1 h serum or glucose starvation, although it was synergistic under nutrient replete condition **(Figure 3.13)**.

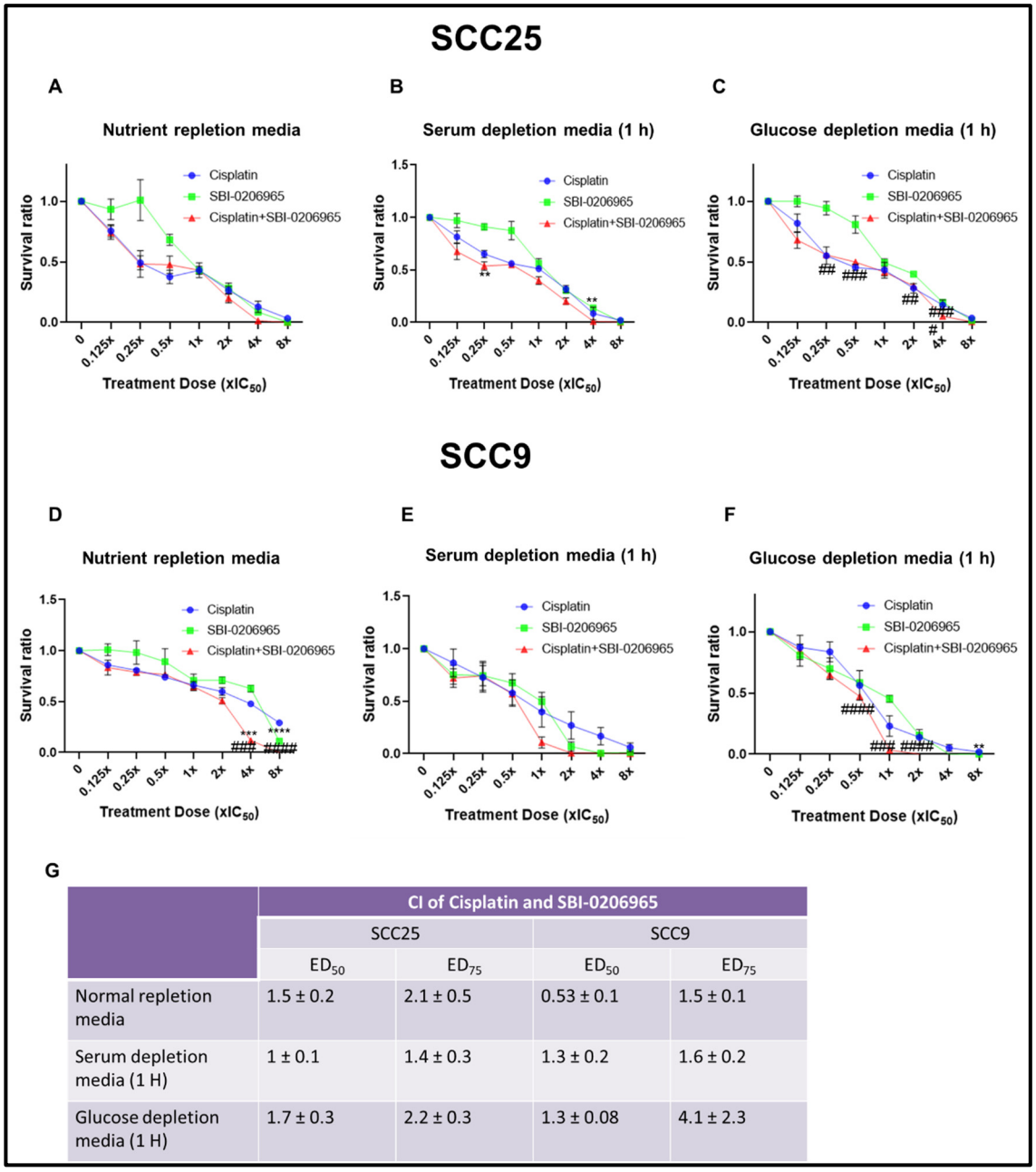

G

	CI of Cisplatin and SBI-0206965			
	SCC25		SCC9	
	ED_{50}	ED_{75}	ED_{50}	ED_{75}
Normal repletion media	1.5 ± 0.2	2.1 ± 0.5	0.53 ± 0.1	1.5 ± 0.1
Serum depletion media (1 H)	1 ± 0.1	1.4 ± 0.3	1.3 ± 0.2	1.6 ± 0.2
Glucose depletion media (1 H)	1.7 ± 0.3	2.2 ± 0.3	1.3 ± 0.08	4.1 ± 2.3

Figure 3.13. Dose response curves and CI for Cisplatin and SBI-0206965 in SCC25 and SCC9 cell lines under nutrient replete, serum deplete, and glucose deplete conditions. (A-C) Dose response curve of Cisplatin and SBI-0206965 in SCC25 under nutrient replete, serum deplete, and glucose deplete conditions respectively. **(D-F)** Dose response curve of Cisplatin and SBI-0206965 in SCC9 under nutrient replete, serum deplete, and glucose deplete conditions respectively. **(G)** Table is showing combination index (CI) of Cisplatin and SBI-0206965 in SCC25 and SCC9 under nutrient replete, serum deplete, and glucose deplete conditions at ED_{50} and ED_{75}. ***p*<0.01, ****p*<0.001, *****p*<0.0001 versus Cisplatin. ##*p*<0.01, ###*p*<0.001, ####*p*<0.0001 versus SBI-0206965. Graphs and CI values are mean ± SEM, n=3.

iii. Paclitaxel and Beclin-1 complex inhibitors (Spautin-1 and SAR405) combination.

- **Paclitaxel and SAR405**

In HCC1806, combination of Paclitaxel and SAR405 showed moderate synergism in nutrient replete condition with significant reduction of cell survival in comparison to SAR405 treatment alone (p<0.01). However, after 1 h serum or glucose starvation the same combination established moderate or slight antagonist, respectively **(Figure 3.14)**.

In MDA-MBA231, Synergism and moderate synergism at ED_{50} were observed on combination of Paclitaxel and SAR405 nutrient replete conditions or when cells were pre-incubated with serum deplete media (1 h), respectively. A significant reduction of cell survival was noted at 2x IC_{50} concentration in contrast to Paclitaxel alone (p<0.01) and SAR405 alone (p<0.0001) under nutrient replete condition. In contrast, after 1 h glucose starvation, Paclitaxel was antagonist with SAR405 **(Figure 3.14)**.

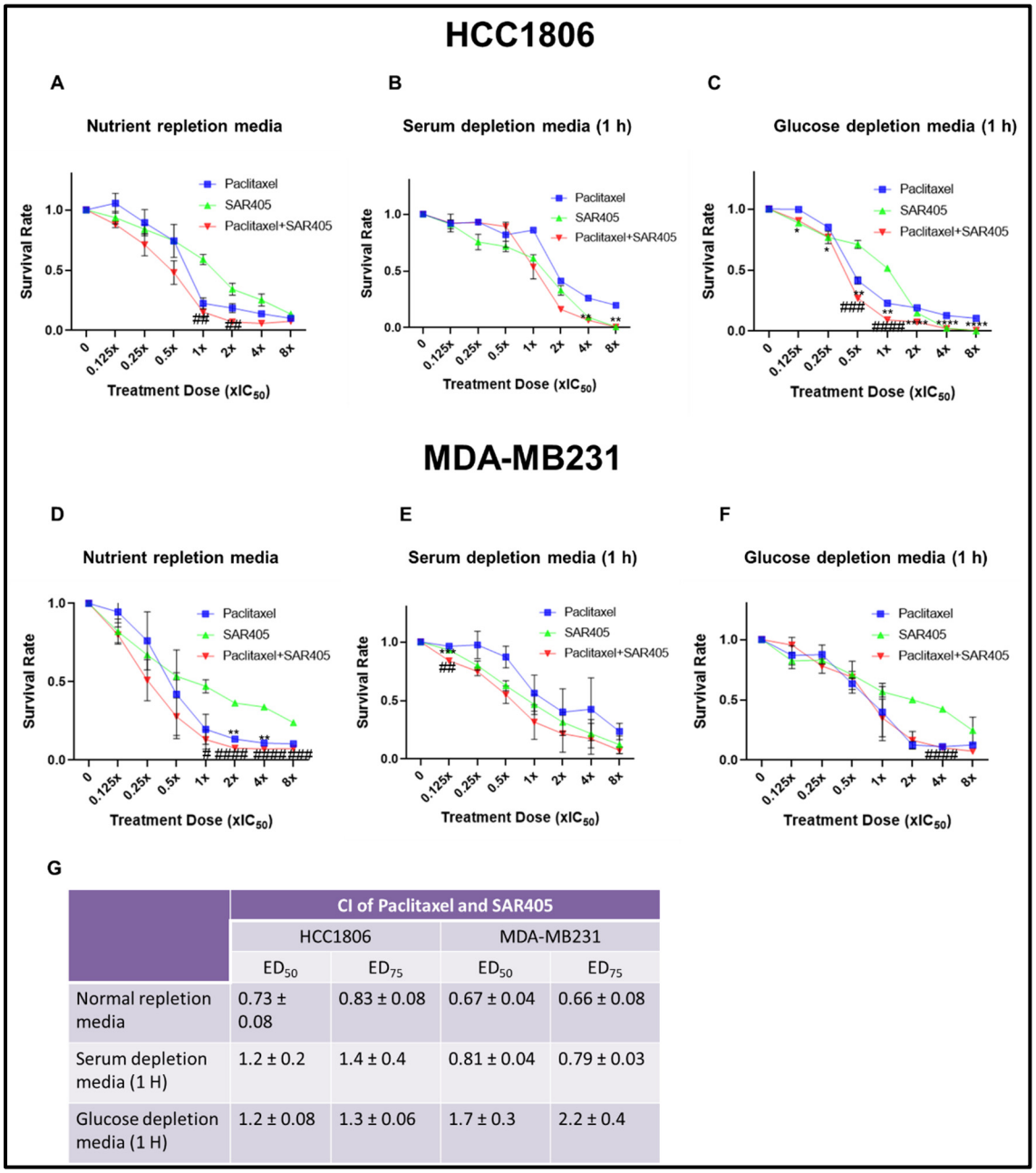

G

	CI of Paclitaxel and SAR405			
	HCC1806		MDA-MB231	
	ED_{50}	ED_{75}	ED_{50}	ED_{75}
Normal repletion media	0.73 ± 0.08	0.83 ± 0.08	0.67 ± 0.04	0.66 ± 0.08
Serum depletion media (1 H)	1.2 ± 0.2	1.4 ± 0.4	0.81 ± 0.04	0.79 ± 0.03
Glucose depletion media (1 H)	1.2 ± 0.08	1.3 ± 0.06	1.7 ± 0.3	2.2 ± 0.4

Figure 3.14. Dose response curves and CI for Paclitaxel and SAR405 in HCC1806 and MDA-MB231 cell lines under nutrient replete, serum deplete, and glucose deplete conditions. (A-C) Dose response curve of Paclitaxel and SAR405 in HCC1806 under nutrient replete, serum deplete, and glucose deplete conditions respectively. **(D-F)** Dose response curve of Paclitaxel and SAR405 in MDA-MB231 under nutrient replete, serum deplete, and glucose deplete conditions respectively. **(G)** Table is showing combination index (CI) of Paclitaxel and SAR405 in HCC1806 and MDA-MB231 under nutrient replete, serum deplete, and glucose deplete conditions at ED_{50} and ED_{75}. **p<0.01, ***p<0.001, ****p<0.0001 versus Paclitaxel. #p<0.05, ##p<0.01, ###p<0.001, ####p<0.0001 versus SAR405. Graphs and CI values are mean ± SEM, n=3.

- **Paclitaxel and Spautin-1**

Paclitaxel was shown to be slightly synergistic with Spautin-1 in HCC1806 cells in nutrient replete condition with significant decrease in cell survival at 0.125-0.5x IC_{50} (p<0.0001-0.01) in comparison to Paclitaxel alone. After pre-treatment with serum or glucose depleted media for 1 h, this combination was nearly additive and slightly antagonist. Likewise, combination of Paclitaxel and Spautin-1 was slight-moderately antagonistic in MDA-MB231 under all conditions **(Figure 3.15)**.

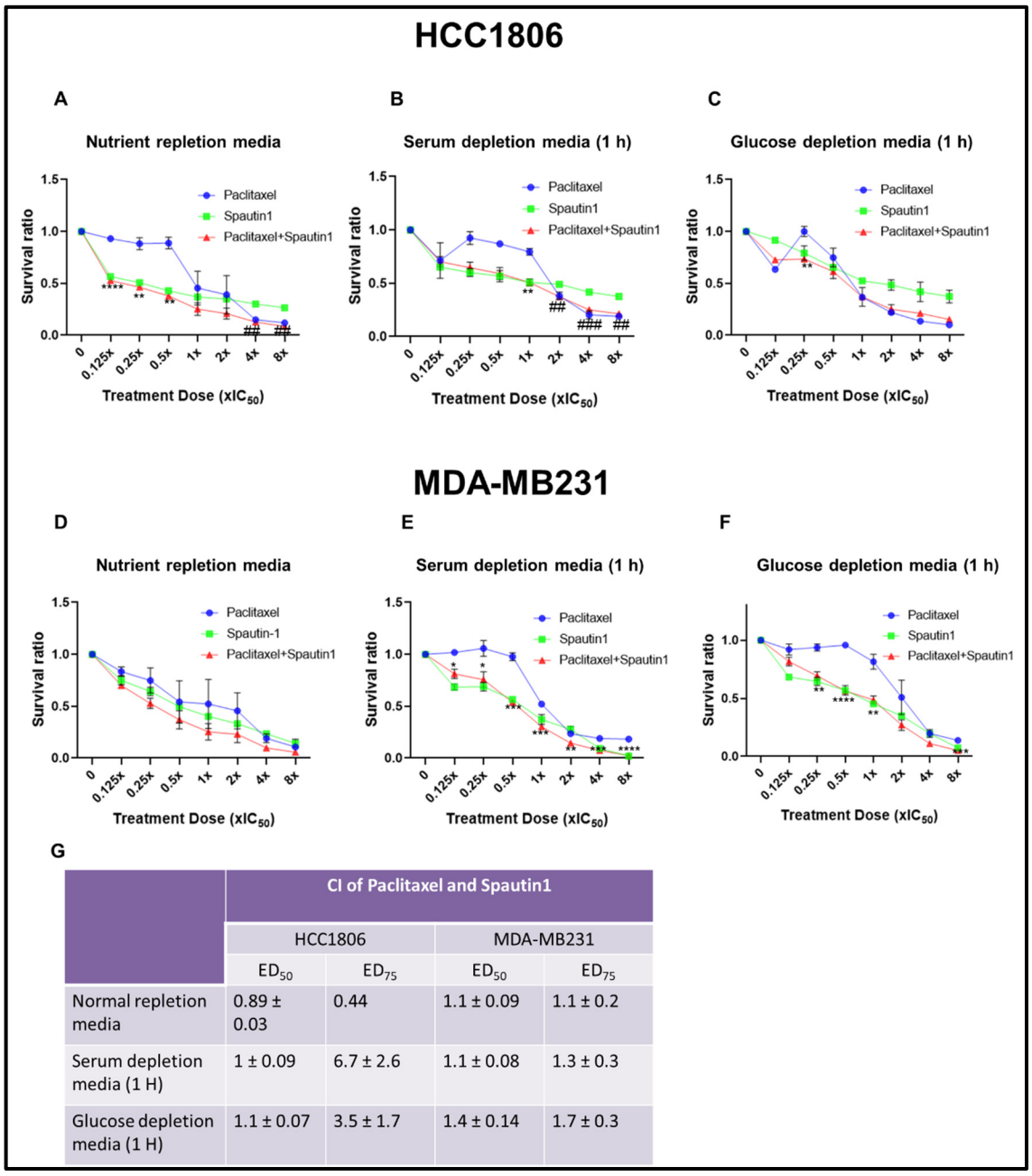

	CI of Paclitaxel and Spautin1			
	HCC1806		MDA-MB231	
	ED_{50}	ED_{75}	ED_{50}	ED_{75}
Normal repletion media	0.89 ± 0.03	0.44	1.1 ± 0.09	1.1 ± 0.2
Serum depletion media (1 H)	1 ± 0.09	6.7 ± 2.6	1.1 ± 0.08	1.3 ± 0.3
Glucose depletion media (1 H)	1.1 ± 0.07	3.5 ± 1.7	1.4 ± 0.14	1.7 ± 0.3

Figure 3.15. Dose response curves and CI for Paclitaxel and Spautin-1 in HCC1806 and MDA-MB231 cell lines under nutrient replete, serum deplete, and glucose deplete conditions. (A-C) Dose response curve of Paclitaxel and Spautin-1 in HCC1806 under nutrient replete, serum deplete, and glucose deplete conditions respectively. **(D-F)** Dose response curve of Paclitaxel and Spautin-1 in MDA-MB231 under nutrient replete, serum deplete, and glucose deplete conditions respectively. **(G)** Table is showing combination index (CI) of Paclitaxel and Spautin-1 in HCC1806 and MDA-MB231 under nutrient replete, serum deplete, and glucose deplete conditions at ED_{50} and ED_{75}. ***p*<0.01, ****p*<0.001, *****p*<0.0001 versus Paclitaxel. ##*p*<0.01, ###*p*<0.001 versus Spautin-1. Graphs and CI values are mean ± SEM, n=3.

iv. Paclitaxel and ULK-1 complex inhibitors (MRT68921 and SBI-0206965) combination

- **Paclitaxel and MRT68921**

When Paclitaxel was combined with MRT68921 in HCC1806 cells, it was synergistic with significant reduction in cell survival at 1-2x IC_{50} (p<0.0001-0.001) in comparison to MRT68921 treatment alone. On the other hand, this combination was moderately antagonist in the same cell line after pre-incubation with serum or glucose depleted medium. On the other hand, in MDA-MB231 cells, the same combination was nearly additive under nutrient replete conditions, while moderate antagonism was observed when cells were pre-incubated in serum or glucose depleted media **(Figure 3.16)**.

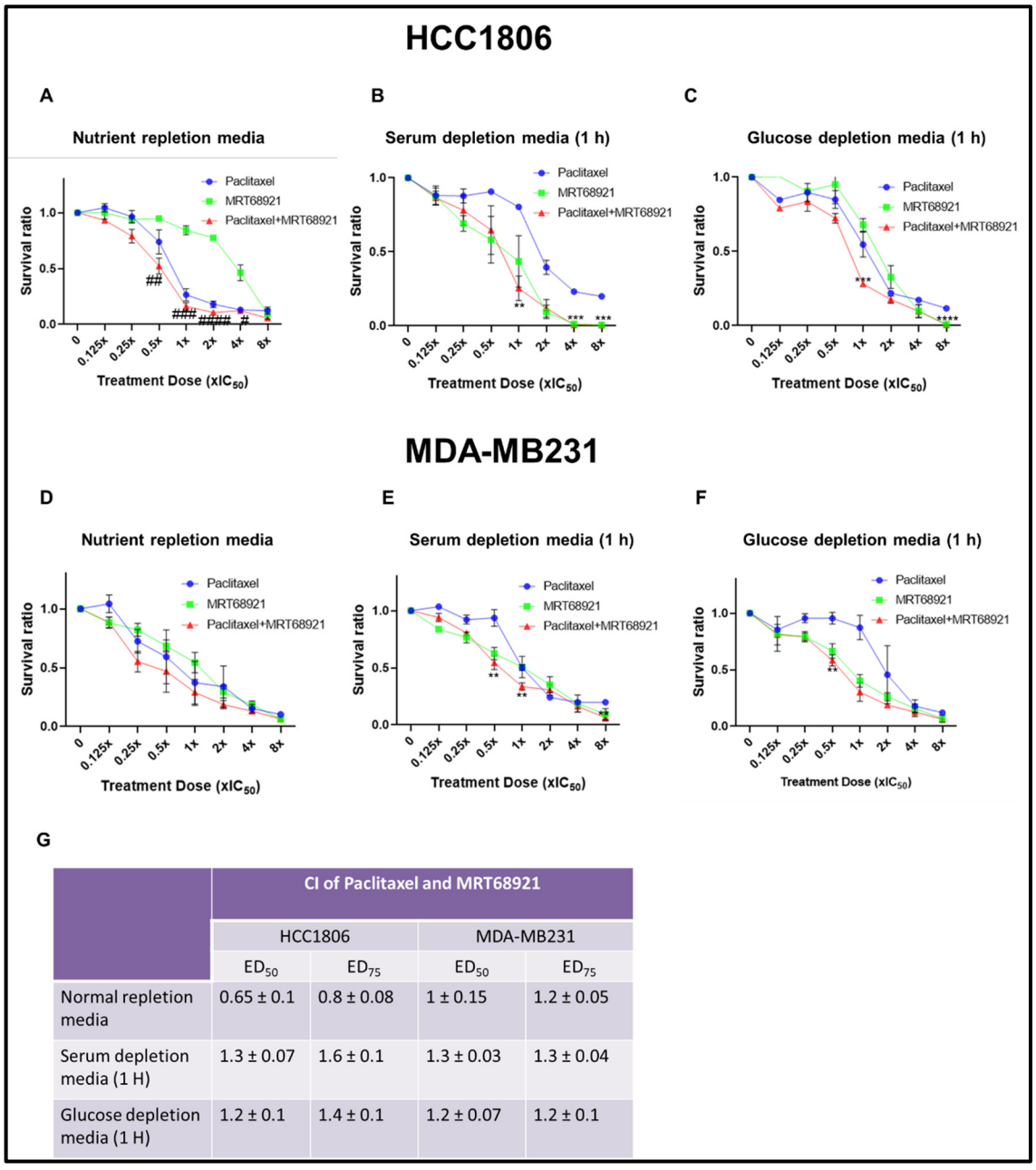

G

	CI of Paclitaxel and MRT68921			
	HCC1806		MDA-MB231	
	ED_{50}	ED_{75}	ED_{50}	ED_{75}
Normal repletion media	0.65 ± 0.1	0.8 ± 0.08	1 ± 0.15	1.2 ± 0.05
Serum depletion media (1 H)	1.3 ± 0.07	1.6 ± 0.1	1.3 ± 0.03	1.3 ± 0.04
Glucose depletion media (1 H)	1.2 ± 0.1	1.4 ± 0.1	1.2 ± 0.07	1.2 ± 0.1

Figure 3.16. Dose response curves and CI for Paclitaxel and MRT68921 in HCC1806 and MDA-MB231 cell lines under nutrient replete, serum deplete, and glucose deplete conditions. (A-C) Dose response curve of Paclitaxel and MRT68921 in HCC1806 under nutrient replete, serum deplete, and glucose deplete conditions respectively. **(D-F)** Dose response curve of Paclitaxel and MRT68921 in MDA-MB231 under nutrient replete, serum deplete, and glucose deplete conditions respectively. **(G)** Table is showing combination index (CI) of Paclitaxel and MRT68921 in HCC1806 and MDA-MB231 under nutrient replete, serum deplete, and glucose deplete conditions at ED_{50} and ED_{75}. ***p*<0.01, ****p*<0.001, *****p*<0.0001 versus Paclitaxel. #*p*<0.05, ##*p*<0.01, ###*p*<0.001, ####*p*<0.0001 versus MRT68921. Graphs and CI values are mean ± SEM, n=3.

- **Paclitaxel and SBI-0206965**

In both HCC1806 and MDA-MB231 cells, combination of Paclitaxel with SBI-0206965 demonstrated antagonism and moderate antagonism, respectively. After 1 h pre-incubation with serum or glucose depleted media, slight to moderate antagonism was observed in both cell lines. Notably, under nutrient replete conditions, significant reduction in cell survival at 1-2x IC_{50} concentrations ($p<0.0001$-0.05) was observed compared to SBI-0206965 or Paclitaxel alone in MDA-MB231 cells **(Figure 3.17)**.

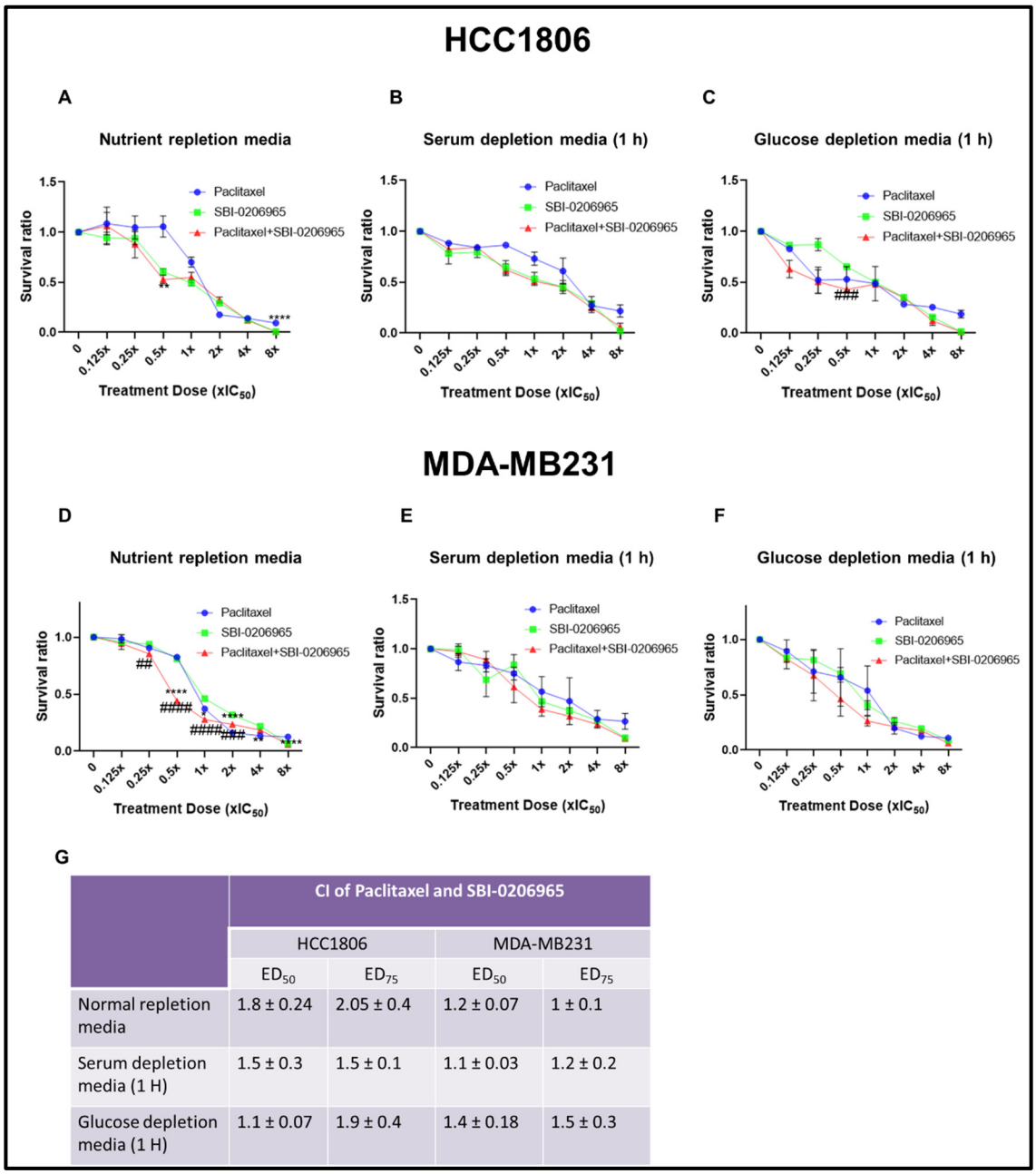

G

	CI of Paclitaxel and SBI-0206965			
	HCC1806		MDA-MB231	
	ED_{50}	ED_{75}	ED_{50}	ED_{75}
Normal repletion media	1.8 ± 0.24	2.05 ± 0.4	1.2 ± 0.07	1 ± 0.1
Serum depletion media (1 H)	1.5 ± 0.3	1.5 ± 0.1	1.1 ± 0.03	1.2 ± 0.2
Glucose depletion media (1 H)	1.1 ± 0.07	1.9 ± 0.4	1.4 ± 0.18	1.5 ± 0.3

Figure 3.17. Dose response curves and CI for Paclitaxel and SBI-0206965 in HCC1806 and MDA-MB231 cell lines under nutrient replete, serum deplete, and glucose deplete conditions. (A-C) Dose response curve of Paclitaxel and SBI-0206965 in HCC1806 under nutrient replete, serum deplete, and glucose deplete conditions respectively. **(D-F)** Dose response curve of Paclitaxel and SBI-0206965 in MDA-MB231 under nutrient replete, serum deplete, and glucose deplete conditions respectively. **(G)** Table is showing combination index (CI) of Paclitaxel and SBI-0206965 in HCC1806 and MDA-MB231 under nutrient replete, serum deplete, and glucose deplete conditions at ED_{50} and ED_{75}. **p<0.01, ****p<0.0001 versus Paclitaxel. ##p<0.01, ###p<0.001, ####p<0.0001 versus SBI-0206965. Graphs and CI values are mean ± SEM, n=3.

3.2.5. Combination of Beclin-1 complex inhibitors (SAR405 and Spautin-1) and ULK-I complex inhibitors (MRT68921 and SBI-0206965) reduce cellular proliferation in both OSCC and TNBC cell models in a dose dependent manner.

- **SAR405 and MRT68921**

SAR405 was synergistic in combination with MRT68921in all 4 cell lines used under nutrient replete conditions. A similar effect was also observed after pre-incubation of cells with serum or glucose deplete media, except in SCC25 where it was moderately synergistic following 1 h glucose starvation. A significant reduction of cell survival across both OSCC and TNBC cell models was observed upon combination of SAR405 and MRT68921 in comparison to either standalone SAR405 or MRT68921 treatment **(Figure 3.18 & 19)**.

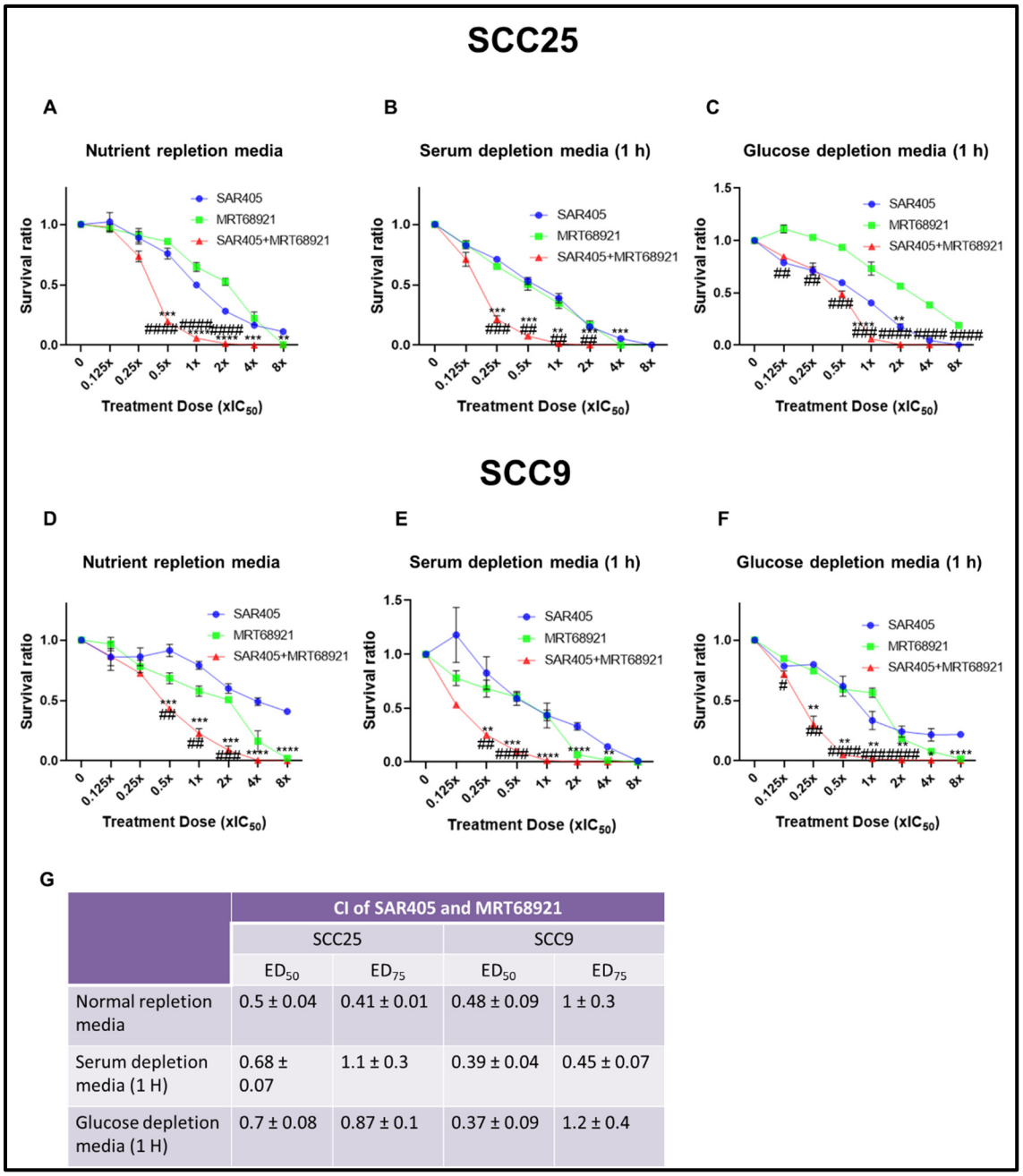

G

	CI of SAR405 and MRT68921			
	SCC25		SCC9	
	ED_{50}	ED_{75}	ED_{50}	ED_{75}
Normal repletion media	0.5 ± 0.04	0.41 ± 0.01	0.48 ± 0.09	1 ± 0.3
Serum depletion media (1 H)	0.68 ± 0.07	1.1 ± 0.3	0.39 ± 0.04	0.45 ± 0.07
Glucose depletion media (1 H)	0.7 ± 0.08	0.87 ± 0.1	0.37 ± 0.09	1.2 ± 0.4

Figure 3.18. Dose response curves and CI for SAR405 and MRT68921 in SCC25 and SCC9 cell lines under nutrient replete, serum deplete, and glucose deplete conditions. (A-C) Dose response curve of SAR405 and MRT68921 in SCC25 under nutrient replete, serum deplete, and glucose deplete conditions respectively. **(D-F)** Dose response curve of SAR405 and MRT68921 in SCC9 under nutrient replete, serum deplete, and glucose deplete conditions respectively. **(G)** Table is showing combination index (CI) of SAR405 and MRT68921 in SCC25 and SCC9 under nutrient replete, serum deplete, and glucose deplete conditions at ED_{50} and ED_{75}. *p<0.05, **p<0.01, ***p<0.001, ****p<0.0001 versus SAR405. #p<0.05, ##p<0.01, ###p<0.001, ####p<0.0001 versus MRT68921. Graphs and CI values are mean ± SEM, n=3.

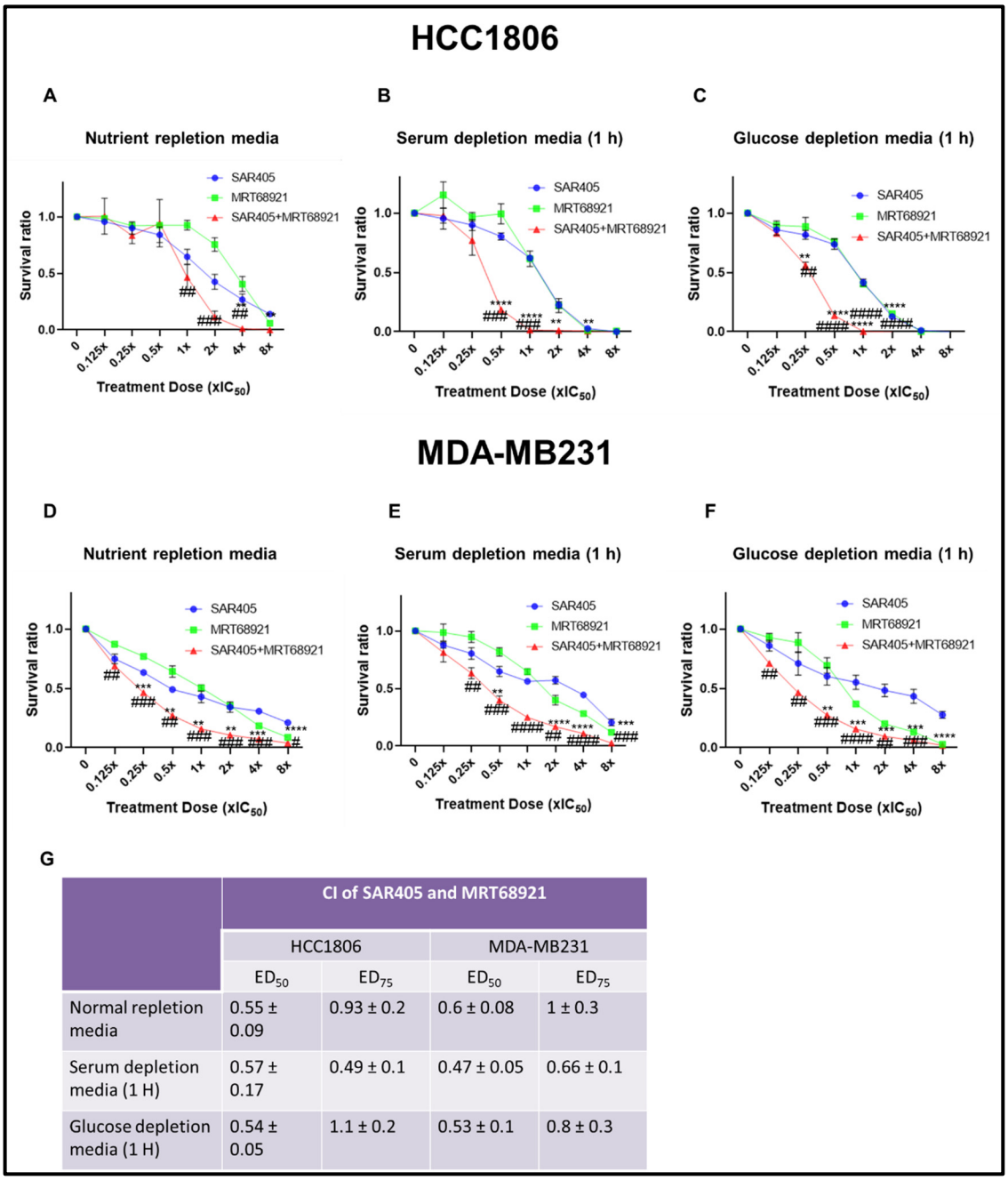

G

	CI of SAR405 and MRT68921			
	HCC1806		MDA-MB231	
	ED_{50}	ED_{75}	ED_{50}	ED_{75}
Normal repletion media	0.55 ± 0.09	0.93 ± 0.2	0.6 ± 0.08	1 ± 0.3
Serum depletion media (1 H)	0.57 ± 0.17	0.49 ± 0.1	0.47 ± 0.05	0.66 ± 0.1
Glucose depletion media (1 H)	0.54 ± 0.05	1.1 ± 0.2	0.53 ± 0.1	0.8 ± 0.3

Figure 3.19. Dose response curves and CI for SAR405 and MRT68921 in HCC1806 and MDA-MB231 cell lines under nutrient replete, serum deplete, and glucose deplete conditions. (A-C) Dose response curve of SAR405 and MRT68921 in HCC1806 under nutrient replete, serum deplete, and glucose deplete conditions respectively. **(D-F)** Dose response curve of SAR405 and MRT68921 in MDA-MB231 under nutrient replete, serum deplete, and glucose deplete conditions respectively. **(G)** Table is showing combination index (CI) of SAR405 and MRT68921 in HCC1806 and MDA-MB231 under nutrient replete, serum deplete, and glucose deplete conditions at ED_{50} and ED_{75}. ***p*<0.01, ****p*<0.001, *****p*<0.0001 versus SAR405. #*p*<0.05, ##*p*<0.01, ###*p*<0.001, ####*p*<0.0001 versus MRT68921. Graphs and CI values are mean ± SEM, n=3.

- **SAR405 and SBI-0206965**

In SCC25, moderate antagonism was seen in combination of SAR405 with SBI-0206965 under nutrient deplete condition. In contrast, this combination demonstrated moderate synergism after 1 h pre-incubation with serum depleted media in the same cell line, with a significant reduction of cell survival compared to either SAR405 or SBI-0206965 alone. Moreover, this combination was nearly additive after 1 h pre-incubation with glucose depleted media, with a significant decrease in cell survival at all concentrations in comparison to SBI-0206965 treatment only **(Figure 3.20)**.

On the other hand, SAR405 was synergistic in combination with SBI-0206965 under nutrient replete conditions in SCC9 cells, while a slightly antagonistic effect was observed after 1 h pre-incubation with serum depleted media. A nearly additive effect was observed with this combination when cells were pre-incubated with glucose depleted media for 1 h **(Figure 3.20)**.

This combination also showed slight synergism in HCC1806 cells under nutrient replete conditions, while antagonism and moderate antagonism was observed after 1 h pre-incubation with serum or glucose depleted media, respectively. In MDA-MB231 cells, SAR405 and SBI-0206965 combination was moderately synergistic under all incubation conditions with significant reduction of cell survival especially at high concentrations (4-8x IC_{50}) in comparison to both SAR405 and SBI-0206965 alone, except, after 1 h glucose starvation where moderate antagonism was observed **(Figure 3.21)**.

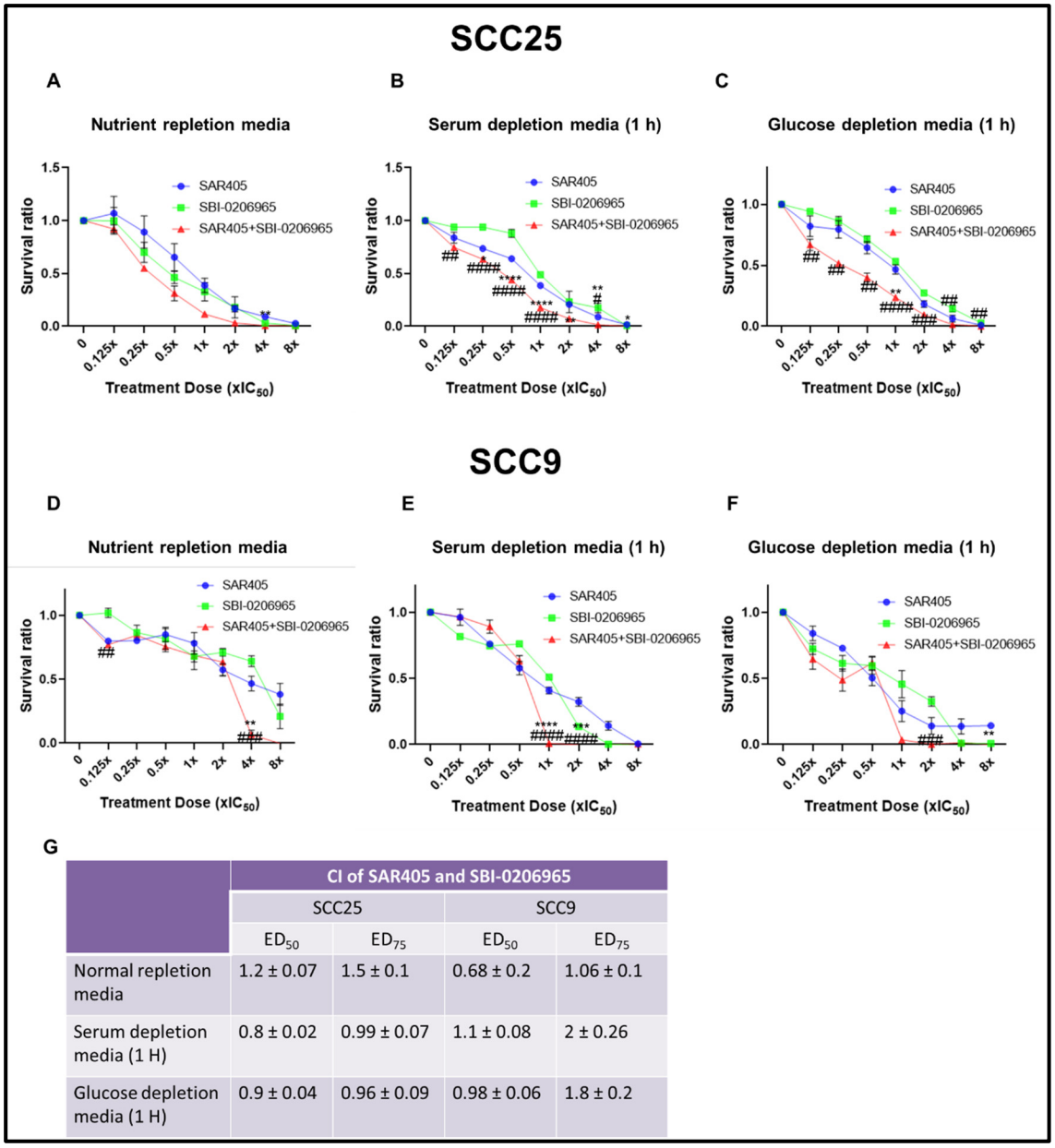

G

	CI of SAR405 and SBI-0206965			
	SCC25		SCC9	
	ED_{50}	ED_{75}	ED_{50}	ED_{75}
Normal repletion media	1.2 ± 0.07	1.5 ± 0.1	0.68 ± 0.2	1.06 ± 0.1
Serum depletion media (1 H)	0.8 ± 0.02	0.99 ± 0.07	1.1 ± 0.08	2 ± 0.26
Glucose depletion media (1 H)	0.9 ± 0.04	0.96 ± 0.09	0.98 ± 0.06	1.8 ± 0.2

Figure 3.20. Dose response curves and CI for SAR405 and SBI-0206965 in SCC25 and SCC9 cell lines under nutrient replete, serum deplete, and glucose deplete conditions. (A-C) Dose response curve of SAR405 and SBI-0206965 in SCC25 under nutrient replete, serum deplete, and glucose deplete conditions respectively. **(D-F)** Dose response curve of SAR405 and SBI-0206965 in SCC9 under nutrient replete, serum deplete, and glucose deplete conditions respectively. **(G)** Table is showing combination index (CI) of SAR405 and SBI-0206965 in SCC25 and SCC9 under nutrient replete, serum deplete, and glucose deplete conditions at ED_{50} and ED_{75}. *p<0.05, **p<0.01, ***p<0.001, ****p<0.0001 versus SAR405. ##p<0.01, ###p<0.001, ####p<0.0001 versus SBI-0206965. Graphs and CI values are mean ± SEM, n=3.

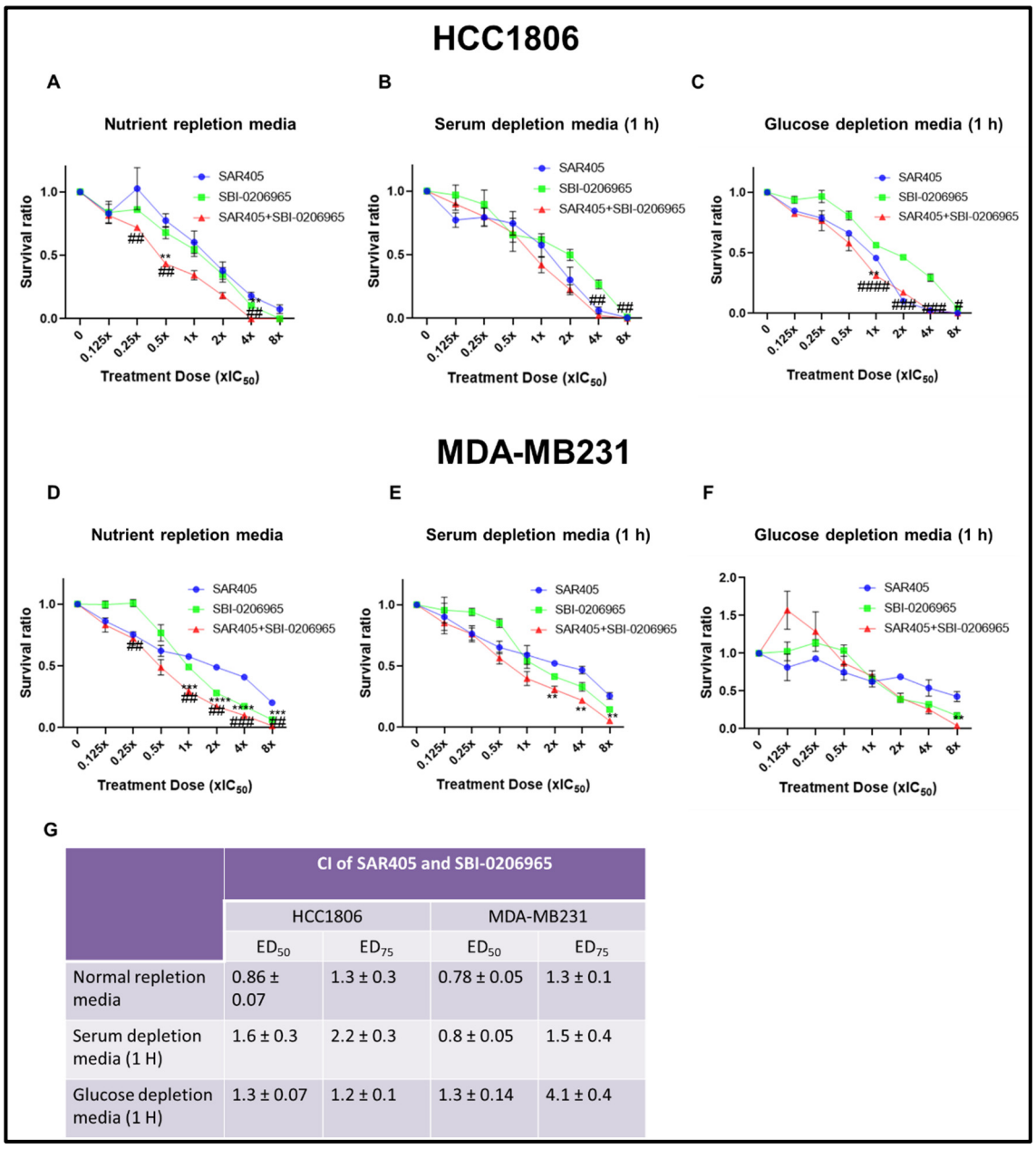

G

	CI of SAR405 and SBI-0206965			
	HCC1806		MDA-MB231	
	ED_{50}	ED_{75}	ED_{50}	ED_{75}
Normal repletion media	0.86 ± 0.07	1.3 ± 0.3	0.78 ± 0.05	1.3 ± 0.1
Serum depletion media (1 H)	1.6 ± 0.3	2.2 ± 0.3	0.8 ± 0.05	1.5 ± 0.4
Glucose depletion media (1 H)	1.3 ± 0.07	1.2 ± 0.1	1.3 ± 0.14	4.1 ± 0.4

Figure 3.21. Dose response curves and CI for SAR405 and SBI-0206965 in HCC1806 and MDA-MB231 cell lines under nutrient replete, serum deplete, and glucose deplete conditions. (A-C) Dose response curve of SAR405 and SBI-0206965 in HCC1806 under nutrient replete, serum deplete, and glucose deplete conditions respectively. **(D-F)** Dose response curve of SAR405 and SBI-0206965 in MDA-MB231 under nutrient replete, serum deplete, and glucose deplete conditions respectively. **(G)** Table is showing combination index (CI) of SAR405 and SBI-0206965 in HCC1806 and MDA-MB231 under nutrient replete, serum deplete, and glucose deplete conditions at ED_{50} and ED_{75}. ***p*<0.01, ****p*<0.001, *****p*<0.0001 versus SAR405. #*p*<0.05, ##*p*<0.01, ###*p*<0.001, ####*p*<0.0001 versus SBI-0206965. Graphs and CI values are mean ± SEM, n=3.

- **Spautin-1 and MRT68921**

Spautin-1 had shown moderate antagonism when combined with MRT68921 in SCC25 cell line under nutrient replete condition and it was nearly additive upon 1 h pre-incubation with serum depleted media, associated with significant reduction of cell survival at 1-2x IC_{50} concentrations (p<0.001) compared to MRT68921 treatment alone and at 2x IC_{50} concentration (p<0.0001) in comparison to Spautin-1 alone. In contrast, this combination showed moderate synergism after 1 h pre-incubation with glucose depleted media **(Figure 3.22).**

In SCC9 cells, synergism was observed when Spautin-1 was combined with MRT68921 under nutrient replete conditions or after pre-incubation with serum deplete media, with significant decrease in cell survival at 2x IC_{50} compared to either Spautin-1 alone (p<0.01) or MRT68921 alone (p<0.001). However, this combination was moderately antagonistic after 1 h pre-incubation with glucose depleted media **(Figure 3.22).**

Likewise, HCC1806 exhibited synergism when Spautin-1 and MRT68921 were co-administrated under nutrient replete conditions, or after pre-incubation with serum or glucose deplete medium. A significant reduction of cell proliferation was noted at 1-2x IC_{50} concentrations (p<0.01) when compared to MRT68921 or Spautin-1 treatment alone in nutrient replete conditions or after pre-incubation with serum deplete media, respectively. After 1 h glucose depletion, a significant decrease in HCC1806 proliferation was observed at 1-2x IC_{50} concentration compared to Spautin-1 alone (p<0.0001-0.01) and at 1x IC_{50} concentration compared to MRT68921 alone (p<0.001) **(Figure 3.23)**.

MDA-MB231 displayed moderate synergism upon combination of Spautin-1 and MRT68921 under all incubation conditions. A significant decrease in MDA-MB231 cell survival was seen at 1-2x IC_{50} concentrations in comparison to Spautin-1 alone (p<0.001) and at 2x IC_{50} compared to MRT68921 alone (p<0.01) under nutrient replete condition. A 1 h pre-incubation with serum depleted media exhibited a significant reduction of cell survival at 1-2x IC_{50} concentrations in comparison to standalone treatment with MRT68921 (p<0.0001) or Spautin-1 (p<0.0001-0.01). Same effect was detected after 1 h pre-incubation with glucose depleted medium at 1-2x IC_{50} concentrations when compared to MRT68921 (p<0.001) or Spautin-1 alone (p<0.0001-0.01) **(Figure 3.23)**

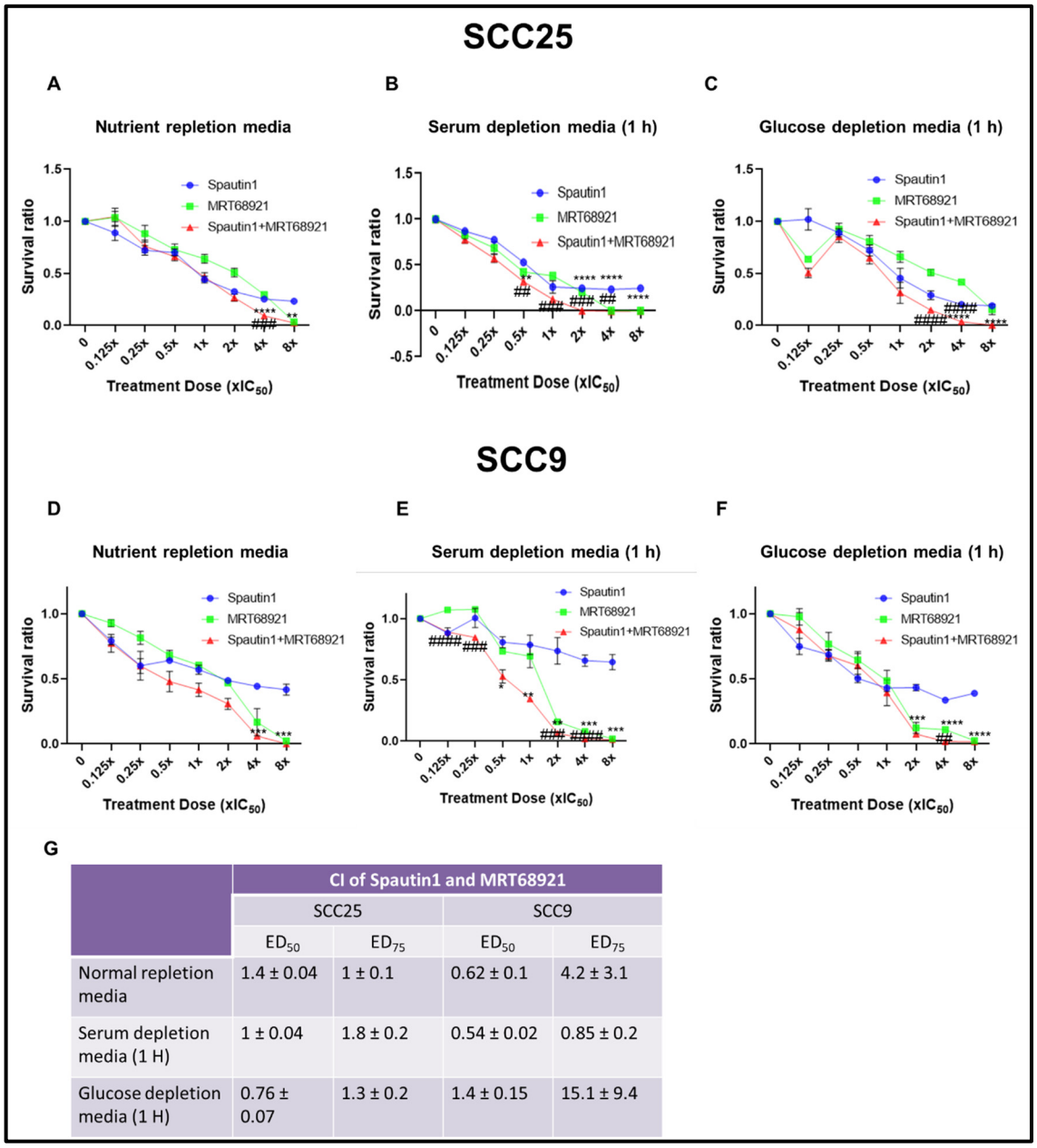

G

	CI of Spautin1 and MRT68921			
	SCC25		SCC9	
	ED_{50}	ED_{75}	ED_{50}	ED_{75}
Normal repletion media	1.4 ± 0.04	1 ± 0.1	0.62 ± 0.1	4.2 ± 3.1
Serum depletion media (1 H)	1 ± 0.04	1.8 ± 0.2	0.54 ± 0.02	0.85 ± 0.2
Glucose depletion media (1 H)	0.76 ± 0.07	1.3 ± 0.2	1.4 ± 0.15	15.1 ± 9.4

Figure 3.22. Dose response curves and CI for Spautin-1 and MRT68921 in SCC25 and SCC9 cell lines under nutrient replete, serum deplete, and glucose deplete conditions. (A-C) Dose response curve of Spautin-1 and MRT68921 in SCC25 under nutrient replete, serum deplete, and glucose deplete conditions respectively. **(D-F)** Dose response curve of Spautin-1 and MRT68921 in SCC9 under nutrient replete, serum deplete, and glucose deplete conditions respectively. **(G)** Table is showing combination index (CI) of Spautin-1 and MRT68921 in SCC25 and SCC9 under nutrient replete, serum deplete, and glucose deplete conditions at ED_{50} and ED_{75}. *p<0.05, **p<0.01, ***p<0.001, ****p<0.0001 versus Spautin-1. ##p<0.01, ###p<0.001, ####p<0.0001 versus MRT68921. Graphs and CI values are mean ± SEM, n=3.

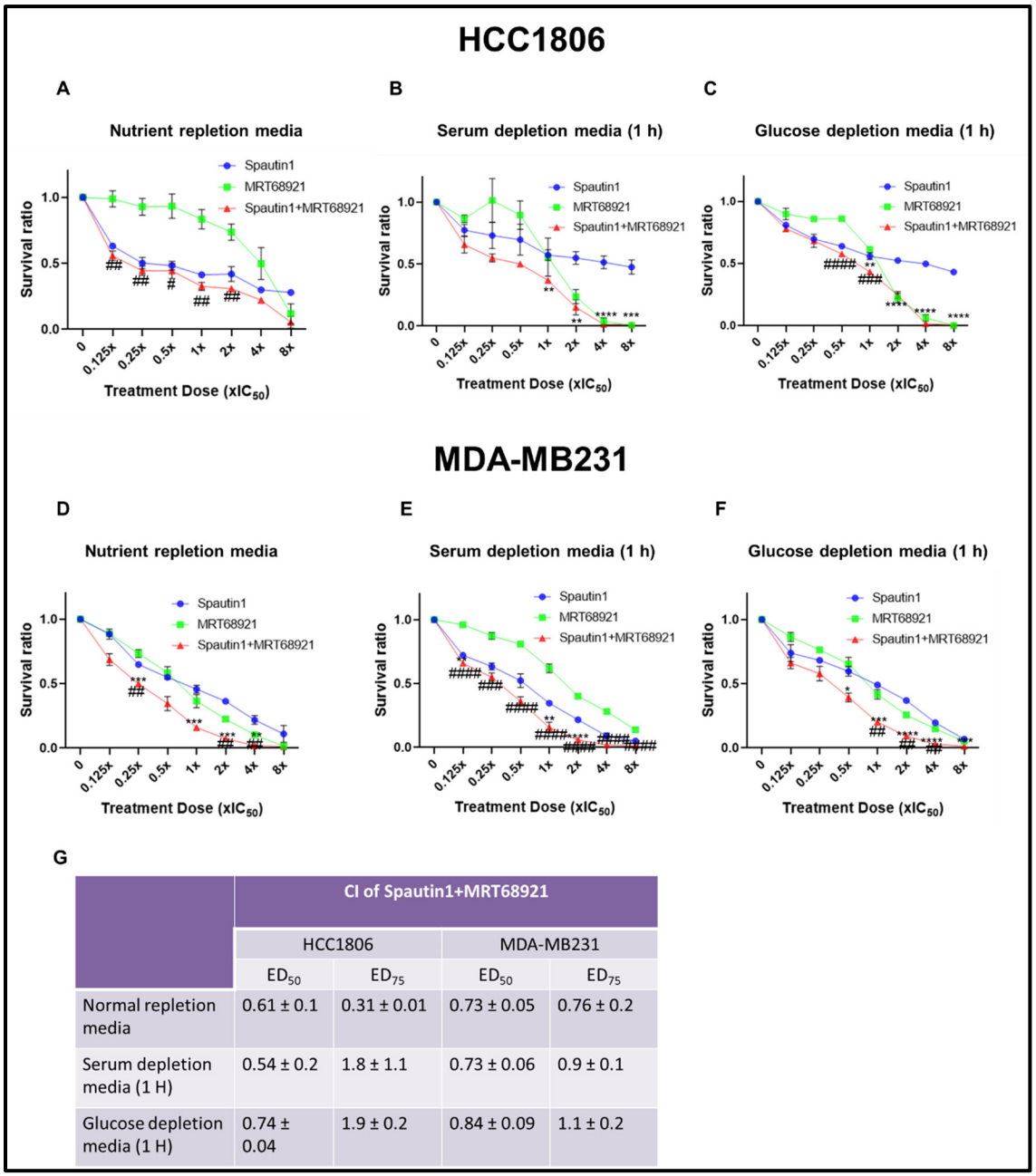

G

	CI of Spautin1+MRT68921			
	HCC1806		MDA-MB231	
	ED_{50}	ED_{75}	ED_{50}	ED_{75}
Normal repletion media	0.61 ± 0.1	0.31 ± 0.01	0.73 ± 0.05	0.76 ± 0.2
Serum depletion media (1 H)	0.54 ± 0.2	1.8 ± 1.1	0.73 ± 0.06	0.9 ± 0.1
Glucose depletion media (1 H)	0.74 ± 0.04	1.9 ± 0.2	0.84 ± 0.09	1.1 ± 0.2

Figure 3.23. Dose response curves and CI for Spautin-1 and MRT68921 in HCC1806 and MDA-MB231 cell lines under nutrient replete, serum deplete, and glucose deplete conditions. (A-C) Dose response curve of Spautin-1 and MRT68921 in HCC1806 under nutrient replete, serum deplete, and glucose deplete conditions respectively. **(D-F)** Dose response curve of Spautin-1 and MRT68921 in MDA-MB231 under nutrient replete, serum deplete, and glucose deplete conditions respectively. **(G)** Table is showing combination index (CI) of Spautin-1 and MRT68921 in HCC1806 and MDA-MB231 under nutrient replete, serum deplete, and glucose deplete conditions at ED_{50} and ED_{75}. **p<0.01, ***p<0.001, ****p<0.0001 versus Spautin-1. #p<0.05, ##p<0.01, ###p<0.001, ####p<0.0001 versus MRT68921. Graphs and CI values are mean ± SEM, n=3.

- **Spautin-1 and SBI-0206965**

Spautin-1 and SBI-0206965 combination was nearly additive in SCC25 cell line under all incubation conditions with significant reduction of cell survival at 1- 2x IC_{50} concentrations in comparison to Spautin-1 or SBI-0206965 alone **(Figure 3.24)**. In SCC9 cell line, synergism was observed with the same combination under all incubation conditions, which was associated with significant decrease in cellular proliferation at 0.5- 4x IC_{50} when compared to SBI-0206965 alone (p<0.01) in case of nutrient replete condition and at concentration of 2x IC_{50} (p<0.01) in serum deplete conditions **(Figure 3.24)**.

In HCC1806, this combination was synergistic and moderate synergistic under nutrient replete conditions, or after pre-incubation with glucose or serum depleted media, respectively. A significant reduction of cell survival was observed at 1-2x IC_{50} concentration under all incubation conditions. In MDA-MB231, the combination of Spautin-1 and SBI-0206695 showed moderate antagonism after pre-incubation with serum or glucose depleted media, while slight synergism was observed under nutrient replete conditions **(Figure 3.25)**.

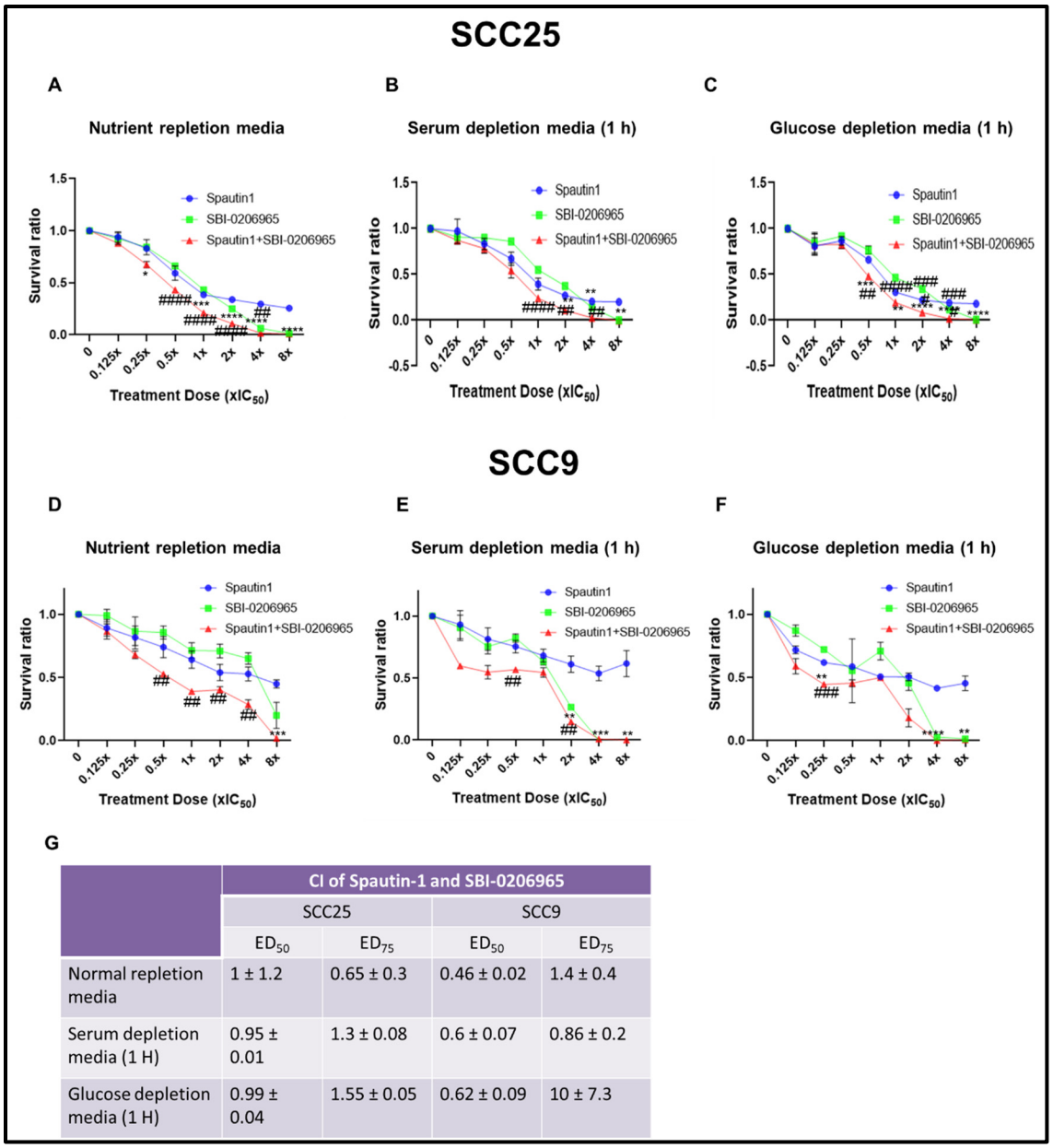

G

	CI of Spautin-1 and SBI-0206965			
	SCC25		SCC9	
	ED_{50}	ED_{75}	ED_{50}	ED_{75}
Normal repletion media	1 ± 1.2	0.65 ± 0.3	0.46 ± 0.02	1.4 ± 0.4
Serum depletion media (1 H)	0.95 ± 0.01	1.3 ± 0.08	0.6 ± 0.07	0.86 ± 0.2
Glucose depletion media (1 H)	0.99 ± 0.04	1.55 ± 0.05	0.62 ± 0.09	10 ± 7.3

Figure 3.24. Dose response curves and CI for Spautin-1 and SBI-0206965 in SCC25 and SCC9 cell lines under nutrient replete, serum deplete, and glucose deplete conditions. (A-C) Dose response curve of Spautin-1 and SBI-0206965 in SCC25 under nutrient replete, serum deplete, and glucose deplete conditions respectively. **(D-F)** Dose response curve of Spautin-1 and SBI-0206965 in SCC9 under nutrient replete, serum deplete, and glucose deplete conditions respectively. **(G)** Table is showing combination index (CI) of Spautin-1 and SBI-0206965 in SCC25 and SCC9 under nutrient replete, serum deplete, and glucose deplete conditions at ED_{50} and ED_{75}. *p<0.05, **p<0.01, ***p<0.001, ****p<0.0001 versus Spautin-1. ##p<0.01, ###p<0.001, ####p<0.0001 versus SBI-0206965. Graphs and CI values are mean ± SEM, n=3.

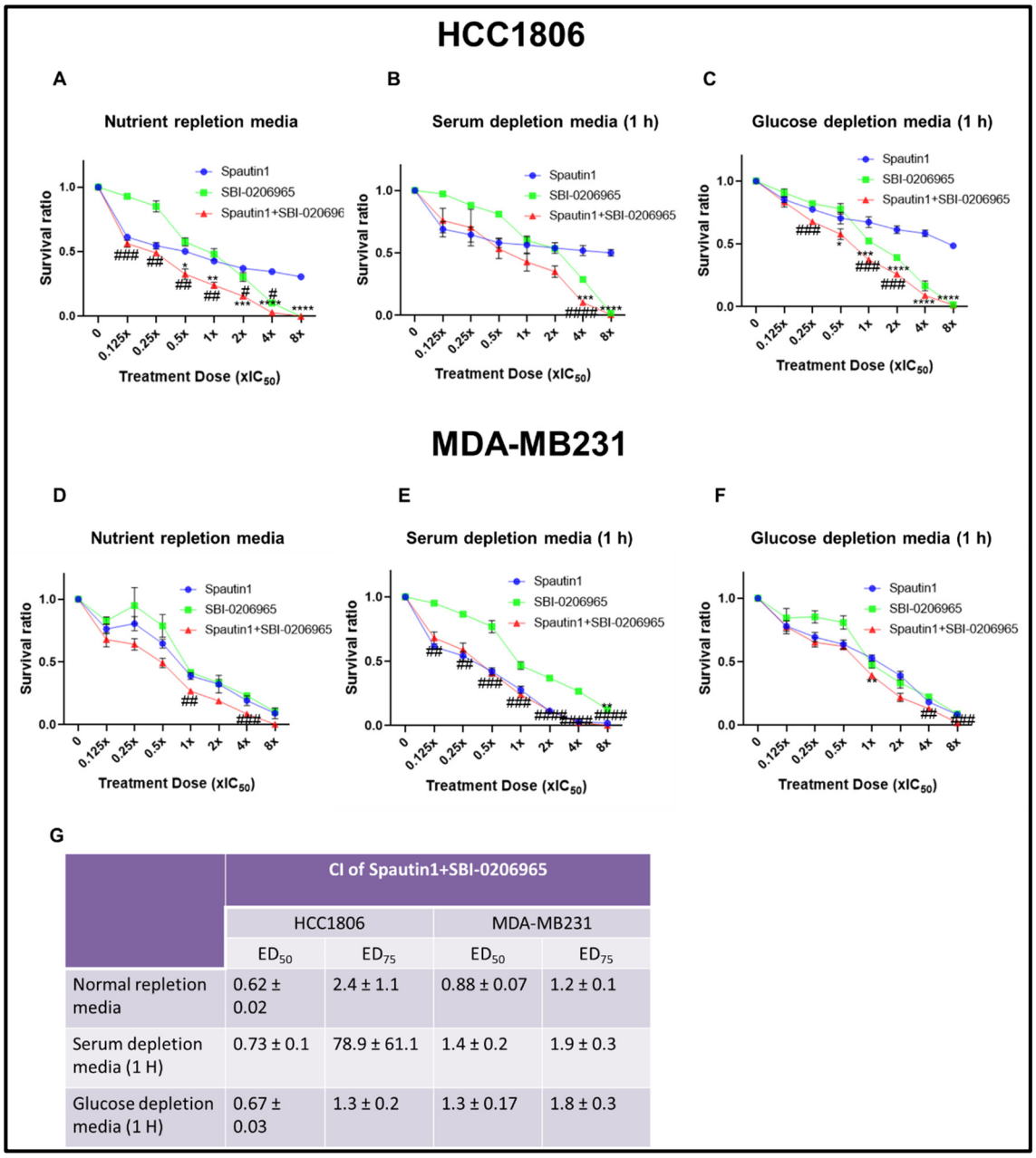

G

	CI of Spautin1+SBI-0206965			
	HCC1806		MDA-MB231	
	ED_{50}	ED_{75}	ED_{50}	ED_{75}
Normal repletion media	0.62 ± 0.02	2.4 ± 1.1	0.88 ± 0.07	1.2 ± 0.1
Serum depletion media (1 H)	0.73 ± 0.1	78.9 ± 61.1	1.4 ± 0.2	1.9 ± 0.3
Glucose depletion media (1 H)	0.67 ± 0.03	1.3 ± 0.2	1.3 ± 0.17	1.8 ± 0.3

Figure 3.25. Dose response curves and CI for Spautin-1 and SBI-0206965 in HCC1806 and MDA-MB231 cell lines under nutrient replete, serum deplete, and glucose deplete conditions. (A-C) Dose response curve of Spautin-1 and SBI-0206965 in HCC1806 under nutrient replete, serum deplete, and glucose deplete conditions respectively. **(D-F**) Dose response curve of Spautin-1 and SBI-0206965 in MDA-MB231 under nutrient replete, serum deplete, and glucose deplete conditions respectively. **(G)** Table is showing combination index (CI) of Spautin-1 and SBI-0206965 in HCC1806 and MDA-MB231 under nutrient replete, serum deplete, and glucose deplete conditions at ED_{50} and ED_{75}. *p<0.05, **p<0.01, ***p<0.001, ****p<0.0001 versus Spautin-1. ##p<0.01, ###p<0.001, ####p<0.0001 versus SBI-0206965. Graphs and CI values are mean ± SEM, n=3.

3.2.6. Combination between standard chemotherapeutics (*i.e.,* Cisplatin, Paclitaxel), Beclin-1 complex inhibitor (SAR405) and ULK-1 complex inhibitor (MRT68921) had a mild inhibitory effect on tumour cell proliferation in both OSCC and TNBC cell models.

As SAR405 and MRT68921 combination showed a significant reduction of cellular proliferation, we attempted to test the effect of combination between standard chemotherapeutic agents (*i.e.,* Cisplatin, Paclitaxel), SAR405 and MRT68921 on tumour cells proliferations. Cells were treated with different concentration of Cisplatin or Paclitaxel (according to cell line used) and fixed dose combination of SAR405-MRT68921 (0.125-8.0x IC_{50}). The IC_{50} for SAR405-MRT68921 combination was derived from previous combination studies for these inhibitors (**Figure 3.18 &19 D-F**).

For OSCC cell model, SCC9 exhibited moderately antagonist effect when Cisplatin, SAR405-MRT68921 were combined with no difference in cellular proliferation observed when compared to either Cisplatin only or SAR405-MRT68921 (**Figure 3.26**). In TNBC cell model, MDA-MB231 demonstrated a moderately antagonist effect when treated with combination of Paclitaxel and SAR405-MRT68921 combination. Despite this, a significant reduction in cellular proliferation was observed at 4-8x IC_{50} concentrations (p<0.001-0.01) in comparison to Paclitaxel and at concentration of 4x IC_{50} (p<0.001) when compared to SAR405-MRT68921 combination (**Figure 3.26**).

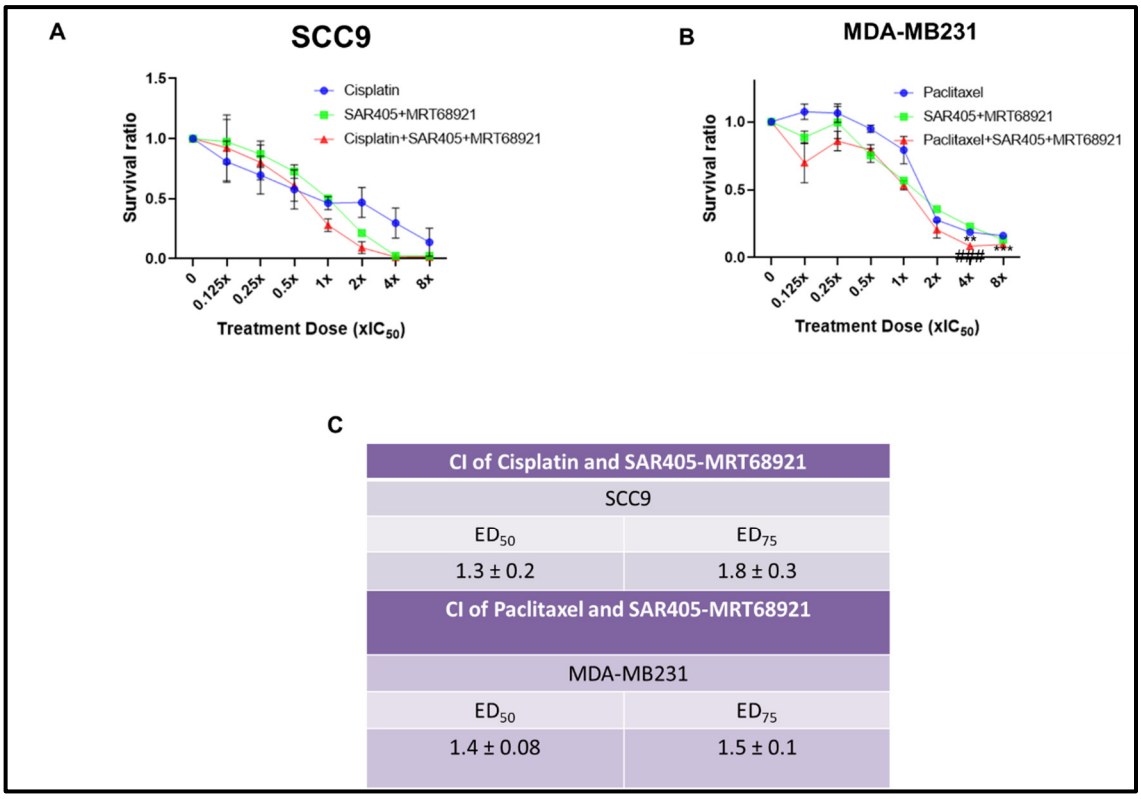

C

CI of Cisplatin and SAR405-MRT68921	
SCC9	
ED_{50}	ED_{75}
1.3 ± 0.2	1.8 ± 0.3
CI of Paclitaxel and SAR405-MRT68921	
MDA-MB231	
ED_{50}	ED_{75}
1.4 ± 0.08	1.5 ± 0.1

Figure 3.26. Dose response curves and CI for Cisplatin- SAR405-MRT68921 and Paclitaxel-SAR405-MRT68921 in OSCC and TNBC cell model respectively. (A) Dose response curve of Cisplatin and SAR405-MRT68921 in SCC9. **(B)** Dose response curve of Paclitaxel and SAR405-MRT68921 in MDA-MB231. **(C)** Table is showing CI of Cisplatin-SAR405-MRT68921 and Paclitaxel-SAR405-MRT68921 in SCC9 and MDA-MB231 respectively. ***p*<0.01,****p*<0.001 versus Paclitaxel, ###*p*<0.001 versus SAR405-MRT68921. Graphs and CI values are mean±SEM, n=3.

3.2.7. Combination between standard chemotherapeutics (Cisplatin and Paclitaxel) and Beclin-1 complex inhibitor (SAR405) impairs tumour cell migration in both OSCC and TNBC cell models.

Tumour metastasis is a biological process by which tumour cells move from the primary neoplasm site to distant sites. It involves invasion of surrounding tissue, entering the lymphatics or blood stream, survival in the circulation, migration to a distant site, and then, extravasation in the new site and grow at this site [382]. Notably, tumour metastasis is the main cause of death for cancer patients and tumour cell migration is a critical phenomenon in the metastatic process [383]. Thus, we aimed to examine the effect of autophagy inhibitors and chemotherapy on cancer cell migration using a scratch wound assay.

Based on the results from cellular proliferation studies, we attempted to test some combination therapies, which significantly reduced the tumour cell proliferation, on tumour cell migration. So, a scratch wound assay was carried out to assess the effect of combination therapy between standard chemotherapeutics, either Cisplatin or Paclitaxel according to the cell line used, and Beclin-1 complex inhibitor (SAR405) on cellular migration. A combination between ULK-1 complex inhibitor (MRT68921) and Beclin-1 complex inhibitor (SAR405) was also tested. Scratch wound assay was carried out as previously described in chapter two using Incucyte.

First, the number of cells for each cell line were optimised to ensure 100% confluency after 24 h of seeding. Different numbers of cells in each cell line were seeded and observed after 24 h to determine cellular confluency. This optimisation process concluded that a number of 24,000 cells/well for SCC25, 30,000 cells/well for SCC9, 32,000 cells/well for HCC1806 and 23,000 cells/well for MDA-MB231 were found to give 100% confluency after

24 h of seeding in a 96 well plate. After that, the optimal dose for each drug was determined by treating each cell line with a range of concentrations for each drug as shown in **Figure 3.27 and 3.28,** 24 h after seeding. The incubation period was determined by the wound closure in the control **(Figure 3.27, 3.28)**. A dose dependent decrease in wound density was observed with increasing doses of drugs (Cisplatin, Paclitaxel, SAR405 or MRT68921) in both OSCC (SCC25 and SCC9) and TNBC (HCC1806 and MDA-MB231) cell lines.

To make sure that the effect exerted by the dose of drug administered was due to migration impairment and not as a result of its effect on cellular proliferation, a parallel MTT proliferation assay was performed using the same concentrations of each drug in each cell line to determine their effect on tumour cell proliferation. No or minimal effect on tumour cell proliferation was observed at different concentrations of each drug (**Figure 3.29 and 3.30**). The dose which had a minimal effect on tumour cell proliferation but had a significant effect on cell migration was selected for each drug for combination studies (**Table 3.8**).

After applying the treatments, relative wound density was calculated using Incucyte ®Scratch Wound Analysis Software which analyse the data based on 2 factors, wound width, and confluency.

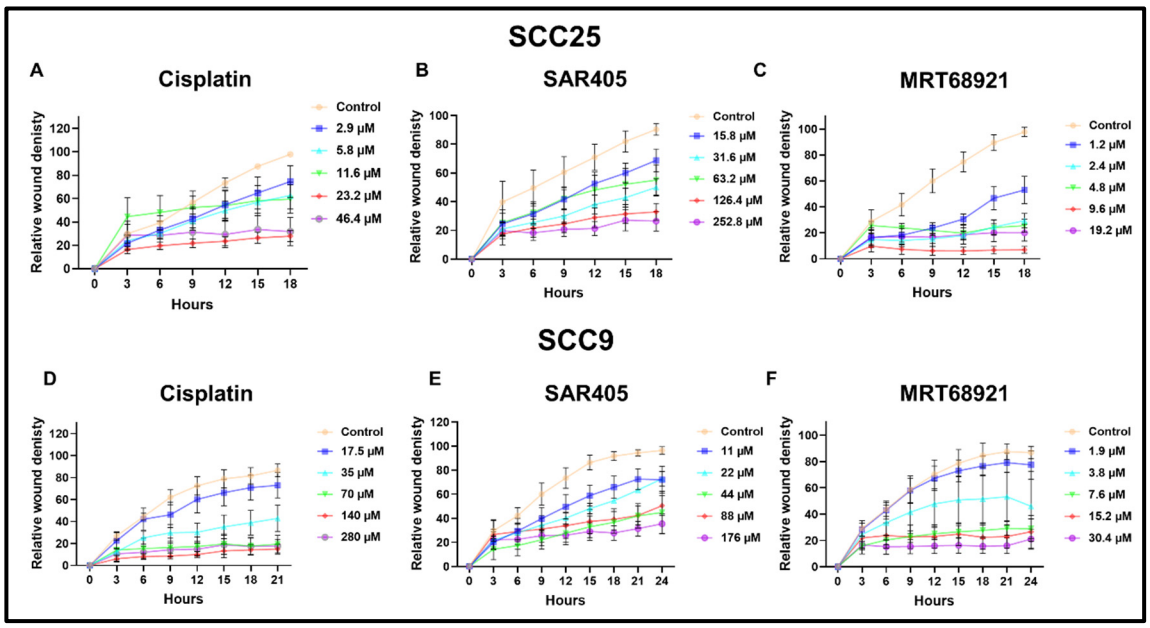

Figure 3.27. Relative wound density in response to Cisplatin, SAR405 and MRT68921 in SCC25 and SCC9 cell lines. (A-C) plot the relative wound density in SCC25 following treatment with different concentration of Cisplatin, SAR405 and MRT68921 respectively. **(D-F)** plot the relative wound density in SCC9 following treatment with different concentration of Cisplatin, SAR405 and MRT68921 respectively. Graphs are mean ± SEM, n=3.

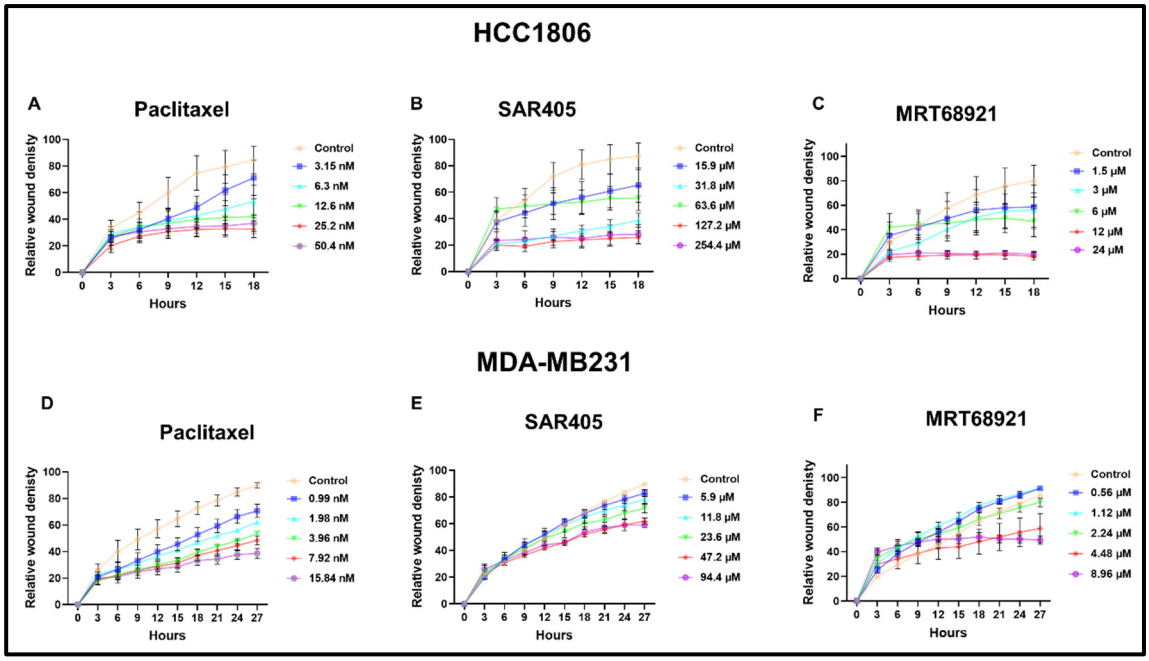

Figure 3.28. Relative wound density in response to Paclitaxel, SAR405 and MRT68921 in HCC1806 and MDA-MB231 cell lines. (A-C) showing the relative wound density in HCC1806 after treatment with different concentration of Paclitaxel, SAR405 and MRT68921 respectively. **(D-F)** showing the relative wound density in MDA-MB231 following treatment with different concentration of Paclitaxel, SAR405 and MRT68921 respectively. Graphs are mean ± SEM, n=3.

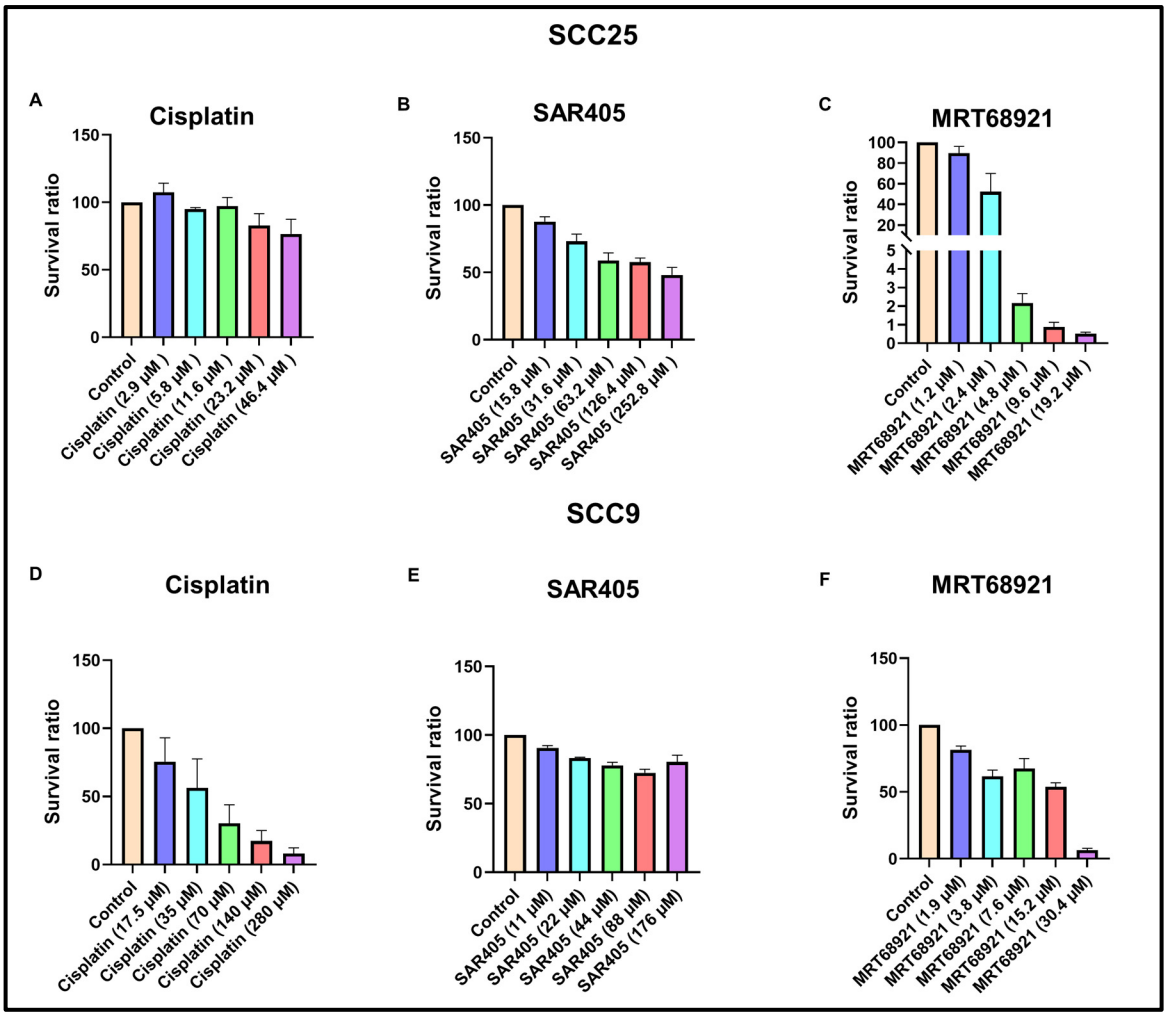

Figure 3.29. Survival ratio in response to Cisplatin, SAR405 and MRT68921 treatment in SCC25 and SCC9 cell lines. (A-C) plot the survival ratio in SCC25 following treatment with different concentration of Cisplatin, SAR405 and MRT68921 respectively. **(D-F)** plot the survival ratio in SCC9 following treatment with different concentration of Cisplatin, SAR405 and MRT68921 respectively. Graphs are mean ± SEM, n=3.

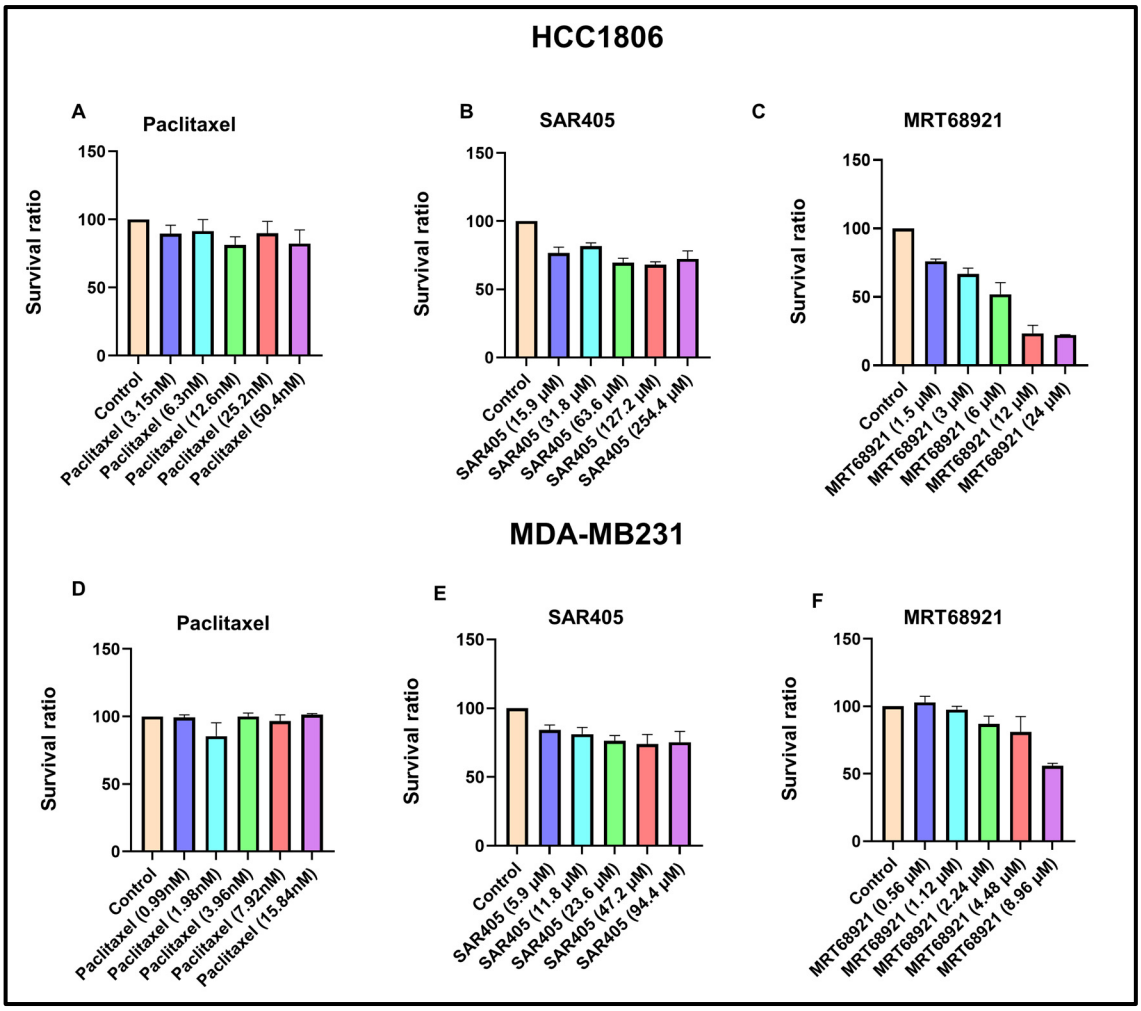

Figure 3.30. Survival ratio in response to Paclitaxel, SAR405 and MRT68921 treatment in HCC1806 and MDA-MB231 cell lines. (A-C) plot the survival ratio in HCC1806 following treatment with different concentration of Paclitaxel, SAR405 and MRT68921 respectively. **(D-F)** plot the survival ratio in MDA-MB231 following treatment with different concentration of Paclitaxel, SAR405 and MRT68921 respectively. Graphs are mean ± SEM, n=3.

Table 3.8. shows selected doses of drugs used for testing the effect of different drug combinations on cell migration.

Drug	Cell lines	
	OSCC	
	SCC25	SCC9
Cisplatin (μM)	2.9	17.5
SAR405 (μM)	15.8	11
MRT68921 (μM)	1.2	1.9
	TNBC	
	HCC1806	MDA-MB231
Paclitaxel (nM)	3.15	0.99
SAR405 (μM)	15.9	5.9
MRT68921 (μM)	1.5	4.48

Both OSCC cell models (*i.e.,* SCC25 and SCC9) exhibited a significant impairment in cell migration upon treatment with combination of Cisplatin and SAR405 when compared to the control, whereas standalone treatment with SAR405 or Cisplatin did not have a significant effect in comparison to the control **(Figure 3.31, 3.32)**. Likewise, combination of Paclitaxel and SAR405 significantly inhibited tumour cell migration in MDA-MB231 cell line in comparison to the control. This effect was not observed in the case of Paclitaxel or SAR405 treatment only **(Figure 3.34)**. However, HCC1806 demonstrated no significant reduction in cell migration when treated with both Paclitaxel and SAR405 **(Figure 3.33)**.

Furthermore, the combination of ULK-1 (*i.e.,* MRT68921) and Beclin-1 inhibitors (*i.e.,* SAR405) did not confer significant inhibition of wound closure compared to the control across all cell lines used **(Figure 3.35, 3.36 and 3.37)**.

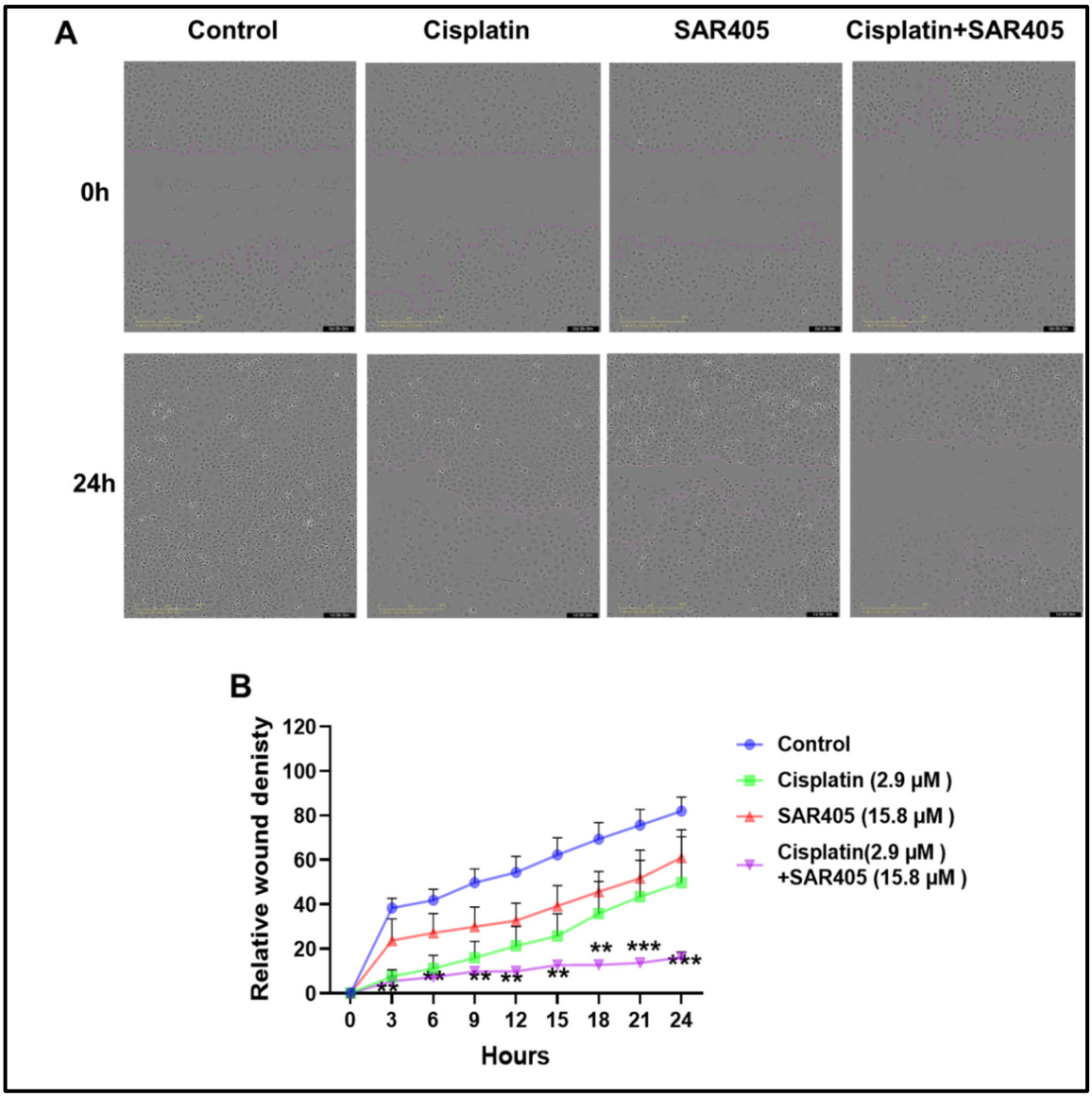

Figure 3.31. Cisplatin-SAR405 combination impairs the cell migration in SCC25 cell line. (A) Representative images of scratch assay for SCC25 with treatment by Cisplatin, SAR405 and combination of both at 0 h and 33 h. **(B)** Relative wound density in SCC25 in response to Cisplatin, SAR405 and Cisplatin-SAR405 combined. **p<0.01, ***p<0.001 versus the control. Graphs are mean ± SEM, n=3. Scale bar: 400μm

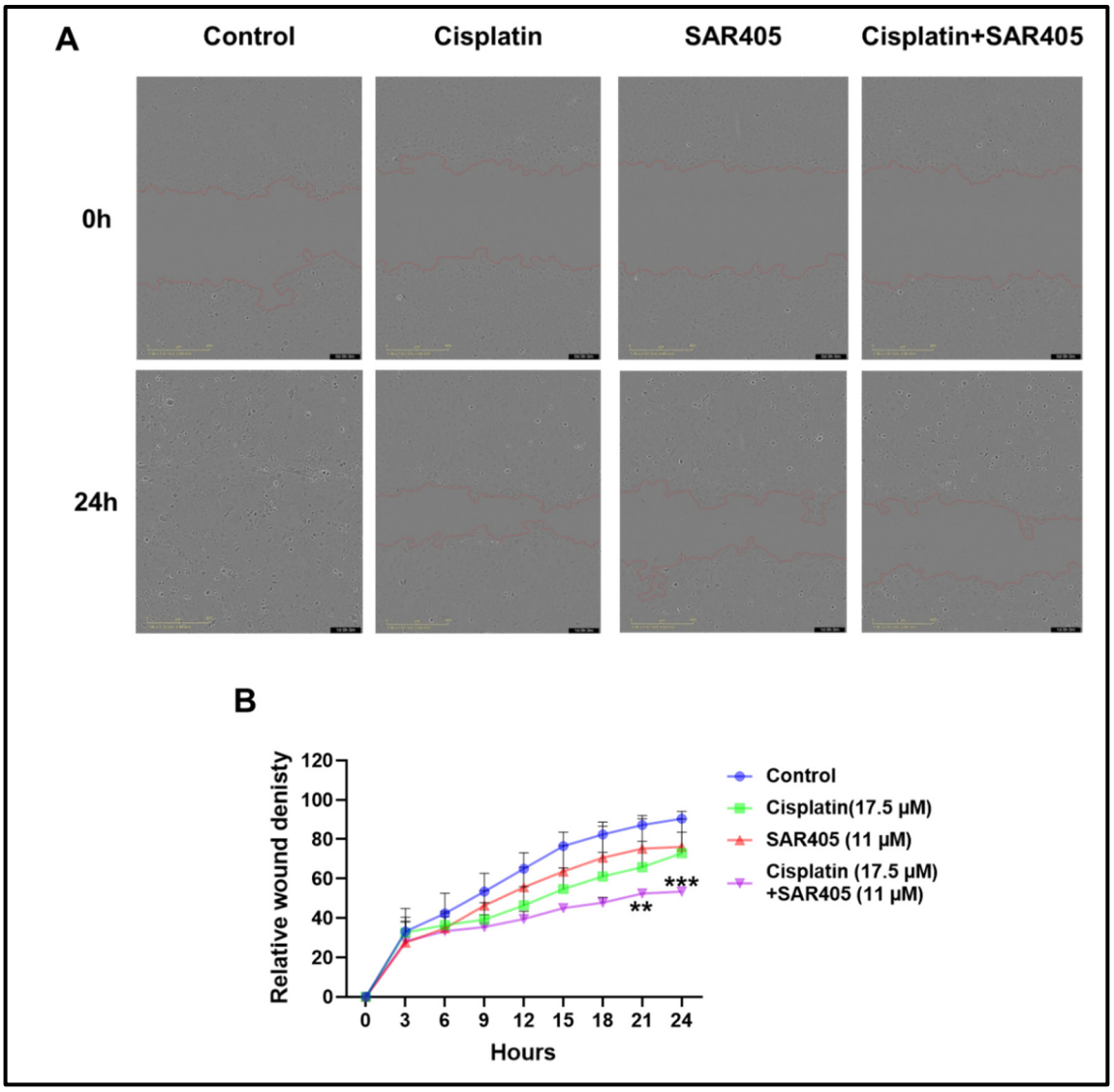

Figure 3.32. Cisplatin-SAR405 combination impairs the cell migration in SCC9 cell line. (A) Representative images of scratch assay for SCC9 with treatment by Cisplatin, SAR405 and combination of both at 0 h and 24 h. **(B)** Relative wound density in SCC9 in response to Cisplatin, SAR405 and Cisplatin-SAR405 combined. **p<0.01, ***p<0.001 versus the control. Graphs are mean ± SEM, n=3. Scale bar: 400μm

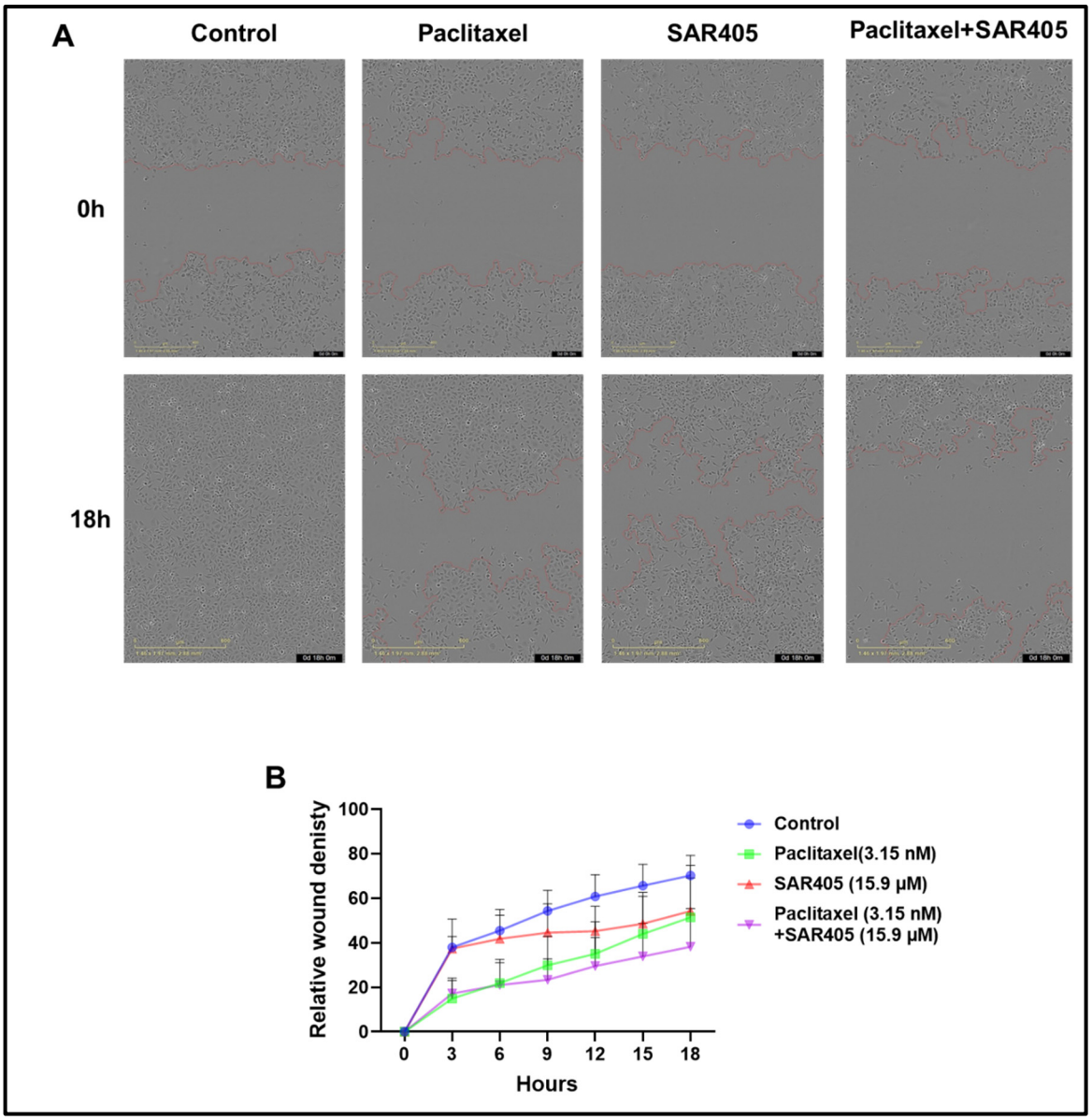

Figure 3.33. Effect of Paclitaxel-SAR405 combination on the cell migration in HCC1806 cell line. (A) Representative images of scratch assay for HCC1806 with treatment by Paclitaxel, SAR405 and combination of both at 0 h and 18 h. **(B)** Relative wound density in HCC1806 in response to Paclitaxel, SAR405 and Paclitaxel-SAR405 combined. Graphs are mean ± SEM, n=3. Scale bar: 400 and 600µm

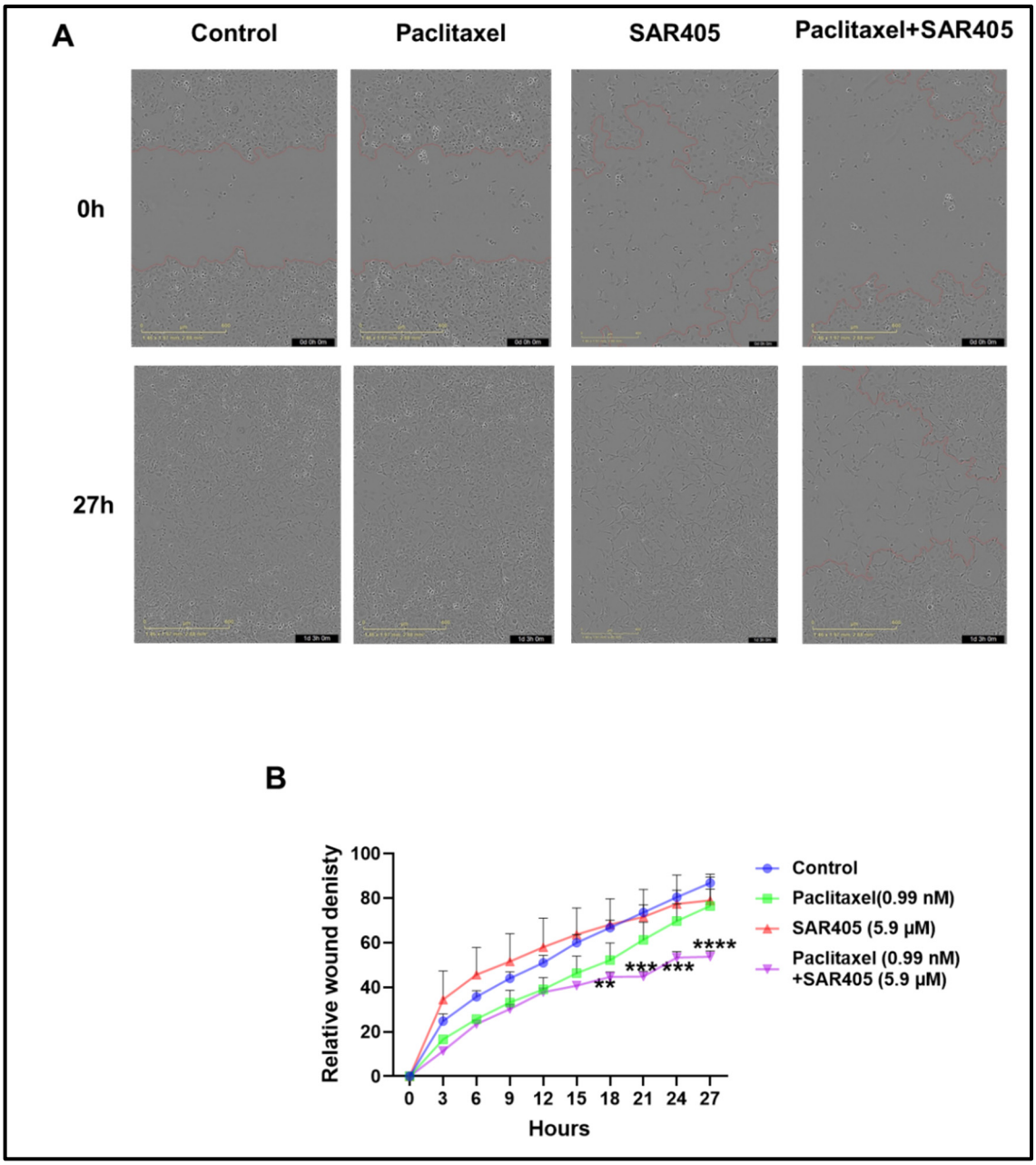

Figure 3.34. Paclitaxel-SAR405 combination impairs the cell migration in MDA-MB231 cell line. (A) Representative images of scratch assay for MDA-MB231 with treatment by Paclitaxel, SAR405 and combination of both at 0 h and 27 h. (B) Relative wound density in MDA-MB231 in response to Paclitaxel, SAR405 and Paclitaxel-SAR405 combined. ** p<0.01, *** p<0.001 versus the control. Graphs are mean ± SEM, n=3. Scale bar: 400 and 600µm

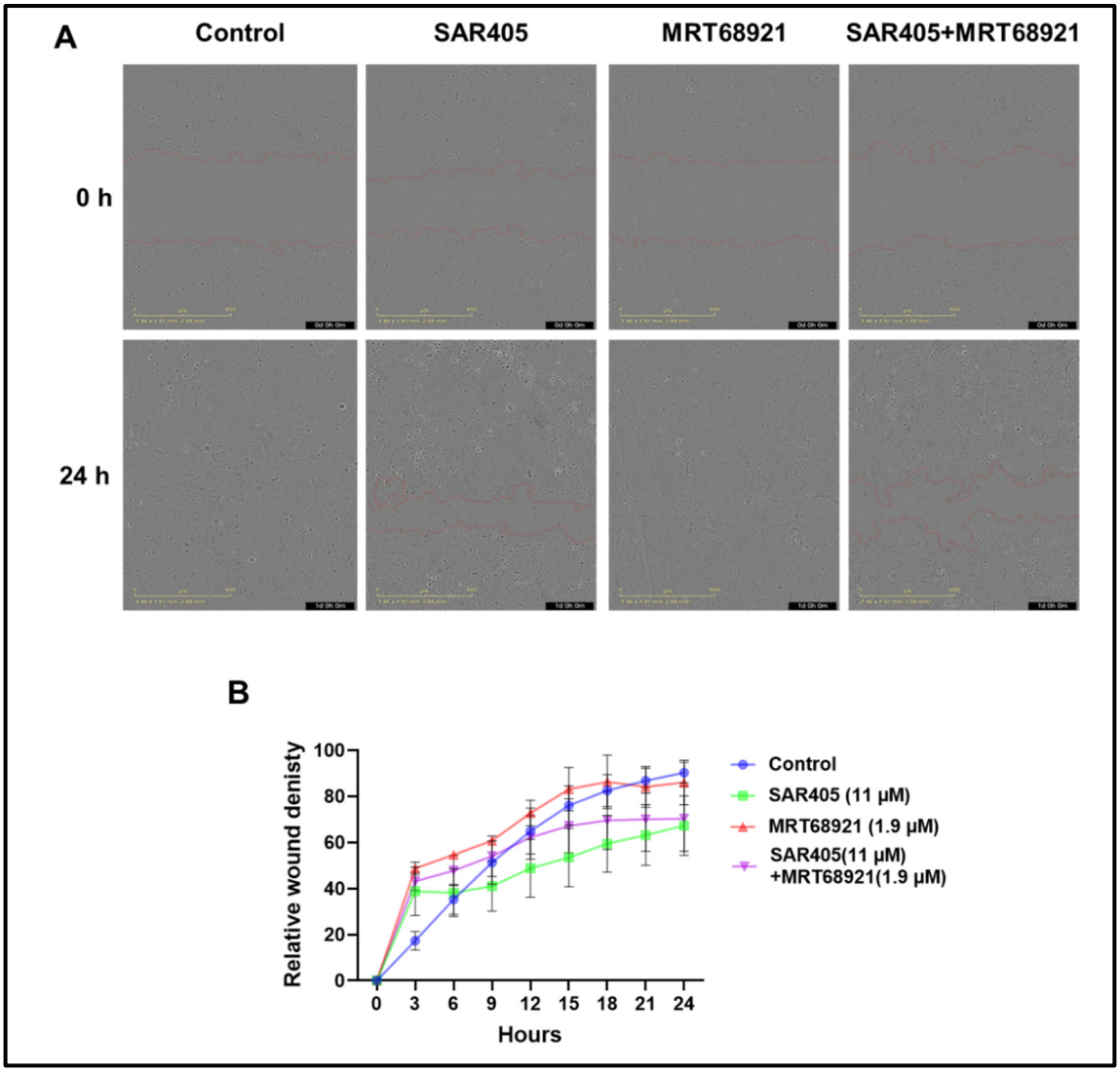

Figure 3.35. SAR405-MRT68921 combination has no effect on the cellular migration in SCC9 cell line. (A) Representative images of scratch assay for SCC9 with treatment by SAR405, MRT68921 and combination of both at 0 h and 24 h. **(B)** Relative wound density in SCC9 in response to SAR405, MRT68921 and SAR405-MRT68921 combined. Graphs are mean ± SEM, n=3. Scale bar: 600μm

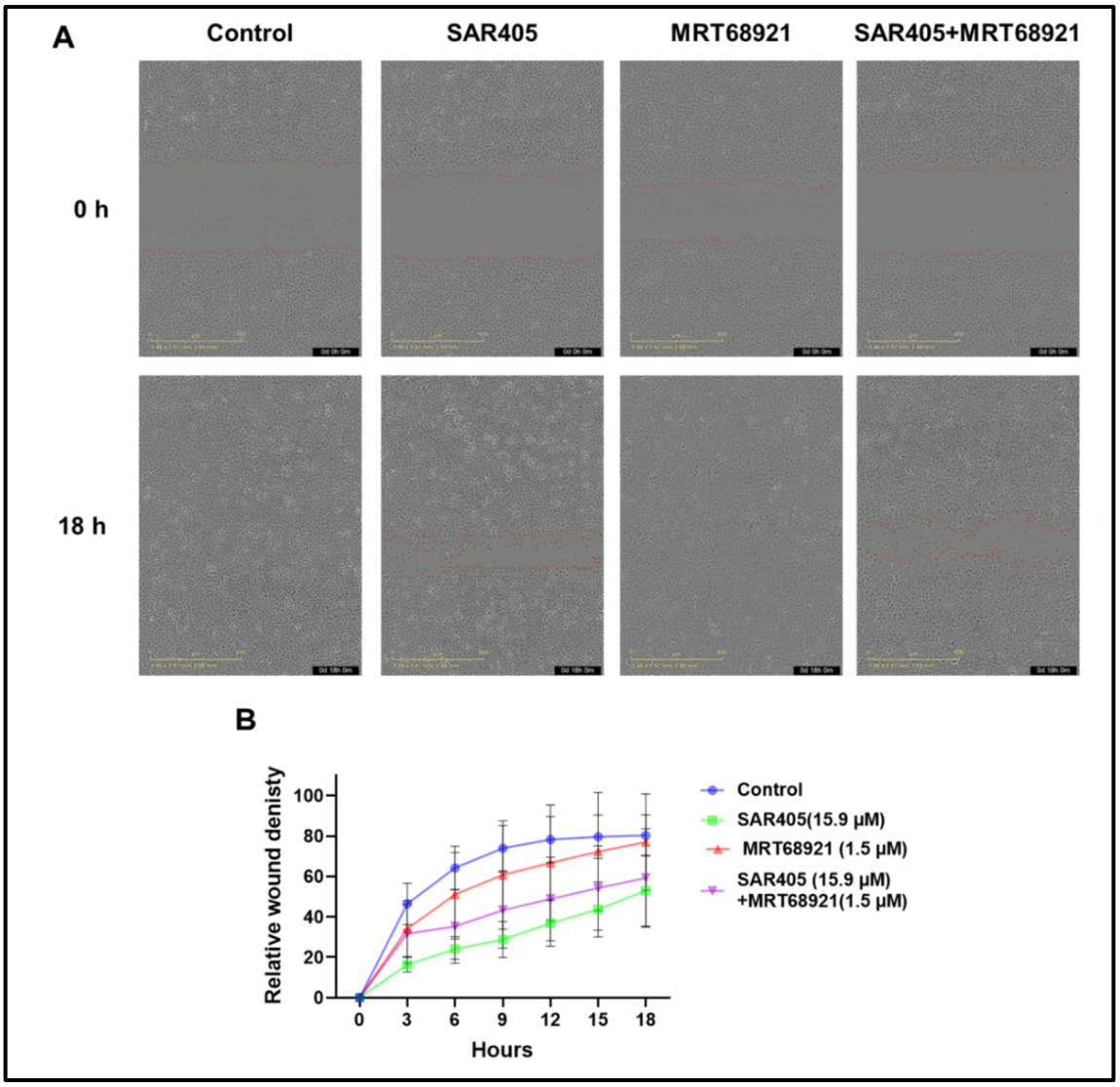

Figure 3.36. SAR405-MRT68921 combination has no effect on the cellular migration in HCC1806 cell line. (A) Representative images of scratch assay for HCC1806 with treatment by SAR405, MRT68921 and combination of both at 0 h and 18 h. **(B)** Relative wound density in HCC1806 in response to SAR405, MRT68921 and SAR405-MRT68921 combined. Graphs are mean ± SEM, n=3. Scale bar: 600μm

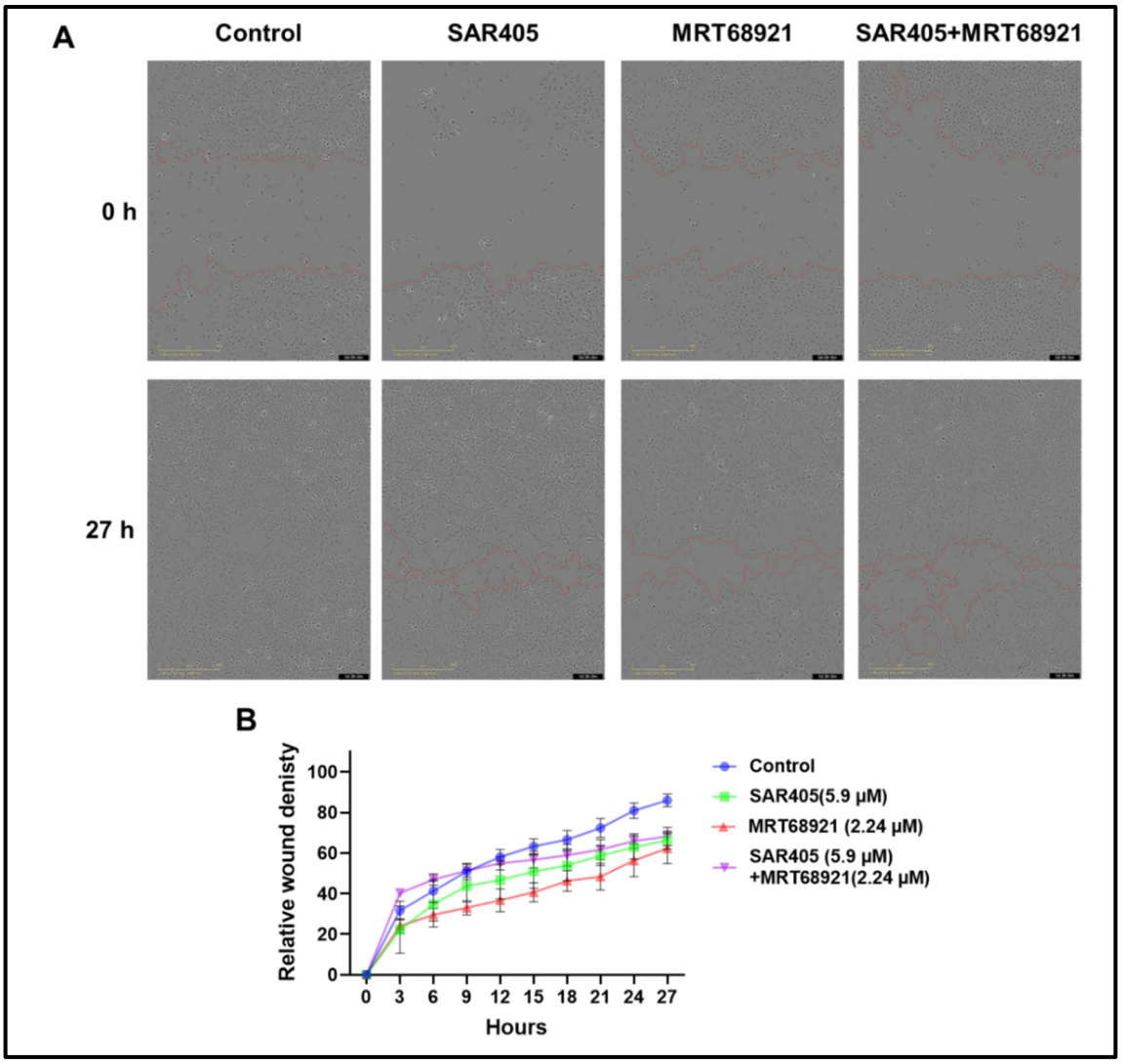

Figure 3.37. SAR405-MRT68921 combination has no effect on the cellular migration in MDA-MB231 cell line. (A) Representative images of scratch assay for MDA-MB231 with treatment by SAR405, MRT68921 and combination of both at 0 h and 27 h. **(B)** Relative wound density in MBA-MD231 in response to SAR405, MRT68921 and SAR405-MRT68921 combined. Graphs are mean ± SEM, n=3. Scale bar: 400µm

3.2.8. Combination between standard chemotherapeutics (*i.e.,* Paclitaxel), Beclin-1 complex inhibitor (SAR405) and ULK-1 complex inhibitor (MRT68921) reduced tumour size in TNBC orthotopic xenograft.

Taking into consideration the previous results, the next step was to evaluate the effect of effective combinations *in vivo*. Initially, a dose escalation study was performed for both SAR405 and MRT68921 to determine the dose which did not lead to any observable adverse effects in the balb/c nude mice. A dose of 20 mg/Kg and 40 mg/Kg from each drug was administered to the mice. For MRT68921, a dose of 40 mg/Kg MRT68921 was toxic to the mice, so a dose of 20 mg/Kg was selected. In case of SAR405, both doses assessed were not toxic in mice, but due to poor solubility of this agent at higher doses, a dose of 20mg/kg was selected. Next, a safety assessment was also performed for combination between SAR405 (20 mg/Kg) and MRT68921 (20 mg/Kg) and was deemed to have no observable adverse events in balb/c nude mice. For Paclitaxel, a dose of 5mg/Kg were used based on previous studies in the literature [384, 385].

To measure the effect of these drugs on tumour growth, an orthotopic xenograft mouse model was performed for TNBCs. The balb/c nude mice were injected with MBA-MD231 tumour cells (5×10^6 cells; 1:1 mixture of Matrigel® and cold PBS) in the 2nd mammary gland, and tumours were allowed to grow *in vivo*. After 14 days from tumour cells implantation (tumours reached size of ~100mm^3), mice were randomly categorised into 8 groups and treated with either vehicle control, SAR405 (20 mg/Kg), MRT68921 (20 mg/Kg), SAR405-MRT68921 combined, Paclitaxel (5 mg/Kg), Paclitaxel-SAR405 combined, Paclitaxel-MRT68921 combined or Paclitaxel-SAR405-MRT68921 combined. Treatments were administered twice/week for 3 weeks, once the majority of tumours were approaching 1000 mm^3, all mice were euthanised and tumours were harvested.

Our data showed no significant reduction in tumour volume in groups treated with either SAR405, MRT68921 or SAR405-MRT68921 in comparison to the control group (**Figure 3.38 A**). A decrease in tumour volume was noted in groups treated with either Paclitaxel, Paclitaxel-SAR405 or Paclitaxel-MRT68921 when compared to the control group, but this decrease was not significant (**Figure 3.38 B**). A significant reduction in tumour volume ($p<0.05$) was noted in the group treated with Paclitaxel-SAR405-MRT68921 in comparison to the control group (**Figure 3.38 B**). A decrease in tumour volume was also noted in the group treated with Paclitaxel-SAR405-MRT68921 when compared to the group treated with Paclitaxel only but it was not significant (**Figure 3.38 B**). Moreover, a decrease in tumour weight was observed in all treatment groups when compared to the control group but did not reach significance (**Figure 3.38 E**). Only the group treated with Paclitaxel-SAR405-MRT68921 showed a significant decrease in tumour weight in comparison to the control group (**Figure 3.38 F**). Hence, Paclitaxel-SAR405-MRT68921 significantly inhibited the growth and progression of tumour xenograft *in vivo* (**Figure 3.39**).

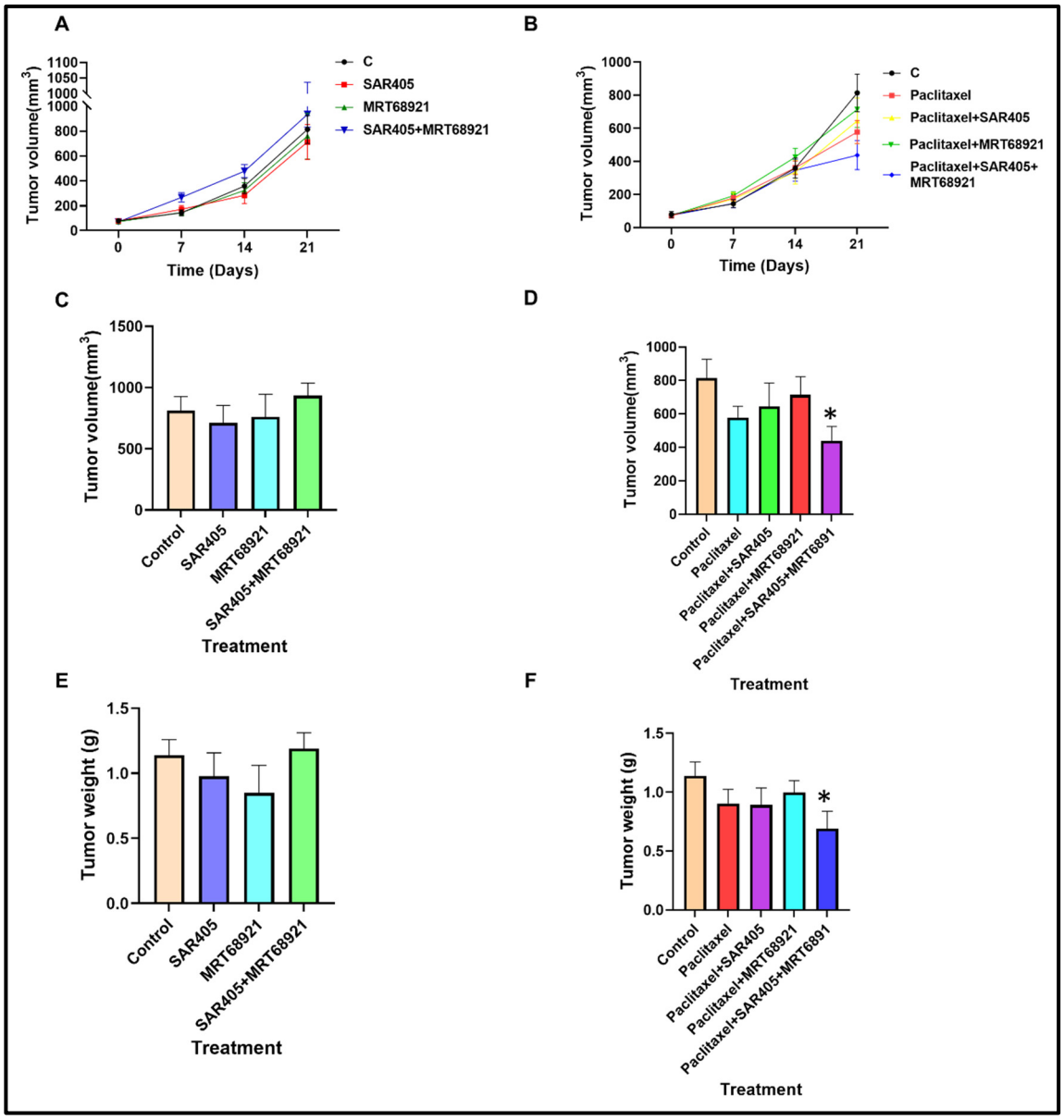

Figure 3.38. Combination of Paclitaxel-SAR405-MRT68921 inhibits TNBC growth *in vivo* (A) Graph of tumour volume between groups treated with either vehicle control, SAR405, MRT68921, SAR405-MRT68921. **(B)** Graph of tumour volume between groups treated with either vehicle control, Paclitaxel, Paclitaxel-SAR405, Paclitaxel-MRT68921 or Paclitaxel-SAR405-MRT68921. **(C)** Bar graph for tumour volume in groups treated with either vehicle control, SAR405, MRT68921, SAR405-MRT68921. **(D)** Bar graph for tumour volume in groups treated with either vehicle control, Paclitaxel, Paclitaxel-SAR405, Paclitaxel-MRT68921 or Paclitaxel-SAR405-MRT68921. *p<0.05 versus control group. **(E)** Bar graph for tumour weight in groups treated with either vehicle control, SAR405, MRT68921, SAR405-MRT68921. **(F)** Bar graph for tumour weight in groups treated with either vehicle control, Paclitaxel, Paclitaxel-SAR405, Paclitaxel-MRT68921 or Paclitaxel-SAR405-MRT68921. *p<0.05 versus control group. Graphs are mean ± SEM, n=8/group.

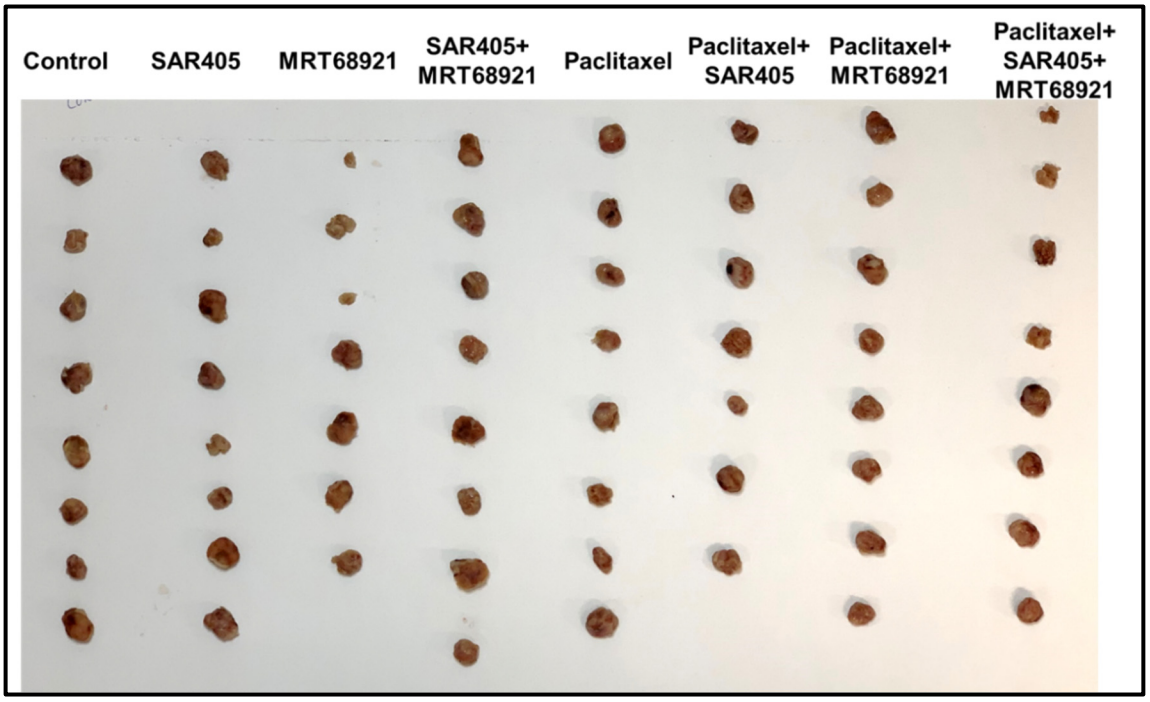

Figure 3.39. Gross pictures for tumours from mice treated with different drug combinations: vehicle control, SAR405, MRT68921, SAR405-MRT68921, Paclitaxel, Paclitaxel-SAR405, Paclitaxel-MRT68921 and Paclitaxel-SAR405-MRT68921.

3.3. Summary of Findings

To achieve the 1st aim, OSCC and TNBC cell models were treated with serum and glucose free media at different time point to determine at which point the autophagy is being upregulated through detection of any change in the levels of autophagic marker LC3-II and lysosomal marker LAMP2 via immunoblotting. It was found that LC3-II levels had been significantly upregulated upon serum or glucose starvation for 0.5-1 h in all cell line used except for MDA-MB231 which suggests either increased autophagy induction or decreased degradation. Comparatively, LAMP2 levels were only significantly increased following 1 h serum starvation in both SCC9 and MDA-MB231. The decreased LAMP2 levels observed in other cell lines (SCC25 and HCC1806) could be due to enhanced degradation of lysosomes as result of active autophagic flux.

To further elucidate if LC3-II upregulation is due to increased autophagy induction, not decreased degradation, cells were pre-incubated with late-stage autophagy inhibitor Baf A1, followed by treatment with serum or glucose depleted media for 1 h. Our results showed that there were significantly increased levels of LC3-II after Baf A1 treatment upon 1 h serum starvation in OSCC cell model, whilst co-incubation of Baf A1 with glucose depleted media for 1 h significantly induced LC3-II levels in both TNBC cell models and SCC25 cell line. Taken together, these results demonstrated that serum starvation induced autophagy induction in OSCC cell models, whereas glucose starvation stimulated autophagy induction in TNBC cell model.

Following these investigations, results from confocal microscopy demonstrated a significant increase in LC3 puncta upon 1 h incubation with serum or glucose free media

with Baf A1 treatment in all cell lines used and similarly increased co-localisation between LC3 and LAMP2 was observed under serum or glucose starvation. Overall, increased autophagic induction and increased LC3-LAMP2 co-localisation under serum or glucose starvation conditions implied enhanced autophagic flux under these conditions.

To achieve the 2nd aim, first, the cells were treated with standard chemotherapy and different autophagy inhibitors. MRT68921 was observed as the most potent autophagy inhibitors as it had the lowest IC_{50} among all autophagy inhibitors across all cell lines used under different conditions. In OSCC, an increase in IC_{50} of Cisplatin was noted in both OSCC cell lines following incubation with serum or glucose free media compared to nutrient replete condition except for glucose starvation in SCC25. A small change was observed in IC_{50} of the autophagic inhibitor after incubation with serum or glucose deplete media compared to nutrient replete conditions except for Spautin-1 and MRT68921 which exhibited marked decrease in their IC_{50} after glucose starvation for 1 h in SCC25. Regarding TNBC, an increase of Paclitaxel's IC_{50} was only noted in MDA-MB231 after 1 h serum starvation in comparison to nutrient replete condition. Similar to OSCC cell lines, a small variability was seen in IC_{50} of the autophagy inhibitors in TNBC cell lines following incubation with serum or glucose free media when compared to nutrient replete condition except for Spautin-1 that showed decrease in IC_{50} after 1 h glucose starvation in HCC1806.

Then, all cell lines were treated with different combinations either combination of standard chemotherapy agents (*i.e.,* Cisplatin or Paclitaxel) with Beclin-1 complex inhibitors or ULK-1 complex inhibitors or combination of ULK-1 complex inhibitors with Beclin-1 complex inhibitors under different conditions (*i.e.,* nutrient repletion and serum or glucose depletion

conditions). These results can be visualised in a heat map in **Figure 3.40**. The combinations that showed consistent results in all 4 cell lines are Cisplatin-SAR405, Paclitaxel-SAR405 and SAR405-MRT68921. The combination of either Cisplatin or Paclitaxel with Beclin-1 complex inhibitor (SAR405) exhibited synergism under nutrient replete condition with significant reduction of cellular proliferation in the 4 cell lines used. However, under serum or glucose depletion conditions, this combination was antagonistic which could be attributed to cancer cells attempting to activate other mechanisms that allow its survival under those stressors. Also, SAR405-MRT68921 combination showed a synergistic effect in all cell lines with significant reduction of tumour cell proliferation under nutrient replete and serum or glucose deplete conditions. Based on these results, combination of standard chemotherapeutics *(i.e.,* Cisplatin or Paclitaxel) with SAR405-MRT68921 combination was tested in SCC9 and MDA-MB231. MDA-MB231 and SCC9 revealed antagonist effect when treated with the latter combination, associated with no difference in cellular proliferation in comparison to each treatment alone.

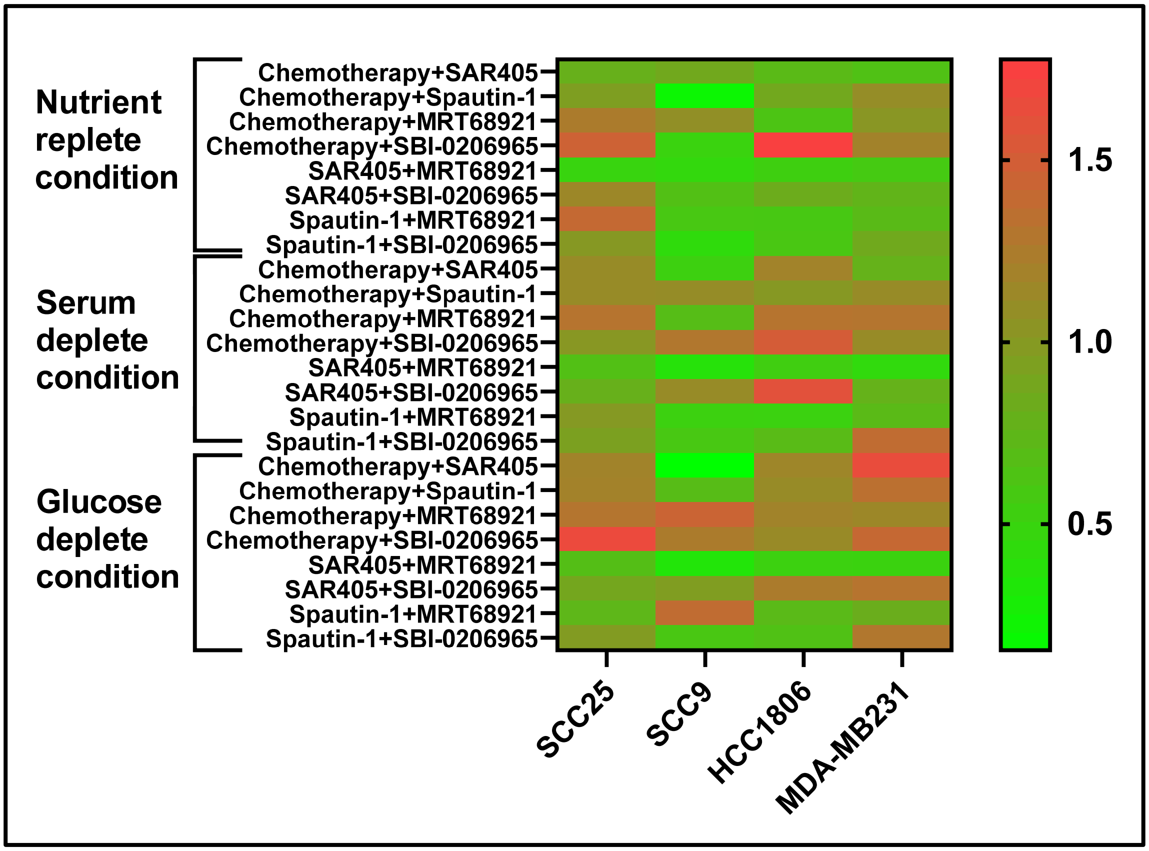

Figure 3.40. Heat map for combination index of different drug combinations across the 4 cell lines (SCC25, SCC9, HCC1806 and MDA-MB231) under different conditions (nutrient replete, serum deplete, and glucose deplete), plotted as mean with shades of green colour indicating different levels of synergism and shades of red colour indicating different levels of antagonism. Chemotherapy refers to Cisplatin for SCC25 and SCC9 and Paclitaxel for HCC1806 and MDA-MB231.

Moreover, the effect of these drugs on cell migration was evaluated by scratch wound assay. A dose dependent decrease in wound density was observed with increasing doses of drugs (Cisplatin, Paclitaxel, SAR405 or MRT68921) in both OSCC (SCC25 and SCC9) and TNBC (HCC1806 and MDA-MB231) cell lines. Also, the effect of combination therapies was examined. The results demonstrated a significant decrease in relative wound density across all cell lines, except for HCC1806, upon treatment with standard chemotherapy agents (*i.e.,* Paclitaxel) in combination with SAR405.

To achieve 3rd aim, a combination of Paclitaxel-SAR405-MRT68921 was examined in TNBC orthotopic xenograft model. Our data demonstrated a significant reduction in tumour volume and tumour weight in the group treated with Paclitaxel-SAR405-MRT68921 combination compared to the control group. From these findings, it can be concluded that targeting autophagy, via novel autophagy inhibitors directed toward major molecules in the autophagic pathway, inhibits tumour cell proliferation and migration both *in vitro* and *in vivo*.

Chapter 4

Assessing expression of LC3 and P62 in OSCC and TNBC Tissue Samples and its correlation with clinical and demographic characteristics

4.1. Introduction

Autophagy is a cell survival mechanism that has been shown to be involved in many pathologies including cancer. The role of autophagy in cancer has been controversial [67]. As mentioned before, in early carcinogenesis, autophagy seems to play a tumour suppressor role, while as the tumour grows it is switched into a tumour promotor role in which autophagy allows the survival of tumour cells under different metabolic stressors [67]. The relationship between autophagy and clinical outcomes of patients had been debatable. Different clinical studies had observed that either low or high expression of autophagy related protein were associated with poor prognosis in various cancer types including oral squamous cell carcinoma (OSCC) [215, 227] and triple negative breast cancer (TNBC) [386, 387].

OSCC is the sixth most common cancer worldwide [151] and has a poor prognosis due to metastasis, recurrence and poor chemosensitivity [163]. The relationship between autophagy related proteins (*i.e.,* LC3 and P62) and clinical parameters had been controversial in OSCC. Some studies demonstrated that high expression of autophagic proteins was associated with aggressive clinical behavior [215], while other studies showed that low expression levels of these proteins was linked to poor prognosis [227].

TNBC is a subtype of breast cancer which is characterised by lack of ER, PR and HER2 receptor expression [237]. It has an aggressive behavior with poor clinical outcome as it does not respond to endocrine or HER2 targeted therapies and conventional chemotherapy is not always effective [240]. Various studies have shown that either low or

high expression of autophagy related proteins (*i.e.,* LC3 and P62) are associated with poor prognosis of TNBC [386, 387].

Thus, the aim of this chapter is to evaluate the expression levels of autophagy related proteins (*i.e.,* LC3 and P62) in OSCC and TNBC tissue section via immunohistochemistry and assess the relationship between their expression level and the clinical characteristics of each cancer type. Further, expression levels of autophagy markers were also compared to the overall patient survival for TNBC cohorts.

4.2. Results

Three cohorts were included for this analysis: one cohort of OSCC tissue tumour specimens and the other two cohorts of TNBC tumour tissue specimens. For OSCC, all samples were obtained from tongue carcinoma patients. A total of 95 tongue tumour tissue specimens (1 H&E tissue section and 2 unstained tissue sections per case) and their clinical data were obtained from the Anatomical Pathology Department in Royal North Shore Hospital (RNSH), Sydney. Regarding TNBC, one cohort (135 tissue specimens in the form of TMAs and their clinical and survival data) was obtained from the Anatomical Pathology Department at the RNSH. The other cohort of TNBC (288 tissue specimens in the form of TMAs and their clinical and survival data) was obtained from the Australian Breast Cancer Tissue Bank (ABCTB), Sydney. All tissue and data were accessed under the purview of approved human ethics (Protocol# 2020/ETH02372) by the Northern Sydney Local Health District (NSLHD) Human Research Ethics Committee (HREC).

All OSCC and TNBC tissue specimens were immunohistochemically stained with LC3 and P62 using the standard procedure outlined in Chapter two. The subcellular localisation and percentage of immunohistochemical staining were evaluated. LC3 staining appeared in the cytoplasm as diffuse brown staining, while P62 exhibited both nuclear and cytoplasmic brown staining pattern. The Immunohistochemical evaluation and scoring was performed by one pathologist, without knowledge of clinicopathological data. For OSCC specimens, LC3 expression was evaluated as either positive or negative and some sections had very weak LC3 staining (<1% cells stained) which was considered as negative. For P62 staining in OSCC, as most of tissue sections had positive staining, the percentage of positive cells (cytoplasmic and nuclear) was recorded from 0-100%, then,

cases were further categorised into 2 groups: ≤50% and >50% positively stained cells. On the other hand, as TNBC specimens were TMAs and had a small tissue area, staining evaluation was recorded as positive or negative for both LC3 and P62.

4.2.1. Evaluation of LC3 and P62 staining in OSCC tissue specimens and their correlation with clinic-pathological characteristics

A total of 95 OSCCs were included in this study. All specimens were obtained from tongue. The clinical information for all OSCC patients is listed in **Table 4.1**.

Table 4.1. Clinical data for OSCC specimens. *Data was only available for 80 patients out of cohort of 95.

Clinical Data	OSCC specimens	
Age (mean ± S.D.; years)	63.1 ± 14.9	
Sex	Male	61
	Female	34
T stage*	T1	37
	T2	22
	T3	14
	T4	7
N Stage*	Positive	51
	Negative	29
Stage*	I	33
	II	15
	III	16
	IV	16
Histological Grade*	I	9
	II	57
	III	14

The relationship between LC3 and P62 (cytoplasmic and nuclear) expression and the clinicopathological characteristics was assessed by chi-square test (**Table 4.2 & 4.3**). 15 cases were excluded from the analysis due to unavailability of the majority of clinicopathological data.

As mentioned earlier, LC3 staining was categorised according to presence or absence of the staining into 2 groups as either negative (-ve) or positive (+ve). A total of 56 cases (70%) were classified as negative and 24 cases (30%) were classified as positive (**Figure 4.1**). LC3 expression was examined in terms of age, sex, T stage, N stage, overall stage, and histological grade, but no significant correlation was observed except positive LC3 expression was significantly (p=0.04) associated with low histologic grade (G1/2) (**Table 4.2**).

P62 was expressed in both nucleus and cytoplasm. The percentage of positive stained cells in each pattern was classified into 2 groups: ≤50 or >50% positively stained cells (**Figure 4.3**). A total of 51 cases (63.75%) were identified as ≤50% cytoplasmic stained cells and 29 cases (36.25%) were classified as >50% cytoplasmic stained cells. No significant correlation was observed between P62 cytoplasmic staining and clinical variables (*i.e.,* age, sex, stage, and grade). For P62 nuclear staining, a total of 56 cases (70%) were classified as ≤50% nuclear stained cells and 24 cases (30%) were assigned as >50% nuclear stained cells. Nuclear P62 exhibited no significant correlation with clinical characteristics (*i.e.,* age, sex, stage, and grade). Interestingly, higher P62 (>50%) nuclear staining was observed in higher stages (III/IV) of OSCC while an opposite association was observed with cytoplasmic staining, however, these relationships did not achieve statistical significance (p=0.09-0.77). Also, higher P62 (>50%) nuclear staining was noted in high OSCC histologic grade (G3) with the opposite relation observed in cytoplasmic staining, but, neither of them was statistically significant. (p=0.059-0.6) (**Table 4.3**).

Table 4.2. Relation between LC3 expression and clinicopathological variables in OSCC patients.

LC3						
Variable	**No of cases**		**-ve**	**+ve**	***p*-value**	**Odds ratio**
Age						
≤65.5	40	≤65.5	27	13	0.62	0.78 (0.28-2)
		vs				
>65.5	40	>65.5	29	11		
Sex						
Male	51	Male	33	18	0.17	0.47 (0.16-1.3)
		vs				
Female	29	Female	23	6		
T stage						
T1/T2	59	T1/T2	43	16	0.34	1.6 (0.5-4.4)
		vs				
T3/T4	21	T3/T4	13	8		
N stage						
N0	51	Negative	34	17	0.38	0.63 (0.24-1.7)
		vs				
N1/N2/N3	29	Positive	22	7		
Stage						
I/II	48	Low	35	13	0.48	1.4 (0.5-3.7)
		vs				
III/IV	32	High	21	11		
Histologic grade						
G1/2	66	Low	43	23	0.04*	0.14 (0.01-0.9)
		vs				
G3	14	High	13	1		

Table 4.3. Relation between P62 expression (cytoplasmic and nuclear) and clinicopathological variables in OSCC patients.

			Cytoplasmic P62				Nuclear P62			
Variable	**No of cases**		**≤50 %**	**>50 %**	***p*-value**	**Odds ratio**	**≤50%**	**>50%**	***p*-value**	**Odds ratio**
Age										
≤65.5	40	≤65.5 *vs* >65.5	25	15	0.81	0.89 (0.37 -2)	27	13	0.62	0.78 (0.28 -2)
>65.5	40		26	14			29	11		
Sex										
Male	51	Male *vs* Female	34	17	0.47	1.4 (0.54 -3.5)	35	16	0.72	0.8 (0.29 -2.2)
Female	29		17	12			21	8		
T stage										
T1/T2	59	T1/T2 *vs* T3/T4	36	23	0.39	0.62 (0.2-1.8)	44	15	0.13	2.2 (0.77 -5.9)
T3/T4	21		15	6			12	9		
N stage										
N0	51	Negative vs Positive	33	18	0.81	1.1 (0.41 -2.7)	37	14	0.50	1.3 (0.55 -3.7)
N1/N2/ N3	29		18	11			19	10		
Stage										
I/II	48	Low *vs* High	30	18	0.77	0.87 (0.33 -2.1)	37	11	0.09	2.3 (0.85 -5.7)
III/IV	32		21	11			19	13		
Histologic grade										
G1/2	66	Low *vs* High	39	27	0.059	0.24 (0.05 -1.1)	47	19	0.60	1.3 (0.4-4.2)
G3	14		12	2			9	5		

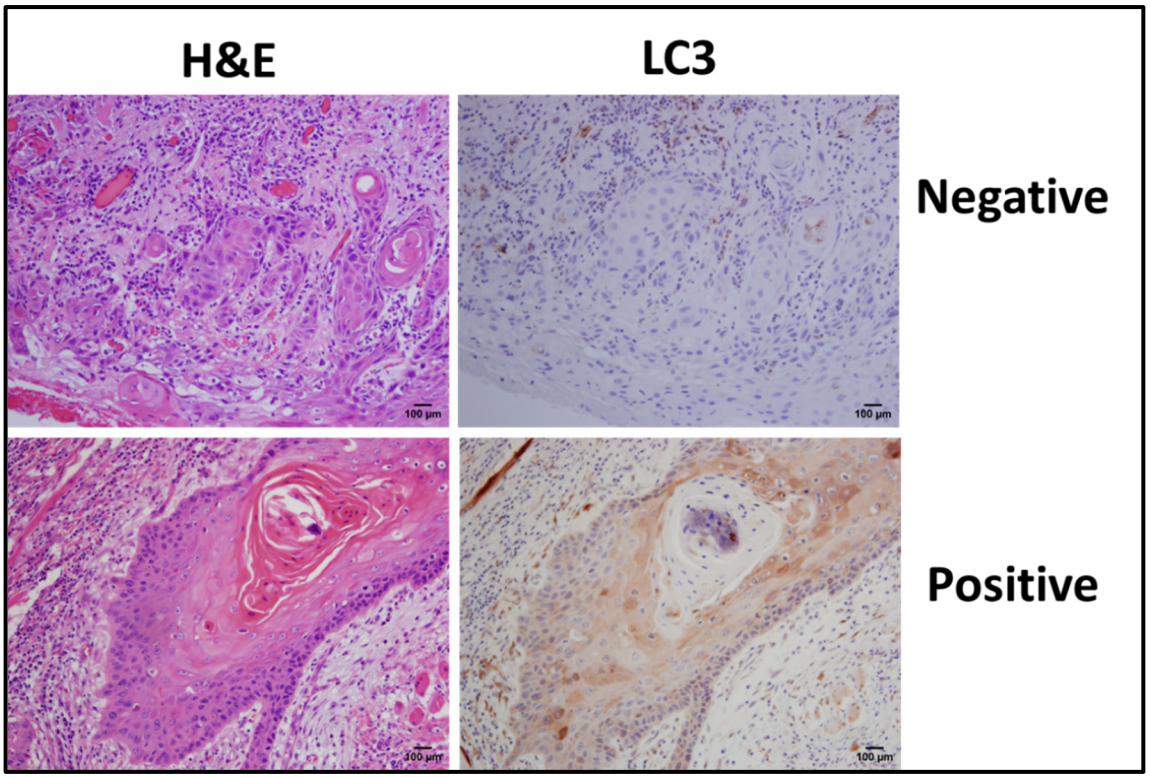

Figure 4.1. H&E and immunohistochemical staining of LC3 in OSCC (original magnification x40). LC3 staining is classified into 2 groups according to presence or absence of the staining (positive or negative). Scale bar: 100µm

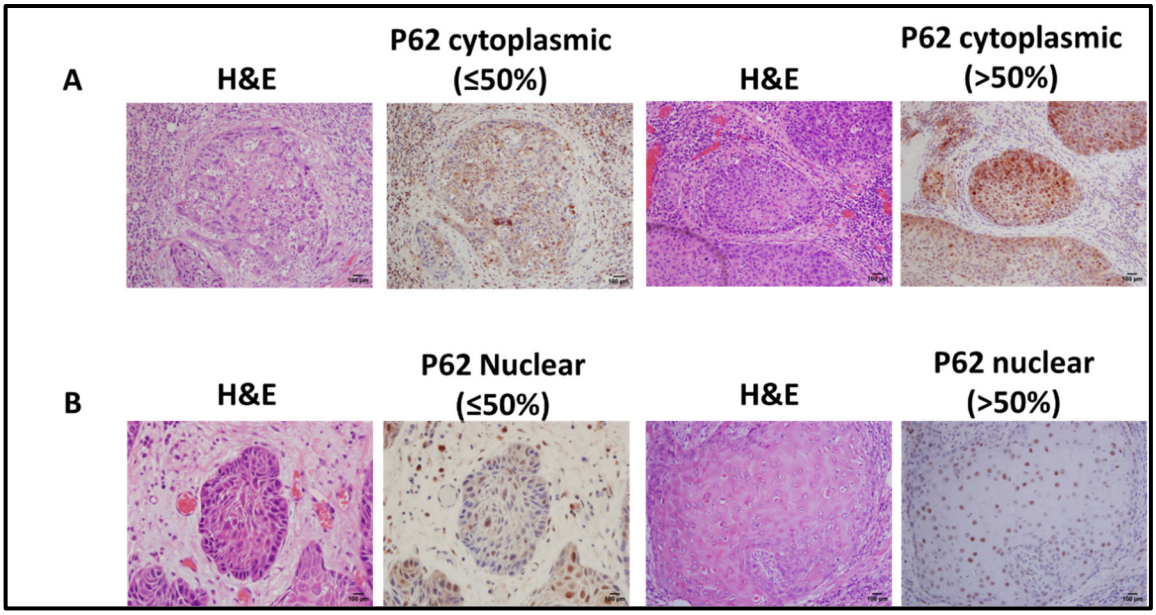

Figure 4.2. H&E and immunohistochemical staining of P62 in OSCC (original magnification x40 and x20). P62 was detected in both cytoplasm and nucleus and is classified into 2 groups according to percentage of immunopositive cells (≤50% or >50%). Scale bar: 100μm

4.2.2. Evaluation of LC3 and P62 staining in TNBC tissue specimens and their correlation with clinicopathological characteristics and overall survival

(A) RNSH TNBC cohort

A total of 135 cases were included in this cohort in the form of TMAs. 3 cases had been excluded from the cohort due to incomplete available clinical data. The clinical data for this cohort are listed in **Table 4.4**

Table 4.4. Clinical data for TNBC specimens from RNSH.

Clinical Data	TNBC specimens from	
Age (mean ±S.D.; years)	60 ±16	
Location	Right	69
	Left	66
Recurrence	Absent	113
	Present	22
Vascular Space invasion	Absent	86
	Present	49
T-stage	T1	58
	T2	65
	T3	7
	T4	5
N-stage	N0	89
	N1	27
	N2	9
	N3	10
Stage	I	49
	II	65
	III	21

The relationship between LC3 and P62 expression and the clinicopathological parameters was assessed by chi-square test (**Table 4.5**). LC3 was expressed as diffuse brown staining in the cytoplasm which was categorised as positive (+ve) or negative (-ve) according to presence or absence of the stain, respectively (**Figure 4.3**). A total of 104 cases (77%) were assessed as negative LC3 staining, whereas 31 cases (22.9%) were

classified as positive LC3 staining. LC3 expression was examined in terms of age, location, vascular invasion, tumour-node stage, and recurrence but no significant correlation was observed (**Table 4.5**).

P62 was expressed as brown cytoplasmic staining, sometimes nuclear staining was observed. P62 was classified as positive (+ve) or negative (-ve) according to presence or absence of P62 staining, respectively (**Figure 4.3**). A total of 117 cases (86.6%) were classified as positive P62 staining, and 18 cases (13.3%) were assessed as negative P62 staining. No significant correlation was observed between P62 expression and any of the clinicopathological parameters (**Table 4.5**).

Survival analysis was performed using Kaplan-Meier analysis using Log-Rank test to identify any relationship between LC3 and P62 expression and overall survival. The median follow-up time for TNBC patients was 43.65 months. Regarding LC3, the median survival for patients with LC3 positive tumours was 107.7 months, which was significantly higher (p<0.05) than that of patients with LC3 negative tumours (92.66 months) (**Figure 4.4 A**). On the other hand, the median survival of patients with P62 positive tumours was 107.7 months, while it was 91.81 months for patients with P62 negative tumours. There was no significant difference (p=0.903) in overall survival was observed between patients with P62 positive and negative tumours (**Figure 4.4B**).

Table 4.5. Relation between LC3 and P62 expression and clinicopathological variables in TNBC patients.

		LC3					P62			
Variable	**No. of cases**	**-ve**	**+ve**	***p*-value**	**Odds ratio**		**-ve**	**+ve**	***p*-value**	**Odds ratio**
Age										
≤59	68	48	20	0.07	0.47 (0.21-1.1)	≤59 *vs* >59	9	59	0.97	0.98 (0.38-2.5)
>59	67	56	11				9	58		
Location										
Right	69	49	20	0.08	2.04 (0.86-4.4)	Left *vs* Right	8	61	0.54	1.36 (0.53-3.7)
Left	66	55	11				10	56		
Vascular space invasion										
Absent	86	67	19	0.75	1.1 (0.5-2.5)	Absent *vs* Present	9	77	0.19	0.5 (0.2-1.3)
Present	49	37	12				9	40		
T stage										
T1/T2	123	93	30	0.20	0.28 (0.02 5-1.7)	T1/T2 *vs* T3/T4	17	106	0.59	1.7 (0.26-20)
T3/T4	12	11	1				1	11		
N stage										
N0	89	66	23	0.26	0.6 (0.25-1.4)	-ve *vs* +ve	12	77	0.94	1 (0.35-3)
N1/N2/ N3	46	38	8				6	40		
Stage										
I/II (low)	114	86	28	0.30	0.5 (0.15-1.8)	Low *vs* High	14	100	0.40	0.59 (0.18-1.8)
III/IV (High)	21	18	3				4	17		
Recurrence										
Absent	113	87	26	0.97	0.98 (0.36-2.8)	Absent *vs* Present	16	97	0.52	1.6 (0.38-7.6)
Present	22	17	5				2	20		

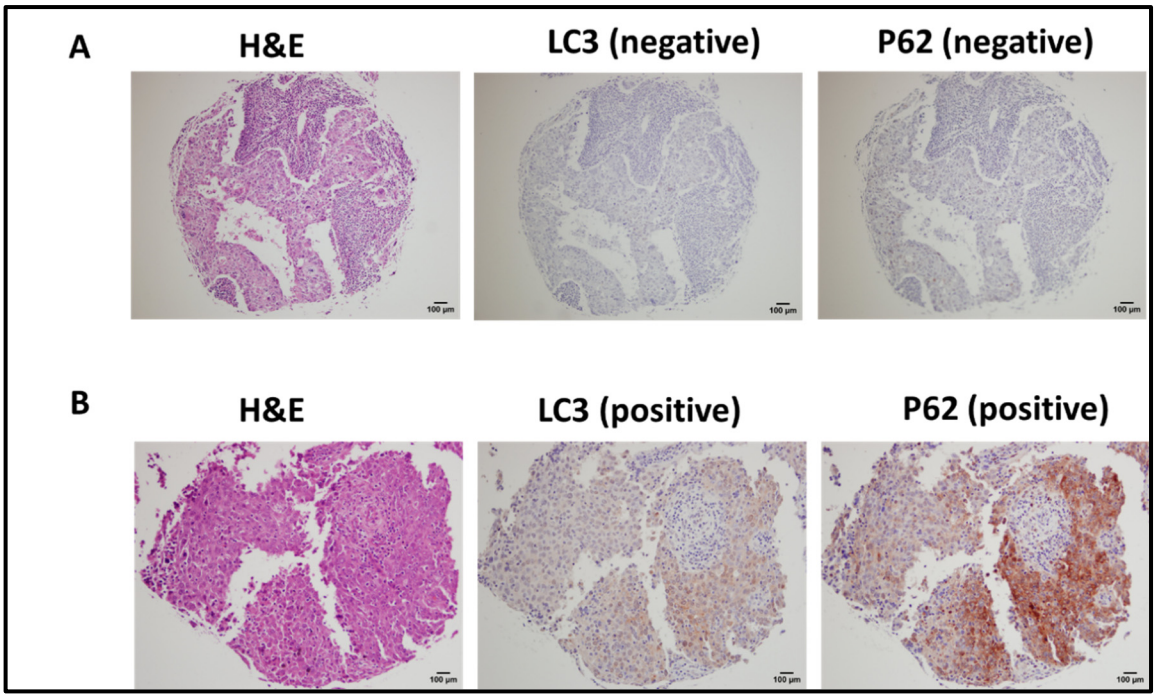

Figure 4.3. H&E and immunohistochemical staining of LC3 and P62 in TNBC. (A) Negative LC3 and P62 staining in TNBC (original magnification x20). (**B)** Positive LC3 and P62 staining in TNBC (original magnification x40). Scale bar: 100μm

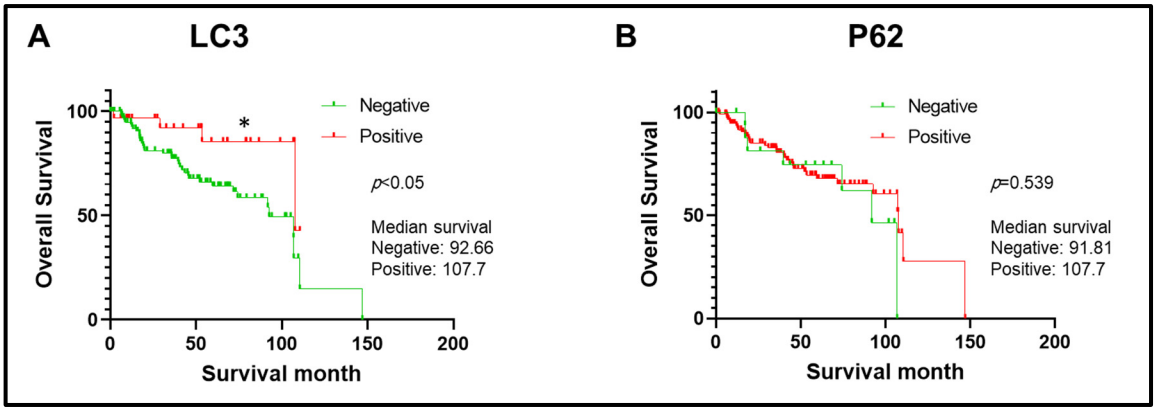

Figure 4.4. Kaplan-Meier curve for overall survival according to (A) LC3 and (B) P62 expression in TNBC cohort from RNSH. Positive LC3 expression was associated with better overall survival.

Furthermore, univariable, and multivariable Cox proportional hazard analysis was carried out to detect any association between the clinicopathological variables and overall survival (**Table 4.6 and 4.7**)**.** Based on the univariable analysis, increasing age, positive lymph node, high overall stage (III/ IV), presence of recurrence and negative LC3 staining in the tumour were associated with poor overall survival (**Table 4.6**). Next, multivariable analysis of parameters which were significant in univariable analysis showed that increasing age, high overall stage, presence of recurrence and negative LC3 staining in the tumour were independently associated with poor overall survival (**Table 4.7**).

Table 4.6. Univariable Cox proportional hazard analysis of clinicopathological variables for overall survival in TNBC patients.

Variable		HR	95% CI	*p*-value
Age		1.052	1.028- 1.077	<0.001*
Location	Left *vs* Right	1.588	0.825- 2.940	0.172
Vascular space invasion	Absent *vs* Present	0.539	0.287-1.011	0.054
T-stage	T1	0.188	0.06- 0.589	0.004*
	T2	0.268	0.09- 0.802	0.019*
	T3	0.8	0.212- 3.011	0.741
N-stage	Negative *vs* Positive	0.233	0.122- 0.447	<0.001*
Overall stage	High (III/IV) *vs* low (I/II)	6.940	3.571- 13.486	<0.001*
Recurrence	Present *vs* Absent	3.399	1.793- 6.444	<0.001*
LC3 expression	Negative *vs* Positive	3.151	1.118-8.883	0.03*
P62 expression	Negative *vs* Positive	1.294	0.567- 2.949	0.540

Table 4.7. Multivariable Cox proportional hazard analysis of clinicopathological variables for overall survival in TNBC patients.

Variable		HR	95% CI	*p*-value
Age		1.051	1.026- 1.078	<0.001*
T-stage	T1	1.4	0.403- 5.5	0.547
	T2	2.7	0.716- 10.5	0.141
	T3	2.2	0.528- 9.3	0.276
N-stage	Negative *vs* Positive	0.579	0.244- 1.5	0.259
Overall stage	High (III/IV) *vs* low (I/II)	5.1	1.8- 14	0.002*
Recurrence	Present *vs* Absent	3	1.5- 5.9	0.001*
LC3 expression	Negative *vs* Positive	3.3	1- 10	0.043*

(B) ABCTB TNBC cohort

A total of 288 cases were obtained from the tumour bank, but only 274 were included in the analysis due to poor sample integrity for a few samples or incomplete clinical data. The clinical data for this cohort are listed in **Table 4.8**

Table 4.8. Clinical data for ABCTB TNBC cohort.

Clinical Data	TNBC specimens from RNSH	
Age (mean ±S.D.; years)	56.1 ± 14.4	
Tumour size (mean ± S.D.; mm^2)	29.4 ± 15.9	
Location	Right	120
	Left	150
	Bilateral	4
T-stage	T1	85
	T2	168
	T3	21
L.N. status	Negative (N)	160
	Positive (P)	114

The relationship between LC3 and P62 expression and the clinicopathological parameters was assessed via chi-square test (**Table 4.9**). Expression of LC3 in the cytoplasm was identified as diffuse brown staining and classified as either positive (+ve) or negative (-ve) (**Figure 4.5**). A total of 99 cases (36.1%) were identified as negative LC3 staining, and 175 cases (63.8%) were classified as positive LC3 staining. However, no significant correlation was noted between age, location, and tumour-node stage and LC3 expression, a significant correlation (p<0.05) was detected between high histologic grade and positive LC3 expression (**Table 4.9**).

P62 was expressed as cytoplasmic brown staining that was categorised into 2 groups: negative (-ve) or positive (+ve) (**Figure 4.6**). A total of 12 cases (4.4%) were classified as negative P62 staining, whereas 262 cases (95.6%) were identified as positive P62 staining. Similar to LC3, a significant correlation (p<0.05) between P62 expression and clinicopathological parameters was only noted in the histologic grade parameter. High histological grade was associated with positive P62 staining (**Table 4.9**).

Moreover, Kaplan-Meier survival analysis was performed to determine the relationship between LC3 and P62 expression and overall survival of the cohort. The median follow-up time for TNBC patients was 50 months. Patients with positive LC3 expression in their tumour had significantly higher overall survival (p<0.01), while no significant difference (p=0.628) in overall survival was observed between patients with P62 negative and positive tumour expression (**Figure 4.7**).

Table 4.9. Relation between LC3 and P62 expression and clinicopathological variables in TNBC patients.

		LC3					P62			
Variable	**No. of cases**	**-ve**	**+ve**	***p*-value**	**Odds ratio**		**-ve**	**+ve**	***p*-value**	**Odds ratio**
Age										
≤56	144	45	99	0.076	0.63 (0.39-1.06)	≤56 *vs* >56	5	139	0.439	0.63 (0.22-1.8)
>56	130	54	76				7	123		
Location										
Right	120	44	76	0.82	0.94 (0.58-1.5)	Left *vs* Right	5	115	0.85	1.1 (0.38-3.1)
Left	150	53	97				7	143		
Histologic grade										
Low grade	21	12	9	0.037*	2.5 (1-6)	Low *vs* high	3	18	0.02*	4.5 (1.2-16)
High grade	253	87	166				9	244		
T stage										
T1/T2	253	89	264	0.254	0.59 (0.25-1.4)	T1/T2 *vs* T3/T4	11	242	0.929	0.9 (0.14-10.2)
T3/T4	21	10	11				1	20		
N stage										
N	160	58	102	0.96	1 (0.62-1.6)	-ve *vs* +ve	9	151	0.232	2.2 (0.58-7.6)
P	114	41	73				3	111		

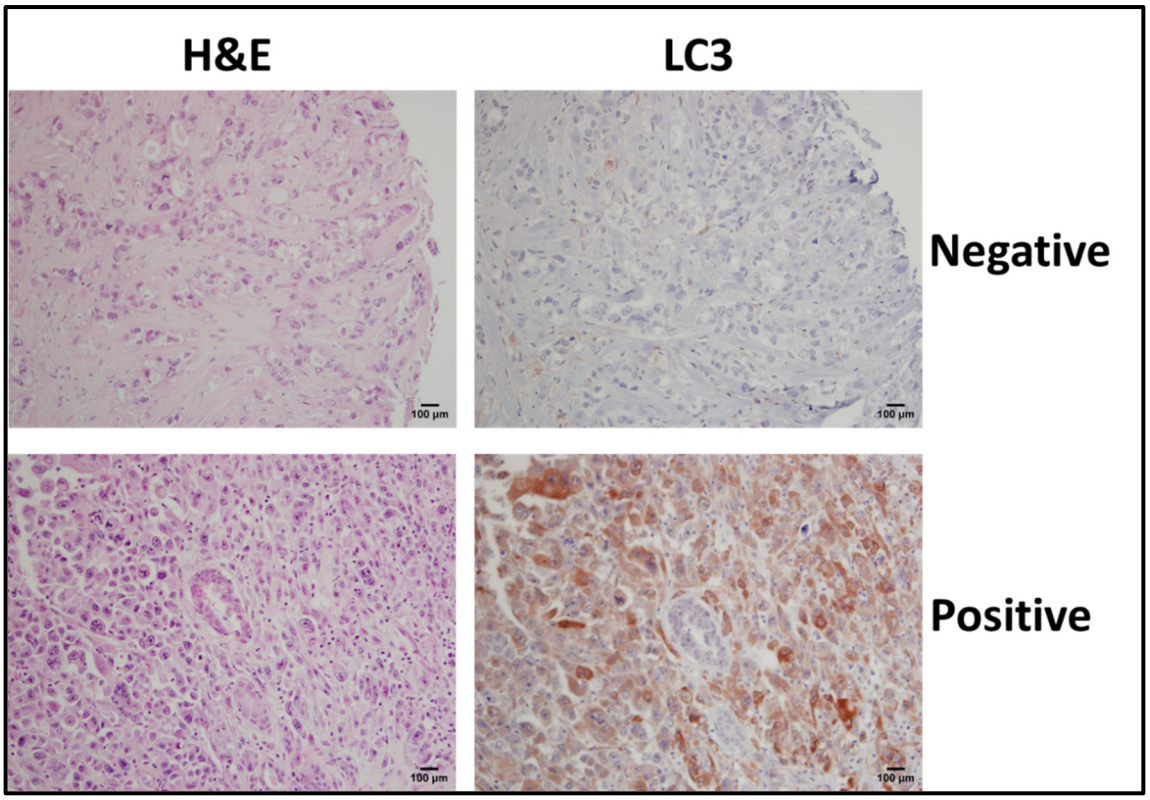

Figure 4.5. H&E and immunohistochemical staining of LC3 in TNBC (original magnification x40). LC3 staining is classified as negative or positive. Scale bar: 100µm

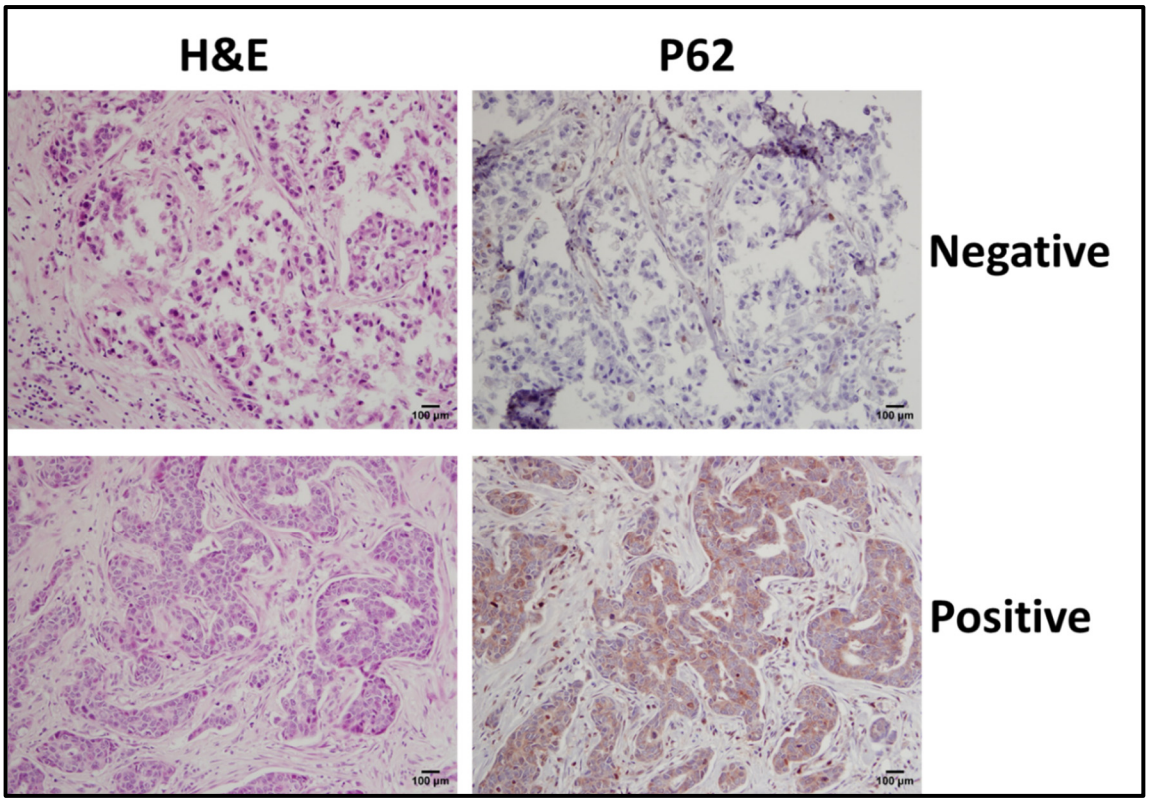

Figure 4.6. H&E and immunohistochemical staining of P62 in TNBC (original magnification x40). P62 staining is classified as negative or positive. Scale bar: 100µm

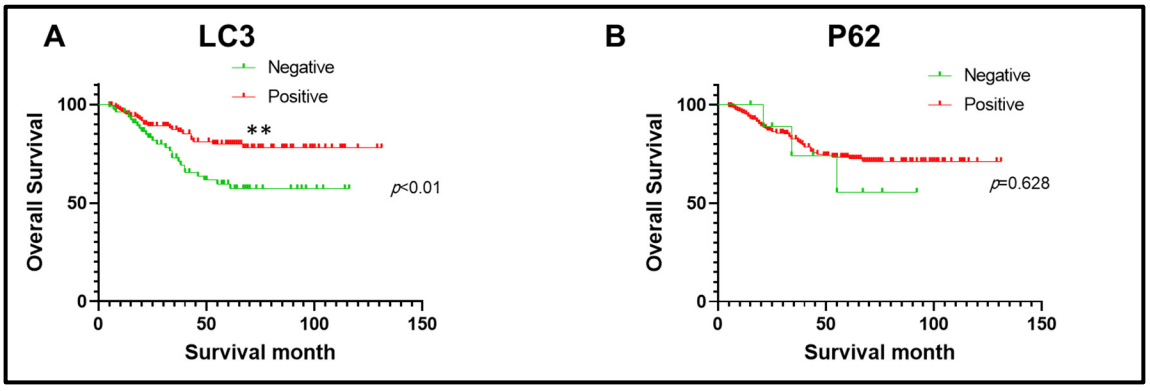

Figure 4.7. Kaplan-Meier curve for overall survival according to (A) LC3 and (B) P62 expression in TNBC cohort from tumour bank. Positive LC3 expression was associated with better overall survival.

Also, the relationship between any of the clinicopathological variables and overall survival was assessed using univariable and multivariable Cox proportional hazard analysis (**Table 4.10 and 4.11).** Based on the univariable analysis, increasing age and tumour size, positive lymph node and negative LC3 staining of tumour were associated with poor overall survival (**Table 4.10**). On the other hand, multivariable analysis of significant variables identified in univariable analysis demonstrated that increasing age and positive lymph node were the only independent variables associated with poor overall survival (**Table 4.11**).

Table 4.10. Univariable Cox proportional hazard analysis of clinicopathological variables for overall survival in TNBC patients.

Variable		HR	95% CI	*p*-value
Age		1.043	1.023-1.063	<0.001***
Location	Left *vs* Right	1.262	0.722- 2.207	0.414
Tumour size		1.024	1.014- 1.035	<0.001***
T-stage	T1	0.177	0.072- 0.435	<0.001***
	T2	0.341	0.167- 0.697	0.003**
N-stage	Negative *vs* Positive	0.470	0.268- 0.826	0.009**
Histologic grade	High *vs* low	2.099	0.510- 8.639	0.304
LC3 expression	Negative *vs* Positive	2.154	1.236- 3.756	0.007**
P62 expression	Negative *vs* Positive	1.336	0.416- 4.295	0.626

Table 4.11. Multivariable Cox proportional hazard analysis of clinicopathological variables for overall survival in TNBC patients.

Variable		HR	95% CI	*p*-value
Age		1	1.019-1.059	<0.001***
Location	Left *vs* Right	1.188	0.662- 2.132	0.563
Tumour size		1	0.982- 1.033	0.582
T-stage	T1	0.407	0.074- 2.2	0.301
	T2	0.65	0.182- 2.3	0.507
N-stage	Negative *vs* Positive	0.468	0.258- 0.847	0.012*
Histologic grade	High *vs* low	2.780	0.648- 11.930	0.169
LC3 expression	Negative *vs* Positive	1.5	0.856- 2.8	0.15
P62 expression	Negative *vs* Positive	1.325	0.375- 4.681	0.663

(C) Analysis of both TNBC cohorts

We combined data from both TNBC cohorts (RNSH and ABCTB) for further analysis. A total of 409 cases were included in this analysis. The clinical data for these cohorts are listed in **Table 4.12**.

Table 4.12. Clinical data for both TNBC cohorts.

Clinical Data	TNBC specimens from both cohorts	
Age (mean ±S.D.; years)	57.3±14.9	
Location	Right	189
	Left	216
	Bilateral	4
T-stage	T1	143
	T2	233
	T3	28
	T4	5
L.N. status	Negative (N)	249
	Positive (P)	160

The relationship between common clinical parameters in both cohorts and expression of LC3 and P62 was assessed using chi-square test (**Table 4.13)**. Negative LC3 and p62 expression was significantly associated (p<0.05) with increasing age. Also, survival analysis for both cohorts was carried out using Kaplan Meier test. The median follow-up time of all TNBC patients was 45.9 months. Patients with positive LC3 expression in their tumours specimens had significantly (p<0.0001) better overall survival (**Figure 4.8A**). On the contrary, there was no significant difference between overall survival of patients with positive and negative P62 expression in their tumour (**Figure 4.8B**).

Table 4.13. Relation between LC3 and P62 expression and clinicopathological variables in both TNBC cohorts.

		LC3					P62			
Variable	**No. of cases**	**-ve**	**+ve**	***p*-value**	**Odds ratio**		**-ve**	**+ve**	***p*-value**	**Odds ratio**
Age										
≤57	209	92	117	0.02*	0.6 (0.42-92)	≤57 *vs* >57	10	199	0.04*	0.45 (0.21 - 0.95)
>57	200	112	88				20	180		
Location										
Right	189	93	96	0.87	1 (0.69-1.5)	Left *vs* Right	13	176	0.7	1.1 (0.55 -2.3)
Left	216	108	108				17	199		
T stage										
T1/T2	367	182	194	0.093	0.54 (0.26-1.1)	T1/T2 *vs* T3/T4	28	348	0.769	1.2 (0.31 -5.5)
T3/T4	33	21	12				2	31		
N stage										
N	249	124	125	0.933	1 (0.68-1.5)	Negative *vs* Positive	21	228	0.287	1.5 (0.71 -3.5)
P	160	79	81				9	151		

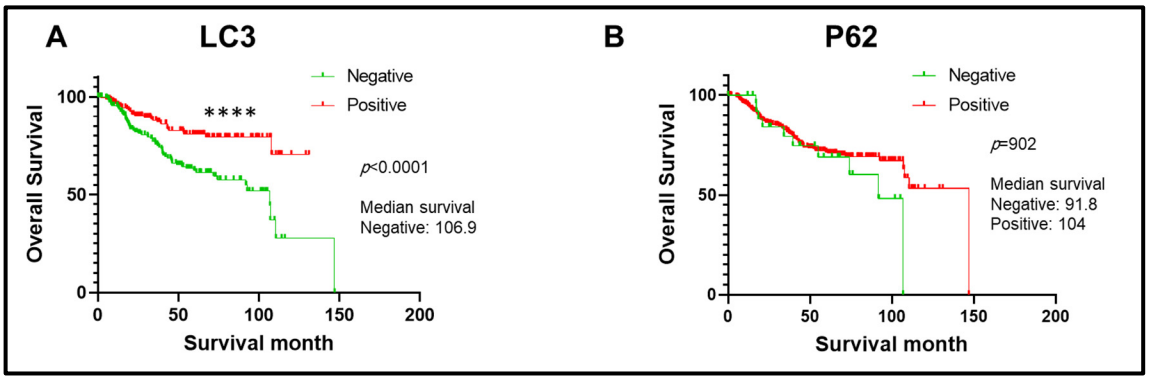

Figure 4.8. Kaplan-Meier curve for overall survival according to (A) LC3 and (B) P62 expression in both TNBC cohort. Positive LC3 expression was associated with better overall survival.

Lastly, univariable, and multivariable Cox regression analysis were performed for both cohorts together to determine any correlation between the common clinical variables in both cohorts and overall survival. **Table 4.14 and 4.15** present the results of univariable and multivariable analysis, respectively. The univariable analysis showed that increasing age and positive lymph node are associated with poor overall survival. Also, T1/T2 and positive LC3 staining of tumour specimen were associated with better overall survival based on the univariable analysis (**Table 4.14**). In multivariate analysis of significant variables from univariable analysis demonstrated that all these variables were independently associated with overall survival outcomes (**Table 4.15**).

Table 4.14. Univariable Cox proportional hazard analysis of clinicopathological variables for overall survival in both TNBC cohorts.

Variable		HR	95% CI	*p*-value
Age		1.047	1.032-1.062	<0.001***
Location	Left *vs* Right	1.380	0.908- 2.098	0.131
T-stage	T1	0.143	0.049- 0.417	<0.001***
	T2	0.235	0.085- 0.652	0.005*
	T3	0.623	0.206- 1.883	0.402
N-stage	Negative *vs* Positive	0.367	0.240- .561	<0.001***
LC3 expression	Negative *vs* Positive	2.368	1.515- 3.704	<0.001***
P62 expression	Negative *vs* Positive	1.422	0.736- 2.749	0.295

Table 4.15. Multivariable Cox proportional hazard analysis of clinicopathological variables for overall survival in both TNBC cohorts.

Variable		HR	95% CI	*p*-value
Age		1.04	1.026-1.055	<0.001***
T-stage	T1	0.306	0.103- 0.912	0.034*
	T2	0.504	0.178- 1.4	0.195
	T3	1.05	0.348- 3.2	0.992
N-stage	Negative *vs* Positive	0.413	0.268- 0.636	<0.001**
LC3 expression	Negative *vs* Positive	1.8	1.1- 2.8	0.017*

4.3. Summary of findings

The aim of this chapter was to assess LC3 and P62 expression in OSCC and TNBC tissue sections by immunohistochemistry. Three cohorts were included in this chapter, one for OSCC and two for TNBC.

In OSCC, LC3 was expressed as brown diffuse staining in the cytoplasm which was categorised into 2 groups: negative or positive according to absence or presence of staining. The relationship between LC3 expression and clinicopathological parameters was evaluated and showed that positive LC3 expression was associated with low histologic grade of OSCC (p<0.05). Regarding P62, it showed nuclear and cytoplasmic patterns in OSCC. Each pattern is classified, according to percentage of immunostained cells, into: ≤50% or >50%. High nuclear P62 was seen in high stage (III/IV) and high histopathological grade (G3) of OSCC, and the reverse association was noted with cytoplasmic P62 staining, but neither of these associations were statistically significant.

In both cohorts of TNBC, LC3 was expressed as cytoplasmic brown staining which was further classified as negative or positive. P62 showed the same pattern of expression as LC3 and was categorised as either negative or positive. The relation between LC3 and P62 expression and clinicopathological characteristics was evaluated for each cohort individually and then combined together. A significant correlation was noted between positive LC3 and P62 expression and high histologic grade (p<0.05) in the ABCTB cohort.

Survival analysis was performed for both TNBC cohorts separately and then combined together. It was observed that patients with positive LC3 expression in tumour tissue specimen had better overall survival in both cohort (p<0.05) and when combined (p<0.0001). Moreover, patients with positive P62 expression in tumour tissue specimen also showed better overall survival but it did not achieve statistical significance in any of the cohorts. These results indicate that patients with better overall survival might have an increased induction of autophagy in their tumours, which was indicated by the observed positive LC3 expression. However, at the same time autophagic flux might have been impaired due to increased P62 expression. This may explain why patient cohort with positive LC3 expression had a better survival, as the whole process of autophagy might be dysfunctional.

Lastly, univariable, and multivariable Cox regression analysis was performed for both cohorts separately and then combined. Based on univariable and multivariable analysis, both cohorts showed poor overall survival with increasing age, positive lymph node status and negative LC3 expression, whereas better overall survival was associated with T1 tumour stage. Taking together, age, lymph node status, LC3 expression and tumour stage were shown to be independent prognostic factors in TNBC patients.

Chapter 5

Development of OSCC and TNBC Resistant Cell Models and Identification of Novel Targets for Chemoresistance

5.1. Introduction

As discussed in chapter one, autophagy plays a crucial role in cancer progression [67]. It allows cancer cells to survive under different tumour microenvironmental stressors such as energy and nutrient deprivation and stress induced by chemotherapy [378]. Chemotherapeutic agents usually act by inducing apoptosis of cancer cells; however, tumour cells sometimes become irresponsive to the chemotherapy and develop chemoresistance [388]. Several studies have indicated that administration of chemotherapeutic agents leads to autophagy induction in tumour cells which had shed some light on a relationship between autophagy and chemoresistance [389, 390]. The role of autophagy in developing chemoresistance has not been fully understood. Thus, more research should be directed toward this field to elucidate the mechanism by which autophagy contributes to chemoresistance and this might open up new strategies to overcome chemoresistance in cancer cells.

Oral squamous cell carcinoma (OSCC) is the sixth most prevalent cancer worldwide [151]. OSCC patients suffer from poor prognosis due to late detection, early metastasis, and high recurrence rates [163]. Despite cisplatin being the gold standard chemotherapeutic agent for OSCC [166], it did not improve the overall survival rate over the last decade [169]. This is mainly due to the development of chemoresistance in cancer cells [170]. Several studies have linked chemoresistance in OSCC with an induction of autophagy [223, 225, 226] and thus, targeting autophagy could be developed as a potential strategy to overcome chemoresistance in OSCC.

Triple negative breast cancer (TNBC) is a subtype of breast cancer that accounts for 15% of all breast cancer types [240]. It has the lowest survival rate of all breast cancer types [241]. This is due to lack of ER, PR and HER2 receptor expression which makes endocrine or HER2 targeted therapies ineffective [240]. Although chemotherapy is the mainstay treatment available, 30-40% of patients develop metastasis which are often chemoresistant [247]. Many studies have correlated TNBC chemoresistance to autophagy [293, 295, 296], which might be a promising target to overcome chemoresistance in TNBC.

Taken together, the aim of this chapter is directed to:

1) Develop OSCC and TNBC resistant cell models.
2) Evaluate the effect of specific autophagy inhibitors on OSCC and TNBC resistant cell models.
3) Proteomic analysis of resistant cell models in both OSCC and TNBC to identify any novel targets for chemoresistance.
4) Evaluate the role of detected novel targets from proteomic analysis in OSCC and TNBC resistant cell models.

5.2. Results

5.2.1. Development of resistant OSCC and TNBC cell models

In OSCC cell model, SCC9 and HN6 cell lines were used to develop chemoresistance as we were unable to develop resistant phenotype of SCC25 and used HN6 cell line instead. OSCC cell lines (SCC9 and HN6) were treated with gradually increasing gradient concentrations of Cisplatin. We started treatments from IC_{30} (10.5 µM for SCC9 and 1.6 µM for HN6) for 3 days then, changed to drug free media to revive the cells. Once the cells were confluent, they were subcultured and treated with two-fold concentrations of the respective drug. This process was continued until a concentration of 280 µM for SCC9 and 425 µM for HN6 was reached where both cell lines were able to grow under these concentrations.

A chemoresistance phenotype was validated by determining the IC_{50} for both cell lines in comparison to the parent cell lines via cellular proliferation assay. For SCC9, IC_{50} of cisplatin-resistant (CR) cell line (*i.e.*, SCC9 CR) was 5-fold higher (87.6 µM ± 7.8) in comparison to the parent cell line (17.5 µM ± 3.7). In case of HN6, IC_{50} for cisplatin-resistant cell line (*i.e.*, HN6 CR) was 60.7 µM ± 5, while IC_{50} for the parent cell line was 7.5 µM ± 1.7 (**Figure 5.1.A**).

As Paclitaxel is the standard chemotherapeutic agent for TNBC, TNBC cell lines (HCC1806 and MDA-MB231) were treated with gradient concentrations of Paclitaxel following the previous described procedure for OSCC cell lines, starting at a concentration of IC_{30} (*i.e.*, 2.1 nM for HCC1806 and 0.59 nM for MDA-MB231). Treatments were continued until a concentration of 1.6 µM for HCC1806 and 1 µM for MDA-MB231 was

achieved where both cell lines were able to grow under these concentrations. Then, IC_{50} of paclitaxel-resistant (PR) cell lines were calculated using cellular proliferation assay. The cellular proliferation assay showed that IC_{50} of resistant HCC1806 (*i.e.*, HCC1806 PR) was 280 nM ± 0.1compared to IC_{50} of the parent cell line that was 3.15 nM ± 0.56. Resistant MDA-MB231 (*i.e.*, MDA-MB231 PR) had IC_{50} of 7.6 µM ± 1.1, while IC_{50} of the parent cells was 0.99 nM ± 0.23 (**Figure 5.1.B**).

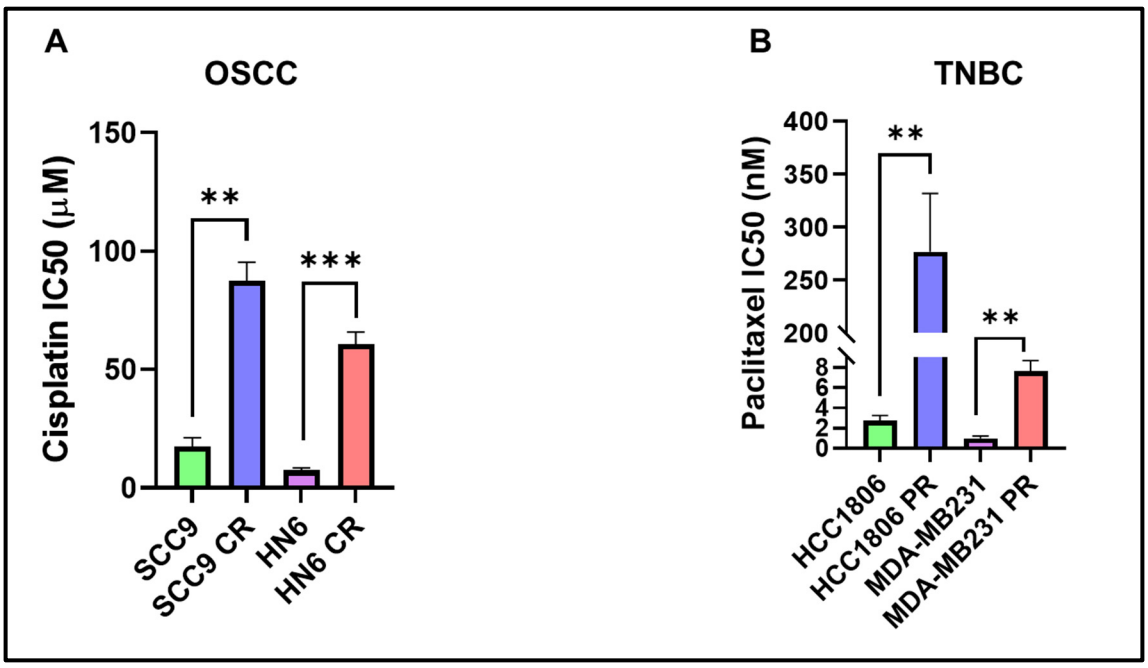

Figure 5.1. Graph showing IC_{50} for each of the parent cell line in comparison to its resistant counterpart for (A) OSCC and (B) TNBC cell models. Graphs are mean ± SEM. **p<0.01, ***p<0.001 compared to respective parent cells.

Moreover, resistant cell lines for both OSCC and TNBC cell models were further characterised using the colony formation assay (CFA). The ability of standard chemotherapeutics to stop initiation of 50% colonies was compared between resistant and parent cell lines. HN6 CR showed a significantly (p<0.0001) higher IC_{50} value for Cisplatin

(5 µM ± 0.1) than the parent cells (0.5 µM ± 0.1) (**Figure 5.2**). Likewise, IC_{50} of Cisplatin in SCC9 CR was significantly (p<0.01) higher (3.2 µM ± 0.6) than that of the parent cells (0.56 µM ± 0.2) (**Figure 5.3**). HCC1806 PR did not produce any colonies under control conditions, and as such we were unable to use it in this assay. Moreover, MDA-MB-231 PR had a significantly (p<0.001) higher IC_{50} for Paclitaxel (2.6 nM ± 0.1) than the parent cells (1.2 nM ± 0.05) (**Figure 5.4**). These results are consistent with data obtained from cellular proliferation assay, which indicate the chemo-resistant phenotype was generated.

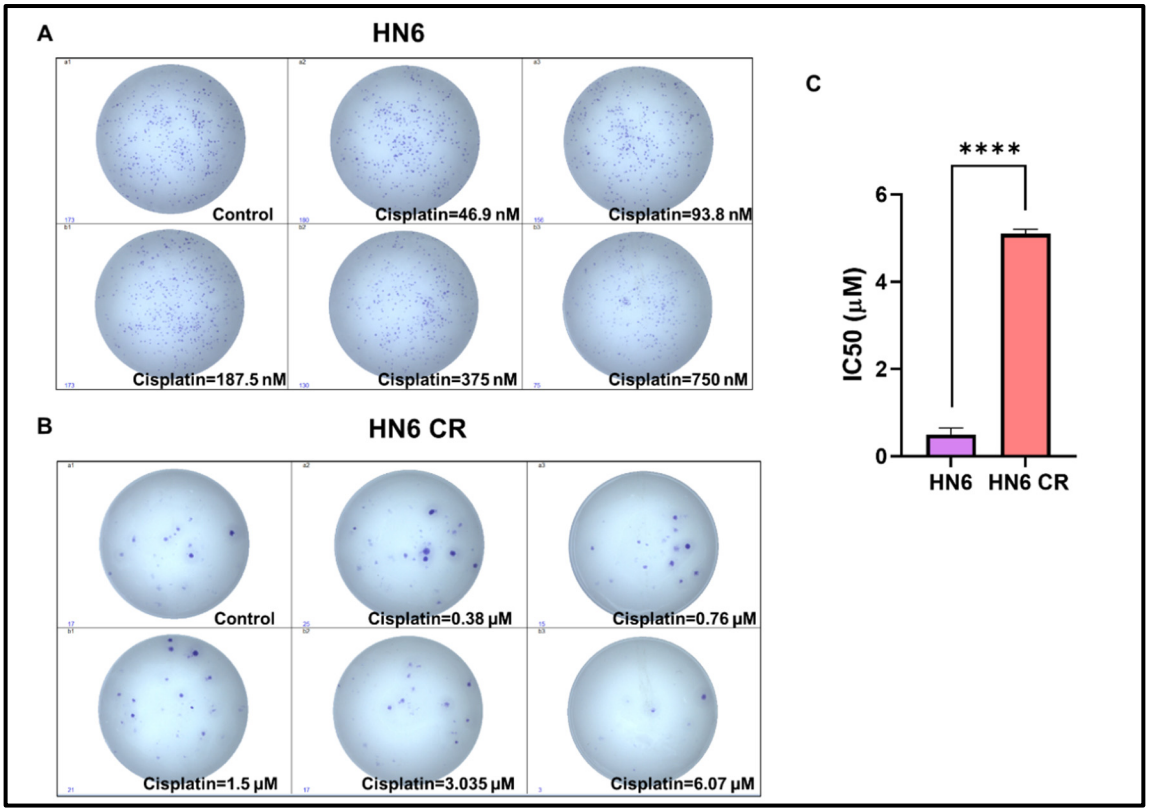

Figure 5.2. HN6 CR had significantly higher IC_{50} of Cisplatin than the parent cells via colony formation assay (CFA). (A) Representative images of CFA for parent HN6 cell line. **(B)** Representative images of CFA for HN6 CR cell line. **(C)** Graph plots the IC_{50} for both parent and resistant HN6 cell line. Graph is mean ± SEM. ****p<0.0001 compared to parent cells.

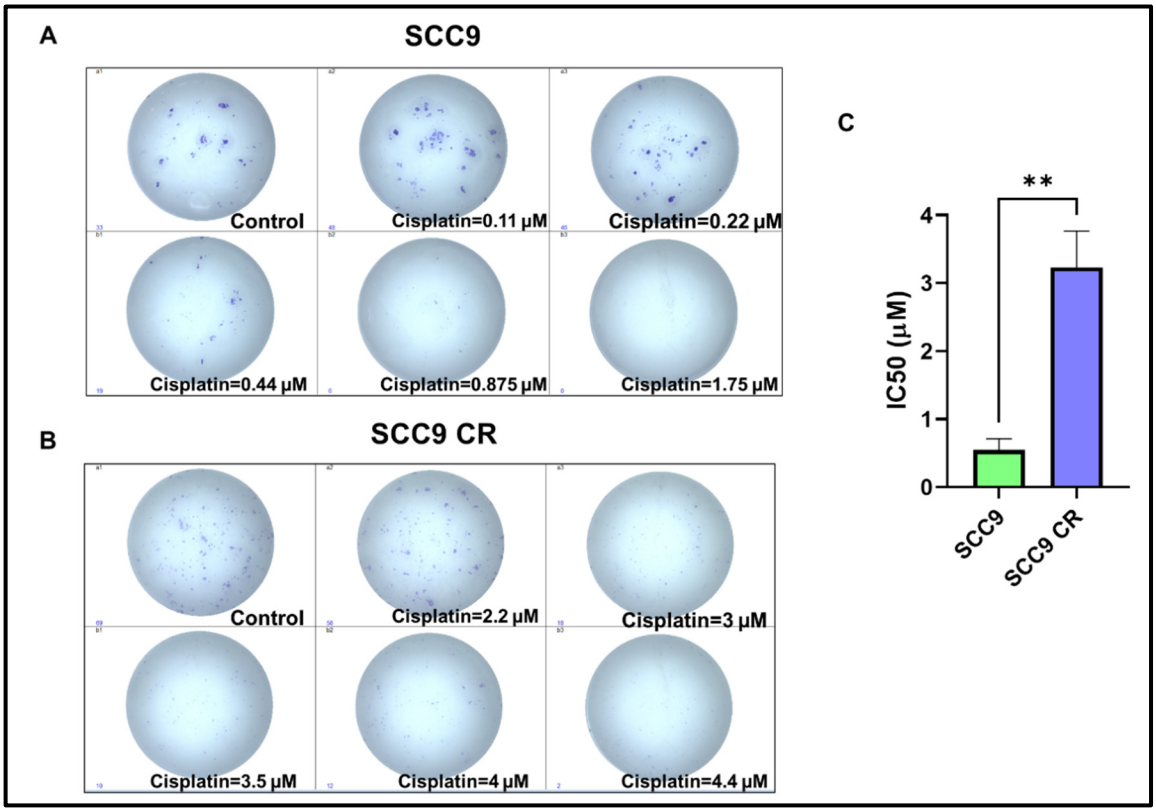

Figure 5.3. SCC9 CR had significantly higher IC_{50} of Cisplatin than the parent cells via colony formation assay (CFA). (A) Representative images of CFA for parent SCC9 cell line. **(B)** Representative images of CFA for SCC9 CR cell line. **(C)** Graph plots the IC_{50} for both parent and resistant SCC9 cell line. Graph is mean ± SEM. ***p*<0.01 compared to parent cells.

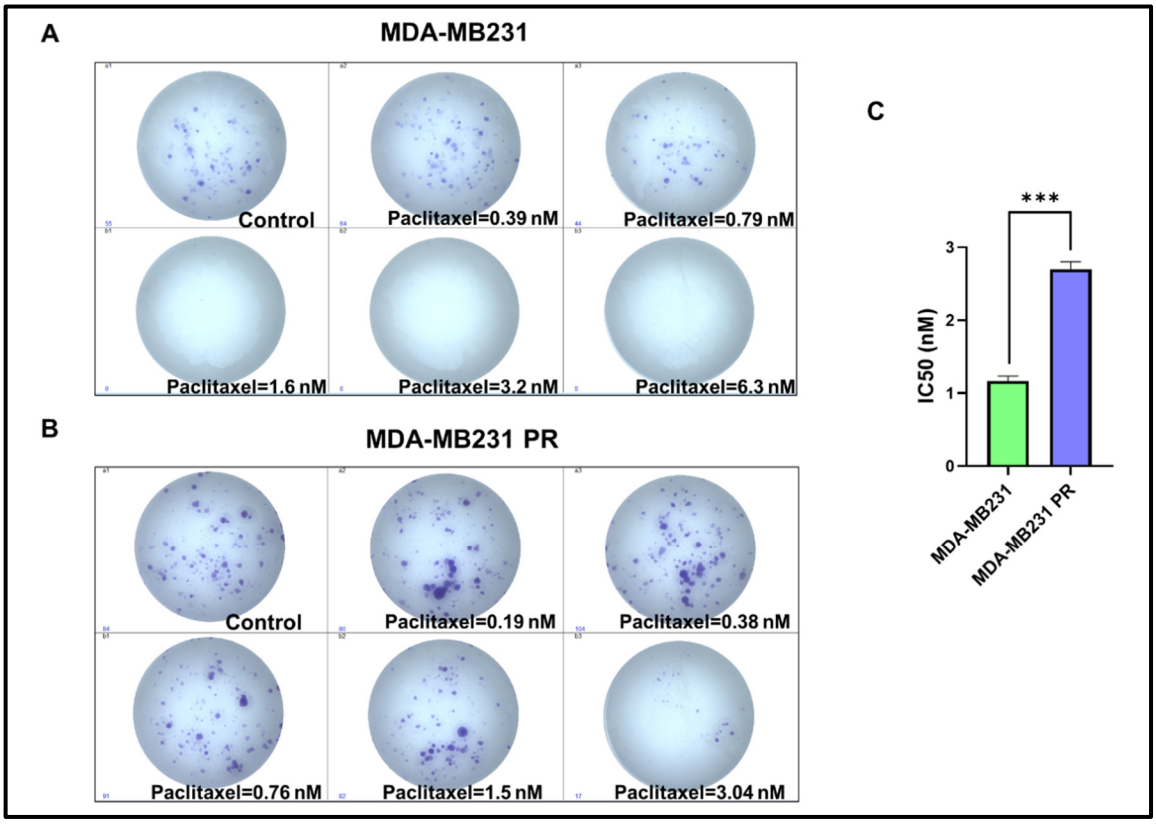

Figure 5.4. MDA-MB231 PR had significantly higher IC_{50} of Paclitaxel than the parent cells via colony formation assay (CFA). (A) Representative images of CFA for parent MDA-MB231 cell line. **(B)** Representative images of CFA for MDA-MB231 PR cell line. **(C)** Graph plots the IC_{50} for both parent and resistant MDA-MB231 cell line. Graph is mean ± SEM. ****p*<0.001 compared to parent cells.

5.2.2. Combination therapy between Beclin-1 complex inhibitor (SAR405) and ULK-1 complex inhibitor (MRT68921) exert an anti- proliferative activity on resistant OSCC and TNBC cell models

Taking into consideration combination therapy results on parent OSCC and TNBC cell lines in Chapter three, we aimed to test some effective autophagy inhibitors-based combination therapies on the resistant cell lines to identify the role that autophagy might play in chemoresistance. As SAR405-MRT68921 had demonstrated a significant anti-proliferative activity on the parent cell lines for both OSCC and TNBC, their activity was examined on resistant OSCC and TNBC cell lines. First, IC_{50} value for both SAR405 and MRT68921 were determined in the 4 resistant cells (*i.e.,* SCC9 CR, HN6 CR, HCC1806 PR and MDA-MB231 PR) via cellular proliferation assay (**Table 5.1**).

Table 5.1. IC_{50} values for both SAR405 and MRT68921 obtained from cell viability assay for resistant OSCC and TNBC cell lines.

Cell line/Treatment	SAR405	MRT68921
SCC9 CR	51.1 µM ± 5.6	8.2 µM ± 0.7
HN6 CR	40.7 µM ± 3.8	2.3 µM ± 0.1
HCC1806 PR	41.8 µM ± 3	3.3µM ± 0.08
MDA-MB-231 PR	34.9 µM ± 5. 8	5.45 µM ± 0.25

Then, combination therapies were performed using *Chou-Talalay* method as described previously in chapter two. SAR405-MRT68921 combination demonstrated a very strong synergism in SCC9 CR cells, associated with significant (p<0.001-0.01) reduction of cellular proliferation at all concentrations in comparison to either SAR405 or MRT68921 treatment alone (**Figure 5.5**). Similarly, HN6 CR observed a synergistic effect on combination of SAR405 and MRT68921 with significant (p<0.001-0.01) decrease of

tumour cell proliferation at concentrations of 2-4x IC_{50} when compared to either SAR405 or MRT68921 treatment alone (**Figure 5.5**). Moreover, both TNBC cell lines (HCC1806 PR and MDA-MB-231 PR) showed a synergism following co-treatment with SAR405 and MRT68921 and a significant reduction of cell proliferation at all concentrations in MDA-MB231 PR cell line and at concentrations of 0.5-1x IC_{50} in HCC1806 PR in comparison to standalone treatment with SAR405 or MRT68921(**Figure 5.6**).

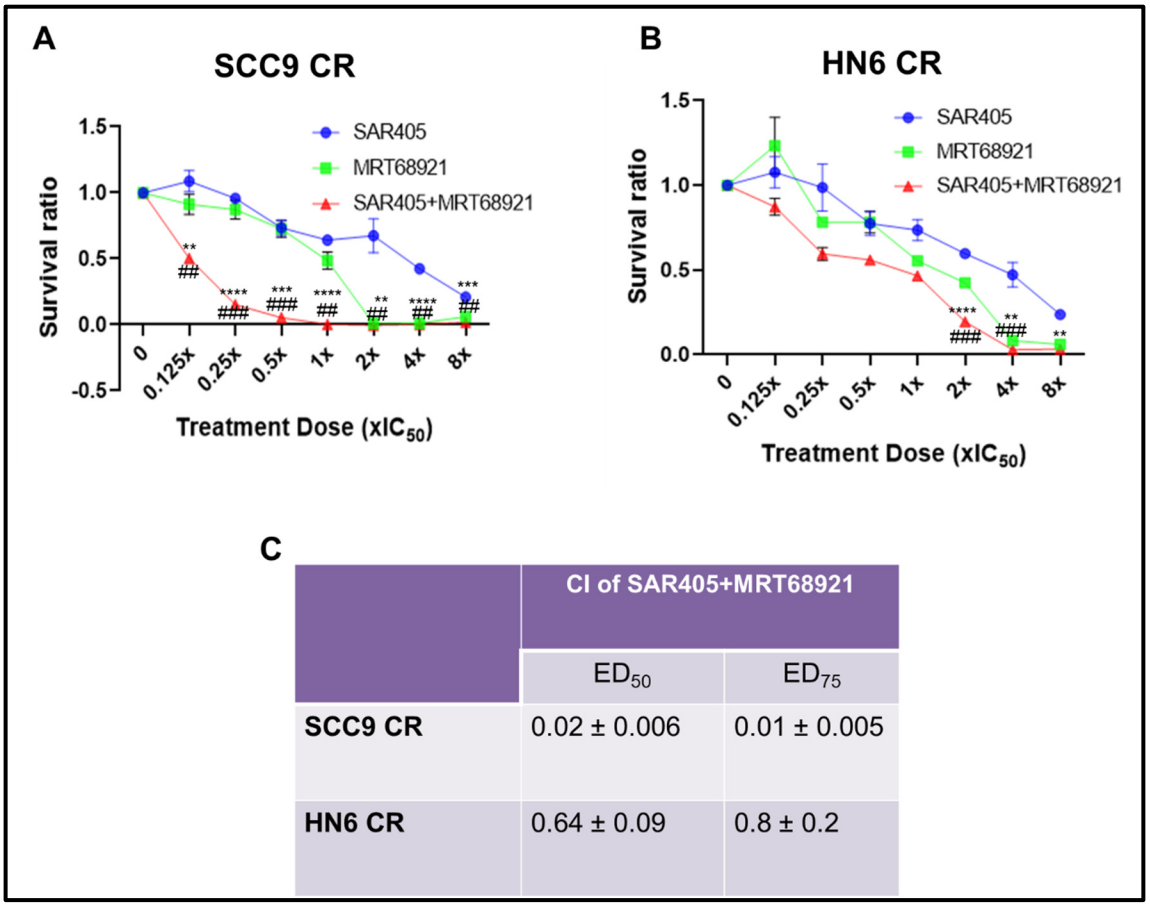

C

	CI of SAR405+MRT68921	
	ED_{50}	ED_{75}
SCC9 CR	0.02 ± 0.006	0.01 ± 0.005
HN6 CR	0.64 ± 0.09	0.8 ± 0.2

Figure 5.5. SAR405-MRT68921 combination significantly decreased cellular proliferation of resistant OSCC cell lines. (A) A dose response curve for SCC9 CR upon treatment with SAR405-MRT68921 combination. **(B)** A dose response curve for HN6 CR upon treatment with SAR405-MRT68921 combination. **(C)** Table showing the combination index (CI) of SAR405-MRT68921 in SCC9 CR and HN6 CR. Graphs are mean ± SEM. n=3. ***p*<0.01, ****p*<0.001, *****p*<0.0001 versus SAR405 treatment only. ##*p*<0.01, ###*p*<0.001 versus MRT68921 treatment only.

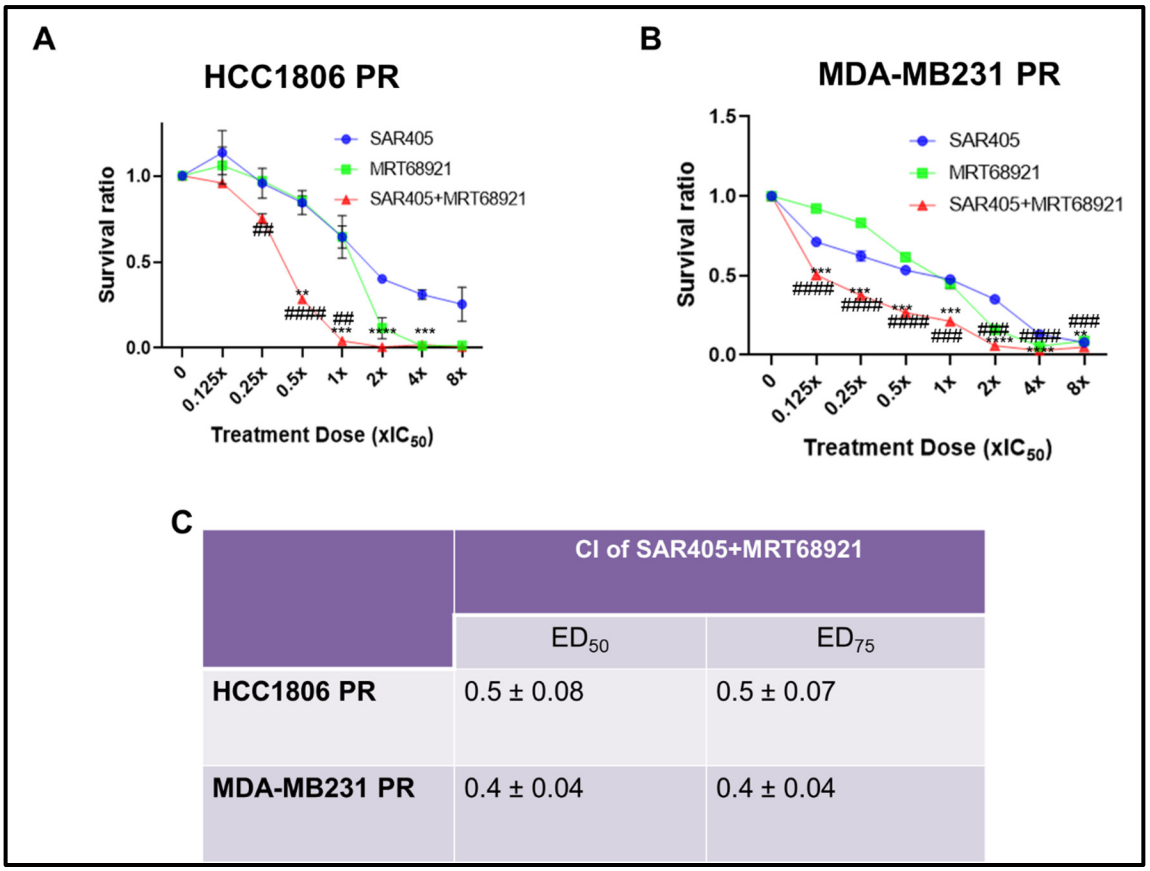

C

	CI of SAR405+MRT68921	
	ED_{50}	ED_{75}
HCC1806 PR	0.5 ± 0.08	0.5 ± 0.07
MDA-MB231 PR	0.4 ± 0.04	0.4 ± 0.04

Figure 5.6. SAR405-MRT68921 combination significantly decreased cellular proliferation of resistant TNBC cell lines. (A) A dose response curve for HCC1806 PR upon treatment with SAR405-MRT68921 combination. **(B)** A dose response curve for MDA-MB231 PR upon treatment with SAR405-MRT68921 combination. **(C)** Table showing the combination index (CI) of SAR405-MRT68921 in HCC1806 PR and MDA-MB231 PR. Graphs are mean ± SEM. n=3. ***p*<0.01, ****p*<0.001, *****p*<0.0001 versus SAR405 only. ##*p*<0.01, ###*p*<0.001, ####*p*<0.0001 versus MRT68921 only.

5.2.3. Combination therapy between standard chemotherapeutic agent and SAR405-MRT68921 synergistically reduce tumour cell proliferation in resistant OSCC cell lines but not in resistant TNBC cell lines

As SAR405-MRT68921 combination was synergistic in both resistant OSCC and TNBC cell models, the next step was to test the combination between these two inhibitors and standard chemotherapy agents either Cisplatin or Paclitaxel according to the cell model used. Cells were treated with different concentrations of Cisplatin or Paclitaxel (according to cell line used) and a fixed dose combination of SAR405-MRT68921 (0.125-8.0x IC_{50}). The IC_{50} for SAR405-MRT68921 combination was derived from previous combination studies for these inhibitors (**Figure 5.5 and 5.6**).

- **Cisplatin and SAR405-MRT68921**

Combination of Cisplatin with SAR405-MRT68921 showed slight to moderate synergism in both HN6 CR and SCC9 CR cell lines, respectively. A significant (p<0.0001) reduction of tumour cell proliferation was observed at a concentration of 1-2x IC_{50} in SCC9 CR after treatment with combination in comparison to Cisplatin treatment only and at all concentrations when compared to SAR405-MRT68921 treatment. In HN6 CR, cellular proliferation was significantly (p<0.01) decreased at 1-8x IC_{50} concentrations compared to treatment with Cisplatin only (**Figure 5.7**).

- **Paclitaxel and SAR405-MRT68921**

Unlike resistant OSCC cell lines, antagonism was noted upon combination of Paclitaxel and SAR405-MRT68921 in MDA-MB231 PR (**Figure 5.8**). Due to prolonged time required

to develop chemoresistance and additional time constraints due to extended COVID lockdowns, this combination could not be performed on HCC1806 PR.

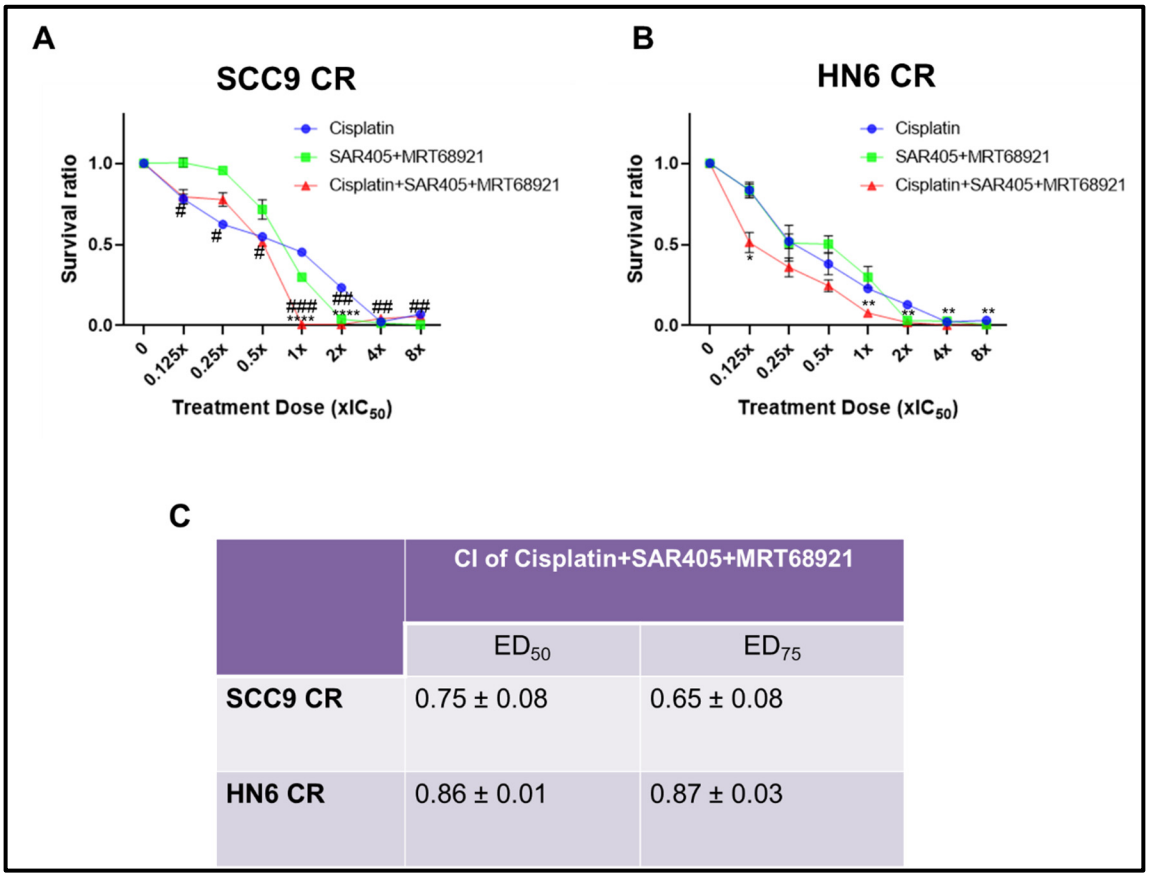

C

	CI of Cisplatin+SAR405+MRT68921	
	ED_{50}	ED_{75}
SCC9 CR	0.75 ± 0.08	0.65 ± 0.08
HN6 CR	0.86 ± 0.01	0.87 ± 0.03

Figure 5.7. Cisplatin-SAR405-MRT68921 combination significantly decreased cellular proliferation of resistant OSCC cell lines. (A) A dose response curve for SCC9 CR upon treatment with Cisplatin-SAR405-MRT68921 combination. **(B)** A dose response curve for HN6 CR upon treatment with Cisplatin-SAR405-MRT68921 combination. **(C)** Table showing the combination index (CI) of Cisplatin-SAR405-MRT68921 in SCC9 CR and HN6 CR. Graphs are mean ± SEM. n=3. ***p*<0.01, *****p*<0.0001 versus Cisplatin only. #*p*<0.05, ##*p*<0.01, ###*p*<0.001 versus SAR405-MRT68921.

A

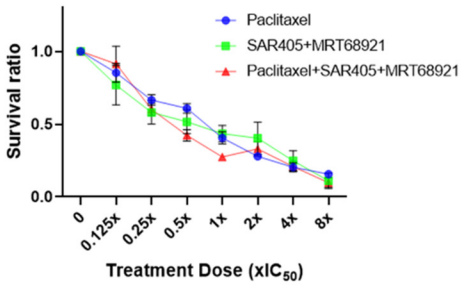

B

	CI of Paclitaxel+SAR405+MRT68921	
	ED_{50}	ED_{75}
MDA-MB231 PR	1.6 ± 0.3	1.5 ± 0.3

Figure 5.8. Paclitaxel-SAR405-MRT68921 combination had antagonist effect in MDA-MB231 PR cell line. **(A)** A dose response curve for MDA-MB231 PR upon treatment with Paclitaxel-SAR405-MRT68921 combination. **(B)** Table showing the combination index (CI) of Paclitaxel-SAR405-MRT68921 in MDA-MB231 PR. Graphs are mean ± SEM. n=3.

5.2.4. Proteomic analysis of the resistant and parent OSCC and TNBC cell models

After assessment of autophagy-based combination therapies in the resistant OSCC and TNBC cell models, high-resolution tandem mass spectrometry based proteomic analysis was performed to identify the altered protein expression between resistant and parent cell lines, that could have played a role in developing chemoresistance. In OSCC cell lines, a remarkable 5155 and 5467 proteins were identified and quantified in SCC9 and HN6 cell lines and their chemo-resistant counterparts, respectively. Similarly, 6730 and 7036 proteins were identified and quantified in HCC1806 and MDA-MB231 TNBC cell lines and their chemo-resistant counterparts, respectively. After statistical analysis and 10% false discovery rate, about 57-77% of total proteins were significantly altered in chemoresistant cells compared to their respective counterparts (**Figure 5.9) (Appendix 1)**.

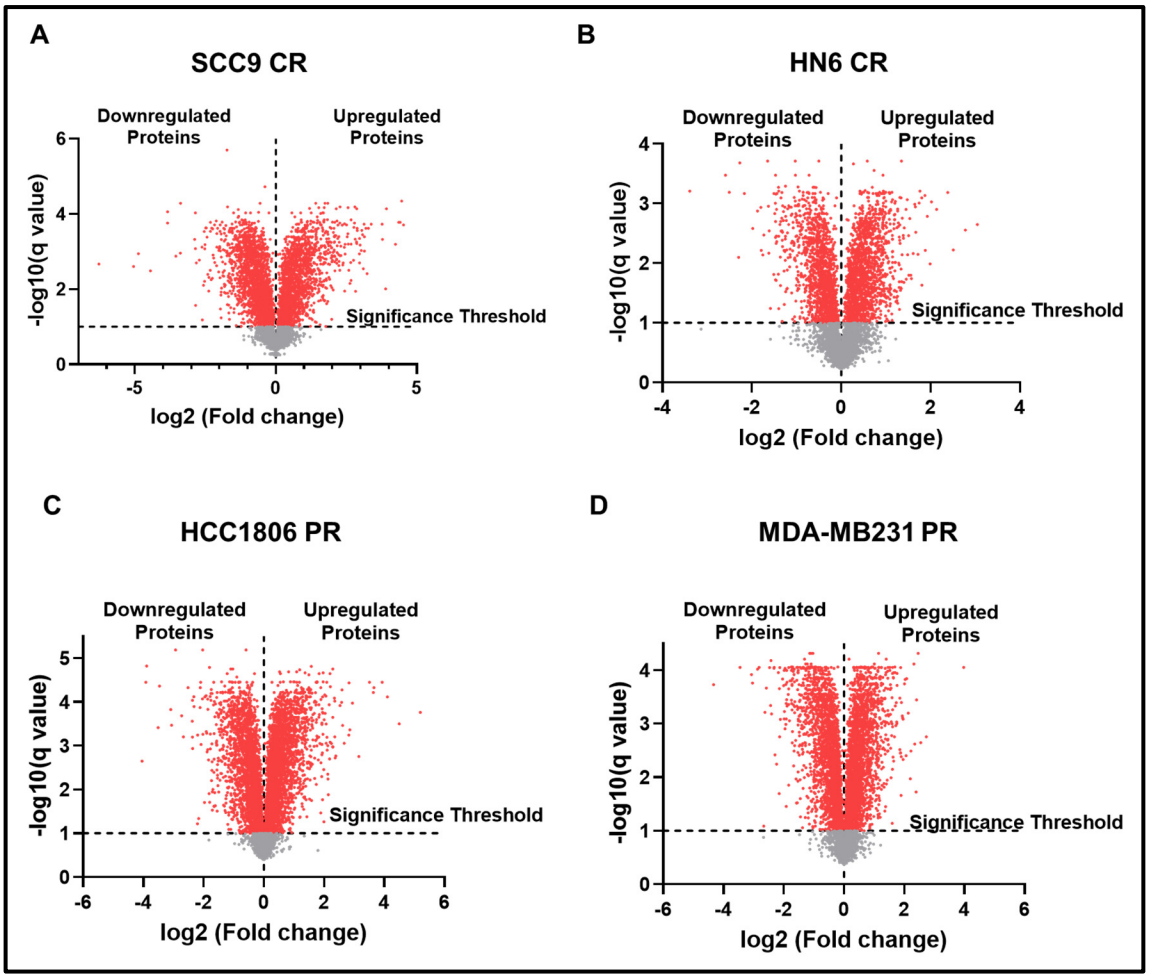

Figure 5.9. Volcano plot graphs display upregulated, dowregulated and unchanged proteins in OSCC and TNBC resistant cell lines. (A) SCC9 CR**, (B)** HN6 CR, **(C)** HCC1806 PR and **(D)** MDA-MB231 PR.

Next, we used Ingenuity Pathway Analysis to identify canonical pathways and key upstream regulators based on the differential proteomic profile obtained between chemoresistant cell lines and their respective parent cells. A cut off for IPA analysis was set at $p<0.05$, Log_2 Fold-Change ($\leq$-1.0 or $\geq$ 1.0) and q-value =0.1 for all data sets when mapping relevant regulators and biological functions, except for HN6 CR data set where no fold-change cut off points were set as the number of significantly altered protein was small.

(A) Proteomic analysis for OSCC cell models

- **Differentially expressed proteins identified in resistant OSCC cell model are involved in different biological functions**

A total of 500 biological functions were identified in both SCC9 CR and HN6 CR. This was narrowed down to include only biological functions related to cancer. The biological functions for both SCC9 CR and HN6 CR were further arranged according to z-score which defines the relation between proteins in our data compared to known relationship in the literature. Positive z-score represents activation, while negative z-score represents inhibition (**Appendix 2: Table 1&2**). Organisation of cytoplasm, metastasis, apoptosis, colony formation and autophagy were the most activated cellular functions in SCC9 CR. While the most inhibited biological functions in the same cell line were cell viability, proliferation of connective tissue cells, cell movement of neutrophils, metabolism of amino acids and cell survival (**Table 5.2**).

In HN6 CR, cell death of cancer cells, endocytosis, cellular homeostasis, formation of cellular protrusion and autophagy were identified as the most activated biological functions, whereas, the most inhibited functions were mitosis of tumour cells, cell survival, cell viability, metabolism of proteins and cell death of fibroblasts. (**Table 5.2**).

A comparison analysis was performed between the two sets of cell lines (SCC9 CR/SCC9 and HN6 CR/ HN6) to find out the common activated biological functions in both cell lines of OSCC (**Appendix 2: Table 3**). The most significantly activated biological functions in both cell lines were autophagy, organisation of cytoskeleton and cytoplasm and formation

of cellular protrusion and vesicles (**Table 5.3**). These findings are consistent with previously mentioned results where autophagy inhibition showed a significant reduction of cell proliferation in resistant OSCC cell lines.

Table 5.2. Top differentially regulated biological functions in both SCC9 CR and HN6 CR compared to their respective parent cell lines. z-scores highlighted with green indicates activation, while red indicates inhibition.

Functions	*p*-value	Z-score
SCC9 CR		
Organisation of cytoplasm	1.65E-12	2.725
Metastasis	0.000000499	1.847
Apoptosis	0.0000361	1.482
Colony formation	4.48E-09	0.946
Autophagy	2.01E-08	0.577
Cell viability	8.64E-11	-1.79
Proliferation of connective tissue cells	0.00000403	-1.57
Cell movement of neutrophils	0.0000198	-1.544
Metabolism of amino acids	3.2E-09	-1.458
Cell survival	2.09E-13	-1.455
HN6 CR		
Cell death of cancer cells	1.73E-15	6.172
Endocytosis	3.7E-29	4.265
Cellular homeostasis	2.3E-16	3.646
Formation of cellular protrusion	7.51E-18	3.547
Autophagy	2.38E-39	2.418
Mitosis of tumour cells	2.13E-17	-1.489
Cell survival	6.47E-44	-1.351
Cell viability	8.99E-45	-1.209
Metabolism of protein	3.23E-53	-0.809
Cell death of fibroblast	5.22E-13	-0.746

Table 5.3. Top differentially activated bio-functions with their relative z-score in both SCC9 CR and HN6 CR compared to their respective parent cell lines.

Top activated bio-functions	Z-score	
	SCC9 CR	HN6 CR
Organisation of cytoskeleton	2.639	3.295
Organisation of cytoplasm	2.725	3.3
Formation of cellular protrusion	1.454	3.547
Formation of vesicles	1.44	3.263
Autophagy	0.577	2.418

- **Canonical pathways implicated in resistant OSCC cell model**

IPA analysis identified 607 and 682 differentially regulated canonical pathways in both SCC9 CR and HN6 CR compared to their parent cells, respectively. This was decreased to 145 and 268 canonical pathways in SCC9 CR and HN6 CR respectively, by applying a cut off point for negative log (*p*-value) at 1.3 which was considered for significance, and also, demonstrating z-score activation or inhibition. The canonical pathways were arranged according to their z-score (**Appendix 2: Table 4&5**). Top activated and inhibited pathways in both SCC9 CR and HN6 CR are present in **Figure 5.10 & 11**.

In SCC9 CR, the most activated canonical pathways were interferon signaling (z-score= 3.3), xenobiotic metabolism AHR signaling pathway (z-score= 2.53), thrombin signaling (z-score= 2.5) and fatty acid β oxidation I (z-score= 2.4). Of note, autophagy (z-score= 0.943) was also one of the activated canonical pathways in SCC9 CR. On the other hand, anti-oxidant action of vitamin C (z-score= -2.2), ferroptosis signaling pathway (z-score= -

1.78), EIF2 signaling (z-score= -1.5) and HIF1α signaling (z-score= -1.34) were the most inhibited canonical pathways in the same cell line (**Figure 5.10**).

In the case of HN6 CR, signaling by Rho family GTPases (z-score= 4.4), Gαq signaling (z-score= 4.2) and FGF signaling (z-score= 3.7) were the most activated pathways. Notably, autophagy regulator, AMPK signaling (z-score= 2.7), and autophagy (z-score= 1.5) were also identified as activated canonical pathways. The most inhibited canonical pathways in the same cell line were oxidative phosphorylation (z-score= -5.1), spliceosomal signaling (z-score= -4), kinetochore metaphase signaling pathway (z-score= -3.7), NER (Nucleotide Excision Repair, Enhanced Pathway) (z-score= -3.5) and RHOGDI signaling (z-score= -3.28) (**Figure 5.11**).

Additionally, a comparative pathway analysis was carried out to identify the common pathways affected among both cell lines (SCC9 CR/ SCC9 and HN6 CR/ HN6) (**Appendix 2: Table 6**). The top activated canonical pathways in both SCC9 CR and HN6 CR were endothelin-1 signaling, NRF2-mediated oxidative stress response and interferon signaling, while RHOGDI signaling, and antioxidant action of vitamin C were the most inhibited canonical pathways (**Table 5.4**).

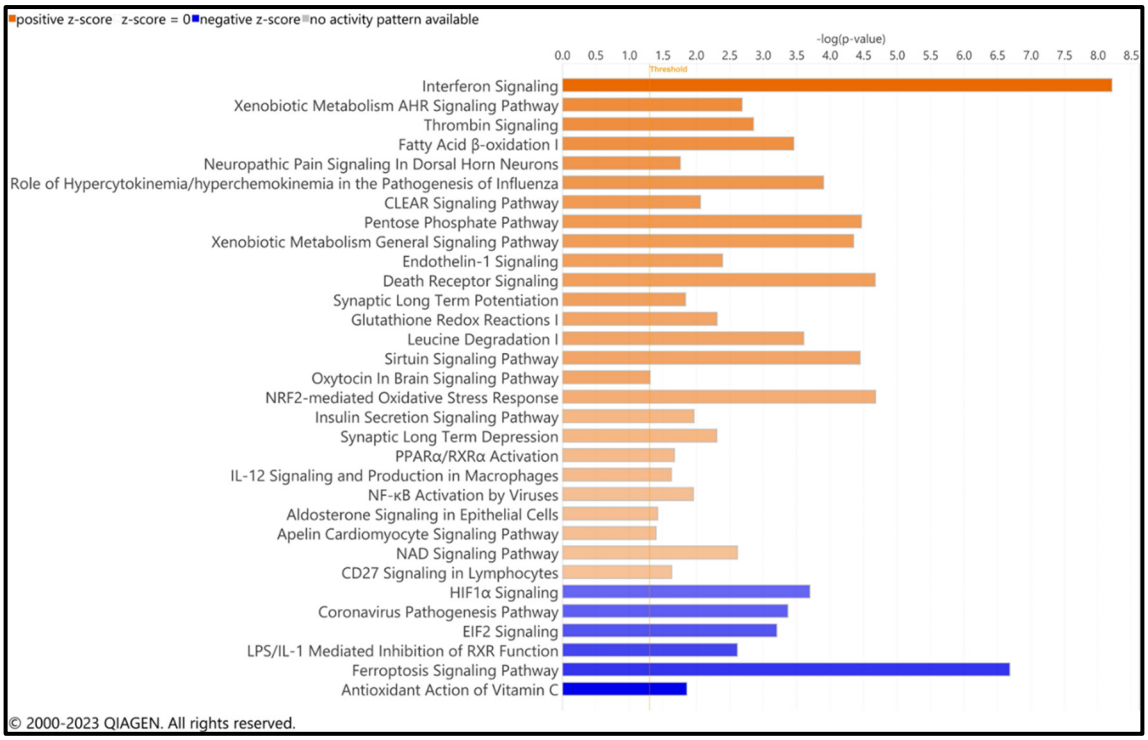

Figure 5.10. Top activated (orange) and inhibited (blue) canonical pathways in SCC9 CR compared to parent cell line. z-score range from -2.2 to 3.3.

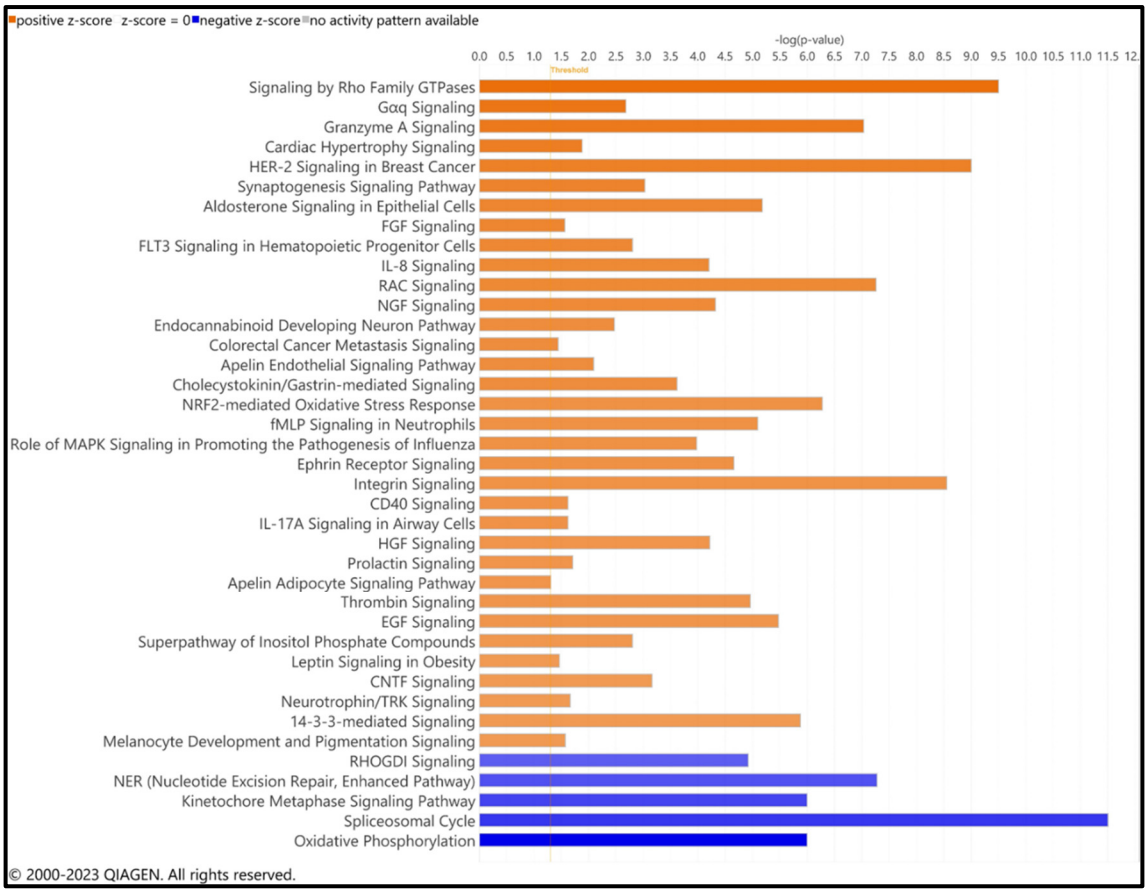

Figure 5.11. Top activated (orange) and inhibited (blue) canonical pathways in HN6 CR compared to the parent cell line. z-score range from -5.1 to 4.4

Table 5.4. Top activated and inhibited canonical pathways with their relative z-score in both resistant SCC9 and HN6 compared to their respective parent cells.

Top activated pathways	Z-score	
	SCC9 CR	HN6 CR
Endothelin-1 signaling	2.138	3.402
NRF2-mediated oxidative stress	1.807	3.413
Interferon signaling	3.317	1.89
Top inhibited pathways		
RHOGDI signaling	-1.897	-3.28
Antioxidant action of vitamin	-2.236	-2.309

- **Upstream regulators detected in resistant OSCC cell models**

A total of 269 and 398 upstream regulators were identified by their predictive activity in both SCC9 CR and HN6 CR cell lines, respectively (**Appendix 2: Table 7&8**). **Table 5.5** lists the top activated or inhibited regulators in each cell line according to their z-score. In regard to SCC9 CR, IRF7, IFNA2, IRF1, IFNL1, NONO, IFNB1 and TGM2 were the top activated upstream regulators, while MAPK1, TREX1, IRGM, NKX2-3, MYC, TRIM24 and RC3H1 being the topmost inhibited upstream regulators (**Table 5.5**).

In the case of HN6 CR, the top activated upstream regulators were LARP1, CDKN2A, XBP1, IL6, TP53, TCF7L2 and TGM2, whereas MYC, MLXIPL, MYCN, CEBPB, CSF2, NPC1 and TBX2 were the top inhibited upstream regulators (**Table 5.5**). Also, a

comparison analysis was performed between both resistant OSCC cell lines to detect the common upstream regulators in both cell lines (**Appendix 2 Table 9**).LARP1, IRF7, IFNL1, IFNA2, IFNG, FOXC1 and TGM2 are the most activated regulators and MYC, MYCN, MLXIPL, IRGM, USP8, MAPK1 and NKX2-3 as the top inhibited regulators (**Table 5.6**).

Table 5.5. Top upstream regulators in both SCC9 CR and HN6 CR compared to their respective parent cells. z-scores highlighted in green indicates activation, while red indicates inhibition.

Upstream regulator	Molecular type	z-score
SCC9 CR		
IRF7	transcription	5.685
IFNA2	cytokine	5.402
IRF1	transcription	4.78
IFNL1	cytokine	4.731
NONO	transcription	4.717
IFNB1	cytokine	4.652
TGM2	enzyme	4.461
STAT1	transcription	4.139
FOXC1	transcription	3.929
IRF3	transcription	3.733
MAPK1	kinase	-5.951
TREX1	enzyme	-5.214
IRGM	enzyme	-5.113
NKX2-3	transcription	-4.747
MYC	transcription	-4.553
TRIM24	transcription	-4.263
RC3H1	enzyme	-4.123
PNPT1	enzyme	-3.973
IL1RN	cytokine	-3.671
MYCN	transcription	-3.62
HN6 CR		
LARP1	translation regulator	6.716
CDKN2A	transcription	5.258
XBP1	transcription	4.409
IL6	cytokine	4.297
TP53	transcription	4.257
TCF7L2	transcription	4.042
TGM2	enzyme	2.417
MAFF	transcription	2.414
ID3	transcription	2.413
SP1	transcription	2.396
MYC	transcription	-6.273
MLXIPL	transcription	-6.131
MYCN	transcription	-5.574
CEBPB	transcription	-5.464
CSF2	cytokine	-4.704
NPC1	transporter	-4.644
TBX2	complex	-4.088
TNFRSF9	transmembrane	-3.578
IL10	cytokine	-3.571
KLF3	transcription	-3.394

Table 5.6. Top activated and inhibited upstream regulators with their z-score in both SCC9 CR and HN6 CR compared to their respective parent cell lines.

Top activated regulators	Z-score	
	SCC9	HN6
LARP1	3.317	6.716
IRF7	5.685	3.708
IFNL1	4.731	2.804
IFNA2	5.402	2.008
IFNG	3.575	3.814
FOXC1	3.929	3.000
TGM2	4.461	2.417
Pyridostatin	5.235	2.496
CHROMR variant 3	4.83	2.652
Lipopolysaccharide	1.482	5.972
Top inhibited regulators		
MYC	-4.553	-6.273
MYCN	-3.62	-5.574
MLXIPL	-2.121	-6.131
IRGM	-5.113	-2.8
USP8	-3.93	-3.57
MAPK1	-5.951	-1.325
NKX2-3	-4.747	-2.353
NPC1	-2.966	-4.644
BCR (complex)	-5.005	-2.421
SN-011	-4.796	-2.496

(B) Proteomic analysis for TNBC cell models

- **Proteins detected in resistant TNBC cell model are involved in different biological functions.**

A total of 311 and 232 biological functions were recognised in both HCC1806 PR and MDA-MB231 PR data sets, respectively. The differentially regulated biological functions identified in both HCC1806 PR and MDA-MB2321 PR, compared to their respective parent cells, were arranged according to z- score (**Appendix 3: Table 1 &2**). In HCC1806 PR, invasion, metastasis, and proliferation of tumour cells were from the most activated biological functions, while the most inhibited functions in the same cell line were sphere formation, tumourigenesis and growth of tumour cells (**Table 5.7**). Similarly, MDA-MB231 PR had apoptosis, invasion, and metastasis as the most activated bio-functions, whereas tumour growth and proliferation of tumour cells were the most inhibited functions (**Table 5.7**). Moreover, a comparative functions analysis was done to identify the common differential biological functions between both cell lines (HCC1806 PR and MDA-MB231 PR) (**Appendix 3: Table 3**). This analysis identified invasion, metastasis, migration, and apoptosis of tumour cells as the top activated functions in both resistant TNBC cell lines, which seems to be consistent with the phenotype characteristic of resistant cell lines (**Table 5.8**).

Table 5.7. Top differentially regulated biological functions in both HCC1806 PR and MDA-MB231 PR compared to their respective parent cell lines. z-scores highlighted with green mean activation and red mean inhibition.

Functions	*p*-value	Z-score
HCC1806 PR		
Metastasis	1.08E-06	2.381
Invasion	1.8E-09	1.918
Cell proliferation	0.000014	0.703
Sphere formation	0.000335	-0.422
Tumourigenesis	3.48E-10	-0.059
Growth of tumour cells	9.83E-07	-0.017
MDA-MB231 PR		
Apoptosis	0.00014	2.796
Invasion	8.13E-10	1.337
Metastasis	5.19E-07	1.336
Tumour growth	6.38E-11	-1.562
Proliferation of tumour cells	1.45E-07	-0.726

Table 5.8. Top differentially activated bio-functions with their relative z-score in both HCC1806 PR and MDA-MB231 PR compared to their respective parent cell lines.

Top activated bio-functions	Z-score	
	HCC1806 PR	MDA-MB231 PR
Invasion	1.918	1.337
Metastasis	1.717	1.336
Apoptosis	1.547	0.95
Migration	0.131	1.454

- **Canonical pathways involved in resistant TNBC cell model**

A total of 110 and 35 differentially regulated canonical pathways were identified in HCC1806 PR and MDA-MB231 PR, respectively, compared to their parent cells. The canonical pathways were arranged according to z-score (**Appendix 3: Table 4&5**). The top activated and inhibited canonical pathways for HCC1806PR and MDA-MB231PR are presented in **Figure 5.12&13**.

In HCC1806 PR, clear signaling pathway (z-score= 2.1), aryl hydrocarbon receptor signaling (z-score= 1.89), Fcy receptor mediated phagocytosis (z-score= 1.89), xenobiotic metabolism AHR signaling pathway (z-score= 1.63) and NAD signaling pathway (z-score= 1.6) were the most activated pathways, while super pathway of cholesterol biosynthesis (z-score= -2.4), tumour microenvironment pathway (z-score= -1.66), AMPK signaling (z-score= -1.66), microRNA biogenesis signaling pathway (z-score= -1.5) and PI3K/AKT signaling (z-score= -1.26) were the most inhibited canonical pathways in the same cell line (**Figure 5.12**).

Regarding MDA-MB231 PR, the most activated canonical pathways were NRF2-mediated oxidative stress response (z-score= 2.4), cell cycle: G2/M DNA damage checkpoint regulation (z-score= 2.3), GADD45 signaling (z-score= 2.2), regulation of cellular mechanics by Calpain protease (z-score= 2.2) and senescence pathway (z-score= 1.5) , while most inhibited pathways were cell cycle control of chromosomal replication (z-score= -3.46), clear signaling pathway (z-score= -3.05), kinetochore metaphase signaling pathway (z-score= -2.84), NER (Nucleotide Excision Repair, Enhanced Pathway) (z-score= -2.449) and Cyclins and Cell Cycle Regulation (z-score= -2.449) (**Figure 5.13**).

Also, comparison analysis was performed to identify the common canonical pathways in both HCC1806 PR and MDA-MB231 PR (**Appendix 3: Table 6**). The top activated canonical pathways in both cell lines were role of hypercytokinemia/hyperchemokinemia in the pathogenesis of Influenza, NRF2-mediated oxidative stress response, xenobiotic metabolism general signaling pathway, HIF1α signaling, Cholecystokinin/Gastrin-mediated signaling and GADD45 signaling, whereas the top inhibited pathways were kinetochore metaphase signaling pathway and semaphorin neuronal repulsive signaling pathway (**Table 5.9**).

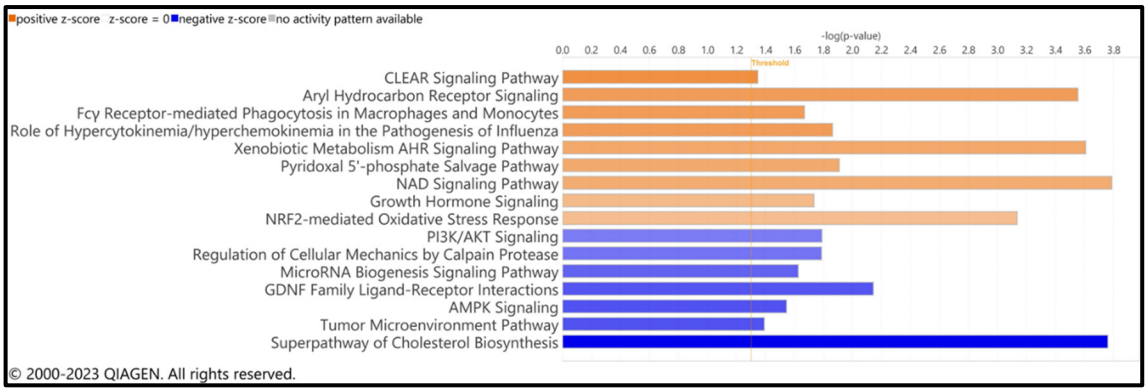

Figure 5.12. lists top activated (orange) and top inhibited (blue) canonical pathways according to their z-score in HCC1806PR. z-score range from -2.4 to 2.1.

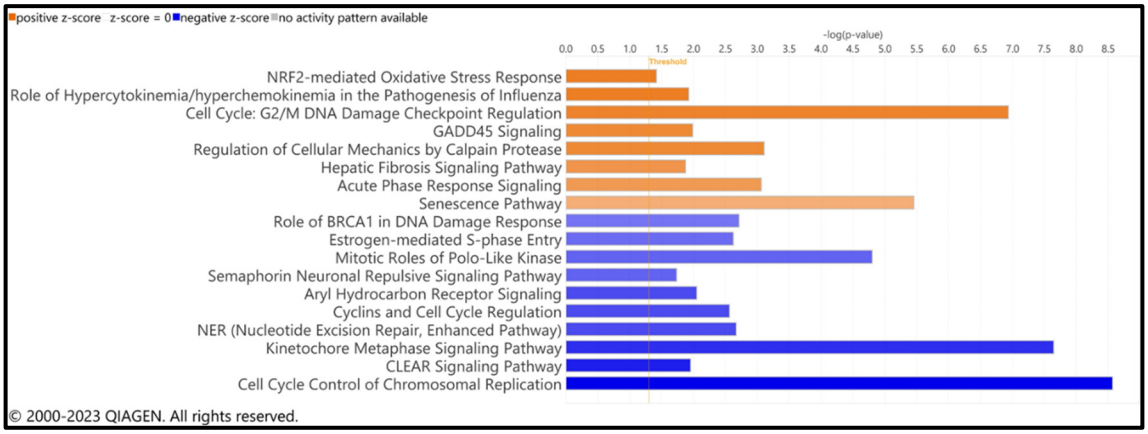

Figure 5.13. lists top activated (orange) and top inhibited (blue) canonical pathways according to their z-score in MDA-MB231PR. z-score range from -3.46 to 2.44.

Table 5.9. Top activated and inhibited canonical pathways with their relative z-score in both HCC1806PR and MDA-MB231PR compared to their respective parent cells.

Top activated pathways	Z-score	
	HCC1806PR	MDA-MB231PR
Role of hypercytokinemia/hyperchemokinemia in the pathogenesis of Influenza	1.89	2.449
NRF2-mediated oxidative stress response	1.265	2.449
Xenobiotic metabolism general signaling pathway	1.155	2.449
HIF1α signaling	0.577	2.449
Cholecystokinin/Gastrin-mediated signaling	0.707	2.236
GADD45 signaling	0.378	2.236
Top inhibited pathways		
Kinetochore metaphase signaling pathway	-0.816	-2.84
Semaphorin neuronal repulsive signaling pathway	-0.447	-2.121

- **Upstream regulators detected in resistant TNBC cell model**

A total of 135 and 233 upstream regulators were identified depending on their predicted activity in both HCC1806PR and MDA-MB231PR, respectively, compared to their parent cell lines. The upstream regulators were arranged according to their z-score (**Appendix 3: Table 7 &8**).

In the case of HCC1806 PR, STAT1, IRF7, STAT5B, ZBTB10, IFNB1, PRL, TPH1, TGM2 and FOXC1 were the most activated regulators, while NUPR1, POU5F1, TREM1, HMG20A, CSF1, SREBF2 and TARDBP being the top inhibited regulators (**Table 5.10**). Regarding MDA-MB231PR, the top activated up-stream regulators were IL1B, CDKN2A,

TNF, TP53, TGFB1, IFNG and TRPS1, while MYC, CSF2, CEBPB, TBX2, CD3E and MITF were the top inhibited regulators (**Table 5.10**).

Additionally, a comparative analysis was performed to detect the common upstream regulator in both TNBC resistant cell lines (**Appendix 3: Table 9**). The analysis showed that IFNB1, TNF, tretinoin, Ifnar, ZBTB10, FOXC1, IFNA2 and TGM2 were the top activated up-stream regulators in both cell lines and STAG2, MYC, TREX1, RNASEH2B and SN-011 being the top inhibited regulators (**Table 5.11**).

Table 5.10. Top upstream regulators in both HCC1806 PR and MDA-MB231 PR compared to their respective parent cells. z-scores highlighted with green mean activation and red mean inhibition.

Upstream regulator	Molecular type	z-score
HCC1806PR		
STAT1	transcription	3.206
IRF7	transcription	2.925
STAT5B	transcription	2.872
ZBTB10	transcription	2.813
IFNB1	cytokine	2.767
PRL	cytokine	2.747
TPH1	enzyme	2.72
TGM2	enzyme	2.704
FOXC1	transcription	2.673
TFEB	transcription	2.602
NUPR1	transcription	-3.938
POU5F1	transcription	-3.555
TREM1	transmembrane	-2.84
HMG20A	transcription	-2.714
CSF1	cytokine	-2.666
SREBF2	transcription	-2.607
TARDBP	transcription	-2.562
MAPK1	kinase	-2.417
PDX1	transcription	-2.377
KDM3B	enzyme	-2.236
MDA-MB231PR		
IL1B	cytokine	3.883
CDKN2A	transcription	3.836
TNF	cytokine	3.836
TP53	transcription	3.817
TGFB1	growth factor	3.617
IFNG	cytokine	3.447
TRPS1	transcription	3.317
RB1	transcription	3.157
NFATC2	transcription	3.108
RELA	transcription	3.09
MYC	transcription	-4.795
CSF2	cytokine	-4.623
CEBPB	transcription	-4.181
TBX2	transcription	-3.871
CD3E	transmembrane	-3.576
MITF	transcription	-3.556
FOXM1	transcription	-3.55
VDR	transcription	-3.503
AREG	growth factor	-3.499
TNFRSF9	transmembrane	-3.464

Table 5.11. Top activated and inhibited upstream regulators with their z-score in both HCC1806 PR and MDA-MB231 PR compared to their respective parent cell lines.

Top activated regulators	Z-score	
	HCC1806PR	MDA-MB231PR
IFNB1	2.767	2.931
TNF	1.619	3.836
tretinoin	1.456	3.614
Ifnar	2.587	2.431
ZBTB10	2.813	2.137
FOXC1	2.673	2.121
IFNA2	1.868	2.81
TGM2	2.704	1.961
MAVS	1.98	2.607
NONO	2.414	1.923
Top inhibited regulators		
STAG2	-2.233	-2.81
MYC	-0.153	-4.795
TREX1	-1.713	-2.736
RNASEH2B	-1.571	-2.791
SN-011	-1.633	-2.646
CBX5	-1.732	-2.236
SOCS1	-2.023	-1.809
NRAS	-1.91	-1.664
CDK19	-0.905	-2.646
ESR2	-1.403	-2.124

5.2.5. TGM2 may serve as a potential target for anti-cancer combination therapy

From proteomic data analysis in both resistant OSCC and TNBC cell models, TGM2 enzyme was identified as a key upstream regulator activated in both resistant cell models which indicated that it may play a crucial role in mediating chemoresistance. Normally, TGM2 is detected in the cytoplasm and responsible for crosslinking between amino group of lysine residue and γ-carboxamide group of glutamine residue into same protein or between different proteins and thus, regulating their activity [391]. It also can be found in the plasma membrane where it binds to GTP and acts as G-protein which help in transduction of external signals intracellularly to downstream effectors [391]. In addition, it can expressed in the ECM where it allows cell-matrix interactions through crosslinking of fibronectin [391]. TGM2 has been implicated to play an important role in many diseases including cancer, where it has been linked to tumour cell survival and motility [392]. Henceforth, *TGM2* silencing was performed in the 4 resistant cell lines to detect its effect on IC_{50} of standard chemotherapeutic agents (*i.e.,* Cisplatin or Paclitaxel). First, *TGM2* silencing was tested via immunoblotting at different time points (24 h and 72 h) to make sure that silencing was working through the time frame of cell proliferation assay. Then, cell proliferation assay was carried out using MTT reagent to determine IC_{50} of the standard chemotherapeutics used after *TGM2* silencing.

The immunoblotting results demonstrated a decrease in TGM2 expression in both resistant OSCC and TNBC cell lines after 24 h of silencing with *TGM2* siRNA compared to negative control siRNA, and this effect was more significantly (p<0.001) pronounced after 72 h of silencing (**Figure 5.14, 5.15**).

Next, to determine the effect of TGM2 silencing on the anti-proliferative ability of standard chemotherapy, cells were either incubated with negative control siRNA or *TGM2* siRNA, followed by incubation with standard chemotherapy at range of concentrations. In SCC9 CR, Cisplatin's IC_{50} (62.3 μM ± 8.1) was reduced after *TGM2* silencing compared to negative control which have no known target in the cell (85.5 μM ± 12.7). Likewise, HN6 CR showed reduced Cisplatin's IC_{50} (24.4 μM ± 5.3) following *TGM2* silencing in comparison to negative control (31.2 μM ± 9.3).

In TNBC cell models, HCC1806 PR showed decreased IC_{50} of Paclitaxel (450 nM ± 70) after *TGM2* silencing in comparison to negative control (650 nM ± 20). Also, MDA-MB231 PR showed reduction in Paclitaxel's IC_{50} (7.9 nM ± 3.9) after *TGM2* silencing when compared to negative control (9.6 nM ± 5.2) (**Figure 5.16**). Hence, these results indicate an important role of TGM2 in mediating chemoresistance in both OSCC and TNBC cell models.

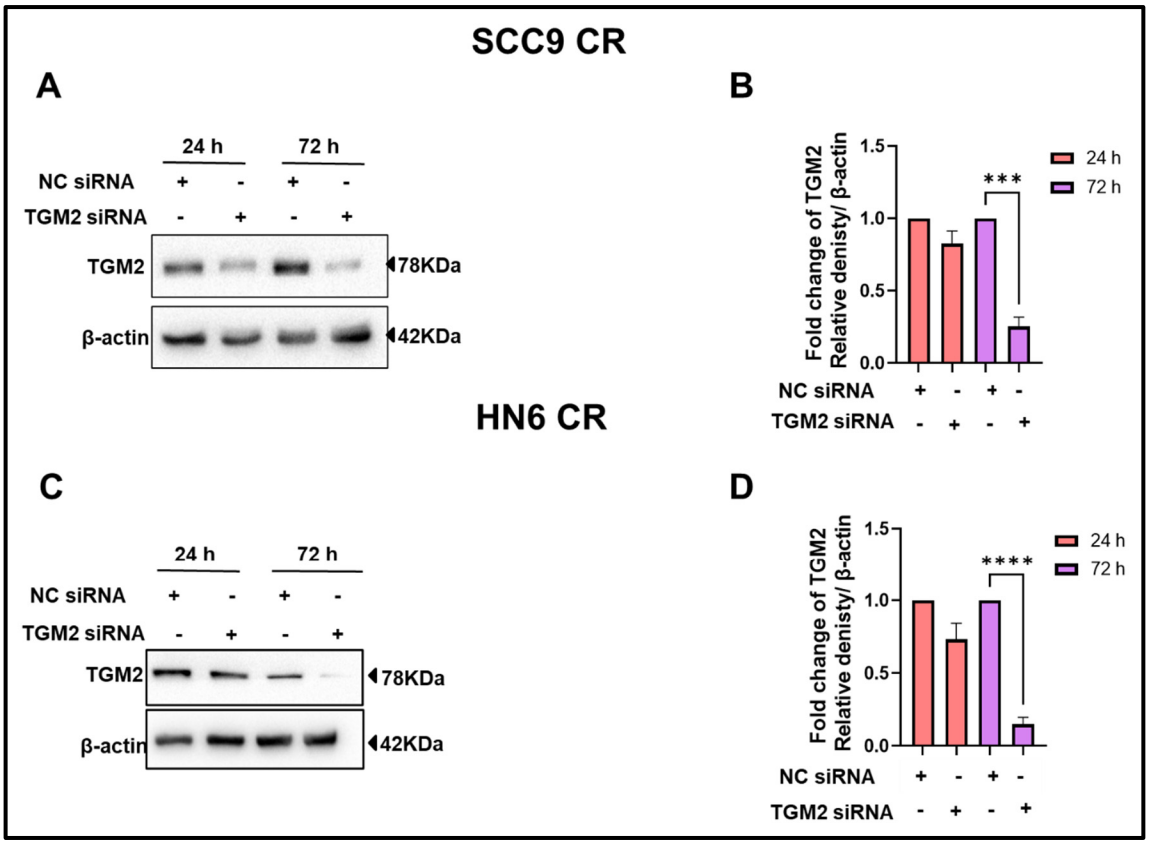

Figure 5.14. TGM2 expression significantly reduced after 72 h of TGM2 silencing in resistant OSCC cell model. (A,C) Western blotting was carried out to detect the effect of TGM2 siRNA in SCC9 CR and HN6 CR at different time point (24 h and 72 h) respectively. **(B,D)** Densitometric analysis for the results shown in **(A,C)** respectively. Blots shown in **(A,C)** are typical of 3 experiments. Densitometric analysis in **(B,D)** are mean ±SEM (3 experiments) normalized to β-actin. ***p<0.001, ****p<0.0001 versus the Control.

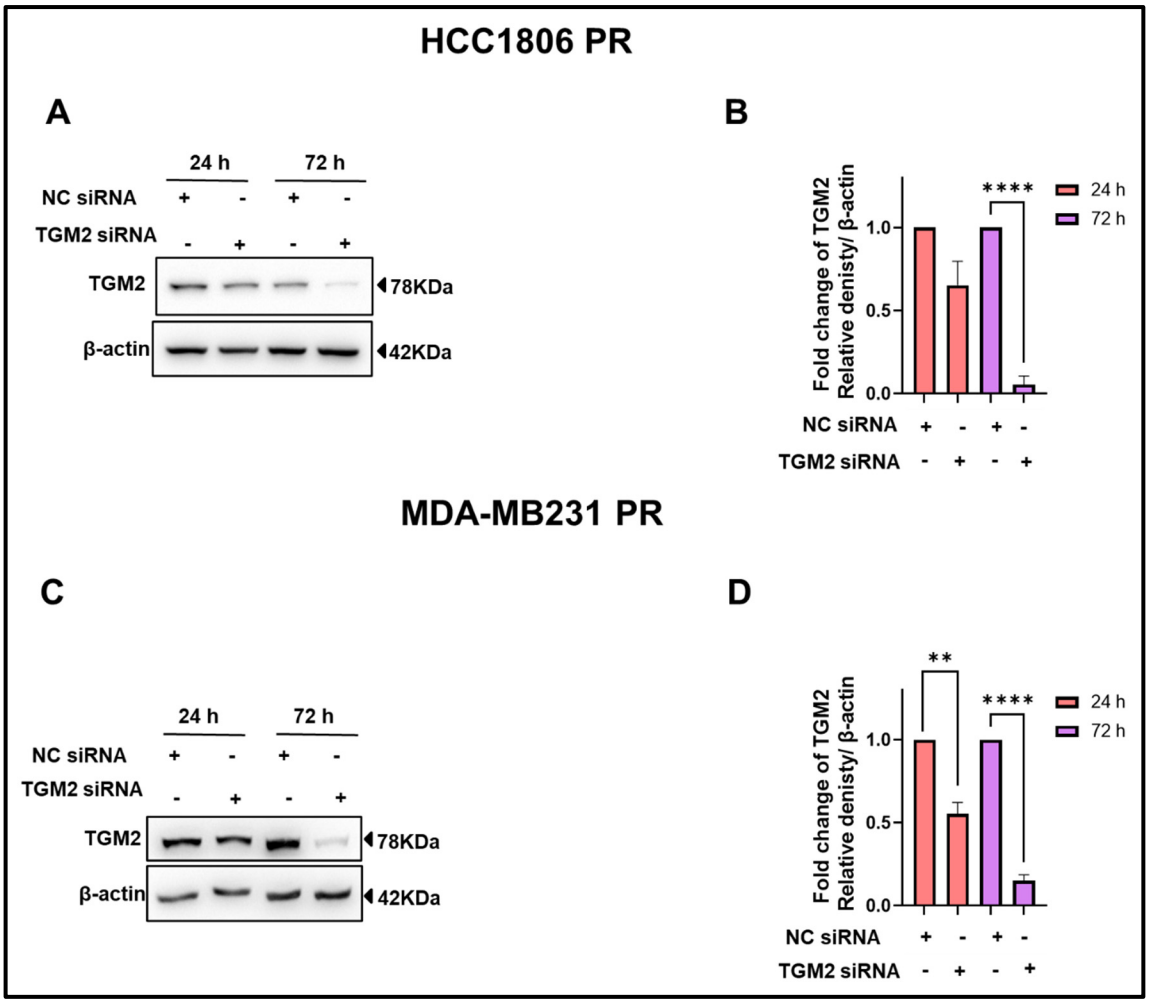

Figure 5.15. TGM2 expression significantly reduced after 72 h of TGM2 silencing in resistant TNBC cell model. (A,C) Western blotting was carried out to detect the effect of TGM2 siRNA in HCC1806 PR and MDA-MB231 PR at different time point (24 h and 72 h) respectively. **(B,D)** Densitometric analysis for the results shown in **(A,C)** respectively. Blots shown in **(A,C)** are typical of 3 experiments. Densitometric analysis in **(B,D)** are mean ±SEM (3 experiments) normalized to β-actin. **p<0.01, ****p<0.0001 versus the Control.

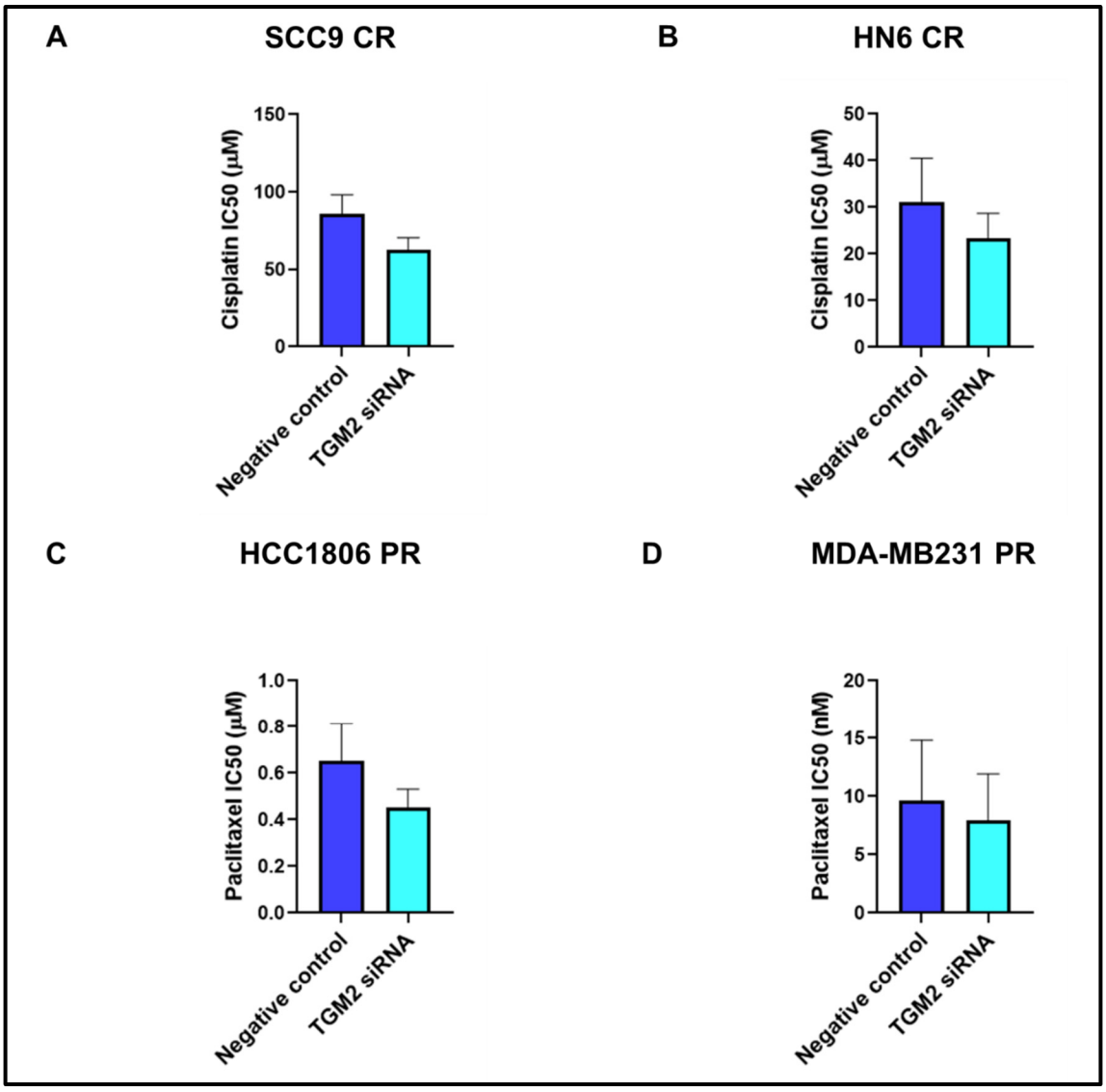

Figure 5.16. *TGM2* silencing decreased IC_{50} of standard chemotherapeutics (*i.e.,* Cisplatin and Paclitaxel) in both OSCC and TNBC resistant cell models respectively. (A) SCC9 CR. **(B)** HN6 CR. **(C)** HCC1806 PR **(D)** MDA-MB231 PR. Graphs are mean ± SEM, n=3.

5.2.6. Combination therapy between standard chemotherapeutic agents *(i.e.*, Cisplatin or Paclitaxel) and TGM2 inhibitor had an inhibitory effect on tumour cell proliferation in both OSCC and TNBC resistant cell models

Based on the previous results, we assessed the effect of combination therapy between standard chemotherapeutic agents and TGM2 inhibitor (*i.e.*, GK921) in the 4 resistant cell lines. First, IC_{50} of GK921 was determined using MTT proliferation assay in both OSCC and TNBC resistant cell lines (**Table 5.12**). Then, combination studies assessing cellular proliferation were performed using *Chou-Talalay* method as mentioned in Chapter 2.

Table 5.12. lists IC_{50} for GK921 in different cell line used. Values are mean ± S.E.M, n=3.

Cell Line	IC_{50} of GK921 (μM)
SCC9 CR	0.62 ± 0.006
HN6 CR	0.25 ± 0.01
HCC1806 PR	0.56 ± 0.02
MDA-MB231 PR	0.35 ± 0.002

- **Cisplatin and GK921**

Moderate antagonism was noted in SCC9 CR when Cisplatin was combined with GK921. Notably, a significant reduction of cellular proliferation (p<0.01) was detected at concentrations of 1-2x IC_{50} in comparison to standalone treatment of either Cisplatin or GK921 (**Figure 5.17A**). On the other hand, Resistant HN6 displayed a synergism following treatment by combination of Cisplatin and GK921 with significant reduction of tumour cell proliferation (p<0.01) at a concentration of 1x IC_{50} when compared to Cisplatin treatment only and at concentrations of 0.25-0.5x (p<0.001-0.01) in comparison to GK921 treatment only (**Figure 5.17B**).

- **Paclitaxel and GK921**

Paclitaxel-GK921 combination showed antagonism in HCC1806 PR (**Figure 5.18A**). On the contrary, MDA-MB231 PR exhibited synergism on combination of Paclitaxel and GK921 with significant (p<0.0001-0.01) decrease in cell proliferation at 1-8x IC_{50} concentrations in comparison to Paclitaxel treatment only (**Figure 5.18 B**).

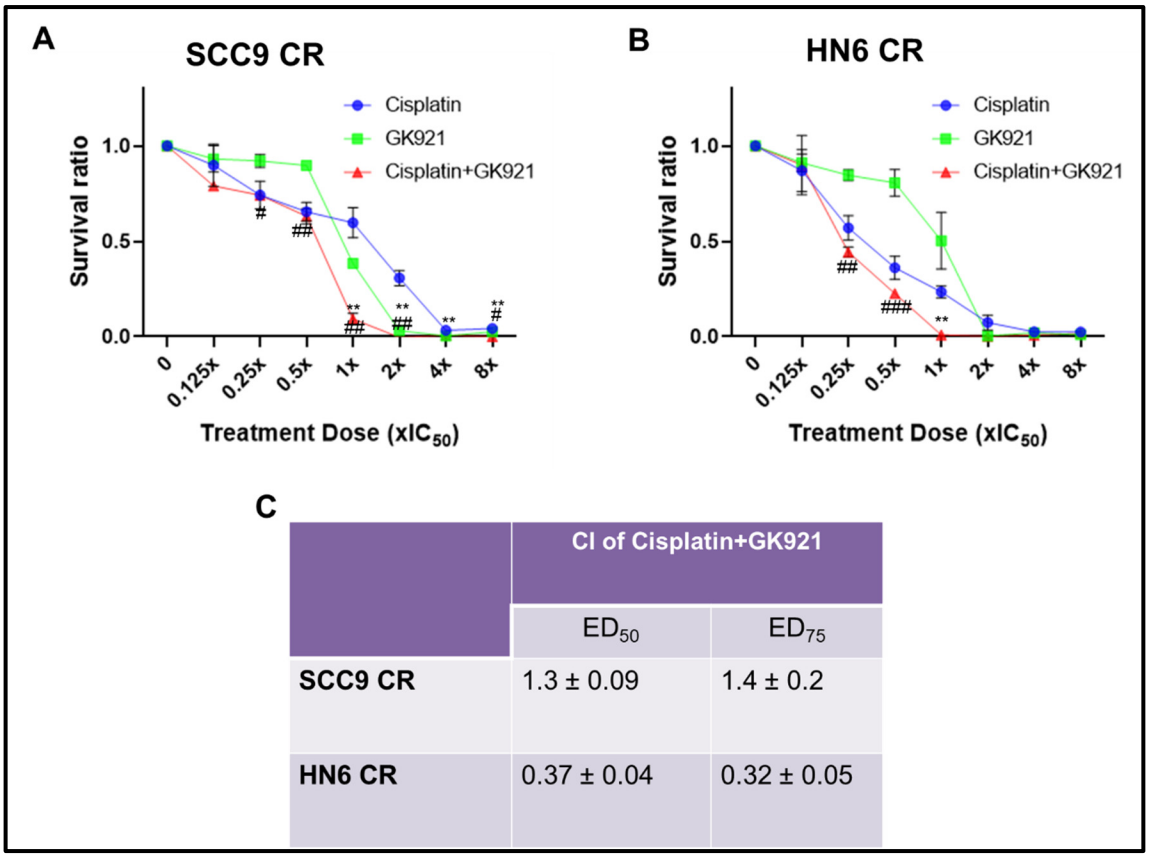

C

	CI of Cisplatin+GK921	
	ED_{50}	ED_{75}
SCC9 CR	1.3 ± 0.09	1.4 ± 0.2
HN6 CR	0.37 ± 0.04	0.32 ± 0.05

Figure 5.17. Cisplatin-GK921 combination significantly decreased cellular proliferation of HN6 CR cell line not SCC9 CR cell line. (A) A dose response curve for SCC9 CR upon treatment with Cisplatin-GK921 combination. **(B)** A dose response curve for HN6 CR upon treatment with Cisplatin-GK921 combination. **(C)** Table showing the combination index (CI) of Cisplatin-GK921 in SCC9 CR and HN6 CR. Graphs are mean ± SEM. n=3. ***p*<0.01 versus Cisplatin only. #*p*<0.05, ##*p*<0.01, ###*p*<0.001 versus GK921 only.

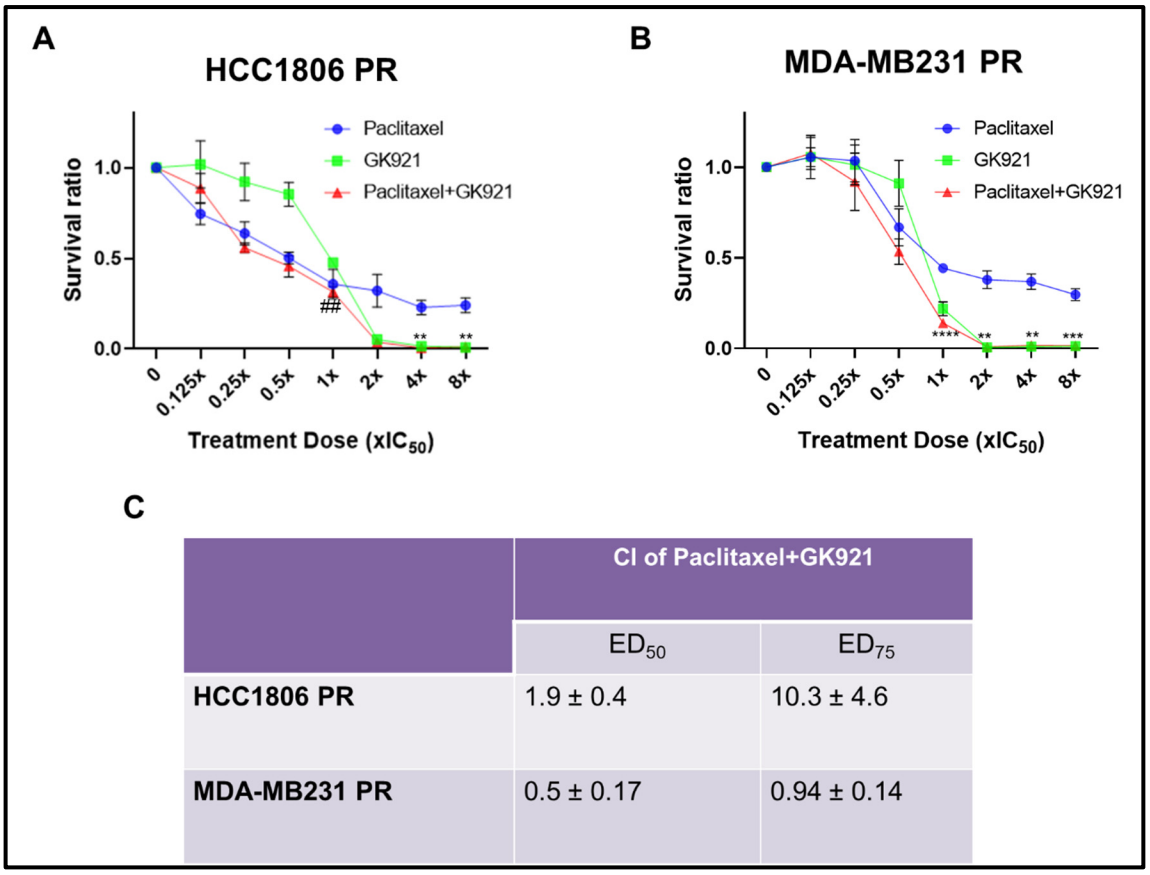

C

	CI of Paclitaxel+GK921	
	ED_{50}	ED_{75}
HCC1806 PR	1.9 ± 0.4	10.3 ± 4.6
MDA-MB231 PR	0.5 ± 0.17	0.94 ± 0.14

Figure 5.18. Paclitaxel-GK921 combination significantly decreased cellular proliferation of MDA-MB231 PR cell line not HCC1806 PR cell line. (A) A dose response curve for HCC1806 PR upon treatment with Paclitaxel-GK921 combination. **(B)** A dose response curve for MDA-MB231PR upon treatment with Paclitaxel-GK921 combination. **(C)** Table showing the combination index (CI) of Paclitaxel-GK921 in HCC1806 PR and MDA-MB231 PR. Graphs are mean ± SEM. n=3. ***p*<0.01, ****p*<0.001, *****p*<0.0001 versus Paclitaxel only. ##*p*<0.01 versus GK921 only.

5.3. Summary of Findings

The main aim of this chapter was to develop resistant OSCC and TNBC cell lines and test the effect of some previously successful combinations in the parent cell lines on the resistant counterparts to determine if autophagy plays a role in chemoresistance. Next, high-resolution data-independent proteomic analysis was carried out to identify any novel regulators that may be implicated in chemoresistance.

Development and characterisation of resistant cell lines were performed using cellular proliferation assay and colony formation assay. In regard to OSCC cell model, IC_{50} for Cisplatin in SCC9 CR and HN6 CR was about 5-8 times higher than that of the respective parent cell line. Similarly, HCC1806 PR and MDA-MB231 PR had higher Paclitaxel's IC_{50} than that of relative parent cell line by 88 and 8 times, respectively. Moreover, this phenotype was further confirmed by colony formation assay which showed that resistant cell lines had a highly chemoresistant phenotype compared to their respective parent cell line.

The role of autophagy in chemoresistance was assessed by examining the effect of some autophagy inhibitors-based combination therapy on the resistant cell lines. SAR405-MRT68921 combination demonstrated a synergistic effect in the 4 resistant cell lines (SCC9 CR, HN6 CR, HCC1806 PR and MDA-MB231PR) with a significant reduction of tumour cell proliferation which was similar to the effect observed in the parent cell lines in chapter three. Moreover, the combination between Cisplatin and SAR405-MRT68921 was synergistic in OSCC resistant cell model with significant reduction of cellular proliferation, although this was antagonist in the parent cell lines. On the other hand, TNBC resistant

cell model (MDA-MB231 PR) showed antagonism following treatment with combination of Paclitaxel and SAR405-MRT68921, with similar effect also observed in the parent cell lines.

Another aim of this chapter was to map OSCC and TNBC resistant cell models on the protein level via high-resolution mass spectrometry based proteomic analysis. In resistant OSCC cell model, pathway analysis identified that autophagy and organisation of cytoskeleton were the top activated cellular functions which was consistent with the significant inhibitory effect exerted by combination of autophagy inhibitors and Cisplatin. In regard to the canonical pathways that were identified via pathway analysis, NRF2-mediated oxidative stress response was found to be from the top activated pathways and antioxidant action of vitamin C was from the top inhibited pathways in both SCC9 CR and HN6 CR. Both pathways are implicated in the tumourigenesis process and should be further investigated in terms of their role in chemoresistance. Additionally, FOXC1 and TGM2 were identified as the top activated upstream regulators with MYC being among the top inhibited regulators.

In regard to resistant TNBC cell models, invasion, metastasis, and migration were the top activated bio-functions which are consistent with the aggressive behavior of resistant cell lines. Similar to OSCC resistant cell model, NRF2-mediated oxidative stress response was from the top activated canonical pathways and FOXC1 and TGM2 as the top activated regulators with MYC was among the top inhibited regulators. Thus, from these findings, TGM2 appeared to be a promising target that could play a role in mediating chemoresistance and was further investigated.

Although about 20-25% decrease in IC_{50} of Cisplatin and Paclitaxel was observed in both OSCC and TNBC resistant cell lines respectively after *TGM2* silencing, this reduction was not statistically significant. On the other hand, combination of Cisplatin and TGM2 inhibitor (GK921) in HN6 CR had a synergistic anti-proliferative effect. However, antagonism was observed in SCC9 CR cell line following treatment with a cisplatin-GK921 combination. The same antagonist effect on cell proliferation was seen in HCC1806 PR upon treatment with Paclitaxel-GK921 combination. On the contrary, a synergistic anti-proliferative effect was detected in MDA-MB231 PR when treated with Paclitaxel combined with GK921. These findings demonstrate that TGM2 could be further developed as a novel target against chemoresistance for certain types of cancer.

Chapter 6

Discussion

6.1. General overview

Autophagy is a cellular catabolic process by which damaged organelles and proteins are being degraded into their primitive biomolecules [1]. It is a mechanism by which cells can survive under microenvironmental stressors such as energy or nutrient deprivation [2]. Autophagy has been implicated in many pathologies including cancer. Role of autophagy in cancer is described as double edge sword as in early carcinogenesis, it has a tumour suppressor role which is switched into tumour promotor role as the tumour grows [67]. As known, tumour cells are subjected to different types of microenvironmental stressors such as nutrient deprivation, hypoxia and stress induced by chemotherapy treatment [377]. In order to survive under these pathological or treatment induced stress conditions, cancer cells try to upregulate autophagy as a cytoprotective mechanism [378]. Notably, autophagy has been linked to various aspects of cancer progression such as tumour growth, invasion, metastasis, and development of chemoresistance [378]. Thus, autophagy could be a promising target to inhibit cancer progression. However, current clinically available autophagy inhibitors (*e.g.,* Chloroquine) only provide modest inhibitory activity [379]. Hence, development of novel strategies to potently inhibit autophagy in cancer cells could lead to the development of more effective anti-cancer therapies.

Oral squamous Cell carcinoma (OSCC) is the sixth most common cancer worldwide [151]. OSCC patients suffer from poor prognosis due to late diagnosis, local recurrence, and early metastasis, which is often resistant to conventional chemotherapy (*i.e.,* Cisplatin) [163]. Several studies have shown that autophagy is associated with aggressive clinicopathological features in OSCC [215, 217]. Thus, targeting autophagy in OSCC may be beneficial that could improve patient's prognosis.

Triple negative breast cancer (TNBC) has the worst prognosis of all subtypes of breast cancers [241]. It does not respond to any endocrine and HER-2 targeted therapy due to lack of PR, ER and HER-2 expression and conventional chemotherapeutic agents are often not effective [240]. Autophagy was found to be correlated with aggressive behavior and poor prognosis in TNBC patients [380] which suggests its role in acquiring this malignant behavior. Hence, targeting autophagy could open up new avenues for developing strategies in inhibiting TNBC progression and re-sensitise tumour cells to standard chemotherapy.

Therefore, in this thesis, we first attempted to identify the effect of some common microenvironmental stressors, namely, glucose- and serum-starvation, on the levels of autophagic marker LC3-II in both OSCC and TNBC models. As autophagy is a dynamic process [1], the next step was to determine if the elevated levels of LC3-II upon serum or glucose starvation is due to increased autophagy induction or decreased degradation. We then assessed the level of autophagy induction, followed by the level of autophagic flux by examining the co-localisation between LC3 and lysosomal marker LAMP2. Then, we tested the effect of combination between ULK-1 complex inhibitors or Beclin-1 complex inhibitors and standard chemotherapeutic agents (*i.e.,* Cisplatin or Paclitaxel) or between ULK-1 inhibitors and Beclin-1 inhibitors on OSCC and TNBC cellular proliferation. Also, the effect of those combinations was assessed on OSCC and TNBC cell migration via scratch wound assay. Some of those combinations were also examined *in vivo* in a TNBC mouse model. Next, the levels of autophagic markers LC3 and P62 were assessed by IHC in OSCC and TNBC tumour tissue sections to identify any correlation between their expression and clinicopathological parameters, and also, survival data.

Furthermore, role of autophagy in chemoresistance was evaluated by developing resistant OSCC and TNBC cell models and testing some of the effective combinations in them. Once the resistant phenotype was established, proteomic analysis of the chemoresistant cell models was also performed to identify the novel drug targets for chemoresistance. In this section, we will discuss our results and recognise any novel findings in our experiments.

6.2. Serum and glucose starvation increased autophagy induction and autophagic flux in OSCC and TNBC cell models

First, the effect of serum and glucose starvation was studied on the autophagic pathway via utilisation of multiple experimental assays, where a 1 h incubation with these stressors was deemed to upregulate autophagic response under the majority of conditions. In OSCC cell lines, both serum and glucose starvation conditions led to increased autophagosome levels (*i.e.,* LC3-II) in the cells after 1 h incubation, except for serum starvation in SCC9 cells. Of note, LAMP2 levels were significantly increased in SCC9 after serum starvation (1 h) which could have elevated the autophagic flux leading to quick removal of autophagosomes. This could have resulted in the observed no net increase in the LC3-II levels under these latter conditions. Further, increased autophagic induction was observed under both stressors, which was confirmed either by increased LC3-II levels or LC3-stained punctas after incubation of cells with stressors in presence of Baf A1(which inhibits autophagic degradation). We also observed increased autophagic flux under these conditions, which was visualised by increased fusion (*i.e.,* co-localisation) between autophagosome (LC3) and lysosome (LAMP2) markers. Taken together, both serum and glucose starvation were shown to increase the autophagic pathway in both OSCC cell lines.

In TNBC cell models, increased autophagosome levels were observed only after 1 h incubation with serum free media in HCC 1806 cells, while increased LAMP2 levels were observed after 1 h serum starvation in MDA-MB-231 cells. The increased autophagosome initiation was observed after serum or glucose starvation in both TNBC cell lines, except for serum starvation in MDA-MB231 cells. Moreover, increased autophagic flux was observed under all conditions. Hence, there is an overall increase in both initiation and degradation stages of autophagic process in response to glucose starvation in both cell lines, while serum starvation led to this effect only in HCC1806 cells. In MDA-MB231 cells, serum starvation conditions led to no autophagic induction, while there was an increase in autophagic degradation process. This result was also consistent with the observed increase in the lysosome (LAMP2) and autolysosome (colocalisation of LAMP2 and LC3) levels.

Overall, enhanced autophagic activity was observed after both serum or glucose starvation in OSCC and TNBC models. Similar results have also been demonstrated in previous studies where glucose and serum starvation induced autophagy in Luminal A Breast, Pancreatic, OSCC and Bladder cancer cells [393-396]. This highlights the role of autophagy under different microenvironmental stressors.

6.3. Microenvironmental stressors increased IC_{50} of standard chemotherapy and decreased IC_{50} of some autophagy inhibitors

After that, IC_{50} of standard chemotherapy and autophagy inhibitors were determined for their anti-proliferative activity under different conditions (nutrient replete conditions or after pre-incubation with serum- or glucose depleted media). Our results showed that

MRT68921 seems to be the most potent autophagy inhibitors, as it had the lowest IC_{50}, across both OSCC and TNBC cell models used under different conditions (nutrient replete or after incubation with serum or glucose deplete media).

In OSCC, increased IC_{50} of Cisplatin was observed in both OSCC cell lines after 1 h pre-incubation with serum or glucose free media in comparison to nutrient replete condition except for glucose starvation in SCC25. Also, small variability in IC_{50} of autophagy inhibitors was observed after incubation with serum or glucose depleted media compared to nutrient replete conditions in OSCC cell lines except for Spautin-1 and MRT68921 in SCC25 that showed marked decrease in their IC_{50} following 1 h incubation with glucose free media. Notably, a huge increase in IC_{50} of SAR405 and SBI-0206965 was observed in SCC9 after 1 h of serum or glucose starvation.

In TNBC, an increase in IC_{50} of Paclitaxel was observed only in MDA-MB231 after 1 h serum starvation compared to nutrient replete condition. While a small changes in IC_{50} of autophagy inhibitors were noted in both TNBC cell lines following incubation with serum or glucose depleted media in comparison to nutrient replete conditions except for Spautin-1 in HCC1806 which exhibited marked decrease in its IC_{50} after 1 h incubation with glucose free media. Of note, marked increase in Spautin-1 IC_{50} was seen in MDA-MB231 following incubation with serum deplete media for 1 h.

Altogether, microenvironmental stressors increased IC_{50} of standard chemotherapy in OSCC cell model, whilst TNBC cell model showed an opposite effect except in MDA-

MB231 which exhibited increased Paclitaxel's IC_{50} after 1 h incubation with serum deplete media. Regarding autophagy inhibitors, a small variability in IC_{50} of the autophagic inhibitors was noted under most of conditions in both cell models except for Spautin-1 which showed decreased IC_{50} after glucose starvation in both SCC25 and HCC1806. This is consistent with our hypothesis that increased autophagy by tumour microenvironmental stressors could lead to the development of chemo-resistance and also, results in sensitisation of cancer cells to novel autophagy inhibitors. Similar results were observed in another study where hypoxia increased IC_{50} of Cisplatin and doxorubicin in lung cancer [397]. This emphasises the role of microenvironmental stressors in activating autophagy and developing resistant to standard chemotherapy.

6.4. Combination between standard chemotherapeutic agents (*i.e.,* Cisplatin, Paclitaxel) and specific autophagy inhibitors (Beclin-1 inhibitors) reduced OSCC and TNBC cellular proliferation

The next step was to test the effect of autophagy inhibition on tumour cell proliferation under nutrient replete or microenvironmental stressors (*i.e.,* serum and glucose depleted conditions). A combination of standard chemotherapy (*i.e.,* Cisplatin or Paclitaxel) and different autophagy inhibitors (ULK-1 complex inhibitors or Beclin-1 complex inhibitors) were examined in both OSCC and TNBC cell models. The combination of either Cisplatin or Paclitaxel and SAR405 showed a consistent synergistic effect in both OSCC and TNBC cell model under nutrient replete conditions. SAR405 is an inhibitor of vps34, which plays a critical role in Beclin-1 complex [341]. The same results were observed in previous studies where combination of standard chemotherapy and SAR405 enhanced the cytotoxicity of the chemotherapy in lung cancer, urothelial carcinoma cell, osteosarcoma and head and neck squamous cell carcinoma (HNSCC) [398, 374, 344, 399]. However,

cell type dependent effects were observed for this combination after incubation of cells with serum or glucose free medium. The observed antagonism under microenvironmental stressors in some cell lines was unexpected, as increased autophagic activity should have increased the susceptibility of cell towards autophagy inhibitors. However, it should be considered that autophagy is one of the mechanisms affected by tumour microenvironmental stressors and there could be potential conflicting pathways which may have been activated to counteract the activity of these inhibitors.

Other combinations of chemotherapy and autophagy inhibitors (Spautin-1, MRT68921 and SBI-0206965) also showed cell type dependent effect in both OSCC and TNBC cell lines. Previous studies have also shown that combination of standard chemotherapy with either Spautin-1 or SBI-0206965 led to improved cytotoxicity of the chemotherapy in prostate cancer, melanoma, and renal carcinoma [400-402]. These differences could be due to different mechanism of action of these inhibitors. For instance, Spautin-1 inhibits USP10/13 deubiquitinases leading to degradation of Beclin-1 [339]. However, USP10/13 can also regulate deubiquitination of other important cellular proteins (*e.g.,* p53) [339], which could potentially cofound the activity of this agent. Moreover, Beclin-1 also has a well-known tumour suppressor role, via interaction with apoptotic proteins, apart from its role in autophagy regulation [48]. Thus, direct inhibition of Beclin-1, rather than other molecules in Beclin-1 complex, could lead to tumour promoting activity as well.

MRT68921 and SBI-0206965 are known to inhibit ULK-1 kinase [348, 349]. However, SBI-0206965 is also shown to inhibit AMPK, which is a master regulator of energy homeostasis and could lead to multiple signaling effects [352]. Furthermore, cell lines from same cancer

type can still have different mutations which could lead to differential effects observed among different combinations of chemotherapy and autophagy inhibitors. Thus, more broad panels of OSCC and TNBC cell lines are required to be assessed in future to further delineate these cell type specific effects.

After incubation with tumour microenvironmental stressors, majority of combinations between chemotherapy and autophagy inhibitors showed antagonistic activity. This could be due to activation of other pathways that allow tumour cell survival under those conditions. One of possible pathways involves activation of the AMPK pathway after glucose deprivation resulting in an enhanced expression of phosphoglucomutase 1. Phosphoglucomutase 1 is a main protein involved in metabolic switch in tumours and could facilitate cancer progression [403]. Another possible mechanism is activation of ATF4, a transcription factor that is responsible for genes involved in amino acids metabolism and ER stress response, which is triggered by glucose deprivation, and is overexpressed in cancer cells [404]. J Ye *et al.* [404] demonstrated that ATF4 inhibition suppressed proliferation and survival of colorectal cancer cells even with activation of cytoprotective autophagy. Also, the ability of different cancer cells (liver, pancreatic, gastric and colon cancer cells) to survive under nutrient starvation condition is associated with high expression of Akt pathway. This pathway not only inhibits autophagy, but also help in recognition of nutrients and stimulates glycogen synthesis [405].

6.5. Combination between ULK-1 inhibitors and Beclin-1 inhibitors reduced OSCC and TNBC cellular proliferation

To the best of our knowledge, this is the first study that examines the effect of combination between different classes of autophagy inhibitors on cellular proliferation. Combination between ULK-1 complex inhibitors (MRT68921 and SBI-0206965) and Beclin-1 complex inhibitors (SAR405 and Spautin-1) was examined in both OSCC and TNBC cell models under nutrient replete conditions or after pre-incubation under serum- and glucose-depleted conditions. The combination of SAR405 (Beclin-1 complex inhibitor) and MRT68921 (ULK-1 complex inhibitor) showed consistent synergistic effect among all cell lines and incubation conditions. Other combinations demonstrated cell type dependent effect, which require further investigation to delineate these differences.

We further examined if combination of SAR405 and MRT68921 could further show anti-proliferative synergy with chemotherapy in OSCC or TNBC cell lines. However, an antagonistic effect was observed when combining SAR405-MRT68921 with Cisplatin or Paclitaxel in SCC9 and MDA-MB231, respectively. This antagonistic effect may be due to the fact that SAR405-MRT68921 exerts a potent anti-proliferative activity, and this effect was not further augmented by addition of chemotherapy.

6.6. Standard chemotherapy (*i.e.,* Cisplatin or Paclitaxel), Beclin-1 inhibitor (SAR405) and ULK-1 inhibitor (MRT68921) reduced tumour cell migration in dose dependent manner in both OSCC and TNBC cell models

The effect of standard chemotherapy and autophagy inhibitors on tumour cell migration was also examined via scratch wound assay. In both OSCC and TNBC cell models, standard chemotherapy (*i.e.,* Cisplatin or Paclitaxel), SAR405 and MRT68921 decreased

wound density in a dose dependent manner. To best of our knowledge, this is the first study to examine the effect of standard chemotherapy and autophagy inhibitors on tumour cell migration in both OSCC and TNBC cell models.

6.7. Combination of standard chemotherapy (*e.g.,* Cisplatin or Paclitaxel) and SAR405 impaired the tumour cell migration in both OSCC and TNBC cell models

We also examined the effect of some combinations, that showed promising results on cellular proliferation, on tumour cell migration via scratch wound assay. Cisplatin-SAR405 combination significantly reduced the relative wound density in OSCC cell model. Likewise, the same effect was observed in MDA-MB231 when treated with Paclitaxel-SAR405 combination. These results indicate the role of autophagy in cell migration, which is an essential step in metastasis [406]. To the best of our knowledge, this is the first study to investigate the effect of these autophagy initiation inhibitors (*i.e.,* Beclin-1 complex inhibitors and ULK-1 complex inhibitors) alone or combined on tumour cell migration. A previous study had investigated the effect of autophagy inhibition, via late stage autophagy inhibitors, on cancer cell migration [407]. Inhibition of autophagy by chloroquine (late autophagy inhibitor) enhanced metastasis suppression by the natural compound phenethyl isothiocyanate in lung cancer cells [407]. On the contrary, autophagy inhibition via 3-methyladenine (3MA) restored the ability of tumour cell migration in nasopharyngeal carcinoma [408]. However, it is important to note that 3-MA lacks specificity for autophagic inhibition. 3-MA inhibits Class III PI3K as well as other major kinases such as MAPK [334]. A recent study demonstrated that incubation of malignant oral keratinocytes (H376) with conditioned media obtained from SAR405 treated natural human oral fibroblast led to increased migration of tumour cells [188].This might reflect that targeting autophagy either

in cancer cells itself or surrounding fibroblast could lead to diverse effects on OSCC migration.

Although SAR405-MRT68921 combination showed synergistic anti-proliferative effect in both OSCC and TNBC cell models, the same combination did not produce any synergistic effect on cell migration in both cell models. This should be considered when designing SAR405-MRT68921 combination therapy as it would be effective mostly in inhibiting primary tumour growth but might not stop the cancer cells from metastasising.

6.8. Combination of standard chemotherapy (Paclitaxel), Beclin-1 (SAR405) and ULK-1 inhibitor (MRT68921) reduced tumour size and weight in TNBC orthotopic xenograft model

Different combinations, which showed promising effect *in vitro*, were tested *in vivo* in TNBC orthotopic xenograft. To best of our knowledge, this is the first study to examine the effect of specific autophagy inhibitors alone or combined with standard chemotherapy *in vivo* in any cancer xenograft model. Our data demonstrated a significant reduction of tumour size and weight in group treated with Paclitaxel-SAR405-MRT68921 when compared to the control group. A decrease in tumour size was noted in the same group in comparison to group treated with Paclitaxel only, but it was not significant. The efficacy of SAR405, MRT68921 alone or in combination in inhibiting tumour growth was not observed. Moreover, none of the inhibitors alone showed synergistic activity with Paclitaxel. One of issues with SAR405 was its poor solubility at the dose administered, and poor cellular uptake of SAR405 *in vivo* [398]. A recent study demonstrated a nanoparticle delivery system for SAR405, not only enhanced the efficacy of autophagy inhibition, but also enhanced the efficacy of doxorubicin treatment in lung cancer cells *in vitro* [398]. Thus,

creating a nanoparticle delivery system for poorly soluble inhibitors, like SAR405 could be a new approach to improve the efficacy of such inhibitors *in vivo***.** Although MRT68921 showed marked anti-proliferative activity *in vitro*, no significant effect was observed *in vivo*. One of the potential reasons for this poor response *in vivo* could also be the use of *intraperitoneal* route of administration and future studies using *intravenous* injections of these agents should be examined.

6.9. Positive LC3 expression is associated with low histologic grade in OSCC patients

Using tumour tissue specimens from OSCC patients, our results demonstrated that no significant association between LC3 expression and clinical variables was noted except for tumour histologic grade where patients with positive LC3 expression were more likely to have a low histological grade OSCC. An opposite trend was observed in previous studies where expression of LC3 A and LC3 B was correlated with tumour recurrence in 71 OSCC patients [409]. Another study on 195 OSCC specimens showed that high LC3 B expression was associated with lymphovascular invasion [217]. In the same context, Tang JY *et al.* [215] demonstrated that high LC3 expression in a cohort of 90 OSCC specimens was correlated with tumour size and tumour stage. However, it should be noted that the latter study did not mention the site of specimens used, opposed to our study where only tongue specimens were used. This discrepancy may also be due to presence of different isoforms of LC3 (LC3 A, B and C) [410] which had different distribution pattern. A previous study compared the expression pattern of the three isoforms of LC3 in different cancer cell lines (lung, glioblastoma and breast cancer cells) where LC3 A was expressed mainly in the nucleus and perinuclear region, whereas, LC3 B was distributed in the cytoplasm and nucleolus and LC3 C was strongly expressed in the nucleus [411]. In our

study, we used a LC3 B antibody, and we therefore might have missed changes in other isoforms.

On the other hand, higher P62 nuclear staining was observed in high histologic grade and advanced stage of OSCC with the reverse association noted for cytoplasmic P62 staining, however, those associations were not significant. Conversely, *Liu JL et al* [217] observed that low P62 nuclear staining and high P62 cytoplasmic staining was correlated with advanced stage and high histologic grade of OSCC. This variance in results could be due to the fact that only tongue specimens were involved in our study, while the latter study does not specify the type of OSCC samples used and hence they could have used a specimen from a different site of oral cavity than us. Thus, additional studies should be performed to explore the exact function of nuclear P62, and also involving normal and precancerous tissues to clarify its role in carcinogenesis and progression of cancer.

6.10. Positive LC3 expression is associated with high histologic grade in TNBC patients and better overall survival

Autophagy markers were also examined in TNBC patients (two cohorts). In one of the cohorts (ABCTB specimens), it was demonstrated that patients with either positive LC3 or P62 expression were more likely to have high grade TNBC which was similar to finding of previous study [386]. Also, increasing age, positive lymph node status and negative LC3 expression in both TNBC cohorts were associated with poor overall survival. Similar results were observed by Chang SJ *et al*. [387], who observed a significant negative association of LC3 expression with overall survival. On the other hand, no significant association was noted between P62 expression and clinical parameters. However, cohorts

with positive P62 expression had better overall survival which was consistent with another study on TNBC [412].

These results suggested that increased autophagy induction by positive LC3 expression could lead to increased survival outcomes. However, it should also be considered that autophagic degradation might be defective in these tumours as P62 expression was also increased. Together, this would lead to dysfunctional autophagy, which could potentially explain why cohorts with positive LC3 and P62 had a better survival outcome. A similar trend was also noted in a previous study on lung cancer where cohorts with high LC3/High P62 expression exhibited better outcome [413]. Another important consideration when analysing LC3 immunostaining is that the antibody detects both LC3-I and LC3-II, although only LC3-II is a marker for autophagosomes and this could potentially confound the results, which should be interpreted with caution in terms of autophagic activity.

6.11. Combination between standard chemotherapy (*e.g.,* Cisplatin or Paclitaxel) and SAR405-MRT68921 exerted anti proliferative effect in resistant OSCC and TNBC cell models

Resistant OSCC and TNBC cell lines were developed by repeated treatment with increasing concentration of Cisplatin or Paclitaxel, respectively. Once resistant cell lines were developed, the role of autophagy in chemoresistance was assessed via examining the effect of some autophagy inhibitors on cellular proliferation in the resistant cell lines. Although, an increase in IC_{50} of SAR405 and MRT68921 respectively was noted in both resistant OSCC and TNBC cell models, combination of SAR405 and MRT68921 showed a synergistic anti-proliferative effect in the 4 resistant cell lines (SCC9 CR, HN6 CR, HCC1806 PR and MDA-MB231 PR) with a significant reduction of tumour cell proliferation.

These results suggest that the increase in IC_{50} could be due to activation of additional pathways leading to multidrug resistance. However, synergistic effect observed on SAR405-MRT68921 combination shows that autophagy is an important pathway and its inhibition along with chemotherapy administration could be an effective treatment strategy.

Furthermore, the combination effect between standard chemotherapeutic agents (Cisplatin or Paclitaxel) and SAR405-MRT68921 on cellular proliferation was tested. In resistant OSCC cell model, Cisplatin-SAR405-MRT68921 combination had a synergistic effect in both SCC9 CR and HN6 CR with significant reduction of tumour cell proliferation. This effect was unlike the effect in the parent cells which displayed antagonism. This could be due to activation of autophagy in resistant OSCC cell lines which was observed in the pathway analysis of the proteomic data. On the other hand, MDA-MB231 PR exhibited an antagonist effect when Paclitaxel was combined with SAR405-MRT68921 which was the same effect observed in the parent cell line. This might be due to minimal activation of autophagy in MDA-MB231 PR (z-score=0.083) which was similarly observed in the pathway analysis of the proteomic data. Overall, these results indicate that SAR405-MRT68921 combination could be a potential therapy to overcome chemo-resistance in OSCC but might not be as effective in TNBC.

6.12. Autophagy is one of the most activated biological functions and TGM2 is one of the most activated up-stream regulators in resistant OSCC cell models

Proteomic data and IPA analysis from resistant OSCC cell lines revealed that cytoskeleton and cytoplasm organisation, formation of cellular protrusion and vesicles and autophagy were the most activated bio-functions in both resistant OSCC cell lines. Notably, previous

studies have also linked autophagy to chemoresistance in OSCC [223-226]. The mechanism by which autophagy induces chemoresistance could be through activation of AMPK signaling and inhibition of mTOR signaling as observed when areca nut extract (ANE) induced cisplatin resistance in SCC9 cancer cells via induction of autophagy [225]. Also, the same study showed that reactive oxygen species (ROS) was involved in chemoresistance by induction of autophagy in ANE treated OSCC cells [225]. Moreover, it was found that sensitivity of tumour cells toward cisplatin in lung cancer was improved by inhibiting ATG3-related autophagy via MicroRNA-1 overexpression [389]. Another study showed that inhibition of autophagy via 3-MA resulted in increased cytotoxicity of doxorubicin in Hela cells via suppression of transcription factor EB (TFEB) (regulator for lysosomal biogenesis and autophagy) induced cell survival [390].

Our analysis further identified endothelin-1 signaling and interferon signaling as one of the most activated canonical pathways in both resistant OSCC cell lines. This is consistent with previously known role of endothelin-1 in cisplatin chemoresistance in ovarian cancer [414-416]. Furthermore, the most inhibited pathway in both cell lines was RHOGDI signaling which was in line with a previous study demonstrating its downregulation in malignant or metastatic breast tumours compared to normal breast tissue or carcinoma *in situ*, respectively [417].

Myc was one of the most inhibited upstream regulators. This might be explained by downregulatory effect of cisplatin on Myc levels as it was found in previous study that chemotherapy treatment (*i.e.,* Doxorubicin) suppressed Myc expression in OSCC cell line (Cal-27) [418]. On the contrary, other studies [419, 420] have shown the involvement of

Myc in cisplatin chemoresistance. This discrepancy may be due to use of different cell lines in our study compared to those studies which may indicate that each cell line could harbor different mutations even within the same type of cancer. Immunity related GTPase M (IRGM) was another top inhibited upstream regulator. IRGM is a GTP protein that regulates autophagy through enhancing the assembly of ULK-1 and Beclin-1 and controls the lysosome biogenesis[421]. The observed inhibition of IRGM was unexcepted as autophagy was one of the most activated functions in resistant OSCC cell lines. Thus, more studies are needed to delineate the role of IRGM in chemoresistance in OSCC and how it correlates to autophagy.

Moreover, TGM2 was one of the most activated up-stream regulators observed in resistant OSCC cell lines. Our results with TGM2 was in line with results in osteosarcoma and lung cancer where TGM2 was linked to cisplatin chemoresistance via MAPK/AKT pathway and NK-κB regulation respectively [422, 423]. Forkhead box C1 (FOXC1) was also identified as one of the top activated upstream regulators. FOXC1 is a transcription factor that is involved in the development of different organs in embryonic life and has been involved in cancer progression as well [424]. FOXC1 knockdown in OSCC cells reduced the migration of tumour cells and impaired tumour cell growth and colony formation [425]. It has been demonstrated that FOXC1 stimulates acquisition of stem cell like properties in lung cancer cells [426]. Acquisition of stemness like cell properties is one of the mechanisms via which cancer cells develop chemoresistant phenotype [427] and this might be linked to the observed FOXC1 upregulation in chemoresistant cell lines.

6.13. HIF-1α is one of the most activated canonical pathways and TGM2 is one of the most activated up-stream regulators in resistant TNBC cell models

Proteomic data and IPA analysis from chemoresistant TNBC cell lines also demonstrated that invasion and metastasis were the top activated biological functions in both HCC1806 PR and MDA-MB231 PR, compared to parent cells. One of the molecules that was upregulated in HCC1806 PR was epidermal growth factor like protein -7 (EGFL7) and analysis showed that it was involved in invasion and metastasis. This is consistent with previous studies that indicated the role of EGFL7 in invasion and metastasis of gastric cancer cells [428, 429]. However, the exact role of EGFL7 in chemoresistance of TNBC is still unclear and needs more investigation. AKT3 was also upregulated in MDA-MB231 PR and IPA analysis revealed that it may be involved in invasion and metastasis. This consistent with other studies where AKT3 was found to be upregulated in thyroid cancer and associated with invasion, cell migration and proliferation [430-432]. Also, AKT3 have been linked to chemoresistance in uterine cancer where downregulation of AKT3 resulted in increased sensitivity of tumour cells toward chemotherapy [433, 434].

Regarding canonical pathways, HIF-1α signaling and NRF2 mediated oxidative stress response were identified as the top activated pathways in both resistant cell lines. HIF-1 α is a major transcription factor which not only allow survival of cancer cells under hypoxic conditions but also regulates many genes responsible for different cellular function such as cell survival under microenvironmental stresses and chemotherapeutic treatment [435, 436]. Notably, a previous study showed that HIF-1α downregulation in TNBC reversed chemoresistance [437]. NRF2 is a transcription factor that allows survival of cancer cells under oxidative stress as it regulates antioxidant genes [438]. Previous studies have also implicated NRF2 in mediating chemoresistance in breast cancer [439, 440]. NRF2

inhibition increased cisplatin cytotoxicity in an *in vivo* breast cancer mouse model [439]. Notably, enhanced chemosensitivity in breast cancer cells was observed when luteolin (flavonoid) was combined with standard chemotherapy (Taxol) via downregulation of NRF2 mediated pathway [440].

Furthermore, similar to chemoresistant OSCC cell model, TGM2 was one of the top activated up-stream regulators in chemoresistant TNBC cell lines. TGM2 has been involved in chemoresistance of different types of cancer [422, 423]. Notably, TGM2 inhibition in a TNBC model has previously been shown to improve the anti-cancer effect of chemotherapy (docetaxel) [441]. This study aligns with our finding about a potential role of TGM2 in chemoresistance. In addition, tumour necrosis factor (TNF) was one of the top activated up-stream regulators. TNF is an inflammatory cytokine that plays role in cell survival and proliferation [442]. Previous studies have linked TNF to chemoresistance in breast cancer [443, 444]. TNF-α was found to be positively associated with anthracycline resistance in breast cancer cells [443]. Likewise, another study demonstrated increased serum level of TNF-α in TNBC xenograft model treated with cisplatin alone, which suggested that chemotherapy induced inflammation can triggers chemoresistance [444].

TREX1 was from the top inhibited upstream regulators, which is a protein known to be involved in removal of extra nucleotides that build up sometimes during DNA replication [445]. The observed inhibition of TREX1 was consistent with previous studies where low TREX1 expression was associated with poor prognosis in breast cancer [446]. In the same context, TREX1 was downregulated in melanoma cells and its overexpression induced apoptosis and diminished proliferation [447]. However, the role of TREX1 in

chemoresistance is not clear and needs further investigation. Moreover, Myc was another inhibited up-stream regulator identified in mediating chemoresistance in TNBC model. Notably, Myc is known as a transcription factor that is persistently expressed in many types of cancer and has been found to be involved in chemoresistance of breast cancer [448, 449], pancreatic cancer [450, 451], and colon cancer [452, 453]. Thus, additional studies need to be performed to uncover the rationale of Myc inhibition in our developed chemoresistant cell line.

6.14. TGM2 may serve as a promising target for chemoresistance in OSCC and TNBC cell models

Targeting the upstream regulators that were identified from IPA analysis could be a promising approach to overcome chemoresistance, as these regulators control multiple pathways that could be involved in mediating chemo-resistance in tumour cells. *TGM2* is a gene encoding for a family of enzymes that induces the formation of a bond between amino group of lysine residue and γ-carboxamide group of glutamine residue of various proteins [454]. TGM2 has been shown to be involved in angiogenesis and metastasis of colorectal cancer [455] and renal cell carcinoma [456], respectively. Our IPA analysis revealed that TGM2 was activated in all 4 chemo-resistant cell lines which indicates that it might have an important role in mediating chemoresistance. To investigate the role of TGM2 in chemoresistance, we assessed the IC_{50} of standard chemotherapy in inhibiting cellular proliferation after *TGM2* silencing. A reduction in IC_{50} of Cisplatin or Paclitaxel was observed in resistant OSCC and TNBC cell lines after *TGM2* silencing, but this effect was not significant. These results were consistent with other studies in breast cancer [441], osteosarcoma [422] and lung cancer [423] where *TGM2* silencing increased the sensitivity

to standard chemotherapy. This indicates that TGM2 could be involved in developing resistance towards standard chemotherapy.

Of note, some studies have also shown a relation between TGM2 and autophagy. Zhang *et al.* demonstrated that autophagy inhibition in TGM2 overexpressing cells of mantle cell lymphoma reduced chemoresistance caused by TGM2 [457]. Another study showed that fusion between autophagosome and lysosomes was inhibited by knockdown of *TGM2* in glioblastoma cells with enhanced radiosensitivity [458]. Those results were consistent with another study where nutrient depletion induced both autophagy and TGM2 expression in breast cancer cells and TGM2 boosted the autophagic flux by amplifying lysosomal clearance and autophagic protein degradation [459].

Moreover, combination of standard chemotherapy (Cisplatin or Paclitaxel) and TGM2 inhibitor (GK921) showed a synergistic anti-proliferative effect in HN6 CR and MDA-MB231 PR. Similar results were observed in other types of cancer such as xenograft model of glioma stem cells [460] and renal squamous cell carcinoma [461]. Also, a study on renal cell carcinoma showed that GK921 treatment only reduced tumour cell growth via P53 stabilisation [462]. Overall, our results and results from others indicate that TGM2 may be an attractive target to re-sensitise tumour cells toward conventional chemotherapy.

Chapter 7

Conclusion

7.1. Conclusion

Recently, autophagy has been implicated in different aspects of cancer such as growth, metastasis, and development of chemoresistance. At the same time, despite the emergence of new treatment modalities over the last two decades, chemotherapy is still the primary treatment modality used in many cancers. Thus, autophagy could be a promising target in inhibiting cancer progression and re-sensitising the tumour cells to conventional chemotherapeutic agents.

This thesis used two cancer models (OSCC and TNBC) as both these cancer types have poor prognosis due to early metastasis and development of chemoresistance. This thesis demonstrated, via multiple assays, that autophagy can be activated by serum or glucose starvation in OSCC and TNBC cell models. Also, the effect of combination between standard chemotherapy and specific autophagy inhibitors directed toward major molecules in the autophagic pathway on tumour cell proliferation was assessed. For the first time, this thesis demonstrated the inhibitory effect of combination between standard chemotherapy and autophagy inhibitors on OSCC and TNBC tumour cell proliferation. Similar effect was also seen when different autophagy inhibitors were combined. Moreover, it further showed that combination between standard chemotherapy and autophagy inhibitors not only inhibited tumour cell proliferation but also impaired tumour cell migration in both OSCC and TNBC cell models. Lastly, the effect of this combination was tested *in vivo* in TNBC xenograft model where it reduced tumour size and weight.

The expression of autophagic markers (LC3 and P62) was examined in OSCC and TNBC tumour specimens from patients where positive LC3 expression was associated with low

histologic grade in OSCC and high histologic grade in TNBC. Further, positive LC3 levels were also associated with better overall survival in TNBC patients.

Additionally, the role of autophagy in chemoresistance were examined by developing a resistant OSCC and TNBC cell model and assessing the effect of combination between standard chemotherapy and autophagy inhibitor on their cellular proliferation. It was demonstrated that these combinations had an inhibitory effect on tumour cell proliferation of resistant OSCC cells, but not in resistant TNBC cells. This was further illustrated by activation of autophagy in resistant OSCC cells that was detected by the pathway analysis of the proteomic data.

Furthermore, the proteomic analysis for the resistant cell lines and their parent counterparts cell lines was performed to identify the activated and inhibited biological functions, canonical pathways, and upstream regulators. The analysis revealed activation of upstream regulator TGM2, which was observed in both resistant OSCC and TNBC cell models, could be a potential key mechanism involved in conferring chemoresistance in these cells. Henceforth, we examined its role by assessing anti-proliferative activity of standard chemotherapy after *TGM2* silencing. The IC_{50} of standard chemotherapy was reduced by 20-25% after *TGM2* silencing in both resistant OSCC and TNBC cell model, respectively. Also, the combination of standard chemotherapy and TGM2 inhibitor exerted an inhibitory effect on tumour cell proliferation in both OSCC and TNBC resistant cell models.

Overall, this study provides a new approach for combination based anti-cancer therapies to inhibit cancer progression and re-sensitise the tumour cells toward the conventional chemotherapeutic agents in OSCC and TNBC models. Also, the upstream regulator (TGM2) identified by the proteomic analysis is a promising target that could open new strategies to overcome chemoresistance in OSCC and TNBC and needs to be further investigated in detail in future studies.

7.2. Limitations

This thesis has faced two major limitations that significantly impacted completion of experiments. The first limitation was that I started my PhD in mid-2019 in another Lab where my supervisor resigned from the University after 6 months of my candidature's start. Thus, I had to find a new lab with a new supervisor and a new project. After everything being settled in early 2020, the second limitation was numerous COVID-19 shutdowns. The emergence of COVID-19 forced us to stop working in the lab for 4 months in 2020 and 6 months again in 2021. These interruptions dramatically affected our experiments, especially when we were trying to develop resistant cell lines which usually take a long time to develop. These limitations brought a time constraint that hindered further investigations to be performed especially in resistant cell lines.

In **Chapter 3**, we were planning to test the effect of hypoxia on autophagy induction in both cell models but due to time constraint and the limited access to a hypoxia chamber as it needed some repairs, those experiments could not be carried out. Also, the limited time hindered us to perform combination experiments between standard chemotherapy and SAR405-MRT68921 on all cell lines, so, experiments were performed only on one cell

line in each model. Moreover, due to limited time, testing the effectiveness of combination therapy *in vivo* in OSCC xenograft model was also difficult to perform.

In **Chapter 4**, the unavailability of survival data for OSCC patient hindered us from performing survival studies as planned. In addition, in **Chapter 5**, again due to time constrain and extended time I take to develop resistance, some combination experiments (Paclitaxel-SAR405-MRT68921) could not be performed on HCC1806 PR. We also could not perform all the planned combinations' experiments *e.g.*, in parent cell lines that was part of the plane.

7.3. Future directions

As mentioned previously, some experiments could have been done to further elucidate the role of autophagy in cancer progression and chemoresistance. Also, more experiments need to be carried out to further elucidate the mechanism by which TGM2 contributes to chemoresistance.

As hypoxia is one of the important tumour microenvironmental stressors, future studies are required to be carried out to evaluate the effect of hypoxia on autophagy in both OSCC and TNBC cell models. In addition, testing the effect of combination therapy between standard chemotherapy and autophagy inhibitors under hypoxic conditions needs to be performed. Moreover, in order to mimic the tumour microenvironmental stress, we would also like to examine the effect of combination between standard chemotherapy and autophagy inhibitors under integrated microenvironmental stress from serum-depletion,

glucose-depleted and hypoxia. Additionally, any combinations experiment that had not been done due to time constraint under any condition in any cell line needs to be performed.

We would like to further expand our combination studies to cover 3D spheroid cell culture [463] where cells will be seeded in 96-well Ultra-Low-Attachment (ULA) plates with addition of Matrigel® (final concentration 2.5% w/v) to help in spheroid formation. After 72 h of seeding, spheroids will be treated with different combinations under nutrient replete, serum deplete, and glucose deplete conditions and 3D cell viability assay will be performed after 72 h of treatment. These studies can also be expanded to include different sub-types of TNBC [238, 239] and OSCC as each sub-types have different genetic profile, which could lead to potential heterogeneity in results and aid in the development of more personalised therapies for patients with particular subtype of cancer.

One of the tumour microenvironment elements that may contribute to autophagy induction is cancer associated fibroblasts (CAFs) [464]. They are known to induce autophagy to provide essential nutrients to pancreatic cancer cells [465]. Thus, the effect of CAFs on levels of autophagy in OSCC and TNBC cancer cells should be evaluated via co-culture of CAFs and cancer cells in trans-well co-culture system [466] under different microenvironmental stressors (hypoxia, serum, or glucose starvation).

In addition to cell migration assay, invasion assay could be carried out to examine the effect of different combinations on tumour cell invasion. Invasion assay could be

performed via trans-well assay [467], where tumour cells will be seeded in the upper compartment and chemoattractant will be placed in the lower compartment. The ability of tumour cells to invade the extracellular matrix coated pores toward the chemoattractant is visualised using live cell bottom imaging reader after applying the treatments.

As combination studies in OSCC cell model had shown promising results *in vitro*, these results need to be further confirmed in an animal model. Also, as we faced problems in solubility of some autophagy inhibitors during our animal study, the use of nanoparticles for drug delivery should be considered in future studies to address this problem.

Another experiment that we would like to do is the survival analysis of OSCC patients and assessing the correlation between LC3 and P62 expression and the overall survival of OSCC patients, as this would aid in development of these proteins as prognostic biomarkers in OSCC patients. In addition to this, P62 levels in tissue specimens should be further investigated as they may change not only due to impaired autophagy, but it could also be due to increased transcription of *SQSTM1* gene [468]. Thus, *SQSTM1* mRNA levels should be examined via RNAscope assay [217].

We would like to further validate the role of autophagy in chemoresistance by testing all combination studies on the resistant cell lines under different conditions (nutrient replete, serum or glucose depleted or hypoxic conditions). Another experiment that could be performed is to examine the secreted proteins from chemoresistant cell lines in the media via proteomic analysis. This could give a solid basis for identifying blood-based biomarkers

for chemoresistance. Lastly, results from our proteomic study results need to be further verified to elucidate the mechanism by which TGM2 contributes to chemoresistance.

Taken together, this thesis identified novel combination therapies for OSCC and TNBC and have laid a solid foundation to further develop anti-cancer therapies targeting autophagy.

References

1. Dikic I, Elazar Z. Mechanism and medical implications of mammalian autophagy. Nat Rev Mol Cell Biol. 2018;19(6):349-64.
2. Viry E, Paggetti J, et al. Autophagy: an adaptive metabolic response to stress shaping the antitumor immunity. Biochem Pharmacol. 2014;92(1):31-42.
3. Fitzwalter BE, Thorburn A. Recent insights into cell death and autophagy. FEBS J. 2015;282(22):4279-88.
4. Clarke AJ, Simon AK. Autophagy in the renewal, differentiation and homeostasis of immune cells. Nature Reviews Immunology. 2019;19(3):170-83.
5. Wong AS, Cheung ZH, et al. Molecular machinery of macroautophagy and its deregulation in diseases. Biochim Biophys Acta. 2011;1812(11):1490-7.
6. Yoshii SR, Mizushima N. Monitoring and Measuring Autophagy. Int J Mol Sci. 2017;18(9).
7. Li WW, Li J, et al. Microautophagy: lesser-known self-eating. Cell Mol Life Sci. 2012;69(7):1125-36.
8. Thorburn A, Thamm DH, et al. Autophagy and cancer therapy. Mol Pharmacol. 2014;85(6):830-8.
9. Yang Z, Klionsky DJ. Mammalian autophagy: core molecular machinery and signaling regulation. Curr Opin Cell Biol. 2010;22(2):124-31.
10. Kim J, Kundu M, et al. AMPK and mTOR regulate autophagy through direct phosphorylation of Ulk1. Nat Cell Biol. 2011;13(2):132-41.
11. Gallagher LE, Chan EY. Early signalling events of autophagy. Essays Biochem. 2013;55:1-15.
12. Simonsen A, Tooze SA. Coordination of membrane events during autophagy by multiple class III PI3-kinase complexes. J Cell Biol. 2009;186(6):773-82.
13. Tooze SA, Yoshimori T. The origin of the autophagosomal membrane. Nat Cell Biol. 2010;12(9):831-5.
14. Nakatogawa H. Two ubiquitin-like conjugation systems that mediate membrane formation during autophagy. Essays Biochem. 2013;55:39-50.
15. Fujita N, Itoh T, et al. The Atg16L complex specifies the site of LC3 lipidation for membrane biogenesis in autophagy. Mol Biol Cell. 2008;19(5):2092-100.
16. Dooley HC, Razi M, et al. WIPI2 links LC3 conjugation with PI3P, autophagosome formation, and pathogen clearance by recruiting Atg12-5-16L1. Mol Cell. 2014;55(2):238-52.
17. Mizushima N, Sugita H, et al. A new protein conjugation system in human: the counterpart of the yeast Apg12p conjugation system essential for autophagy. J Biol Chem. 1998;273(51):33889-92.
18. Webb JL, Ravikumar B, et al. Microtubule disruption inhibits autophagosome-lysosome fusion: implications for studying the roles of aggresomes in polyglutamine diseases. The international journal of biochemistry & cell biology. 2004;36(12):2541-50.
19. Klionsky DJ, Abeliovich H, et al. Guidelines for the use and interpretation of assays for monitoring autophagy in higher eukaryotes. Autophagy. 2008;4(2):151-75.
20. Satoo K, Noda NN, et al. The structure of Atg4B-LC3 complex reveals the mechanism of LC3 processing and delipidation during autophagy. EMBO J. 2009;28(9):1341-50.
21. Geng J, Klionsky DJ. The Atg8 and Atg12 ubiquitin-like conjugation systems in macroautophagy. EMBO reports. 2008;9(9):859-64.
22. Weidberg H, Shvets E, et al. LC3 and GATE-16/GABARAP subfamilies are both essential yet act differently in autophagosome biogenesis. EMBO J. 2010;29(11):1792-802.
23. Noda T, Fujita N, et al. The late stages of autophagy: how does the end begin? Cell Death Differ. 2009;16(7):984-90.

24. Kouno T, Mizuguchi M, et al. Solution structure of microtubule-associated protein light chain 3 and identification of its functional subdomains. J Biol Chem. 2005;280(26):24610-7.
25. Lieberman AP, Puertollano R, et al. Autophagy in lysosomal storage disorders. Autophagy. 2012;8(5):719-30.
26. Itakura E, Kishi C, et al. Beclin 1 forms two distinct phosphatidylinositol 3-kinase complexes with mammalian Atg14 and UVRAG. Mol Biol Cell. 2008;19(12):5360-72.
27. Liang C, Lee JS, et al. Beclin1-binding UVRAG targets the class C Vps complex to coordinate autophagosome maturation and endocytic trafficking. Nat Cell Biol. 2008;10(7):776-87.
28. Matsunaga K, Saitoh T, et al. Two Beclin 1-binding proteins, Atg14L and Rubicon, reciprocally regulate autophagy at different stages. Nat Cell Biol. 2009;11(4):385-96.
29. Eskelinen E-L. Maturation of autophagic vacuoles in mammalian cells. Autophagy. 2005;1(1):1-10.
30. Hamacher-Brady A. Autophagy regulation and integration with cell signaling. Antioxid Redox Signal. 2012;17(5):756-65.
31. Yu L, McPhee CK, et al. Termination of autophagy and reformation of lysosomes regulated by mTOR. Nature. 2010;465(7300):942-6.
32. Ravikumar B, Sarkar S, et al. Regulation of mammalian autophagy in physiology and pathophysiology. Physiol Rev. 2010;90(4):1383-435.
33. Kristensen AR, Schandorff S, et al. Ordered organelle degradation during starvation-induced autophagy. Mol Cell Proteomics. 2008;7(12):2419-28.
34. Khaminets A, Behl C, et al. Ubiquitin-Dependent And Independent Signals In Selective Autophagy. Trends Cell Biol. 2016;26(1):6-16.
35. Birgisdottir ÅB, Lamark T, et al. The LIR motif–crucial for selective autophagy. J Cell Sci. 2013;126(15):3237-47.
36. Johansen T, Lamark T. Selective autophagy mediated by autophagic adapter proteins. Autophagy. 2011;7(3):279-96.
37. Zheng YT, Shahnazari S, et al. The adaptor protein p62/SQSTM1 targets invading bacteria to the autophagy pathway. J Immunol. 2009;183(9):5909-16.
38. Mancias JD, Wang X, et al. Quantitative proteomics identifies NCOA4 as the cargo receptor mediating ferritinophagy. Nature. 2014;509(7498):105-9.
39. Asano T, Komatsu M, et al. Distinct mechanisms of ferritin delivery to lysosomes in iron-depleted and iron-replete cells. Mol Cell Biol. 2011;31(10):2040-52.
40. Williams A, Sarkar S, et al. Novel targets for Huntington's disease in an mTOR-independent autophagy pathway. Nat Chem Biol. 2008;4(5):295-305.
41. Alers S, Löffler AS, et al. Role of AMPK-mTOR-Ulk1/2 in the regulation of autophagy: cross talk, shortcuts, and feedbacks. Mol Cell Biol. 2012;32(1):2-11.
42. Li Y, Chen Y. AMPK and autophagy. Autophagy: Biology and Diseases. 2019:85-108.
43. Di Bartolomeo S, Corazzari M, et al. The dynamic interaction of AMBRA1 with the dynein motor complex regulates mammalian autophagy. J Cell Biol. 2010;191(1):155-68.
44. Cory S, Adams JM. The Bcl2 family: regulators of the cellular life-or-death switch. Nat Rev Cancer. 2002;2(9):647-56.
45. Levine B, Sinha SC, et al. Bcl-2 family members: dual regulators of apoptosis and autophagy. Autophagy. 2008;4(5):600-6.
46. Kroemer G, Galluzzi L, et al. Mitochondrial membrane permeabilization in cell death. Physiol Rev. 2007;87(1):99-163.
47. Wirawan E, Lippens S, et al. Beclin1: a role in membrane dynamics and beyond. Autophagy. 2012;8(1):6-17.

48. Liang XH, Kleeman LK, et al. Protection against fatal Sindbis virus encephalitis by beclin, a novel Bcl-2-interacting protein. J Virol. 1998;72(11):8586-96.
49. Pattingre S, Tassa A, et al. Bcl-2 antiapoptotic proteins inhibit Beclin 1-dependent autophagy. Cell. 2005;122(6):927-39.
50. Marquez RT, Xu L. Bcl-2: Beclin 1 complex: multiple, mechanisms regulating autophagy/apoptosis toggle switch. Am J Cancer Res. 2012;2(2):214.
51. Chang NC, Nguyen M, et al. Antagonism of Beclin 1-dependent autophagy by BCL-2 at the endoplasmic reticulum requires NAF-1. EMBO J. 2010;29(3):606-18.
52. Tang D, Kang R, et al. Endogenous HMGB1 regulates autophagy. J Cell Biol. 2010;190(5):881-92.
53. Bellot G, Garcia-Medina R, et al. Hypoxia-induced autophagy is mediated through hypoxia-inducible factor induction of BNIP3 and BNIP3L via their BH3 domains. Mol Cell Biol. 2009;29(10):2570-81.
54. Wei Y, Pattingre S, et al. JNK1-mediated phosphorylation of Bcl-2 regulates starvation-induced autophagy. Mol Cell. 2008;30(6):678-88.
55. Zalckvar E, Berissi H, et al. Phosphorylation of Beclin 1 by DAP-kinase promotes autophagy by weakening its interactions with Bcl-2 and Bcl-XL. Autophagy. 2009;5(5):720-2.
56. Li H, Wang P, et al. Following cytochrome c release, autophagy is inhibited during chemotherapy-induced apoptosis by caspase 8-mediated cleavage of Beclin 1. Cancer Res. 2011;71(10):3625-34.
57. Wirawan E, Vande Walle L, et al. Caspase-mediated cleavage of Beclin-1 inactivates Beclin-1-induced autophagy and enhances apoptosis by promoting the release of proapoptotic factors from mitochondria. Cell Death Dis. 2010;1:e18.
58. Yousefi S, Perozzo R, et al. Calpain-mediated cleavage of Atg5 switches autophagy to apoptosis. Nat Cell Biol. 2006;8(10):1124-32.
59. Glick D, Barth S, et al. Autophagy: cellular and molecular mechanisms. The Journal of pathology. 2010;221(1):3-12.
60. Nixon RA. The role of autophagy in neurodegenerative disease. Nat Med. 2013;19(8):983.
61. Rabinowitz JD, White E. Autophagy and metabolism. Science. 2010;330(6009):1344-8.
62. Chandra P, Kumar D. Selective autophagy gets more selective: Uncoupling of autophagy flux and xenophagy flux in Mycobacterium tuberculosis-infected macrophages. Autophagy. 2016;12(3):608-9.
63. Son Y, Cheong Y-K, et al. Mitogen-activated protein kinases and reactive oxygen species: how can ROS activate MAPK pathways? Journal of signal transduction. 2011;2011.
64. Oberstein A, Jeffrey PD, et al. Crystal structure of the Bcl-XL-Beclin 1 peptide complex Beclin 1 is a novel BH3-only protein. J Biol Chem. 2007;282(17):13123-32.
65. Bialik S, Dasari SK, et al. Autophagy-dependent cell death - where, how and why a cell eats itself to death. J Cell Sci. 2018;131(18).
66. Dasari SK, Bialik S, et al. Signalome-wide RNAi screen identifies GBA1 as a positive mediator of autophagic cell death. Cell Death Differ. 2017;24(7):1288-302.
67. Wilkinson S, Ryan KM. Autophagy: an adaptable modifier of tumourigenesis. Curr Opin Genet Dev. 2010;20(1):57-64.
68. Lorin S, Hamaï A, et al., editors. Autophagy regulation and its role in cancer. Semin Cancer Biol; 2013: Elsevier.
69. Bensaad K, Cheung EC, et al. Modulation of intracellular ROS levels by TIGAR controls autophagy. EMBO J. 2009;28(19):3015-26.
70. Muller PA, Vousden KH. p53 mutations in cancer. Nat Cell Biol. 2013;15(1):2-8.

71. Vousden KH, Lane DP. p53 in health and disease. Nat Rev Mol Cell Biol. 2007;8(4):275-83.
72. Vousden KH, Ryan KM. p53 and metabolism. Nat Rev Cancer. 2009;9(10):691-700.
73. Amaral JD, Xavier JM, et al. The role of p53 in apoptosis. Discov Med. 2010;9(45):145-52.
74. Sui X, Jin L, et al. p53 signaling and autophagy in cancer: a revolutionary strategy could be developed for cancer treatment. Autophagy. 2011;7(6):565-71.
75. Feng Z, Hu W, et al. The regulation of AMPK β1, TSC2, and PTEN expression by p53: stress, cell and tissue specificity, and the role of these gene products in modulating the IGF-1-AKT-mTOR pathways. Cancer Res. 2007;67(7):3043-53.
76. Gao W, Shen Z, et al. Upregulation of human autophagy-initiation kinase ULK1 by tumor suppressor p53 contributes to DNA-damage-induced cell death. Cell Death Differ. 2011;18(10):1598-607.
77. Morselli E, Shen S, et al. p53 inhibits autophagy by interacting with the human ortholog of yeast Atg17, RB1CC1/FIP200. Cell cycle. 2011;10(16):2763-9.
78. Schubbert S, Shannon K, et al. Hyperactive Ras in developmental disorders and cancer. Nat Rev Cancer. 2007;7(4):295-308.
79. Elgendy M, Sheridan C, et al. Oncogenic Ras-induced expression of Noxa and Beclin-1 promotes autophagic cell death and limits clonogenic survival. Mol Cell. 2011;42(1):23-35.
80. Guo JY, Chen H-Y, et al. Activated Ras requires autophagy to maintain oxidative metabolism and tumorigenesis. Genes Dev. 2011;25(5):460-70.
81. Yang S, Wang X, et al. Pancreatic cancers require autophagy for tumor growth. Genes Dev. 2011;25(7):717-29.
82. Young AR, Narita M, et al. Autophagy mediates the mitotic senescence transition. Genes Dev. 2009;23(7):798-803.
83. Lock R, Roy S, et al. Autophagy facilitates glycolysis during Ras-mediated oncogenic transformation. Mol Biol Cell. 2011;22(2):165-78.
84. White E. Deconvoluting the context-dependent role for autophagy in cancer. Nat Rev Cancer. 2012;12(6):401-10.
85. Yang ZJ, Chee CE, et al. The role of autophagy in cancer: therapeutic implications. Mol Cancer Ther. 2011;10(9):1533-41.
86. Shachaf CM, Kopelman AM, et al. MYC inactivation uncovers pluripotent differentiation and tumour dormancy in hepatocellular cancer. Nature. 2004;431(7012):1112-7.
87. Amati B, Alevizopoulos K, et al. Myc and the cell cycle. Front Biosci. 1998;3(D250-D268):5x3.
88. Wang Y-h, Liu S, et al. Knockdown of c-Myc expression by RNAi inhibits MCF-7 breast tumor cells growth in vitro and in vivo. Breast Cancer Res. 2005;7(2):1-9.
89. Iversen PL, Arora V, et al. Efficacy of antisense morpholino oligomer targeted to c-myc in prostate cancer xenograft murine model and a Phase I safety study in humans. Clin Cancer Res. 2003;9(7):2510-9.
90. Schaub FX, Li W, et al. Myc-Directed Suppression of Autophagy Provides Therapeutic Vulnerabilities Targeting Amino Acid Homeostasis. Blood2015. p. 2450.
91. Annunziata I, van de Vlekkert D, et al. MYC competes with MiT/TFE in regulating lysosomal biogenesis and autophagy through an epigenetic rheostat. Nature communications. 2019;10(1):1-18.
92. Toh PP, Luo S, et al. Myc inhibition impairs autophagosome formation. Hum Mol Genet. 2013;22(25):5237-48.
93. Hart LS, Cunningham JT, et al. ER stress–mediated autophagy promotes Myc-dependent transformation and tumor growth. J Clin Invest. 2012;122(12):4621-34.

94. Levine B, Mizushima N, et al. Autophagy in immunity and inflammation. Nature. 2011;469(7330):323-35.
95. Qu X, Yu J, et al. Promotion of tumorigenesis by heterozygous disruption of the beclin 1 autophagy gene. J Clin Invest. 2003;112(12):1809-20.
96. Liang XH, Jackson S, et al. Induction of autophagy and inhibition of tumorigenesis by beclin 1. Nature. 1999;402(6762):672-6.
97. Kang MR, Kim MS, et al. Frameshift mutations of autophagy-related genes ATG2B, ATG5, ATG9B and ATG12 in gastric and colorectal cancers with microsatellite instability. The Journal of Pathology: A Journal of the Pathological Society of Great Britain and Ireland. 2009;217(5):702-6.
98. Hayashi K, Suzuki Y, et al. Molecular Mechanisms and Biological Functions of Autophagy for Genetics of Hearing Impairment. Genes. 2020;11(11):1331.
99. Mathew R, Karantza-Wadsworth V, et al. Role of autophagy in cancer. Nat Rev Cancer. 2007;7(12):961-7.
100. Gewirtz DA. Autophagy, senescence and tumor dormancy in cancer therapy. Autophagy. 2009;5(8):1232-4.
101. Moscat J, Diaz-Meco MT. p62 at the crossroads of autophagy, apoptosis, and cancer. Cell. 2009;137(6):1001-4.
102. Takamura A, Komatsu M, et al. Autophagy-deficient mice develop multiple liver tumors. Genes Dev. 2011;25(8):795-800.
103. Duran A, Amanchy R, et al. p62 is a key regulator of nutrient sensing in the mTORC1 pathway. Mol Cell. 2011;44(1):134-46.
104. Nezis IP, Stenmark H. p62 at the interface of autophagy, oxidative stress signaling, and cancer. Antioxid Redox Signal. 2012;17(5):786-93.
105. Degenhardt K, Mathew R, et al. Autophagy promotes tumor cell survival and restricts necrosis, inflammation, and tumorigenesis. Cancer Cell. 2006;10(1):51-64.
106. Qu X, Zou Z, et al. Autophagy gene-dependent clearance of apoptotic cells during embryonic development. Cell. 2007;128(5):931-46.
107. Wei H, Wei S, et al. Suppression of autophagy by FIP200 deletion inhibits mammary tumorigenesis. Genes Dev. 2011;25(14):1510-27.
108. Harris AL. Hypoxia—a key regulatory factor in tumour growth. Nat Rev Cancer. 2002;2(1):38-47.
109. Liu XW, Su Y, et al. HIF-1α-dependent autophagy protects HeLa cells from fenretinide (4-HPR)-induced apoptosis in hypoxia. Pharmacol Res. 2010;62(5):416-25.
110. Mathew R, Kongara S, et al. Autophagy suppresses tumor progression by limiting chromosomal instability. Genes Dev. 2007;21(11):1367-81.
111. Hanahan D, Weinberg RA. The hallmarks of cancer. Cell. 2000;100(1):57-70.
112. Hanahan D, Weinberg RA. Hallmarks of cancer: the next generation. Cell. 2011;144(5):646-74.
113. Yang A, Rajeshkumar N, et al. Autophagy is critical for pancreatic tumor growth and progression in tumors with p53 alterations. Cancer Discov. 2014;4(8):905-13.
114. Guo JY, Karsli-Uzunbas G, et al. Autophagy suppresses progression of K-ras-induced lung tumors to oncocytomas and maintains lipid homeostasis. Genes Dev. 2013;27(13):1447-61.
115. Hashimoto D, Bläuer M, et al. Autophagy is needed for the growth of pancreatic adenocarcinoma and has a cytoprotective effect against anticancer drugs. Eur J Cancer. 2014;50(7):1382-90.
116. Guo JY, White E. Autophagy is required for mitochondrial function, lipid metabolism, growth, and fate of KRASG12D-driven lung tumors. Autophagy. 2013;9(10):1636-8.

117. Liu F, Shang Y, et al. Chloroquine potentiates the anti-cancer effect of lidamycin on non-small cell lung cancer cells in vitro. Acta Pharmacol Sin. 2014;35(5):645-52.
118. Ameisen JC. On the origin, evolution, and nature of programmed cell death: a timeline of four billion years. Cell Death Differ. 2002;9(4):367-93.
119. Maiuri MC, Zalckvar E, et al. Self-eating and self-killing: crosstalk between autophagy and apoptosis. Nat Rev Mol Cell Biol. 2007;8(9):741-52.
120. Singh SS, Vats S, et al. Dual role of autophagy in hallmarks of cancer. Oncogene. 2018;37(9):1142-58.
121. Abedin M, Wang D, et al. Autophagy delays apoptotic death in breast cancer cells following DNA damage. Cell Death Differ. 2007;14(3):500-10.
122. Xie X, White EP, et al. Coordinate autophagy and mTOR pathway inhibition enhances cell death in melanoma. PLoS One. 2013;8(1):e55096.
123. Yang Y, Xing D, et al. Mitochondrial autophagy protects against heat shock-induced apoptosis through reducing cytosolic cytochrome c release and downstream caspase-3 activation. Biochem Biophys Res Commun. 2010;395(2):190-5.
124. Levine B, Yuan J. Autophagy in cell death: an innocent convict? J Clin Invest. 2005;115(10):2679-88.
125. Josset E, Burckel H, et al. The mTOR inhibitor RAD001 potentiates autophagic cell death induced by temozolomide in a glioblastoma cell line. Anticancer Res. 2013;33(5):1845-51.
126. Bergers G, Benjamin LE. Tumorigenesis and the angiogenic switch. Nat Rev Cancer. 2003;3(6):401-10.
127. Cavallaro U, Christofori G. Molecular mechanisms of tumor angiogenesis and tumor progression. J Neurooncol. 2000;50(1):63-70.
128. Du J, Teng R-J, et al. Role of autophagy in angiogenesis in aortic endothelial cells. Am J Physiol. 2012;302(2):C383-C91.
129. Kang R, Livesey KM, et al. HMGB1: a novel Beclin 1-binding protein active in autophagy. Autophagy. 2010;6(8):1209-11.
130. Yang S, Xu L, et al. High-mobility group box-1 and its role in angiogenesis. J Leukoc Biol. 2014;95(4):563-74.
131. Sharifi MN, Mowers EE, et al. Autophagy promotes focal adhesion disassembly and cell motility of metastatic tumor cells through the direct interaction of paxillin with LC3. Cell Rep. 2016;15(8):1660-72.
132. Sosa MS, Bragado P, et al. Mechanisms of disseminated cancer cell dormancy: an awakening field. Nat Rev Cancer. 2014;14(9):611-22.
133. Macintosh RL, Timpson P, et al. Inhibition of autophagy impairs tumor cell invasion in an organotypic model. Cell Cycle. 2012;11(10):2022-9.
134. Galavotti S, Bartesaghi S, et al. The autophagy-associated factors DRAM1 and p62 regulate cell migration and invasion in glioblastoma stem cells. Oncogene. 2013;32(6):699-712.
135. Li J, Yang B, et al. Autophagy promotes hepatocellular carcinoma cell invasion through activation of epithelial–mesenchymal transition. Carcinogenesis. 2013;34(6):1343-51.
136. Zhai H, Fesler A, et al. Inhibition of colorectal cancer stem cell survival and invasive potential by hsa-miR-140-5p mediated suppression of Smad2 and autophagy. Oncotarget. 2015;6(23):19735.
137. Fung C, Lock R, et al. Induction of autophagy during extracellular matrix detachment promotes cell survival. Mol Biol Cell. 2008;19(3):797-806.
138. Cai Q, Yan L, et al. Anoikis resistance is a critical feature of highly aggressive ovarian cancer cells. Oncogene. 2015;34(25):3315-24.

139. Avivar-Valderas A, Salas E, et al. PERK integrates autophagy and oxidative stress responses to promote survival during extracellular matrix detachment. Mol Cell Biol. 2011;31(17):3616-29.
140. Peng Y-F, Shi Y-H, et al. Autophagy inhibition suppresses pulmonary metastasis of HCC in mice via impairing anoikis resistance and colonization of HCC cells. Autophagy. 2013;9(12):2056-68.
141. Sun L, Li T, et al. Upregulation of BNIP3 mediated by ERK/HIF-1α pathway induces autophagy and contributes to anoikis resistance of hepatocellular carcinoma cells. Future Oncol. 2014;10(8):1387-98.
142. Chen JL, David J, et al. Autophagy induction results in enhanced anoikis resistance in models of peritoneal disease. Mol Cancer Res. 2017;15(1):26-34.
143. Akalay I, Janji B, et al. Epithelial-to-mesenchymal transition and autophagy induction in breast carcinoma promote escape from T-cell–mediated lysis. Cancer Res. 2013;73(8):2418-27.
144. Tittarelli A, Janji B, et al. The selective degradation of synaptic connexin 43 protein by hypoxia-induced autophagy impairs natural killer cell-mediated tumor cell killing. J Biol Chem. 2015;290(39):23670-9.
145. Yamamoto K, Venida A, et al. Autophagy promotes immune evasion of pancreatic cancer by degrading MHC-I. Nature. 2020;581(7806):100-5.
146. Messai Y, Noman MZ, et al. ITPR1 protects renal cancer cells against natural killer cells by inducing autophagy. Cancer Res. 2014;74(23):6820-32.
147. DeBerardinis RJ, Lum JJ, et al. The biology of cancer: metabolic reprogramming fuels cell growth and proliferation. Cell Metab. 2008;7(1):11-20.
148. Dang CV, Semenza GL. Oncogenic alterations of metabolism. Trends Biochem Sci. 1999;24(2):68-72.
149. Gordan JD, Thompson CB, et al. HIF and c-Myc: sibling rivals for control of cancer cell metabolism and proliferation. Cancer Cell. 2007;12(2):108-13.
150. Karvela M, Baquero P, et al. ATG7 regulates energy metabolism, differentiation and survival of Philadelphia-chromosome-positive cells. Autophagy. 2016;12(6):936-48.
151. Bishop JA, Sciubba JJ, et al. Squamous cell carcinoma of the oral cavity and oropharynx. Surg Pathol Clin. 2011;4(4):1127-51.
152. Sung H, Ferlay J, et al. Global cancer statistics 2020: GLOBOCAN estimates of incidence and mortality worldwide for 36 cancers in 185 countries. CA Cancer J Clin. 2021;71(3):209-49.
153. Ferlay J, Soerjomataram I, et al. Cancer incidence and mortality worldwide: sources, methods and major patterns in GLOBOCAN 2012. Int J Cancer. 2015;136(5):E359-86.
154. Farah C, Simanovic B, et al. Oral cancer in Australia 1982–2008: a growing need for opportunistic screening and prevention. Aust Dent J. 2014;59(3):349-59.
155. Park J, Slack-Smith L, et al. Knowledge and perceptions regarding oral and pharyngeal carcinoma among adult dental patients. Aust Dent J. 2011;56(3):284-9.
156. Warnakulasuriya S. Global epidemiology of oral and oropharyngeal cancer. Oral Oncol. 2009;45(4-5):309-16.
157. Ariyawardana A, Johnson NW. Trends of lip, oral cavity and oropharyngeal cancers in Australia 1982–2008: overall good news but with rising rates in the oropharynx. BMC Cancer. 2013;13(1):1-10.
158. Hashibe M, Brennan P, et al. Interaction between tobacco and alcohol use and the risk of head and neck cancer: pooled analysis in the International Head and Neck Cancer Epidemiology Consortium. Cancer Epidemiology and Prevention Biomarkers. 2009;18(2):541-50.

159. Vargas-Ferreira F, Nedel F, et al. Etiologic factors associated with oral squamous cell carcinoma in non-smokers and non-alcoholic drinkers: a brief approach. Braz Dent J. 2012;23(5):586-90.
160. Lubin JH, Purdue M, et al. Total exposure and exposure rate effects for alcohol and smoking and risk of head and neck cancer: a pooled analysis of case-control studies. Am J Epidemiol. 2009;170(8):937-47.
161. Johnson N. Tobacco use and oral cancer: a global perspective. J Dent Educ. 2001;65(4):328-39.
162. Gies P, Roy C, et al. Global solar UV index: Australian measurements, forecasts and comparison with the UK. Photochem Photobiol. 2004;79(1):32-9.
163. Rao SK, Pavicevic Z, et al. Pro-inflammatory genes as biomarkers and therapeutic targets in oral squamous cell carcinoma. J Biol Chem. 2010;285(42):32512-21.
164. Lin Y-M, Lin C-W, et al. Decreased cytoplasmic expression of ADAMTS14 is correlated with reduced survival rates in oral squamous cell carcinoma patients. Diagnostics. 2020;10(2):122.
165. Chatzistefanou I, Lubek J, et al. The role of neck dissection and postoperative adjuvant radiotherapy in cN0 patients with PNI-positive squamous cell carcinoma of the oral cavity. Oral Oncol. 2014;50(8):753-8.
166. Greaves M, Maley CC. Clonal evolution in cancer. Nature. 2012;481(7381):306-13.
167. Sancho-Martínez SM, Prieto-García L, et al. Subcellular targets of cisplatin cytotoxicity: an integrated view. Pharmacol Ther. 2012;136(1):35-55.
168. Lau A, Li K-Y, et al. Induction chemotherapy for squamous cell carcinomas of the oral cavity: a cumulative meta-analysis. Oral Oncol. 2016;61:104-14.
169. Busch C-J, Tribius S, et al. The current role of systemic chemotherapy in the primary treatment of head and neck cancer. Cancer Treat Rev. 2015;41(3):217-21.
170. Galluzzi L, Senovilla L, et al. Molecular mechanisms of cisplatin resistance. Oncogene. 2012;31(15):1869-83.
171. Gibson MK, Li Y, et al. Randomized phase III evaluation of cisplatin plus fluorouracil versus cisplatin plus paclitaxel in advanced head and neck cancer (E1395): an intergroup trial of the Eastern Cooperative Oncology Group. J Clin Oncol. 2005;23(15):3562-7.
172. Güneri P, Epstein JB. Late stage diagnosis of oral cancer: components and possible solutions. Oral Oncol. 2014;50(12):1131-6.
173. Ronca R, Van Ginderachter JA, et al. Paracrine interactions of cancer-associated fibroblasts, macrophages and endothelial cells: tumor allies and foes. Curr Opin Oncol. 2018;30(1):45-53.
174. Burkholder B, Huang R-Y, et al. Tumor-induced perturbations of cytokines and immune cell networks. Biochim Biophys Acta. 2014;1845(2):182-201.
175. Dourado MR, Guerra EN, et al. Prognostic value of the immunohistochemical detection of cancer-associated fibroblasts in oral cancer: A systematic review and meta-analysis. J Oral Pathol Med. 2018;47(5):443-53.
176. Madar S, Goldstein I, et al. 'Cancer associated fibroblasts'–more than meets the eye. Trends Mol Med. 2013;19(8):447-53.
177. Kellermann MG, Sobral LM, et al. Mutual paracrine effects of oral squamous cell carcinoma cells and normal oral fibroblasts: induction of fibroblast to myofibroblast transdifferentiation and modulation of tumor cell proliferation. Oral Oncol. 2008;44(5):509-17.
178. Wei L-Y, Lee J-J, et al. Reciprocal activation of cancer-associated fibroblasts and oral squamous carcinoma cells through CXCL1. Oral Oncol. 2019;88:115-23.

179. Kim EK, Moon S, et al. CXCL1 induces senescence of cancer-associated fibroblasts via autocrine loops in oral squamous cell carcinoma. PLoS One. 2018;13(1):e0188847.
180. Bello IO, Vered M, et al. Cancer-associated fibroblasts, a parameter of the tumor microenvironment, overcomes carcinoma-associated parameters in the prognosis of patients with mobile tongue cancer. Oral Oncol. 2011;47(1):33-8.
181. Vered M, Dobriyan A, et al. Tumor-host histopathologic variables, stromal myofibroblasts and risk score, are significantly associated with recurrent disease in tongue cancer. Cancer Sci. 2010;101(1):274-80.
182. Wang Y, Jing Y, et al. Epiregulin reprograms cancer-associated fibroblasts and facilitates oral squamous cell carcinoma invasion via JAK2-STAT3 pathway. J Exp Clin Cancer Res. 2019;38(1):1-13.
183. Jung DW, Che ZM, et al. Tumor-stromal crosstalk in invasion of oral squamous cell carcinoma: a pivotal role of CCL7. Int J Cancer. 2010;127(2):332-44.
184. Takahashi H, Sakakura K, et al. Cancer-associated fibroblasts promote an immunosuppressive microenvironment through the induction and accumulation of protumoral macrophages. Oncotarget. 2017;8(5):8633.
185. Fabriek BO, Dijkstra CD, et al. The macrophage scavenger receptor CD163. Immunobiology. 2005;210(2-4):153-60.
186. Norton J, Foster D, et al. Pancreatic cancer associated fibroblasts (CAF): under-explored target for pancreatic cancer treatment. Cancers (Basel). 2020;12(5):1347.
187. Qu C, Wang Q, et al. Cancer-associated fibroblasts in pancreatic cancer: should they be deleted or reeducated? Integr Cancer Ther. 2018;17(4):1016-9.
188. Tan ML, Parkinson EK, et al. Autophagy is deregulated in cancer-associated fibroblasts from oral cancer and is stimulated during the induction of fibroblast senescence by TGF-β1. Sci Rep. 2021;11(1):1-14.
189. Hassona Y, Cirillo N, et al. Progression of genotype-specific oral cancer leads to senescence of cancer-associated fibroblasts and is mediated by oxidative stress and TGF-β. Carcinogenesis. 2013;34(6):1286-95.
190. Koontongkaew S. The tumor microenvironment contribution to development, growth, invasion and metastasis of head and neck squamous cell carcinomas. J Cancer. 2013;4(1):66.
191. He K-F, Zhang L, et al. CD163+ tumor-associated macrophages correlated with poor prognosis and cancer stem cells in oral squamous cell carcinoma. BioMed research international. 2014;2014.
192. Gomes FG, Nedel F, et al. Tumor angiogenesis and lymphangiogenesis: tumor/endothelial crosstalk and cellular/microenvironmental signaling mechanisms. Life Sci. 2013;92(2):101-7.
193. Haque AR, Moriyama M, et al. CD206+ tumor-associated macrophages promote proliferation and invasion in oral squamous cell carcinoma via EGF production. Sci Rep. 2019;9(1):1-10.
194. Fujii N, Shomori K, et al. Cancer-associated fibroblasts and CD163-positive macrophages in oral squamous cell carcinoma: their clinicopathological and prognostic significance. J Oral Pathol Med. 2012;41(6):444-51.
195. Chang C, Su Y, et al. TLR2-dependent selective autophagy regulates NF-κ B lysosomal degradation in hepatoma-derived M2 macrophage differentiation. Cell Death Differ. 2013;20(3):515-23.
196. Chang C-P, Su Y-C, et al. Targeting NFKB by autophagy to polarize hepatoma-associated macrophage differentiation. Autophagy. 2013;9(4):619-21.

197. Yang M, Liu J, et al. Cathepsin S-mediated autophagic flux in tumor-associated macrophages accelerate tumor development by promoting M2 polarization. Mol Cancer. 2014;13(1):1-15.
198. Zhang X, Wang X, et al. Effect of hypoxia inducible factor-1 alpha on vascular endothelial growth factor expression in human tongue squamous carcinoma cells (Tca8113) under hypoxia. Zhonghua Kou Qiang Yi Xue Za Zhi. 2007;42(12):747-9.
199. Goetz JG, Minguet S, et al. Biomechanical remodeling of the microenvironment by stromal caveolin-1 favors tumor invasion and metastasis. Cell. 2011;146(1):148-63.
200. King RJB, Robins MW. Cancer biology: Pearson Education; 2006.
201. Pouysségur J, Dayan F, et al. Hypoxia signalling in cancer and approaches to enforce tumour regression. Nature. 2006;441(7092):437-43.
202. Yang M-H, Wu K-J. TWIST activation by hypoxia inducible factor-1 (HIF-1): implications in metastasis and development. Cell cycle. 2008;7(14):2090-6.
203. Tracy K, Dibling BC, et al. BNIP3 is an RB/E2F target gene required for hypoxia-induced autophagy. Mol Cell Biol. 2007;27(17):6229-42.
204. Deng J, Huang Q, et al. Hypoxia-inducible factor-1alpha regulates autophagy to activate hepatic stellate cells. Biochem Biophys Res Commun. 2014;454(2):328-34.
205. Qureshi-Baig K, Kuhn D, et al. Hypoxia-induced autophagy drives colorectal cancer initiation and progression by activating the PRKC/PKC-EZR (ezrin) pathway. Autophagy. 2020;16(8):1436-52.
206. Yang X, Yin H, et al. Hypoxia-induced autophagy promotes gemcitabine resistance in human bladder cancer cells through hypoxia-inducible factor 1α activation. Int J Oncol. 2018;53(1):215-24.
207. Tanis T, Cincin ZB, et al. The role of components of the extracellular matrix and inflammation on oral squamous cell carcinoma metastasis. Arch Oral Biol. 2014;59(11):1155-63.
208. Levental KR, Yu H, et al. Matrix crosslinking forces tumor progression by enhancing integrin signaling. Cell. 2009;139(5):891-906.
209. Méndez E, Houck JR, et al. A genetic expression profile associated with oral cancer identifies a group of patients at high risk of poor survival. Clin Cancer Res. 2009;15(4):1353-61.
210. Kainulainen T, Grenman R, et al. Distribution and synthesis of type VII collagen in oral squamous cell carcinoma. J Oral Pathol Med. 1997;26(9):414-8.
211. Harada T, Shinohara M, et al. An immunohistochemical study of the extracellular matrix in oral squamous cell carcinoma and its association with invasive and metastatic potential. Virchows Archiv. 1994;424(3):257-66.
212. Li Y, Randriantsilefisoa R, et al. Matrix stiffness regulates chemosensitivity, stemness characteristics, and autophagy in breast cancer cells. ACS Applied Bio Materials. 2020;3(7):4474-85.
213. Jones PA, Baylin SB. The epigenomics of cancer. Cell. 2007;128(4):683-92.
214. de Lima T, Paz A, et al. Autophagy analysis in oral carcinogenesis. Pathol Res Pract. 2017;213(9):1072-7.
215. Tang J-Y, Hsi E, et al. High LC3 expression correlates with poor survival in patients with oral squamous cell carcinoma. Hum Pathol. 2013;44(11):2558-62.
216. Tang J-Y, Hsi E, et al. Overexpression of autophagy-related 16-like 1 in patients with oral squamous cell carcinoma. Pathol Oncol Res. 2015;21(2):301-5.
217. Liu J, Chen F, et al. Prognostic significance of p62/SQSTM1 subcellular localization and LC3B in oral squamous cell carcinoma. Br J Cancer. 2014;111(5):944-54.
218. Liang L, Luo H, et al. Investigation of cancer-associated fibroblasts and p62 expression in oral cancer before and after chemotherapy. J Craniomaxillofac Surg. 2018;46(4):605-10.

219. Park B-S, Choi N-E, et al. Crosstalk between fisetin-induced apoptosis and autophagy in human oral squamous cell carcinoma. J Cancer. 2019;10(1):138.
220. Lin CW, Chin HK, et al. Ursolic acid induces apoptosis and autophagy in oral cancer cells. Environ Toxicol. 2019;34(9):983-91.
221. Gao L, Dou Z-C, et al. CircCDR1as upregulates autophagy under hypoxia to promote tumor cell survival via AKT/ERK½/mTOR signaling pathways in oral squamous cell carcinomas. Cell Death Dis. 2019;10(10):745.
222. Naik PP, Mukhopadhyay S, et al. Secretory clusterin promotes oral cancer cell survival via inhibiting apoptosis by activation of autophagy in AMPK/mTOR/ULK1 dependent pathway. Life Sci. 2021;264:118722.
223. Naik PP, Mukhopadhyay S, et al. Autophagy regulates cisplatin-induced stemness and chemoresistance via the upregulation of CD 44, ABCB 1 and ADAM 17 in oral squamous cell carcinoma. Cell Prolif. 2018;51(1):e12411.
224. Li S, Wu Y, et al. CerS6 regulates cisplatin resistance in oral squamous cell carcinoma by altering mitochondrial fission and autophagy. J Cell Physiol. 2018;233(12):9416-25.
225. Xu Z, Huang C-M, et al. Autophagy Induced by Areca Nut Extract Contributes to Decreasing Cisplatin Toxicity in Oral Squamous Cell Carcinoma Cells: Roles of Reactive Oxygen Species/AMPK Signaling. Int J Mol Sci. 2017;18(3):524.
226. Huang K, Liu D. Targeting non-canonical autophagy overcomes erlotinib resistance in tongue cancer. Tumor Biol. 2016;37:9625-33.
227. Wang Y, Wang C, et al. Decrease of autophagy activity promotes malignant progression of tongue squamous cell carcinoma. J Oral Pathol Med. 2013;42(7):557-64.
228. Kapoor V, Paliwal D, et al. Deregulation of Beclin 1 in patients with tobacco-related oral squamous cell carcinoma. Biochem Biophys Res Commun. 2012;422(4):764-9.
229. Weng J, Wang C, et al. Beclin1 inhibits proliferation, migration and invasion in tongue squamous cell carcinoma cell lines. Oral Oncol. 2014;50(10):983-90.
230. Wang X, Li S, et al. Silence of Beclin1 in oral squamous cell carcinoma cells promotes proliferation, inhibits apoptosis, and enhances chemosensitivity. Int J Clin Exp Pathol. 2017;10(8):8424.
231. Sahni S, Merlot AM, et al. Gene of the month: BECN1. J Clin Pathol. 2014;67(8):656-60.
232. Kong Q, Liang Y, et al. Autophagy inhibits TLR4-mediated invasiveness of oral cancer cells via the NF-κB pathway. Oral Dis. 2020;26(6):1165-74.
233. Kim JY, Cho TJ, et al. Curcumin-induced autophagy contributes to the decreased survival of oral cancer cells. Arch Oral Biol. 2012;57(8):1018-25.
234. Qiu Y, Li C, et al. Tanshinone IIA induces cell death via Beclin-1-dependent autophagy in oral squamous cell carcinoma SCC-9 cell line. Cancer Med. 2018;7(2):397-407.
235. Hsiao Y-T, Kuo C-L, et al. Curcuminoids induce reactive oxygen species and autophagy to enhance apoptosis in human oral cancer cells. Am J Chin Med. 2018;46(05):1145-68.
236. Ho-Huynh A, Tran A, et al. Factors influencing breast cancer outcomes in Australia: a systematic review. Eur J Cancer Care. 2019;28(4):e13038.
237. Grandvallet C, Feugeas JP, et al. Autophagy is associated with a robust specific transcriptional signature in breast cancer subtypes. Genes Cancer. 2020;11(3-4):154.
238. Burstein MD, Tsimelzon A, et al. Comprehensive genomic analysis identifies novel subtypes and targets of triple-negative breast cancer. Clin Cancer Res. 2015;21(7):1688-98.
239. Lehmann BD, Bauer JA, et al. Identification of human triple-negative breast cancer subtypes and preclinical models for selection of targeted therapies. The Journal of clinical investigation. 2011;121(7):2750-67.

240. Engebraaten O, Vollan HKM, et al. Triple-negative breast cancer and the need for new therapeutic targets. Am J Path. 2013;183(4):1064-74.
241. Bray F, Ferlay J, et al. Global cancer statistics 2018: GLOBOCAN estimates of incidence and mortality worldwide for 36 cancers in 185 countries. CA Cancer J Clin. 2018;68(6):394-424.
242. Lebert J, Lester R, et al. Advances in the systemic treatment of triple-negative breast cancer. Current Oncol. 2018;25(Suppl 1):S142.
243. Lehmann BD, Jovanović B, et al. Refinement of triple-negative breast cancer molecular subtypes: implications for neoadjuvant chemotherapy selection. PLoS One. 2016;11(6):e0157368.
244. van Mackelenberg M, Seither F, et al. Effects of capecitabine as part of neo-/adjuvant chemotherapy. A meta-analysis of individual patient data from.12:10-4.
245. Yu K-D, Ye F-G, et al. Effect of adjuvant paclitaxel and carboplatin on survival in women with triple-negative breast cancer: a phase 3 randomized clinical trial. JAMA Oncol. 2020;6(9):1390-6.
246. Poggio F, Bruzzone M, et al. Platinum-based neoadjuvant chemotherapy in triple-negative breast cancer: a systematic review and meta-analysis. Ann Oncol. 2018;29(7):1497-508.
247. Haffty BG, Yang Q, et al. Locoregional relapse and distant metastasis in conservatively managed triple negative early-stage breast cancer. J Clin Oncol. 2006;24(36):5652-7.
248. Emens LA. Immunotherapy in triple-negative breast cancer. Cancer J. 2021;27(1):59-66.
249. Place AE, Huh SJ, et al. The microenvironment in breast cancer progression: biology and implications for treatment. Breast Cancer Res. 2011;13(6):1-11.
250. Willumsen N, Thomsen LB, et al. Quantification of altered tissue turnover in a liquid biopsy: a proposed precision medicine tool to assess chronic inflammation and desmoplasia associated with a pro-cancerous niche and response to immuno-therapeutic anti-tumor modalities. Cancer Immunol Immunother. 2018;67(1):1-12.
251. Matsumoto H, Koo S-l, et al. Role of inflammatory infiltrates in triple negative breast cancer. J Clin Pathol. 2015;68(7):506-10.
252. García-Teijido P, Cabal ML, et al. Tumor-infiltrating lymphocytes in triple negative breast cancer: the future of immune targeting. Clin Med Insights Oncol. 2016;10:CMO. S34540.
253. Huang Y, Ma C, et al. CD4+ and CD8+ T cells have opposing roles in breast cancer progression and outcome. Oncotarget. 2015;6(19):17462.
254. Stanton SE, Disis ML. Clinical significance of tumor-infiltrating lymphocytes in breast cancer. Journal for immunotherapy of cancer. 2016;4(1):1-7.
255. Schreiber RD, Old LJ, et al. Cancer immunoediting: integrating immunity's roles in cancer suppression and promotion. Science. 2011;331(6024):1565-70.
256. Loi S, Sirtaine N, et al. Prognostic and predictive value of tumor-infiltrating lymphocytes in a phase III randomized adjuvant breast cancer trial in node-positive breast cancer comparing the addition of docetaxel to doxorubicin with doxorubicin-based chemotherapy: BIG 02-98. J Clin Oncol. 2013;31(7):860-7.
257. Li ZL, Zhang HL, et al. Autophagy deficiency promotes triple-negative breast cancer resistance to T cell-mediated cytotoxicity by blocking tenascin-C degradation. Nat Commun. 2020;11(1):3806.
258. Qian B-Z, Li J, et al. CCL2 recruits inflammatory monocytes to facilitate breast-tumour metastasis. Nature. 2011;475(7355):222-5.
259. Allen M, Louise Jones J. Jekyll and Hyde: the role of the microenvironment on the progression of cancer. The Journal of pathology. 2011;223(2):163-77.
260. Qian B-Z, Pollard JW. Macrophage diversity enhances tumor progression and metastasis. Cell. 2010;141(1):39-51.

261. Laoui D, Movahedi K, et al. Tumor-associated macrophages in breast cancer: distinct subsets, distinct functions. Int J Dev Biol. 2011;55(7-8-9):861-7.
262. Sousa S, Brion R, et al. Human breast cancer cells educate macrophages toward the M2 activation status. Breast Cancer Res. 2015;17(1):1-14.
263. Hollmén M, Roudnicky F, et al. Characterization of macrophage-cancer cell crosstalk in estrogen receptor positive and triple-negative breast cancer. Sci Rep. 2015;5(1):1-10.
264. Mao Y, Keller ET, et al. Stromal cells in tumor microenvironment and breast cancer. Cancer Metastasis Rev. 2013;32(1):303-15.
265. Shiga K, Hara M, et al. Cancer-associated fibroblasts: their characteristics and their roles in tumor growth. Cancers (Basel). 2015;7(4):2443-58.
266. Luo H, Tu G, et al. Cancer-associated fibroblasts: a multifaceted driver of breast cancer progression. Cancer Lett. 2015;361(2):155-63.
267. Camp JT, Elloumi F, et al. Interactions with fibroblasts are distinct in Basal-like and luminal breast cancers. Mol Cancer Res. 2011;9(1):3-13.
268. Takai K, Le A, et al. Targeting the cancer-associated fibroblasts as a treatment in triple-negative breast cancer. Oncotarget. 2016;7(50):82889.
269. Zhu X, Wang K, et al. Galectin-1 knockdown in carcinoma-associated fibroblasts inhibits migration and invasion of human MDA-MB-231 breast cancer cells by modulating MMP-9 expression. Acta Biochim Biophys Sin. 2016;48(5):462-7.
270. Angelucci C, Maulucci G, et al. Epithelial-stromal interactions in human breast cancer: effects on adhesion, plasma membrane fluidity and migration speed and directness. PLoS One. 2012;7(12):e50804.
271. Wang M, Zhang J, et al. Cancer-associated fibroblasts autophagy enhances progression of triple-negative breast cancer cells. Medical science monitor: international medical journal of experimental and clinical research. 2017;23:3904.
272. Vaupel P, Mayer A. Hypoxia in cancer: significance and impact on clinical outcome. Cancer Metastasis Rev. 2007;26(2):225-39.
273. Ziello JE, Jovin IS, et al. Hypoxia-Inducible Factor (HIF)-1 regulatory pathway and its potential for therapeutic intervention in malignancy and ischemia. The Yale journal of biology and medicine. 2007;80(2):51.
274. Bender RJ, Mac Gabhann F. Expression of VEGF and semaphorin genes define subgroups of triple negative breast cancer. PLoS One. 2013;8(5):e61788.
275. Plantamura I, Casalini P, et al. PDGFRβ and FGFR2 mediate endothelial cell differentiation capability of triple negative breast carcinoma cells. Mol Oncol. 2014;8(5):968-81.
276. Zaarour RF, Azakir B, et al. Role of hypoxia-mediated autophagy in tumor cell death and survival. Cancers (Basel). 2021;13(3):533.
277. Azad MB, Gibson SB. Role of BNIP3 in proliferation and hypoxia-induced autophagy: implications for personalized cancer therapies. Ann N Y Acad Sci. 2010;1210(1):8-16.
278. Bousquet G, El Bouchtaoui M, et al. Targeting autophagic cancer stem-cells to reverse chemoresistance in human triple negative breast cancer. Oncotarget. 2017;8(21):35205.
279. He W-S, Dai X-F, et al. Hypoxia-induced autophagy confers resistance of breast cancer cells to ionizing radiation. Oncology Research Featuring Preclinical and Clinical Cancer Therapeutics. 2012;20(5-6):251-8.
280. Lu P, Weaver VM, et al. The extracellular matrix: a dynamic niche in cancer progression. J Cell Biol. 2012;196(4):395-406.
281. Brabrand A, Kariuki II, et al. Alterations in collagen fibre patterns in breast cancer. A premise for tumour invasiveness? APMIS. 2015;123(1):1-8.

282. Roy DM, Walsh LA. Candidate prognostic markers in breast cancer: focus on extracellular proteases and their inhibitors. Breast Cancer (London). 2014;6:81.
283. Kim SH, Lee HY, et al. Role of secreted type I collagen derived from stromal cells in two breast cancer cell lines. Oncol Lett. 2014;8(2):507-12.
284. Castro-Sanchez L, Soto-Guzman A, et al. Native type IV collagen induces cell migration through a CD9 and DDR1-dependent pathway in MDA-MB-231 breast cancer cells. Eur J Cell Biol. 2010;89(11):843-52.
285. Acerbi I, Cassereau L, et al. Human breast cancer invasion and aggression correlates with ECM stiffening and immune cell infiltration. Integrative Biology. 2015;7(10):1120-34.
286. Abdelbary EH, Ibrahim DA, et al. Autophagy-related molecules, light chain 3B, p62, and beclin 1, as prognostic markers in triple-negative breast cancer. Egyptian Journal of Pathology. 2017;37(1):8-16.
287. Bortnik S, Tessier-Cloutier B, et al. Differential expression and prognostic relevance of autophagy-related markers ATG4B, GABARAP, and LC3B in breast cancer. Breast Cancer Res Treat. 2020;183(3):525-47.
288. Wang R-X, Xu X-E, et al. eEF2 kinase mediated autophagy as a potential therapeutic target for paclitaxel-resistant triple-negative breast cancer. Annals of translational medicine. 2019;7(23).
289. Hamurcu Z, Delibaşı N, et al. Targeting LC3 and Beclin-1 autophagy genes suppresses proliferation, survival, migration and invasion by inhibition of Cyclin-D1 and uPAR/Integrin β1/Src signaling in triple negative breast cancer cells. J Cancer Res Clin Oncol. 2018;144(3):415-30.
290. Chen W, Bai Y, et al. Autophagy promotes triple negative breast cancer metastasis via YAP nuclear localization. Biochem Biophys Res Commun. 2019;520(2):263-8.
291. Li H-c, Xia Z-h, et al. Cantharidin inhibits the growth of triple-negative breast cancer cells by suppressing autophagy and inducing apoptosis in vitro and in vivo. Cell Physiol Biochem. 2017;43(5):1829-40.
292. Wang J, Dang MN, et al. Inhibition of Wnt signaling by Frizzled7 antibody-coated nanoshells sensitizes triple-negative breast cancer cells to the autophagy regulator chloroquine. Nano research. 2020;13(6):1693.
293. Liu Z, He K, et al. Autophagy inhibitor facilitates gefitinib sensitivity in vitro and in vivo by activating mitochondrial apoptosis in triple negative breast cancer. PLoS One. 2017;12(5):e0177694.
294. Liu C, Sun L, et al. FSIP1 regulates autophagy in breast cancer. Proc Natl Acad Sci. 2018;115(51):13075-80.
295. Lin H-Y, Kuei C-H, et al. TNFSF13 upregulation confers chemotherapeutic resistance via triggering autophagy initiation in triple-negative breast cancer. J Mol Med. 2020;98(9):1255-67.
296. Huo L, Deng X, et al. Abstract P6-03-16: Role of autophagy in CD24-mediated TNBC drug resistance. Cancer Res2020. p. 6-03-16.
297. Li W, Tanikawa T, et al. Aerobic glycolysis controls myeloid-derived suppressor cells and tumor immunity via a specific CEBPB isoform in triple-negative breast cancer. Cell Metab. 2018;28(1):87-103. e6.
298. Li M, Liu J, et al. Autophagy-related 7 modulates tumor progression in triple-negative breast cancer. Lab Invest. 2019;99(9):1266-74.
299. Li Z-L, Zhang H-L, et al. Autophagy deficiency promotes triple-negative breast cancer resistance to T cell-mediated cytotoxicity by blocking tenascin-C degradation. Nature communications. 2020;11(1):1-19.

300. Qiao Z, Li X, et al. A novel specific anti-CD73 antibody inhibits triple-negative breast cancer cell motility by regulating autophagy. Int J Mol Sci. 2019;20(5):1057.
301. Tanida I, Ueno T, et al. LC3 and Autophagy. Autophagosome and phagosome: Springer; 2008. p. 77-88.
302. Savarino A, Lucia MB, et al. Risks and benefits of chloroquine use in anticancer strategies. Lancet Oncol. 2006;7(10):792-3.
303. Homewood C, Warhurst D, et al. Lysosomes, p H and the Anti-malarial Action of Chloroquine. Nature. 1972;235(5332):50-2.
304. Kremer JM. Rational use of new and existing disease-modifying agents in rheumatoid arthritis. Ann Intern Med. 2001;134(8):695-706.
305. Rainsford K, Parke AL, et al. Therapy and pharmacological properties of hydroxychloroquine and chloroquine in treatment of systemic lupus erythematosus, rheumatoid arthritis and related diseases. Inflammopharmacology. 2015;23(5):231-69.
306. Ben-Zvi I, Kivity S, et al. Hydroxychloroquine: from malaria to autoimmunity. Clin Rev Allergy Immunol. 2012;42(2):145-53.
307. Levy G, Munz S, et al. Incidence of hydroxychloroquine retinopathy in 1,207 patients in a large multicenter outpatient practice. Arthritis Rheum. 1997;40(8):1482-6.
308. Zhao H, Cai Y, et al. Chloroquine-mediated radiosensitization is due to the destabilization of the lysosomal membrane and subsequent induction of cell death by necrosis. Radiat Res. 2005;164(3):250-7.
309. Hori YS, Hosoda R, et al. Chloroquine potentiates temozolomide cytotoxicity by inhibiting mitochondrial autophagy in glioma cells. J Neurooncol. 2015;122(1):11-20.
310. Golden EB, Cho H-Y, et al. Chloroquine enhances temozolomide cytotoxicity in malignant gliomas by blocking autophagy. Neurosurg Focus. 2014;37(6):E12.
311. Grimaldi A, Balestrieri ML, et al. The synergistic effect of everolimus and chloroquine on endothelial cell number reduction is paralleled by increased apoptosis and reduced autophagy occurrence. PLoS One. 2013;8(11):e79658.
312. Zhao L, Yang G, et al. Co-delivery of Gefitinib and chloroquine by chitosan nanoparticles for overcoming the drug acquired resistance. J Nanobiotechnology. 2015;13(1):1-10.
313. Bokobza SM, Jiang Y, et al. Combining AKT inhibition with chloroquine and gefitinib prevents compensatory autophagy and induces cell death in EGFR mutated NSCLC cells. Oncotarget. 2014;5(13):4765.
314. Fukuda T, Oda K, et al. The anti-malarial chloroquine suppresses proliferation and overcomes cisplatin resistance of endometrial cancer cells via autophagy inhibition. Gynecol Oncol. 2015;137(3):538-45.
315. Wu Z, Chang P-C, et al. Autophagy blockade sensitizes prostate cancer cells towards Src family kinase inhibitors. Genes Cancer. 2010;1(1):40-9.
316. Carew JS, Medina EC, et al. Autophagy inhibition enhances vorinostat-induced apoptosis via ubiquitinated protein accumulation. J Cell Mol Med. 2010;14(10):2448-59.
317. Amaravadi RK, Lippincott-Schwartz J, et al. Principles and current strategies for targeting autophagy for cancer treatment. Clin Cancer Res. 2011;17(4):654-66.
318. Hara T, Nakamura K, et al. Suppression of basal autophagy in neural cells causes neurodegenerative disease in mice. Nature. 2006;441(7095):885-9.
319. Komatsu M, Waguri S, et al. Loss of autophagy in the central nervous system causes neurodegeneration in mice. Nature. 2006;441(7095):880-4.
320. Sotelo J, Briceño E, et al. Adding chloroquine to conventional treatment for glioblastoma multiforme: a randomized, double-blind, placebo-controlled trial. Ann Intern Med. 2006;144(5):337-43.

321. Rangwala R, Chang YC, et al. Combined MTOR and autophagy inhibition: phase I trial of hydroxychloroquine and temsirolimus in patients with advanced solid tumors and melanoma. Autophagy. 2014;10(8):1391-402.
322. Rangwala R, Leone R, et al. Phase I trial of hydroxychloroquine with dose-intense temozolomide in patients with advanced solid tumors and melanoma. Autophagy. 2014;10(8):1369-79.
323. Vogl DT, Stadtmauer EA, et al. Combined autophagy and proteasome inhibition: a phase 1 trial of hydroxychloroquine and bortezomib in patients with relapsed/refractory myeloma. Autophagy. 2014;10(8):1380-90.
324. Loaiza-Bonilla A, O'Hara MH, et al. Phase II trial of autophagy inhibition using hydroxychloroquine (HCQ) with FOLFOX/bevacizumab in the first-line treatment of advanced colorectal cancer. American Society of Clinical Oncology; 2015. p. 3614.
325. Wolpin BM, Rubinson DA, et al. Phase II and pharmacodynamic study of autophagy inhibition using hydroxychloroquine in patients with metastatic pancreatic adenocarcinoma. The oncologist. 2014;19(6):637.
326. Mahalingam D, Mita M, et al. Combined autophagy and HDAC inhibition: a phase I safety, tolerability, pharmacokinetic, and pharmacodynamic analysis of hydroxychloroquine in combination with the HDAC inhibitor vorinostat in patients with advanced solid tumors. Autophagy. 2014;10(8):1403-14.
327. Pasquier B. Autophagy inhibitors. Cell Mol Life Sci. 2016;73(5):985-1001.
328. McAfee Q, Zhang Z, et al. Autophagy inhibitor Lys05 has single-agent antitumor activity and reproduces the phenotype of a genetic autophagy deficiency. Proc Natl Acad Sci U S A. 2012;109(21):8253-8.
329. Wang C, Hu Q, et al. Pharmacological inhibitors of autophagy as novel cancer therapeutic agents. Pharmacol Res. 2016;105:164-75.
330. Yu X, Long YC, et al. Differential regulatory functions of three classes of phosphatidylinositol and phosphoinositide 3-kinases in autophagy. Autophagy. 2015;11(10):1711-28.
331. Seglen PO, Gordon PB. 3-Methyladenine: specific inhibitor of autophagic/lysosomal protein degradation in isolated rat hepatocytes. Proc Natl Acad Sci U S A. 1982;79(6):1889-92.
332. Petiot A, Ogier-Denis E, et al. Distinct classes of phosphatidylinositol 3'-kinases are involved in signaling pathways that control macroautophagy in HT-29 cells. J Biol Chem. 2000;275(2):992-8.
333. Wu Y-T, Tan H-L, et al. Dual role of 3-methyladenine in modulation of autophagy via different temporal patterns of inhibition on class I and III phosphoinositide 3-kinase. J Biol Chem. 2010;285(14):10850-61.
334. CARO LHP, PLOMP PJ, et al. 3-Methyladenine, an inhibitor of autophagy, has multiple effects on metabolism. Eur J Biochem. 1988;175(2):325-9.
335. Ihle NT, Williams R, et al. Molecular pharmacology and antitumor activity of PX-866, a novel inhibitor of phosphoinositide-3-kinase signaling. Mol Cancer Ther. 2004;3(7):763-72.
336. Wiesinger D, Gubler H, et al. Antiinflammatory activity of the new mould metabolite 11-desacetoxy-wortmannin and of some of its derivatives. Experientia. 1974;30(2):135-6.
337. Knight ZA, Shokat KM. Chemically targeting the PI3K family. Biochem Soc Trans. 2007;35(Pt 2):245-9.
338. Takase Y, Saeki T, et al. Cyclic GMP phosphodiesterase inhibitors. 2. Requirement of 6-substitution of quinazoline derivatives for potent and selective inhibitory activity. J Med Chem. 1994;37(13):2106-11.

339. Liu J, Xia H, et al. Beclin1 controls the levels of p53 by regulating the deubiquitination activity of USP10 and USP13. Cell. 2011;147(1):223-34.
340. Shao S, Li S, et al. Spautin-1, a novel autophagy inhibitor, enhances imatinib-induced apoptosis in chronic myeloid leukemia. Int J Oncol. 2014;44(5):1661-8.
341. Ronan B, Flamand O, et al. A highly potent and selective Vps34 inhibitor alters vesicle trafficking and autophagy. Nat Chem Biol. 2014;10(12):1013-9.
342. Pasquier B. SAR405, a PIK3C3/Vps34 inhibitor that prevents autophagy and synergizes with MTOR inhibition in tumor cells. Autophagy. 2015;11(4):725-6.
343. Young CD, Arteaga CL, et al. Dual inhibition of Type I and Type III PI3 kinases increases tumor cell apoptosis in HER2+ breast cancers. Breast Cancer Res. 2015;17(1):1-11.
344. Zhou P, Li Y, et al. Autophagy inhibition enhances celecoxib-induced apoptosis in osteosarcoma. Cell Cycle. 2018;17(8):997-1006.
345. Schlütermann D, Skowron MA, et al. Targeting urothelial carcinoma cells by combining cisplatin with a specific inhibitor of the autophagy-inducing class III PtdIns3K complex. Urol Oncol. 2018;36(4):160.e1-.e13.
346. Dowdle WE, Nyfeler B, et al. Selective VPS34 inhibitor blocks autophagy and uncovers a role for NCOA4 in ferritin degradation and iron homeostasis in vivo. Nat Cell Biol. 2014;16(11):1069-79.
347. Ganley IG, Lam DH, et al. ULK1· ATG13· FIP200 complex mediates mTOR signaling and is essential for autophagy. J Biol Chem. 2009;284(18):12297-305.
348. Egan D, Kim J, et al. The autophagy initiating kinase ULK1 is regulated via opposing phosphorylation by AMPK and mTOR. Autophagy. 2011;7(6):643-4.
349. Petherick KJ, Conway OJ, et al. Pharmacological inhibition of ULK1 kinase blocks mammalian target of rapamycin (mTOR)-dependent autophagy. J Biol Chem. 2015;290(18):11376-83.
350. Egan DF, Chun MG, et al. Small molecule inhibition of the autophagy kinase ULK1 and identification of ULK1 substrates. Mol Cell. 2015;59(2):285-97.
351. Tang F, Hu P, et al. SBI0206965, a novel inhibitor of Ulk1, suppresses non-small cell lung cancer cell growth by modulating both autophagy and apoptosis pathways. Oncol Rep. 2017;37(6):3449-58.
352. Dite TA, Langendorf CG, et al. AMP-activated protein kinase selectively inhibited by the type II inhibitor SBI-0206965. J Biol Chem. 2018;293(23):8874-85.
353. Ahwazi D, Neopane K, et al. Investigation of the specificity and mechanism of action of the ULK1/AMPK inhibitor SBI-0206965. Biochem J. 2021;478(15):2977-97.
354. Zhou Z-H, Zhao T-C, et al. A therapeutic approach with combination of interferon-gamma and autophagy inhibitor for oral squamous cell carcinoma. Am J Cancer Res. 2021;11(4):1503.
355. Ahn M-Y, Ahn S-G, et al. Apicidin, a histone deaceylase inhibitor, induces both apoptosis and autophagy in human oral squamous carcinoma cells. Oral Oncol. 2011;47(11):1032-8.
356. Jia L, Wang J, et al. In vitro and in vivo antitumor effects of chloroquine on oral squamous cell carcinoma. Mol Med Report. 2017;16(5):5779-86.
357. Magnano S, Barroeta PH, et al. Cisplatin induces autophagy-associated apoptosis in human oral squamous cell carcinoma (OSCC) mediated in part through reactive oxygen species. Toxicol Appl Pharmacol. 2021:115646.
358. Li B, Lu M, et al. Inhibiting reactive oxygen species-dependent autophagy enhanced baicalein-induced apoptosis in oral squamous cell carcinoma. J Nat Med. 2017;71(2):433-41.
359. Jiang LC, Xin ZY, et al. Inhibition of autophagy augments apoptosis in human oral squamous cell carcinoma under nutrient depletion. J Oral Pathol Med. 2015;44(5):361-6.

360. Li J, Yang D, et al. Inhibition of autophagy by 3-MA enhances IL-24-induced apoptosis in human oral squamous cell carcinoma cells. J Exp Clin Cancer Res. 2015;34(1):1-13.
361. Saiyin W, Wang D, et al. Sequential release of autophagy inhibitor and chemotherapeutic drug with polymeric delivery system for oral squamous cell carcinoma therapy. Mol Pharm. 2014;11(5):1662-75.
362. Mauthe M, Orhon I, et al. Chloroquine inhibits autophagic flux by decreasing autophagosome-lysosome fusion. Autophagy. 2018;14(8):1435-55.
363. Bouchard G, Therriault H, et al. Stimulation of triple negative breast cancer cell migration and metastases formation is prevented by chloroquine in a pre-irradiated mouse model. BMC Cancer. 2016;16(1):1-14.
364. Liang DH, Choi DS, et al. The autophagy inhibitor chloroquine targets cancer stem cells in triple negative breast cancer by inducing mitochondrial damage and impairing DNA break repair. Cancer Lett. 2016;376(2):249-58.
365. Abdel-Mohsen MA, Malak CAA, et al. Influence of copper (I) nicotinate complex and autophagy modulation on doxorubicin-induced cytotoxicity in HCC1806 breast cancer cells. Adv Med Sci. 2019;64(1):202-9.
366. Rao R, Balusu R, et al. Combination of pan-histone deacetylase inhibitor and autophagy inhibitor exerts superior efficacy against triple-negative human breast cancer cells. Mol Cancer Ther. 2012;11(4):973-83.
367. Chittaranjan S, Bortnik S, et al. Autophagy inhibition augments the anticancer effects of epirubicin treatment in anthracycline-sensitive and-resistant triple-negative breast cancer. Clin Cancer Res. 2014;20(12):3159-73.
368. Fleisher B, Mody H, et al. Chloroquine sensitizes MDA-MB-231 cells to osimertinib through autophagy–apoptosis crosstalk pathway. Breast Cancer (London). 2019;11:231.
369. Choi DS, Blanco E, et al. Chloroquine eliminates cancer stem cells through deregulation of Jak2 and DNMT1. Stem Cells. 2014;32(9):2309-23.
370. Schrezenmeier E, Dörner T. Mechanisms of action of hydroxychloroquine and chloroquine: implications for rheumatology. Nature Reviews Rheumatology. 2020;16(3):155-66.
371. Chen W-C, Hsu K-Y, et al. The anti-tumor efficiency of pterostilbene is promoted with a combined treatment of Fas signaling or autophagy inhibitors in triple negative breast cancer cells. Food Funct. 2014;5(8):1856-65.
372. Chen F, Song Q, et al. Axl inhibitor R428 induces apoptosis of cancer cells by blocking lysosomal acidification and recycling independent of Axl inhibition. Am J Cancer Res. 2018;8(8):1466.
373. Wen J, Yeo S, et al. Autophagy inhibition re-sensitizes pulse stimulation-selected paclitaxel-resistant triple negative breast cancer cells to chemotherapy-induced apoptosis. Breast Cancer Res Treat. 2015;149(3):619-29.
374. Schluetermann D, Skowron MA, et al., editors. Targeting urothelial carcinoma cells by combining cisplatin with a specific inhibitor of the autophagy-inducing class III PtdIns3K complex. Urologic Oncology: Seminars and Original Investigations; 2018: Elsevier.
375. Ramos-Vara JA. Principles and methods of immunohistochemistry. Methods Mol Biol. 2011:83-96.
376. Meijer AJ, Codogno P. Regulation and role of autophagy in mammalian cells. The international journal of biochemistry & cell biology. 2004;36(12):2445-62.
377. Nagano O, Okazaki S, et al. Redox regulation in stem-like cancer cells by CD44 variant isoforms. Oncogene. 2013;32(44):5191-8.
378. Chavez-Dominguez R, Perez-Medina M, et al. The double-edge sword of autophagy in cancer: from tumor suppression to pro-tumor activity. Front Oncol. 2020;10:578418.

379. Taylor MA, Das BC, et al. Targeting autophagy for combating chemoresistance and radioresistance in glioblastoma. Apoptosis. 2018;23(11-12):563-75.
380. Zhao H, Yang M, et al. High expression of LC3B is associated with progression and poor outcome in triple-negative breast cancer. Med Oncol. 2013;30(1):475.
381. Cai Y, Wang X-L, et al. Inhibition of endo-lysosomal function exacerbates vascular calcification. Sci Rep. 2018;8(1):1-11.
382. van Zijl F, Krupitza G, et al. Initial steps of metastasis: cell invasion and endothelial transmigration. Mutat Res. 2011;728(1-2):23-34.
383. Fares J, Fares MY, et al. Molecular principles of metastasis: a hallmark of cancer revisited. Signal Transduct Target Ther. 2020;5(1):28.
384. Ward SJ, Ramirez MD, et al. Cannabidiol prevents the development of cold and mechanical allodynia in paclitaxel-treated female C57Bl6 mice. Anesth Analg. 2011;113(4):947-50.
385. Aggarwal BB, Shishodia S, et al. Curcumin suppresses the paclitaxel-induced nuclear factor-κB pathway in breast cancer cells and inhibits lung metastasis of human breast cancer in nude mice. Clin Cancer Res. 2005;11(20):7490-8.
386. Choi J, Jung W, et al. Expression of autophagy-related markers beclin-1, light chain 3A, light chain 3B and p62 according to the molecular subtype of breast cancer. Histopathology. 2013;62(2):275-86.
387. Chang S-J, Ou-Yang F, et al. Decreased expression of autophagy protein LC3 and stemness (CD44+/CD24−/low) indicate poor prognosis in triple-negative breast cancer. Hum Pathol. 2016;48:48-55.
388. Amjad MT, Chidharla A, et al. Cancer chemotherapy. 2020.
389. Hua L, Zhu G, et al. MicroRNA-1 overexpression increases chemosensitivity of non-small cell lung cancer cells by inhibiting autophagy related 3-mediated autophagy. Cell Biol Int. 2018;42(9):1240-9.
390. Fang L-m, Li B, et al. Transcription factor EB is involved in autophagy-mediated chemoresistance to doxorubicin in human cancer cells. Acta Pharmacol Sin. 2017;38(9):1305-16.
391. Tovar-Vidales T, Roque R, et al. Tissue transglutaminase expression and activity in normal and glaucomatous human trabecular meshwork cells and tissues. Invest Ophthalmol Vis Sci. 2008;49(2):622-8.
392. Tovar-Vidales T, Clark AF, et al. Focus on molecules: transglutaminase 2. Exp Eye Res. 2011;93(1):2.
393. Walker A, Singh A, et al. Nrf2 signaling and autophagy are complementary in protecting breast cancer cells during glucose deprivation. Free Radic Biol Med. 2018;120:407-13.
394. Meng Q, Xu J, et al. GPx1 is involved in the induction of protective autophagy in pancreatic cancer cells in response to glucose deprivation. Cell Death Dis. 2018;9(12):1187.
395. Chen G, Liu H, et al. Silencing PFKP inhibits starvation-induced autophagy, glycolysis, and epithelial mesenchymal transition in oral squamous cell carcinoma. Exp Cell Res. 2018;370(1):46-57.
396. Li T, Tong H, et al. Starvation induced autophagy promotes the progression of bladder cancer by LDHA mediated metabolic reprogramming. Cancer Cell Int. 2021;21:1-16.
397. Song X, Liu X, et al. Hypoxia-induced resistance to cisplatin and doxorubicin in non-small cell lung cancer is inhibited by silencing of HIF-1α gene. Cancer Chemother Pharmacol. 2006;58:776-84.
398. Alamassi MN, Chia SL, et al. Increased efficacy of biologics following inhibition of autophagy in A549 lung cancer cells in bimodal treatment of doxorubicin and SAR405-loaded chitosan nanoparticles. OpenNano. 2023;11:100142.

399. Bradley ST, Lee Y-S, et al. The effects of autophagy inhibition on HNSCC sensitivity to CTX. Cancer Res. 2022;82(12_Supplement):3003-.
400. Liao Y, Guo Z, et al. Inhibition of EGFR signaling with Spautin-1 represents a novel therapeutics for prostate cancer. J Exp Clin Cancer Res. 2019;38:1-16.
401. Guo J, Zhang J, et al. Potent USP10/13 antagonist spautin-1 suppresses melanoma growth via ROS-mediated DNA damage and exhibits synergy with cisplatin. J Cell Mol Med. 2020;24(7):4324-40.
402. Lu J, Zhu L, et al. Overexpression of ULK1 represents a potential diagnostic marker for clear cell renal carcinoma and the antitumor effects of SBI-0206965. EBioMedicine. 2018;34:85-93.
403. Li Y, Liang R, et al. AMPK-dependent phosphorylation of HDAC8 triggers PGM1 expression to promote lung cancer cell survival under glucose starvation. Cancer Lett. 2020;478:82-92.
404. Ye J, Kumanova M, et al. The GCN2-ATF4 pathway is critical for tumour cell survival and proliferation in response to nutrient deprivation. EMBO J. 2010;29(12):2082-96.
405. Izuishi K, Kato K, et al. Remarkable tolerance of tumor cells to nutrient deprivation: possible new biochemical target for cancer therapy. Cancer Res. 2000;60(21):6201-7.
406. Bravo-Cordero JJ, Hodgson L, et al. Directed cell invasion and migration during metastasis. Curr Opin Cell Biol. 2012;24(2):277-83.
407. Wang H, Wang L, et al. Inhibition of autophagy potentiates the anti-metastasis effect of phenethyl isothiocyanate through JAK2/STAT3 pathway in lung cancer cells. Mol Carcinog. 2018;57(4):522-35.
408. Zhu J-F, Huang W, et al. Annexin A1-suppressed autophagy promotes nasopharyngeal carcinoma cell invasion and metastasis by PI3K/AKT signaling activation. Cell Death Dis. 2018;9(12):1154.
409. Terabe T, Uchida F, et al. Expression of autophagy-related markers at the surgical margin of oral squamous cell carcinoma correlates with poor prognosis and tumor recurrence. Hum Pathol. 2018;73:156-63.
410. Zois CE, Giatromanolaki A, et al. " Autophagic flux" in normal mouse tissues: focus on endogenous LC3A processing. Autophagy. 2011;7(11):1371-8.
411. Koukourakis MI, Kalamida D, et al. Autophagosome proteins LC3A, LC3B and LC3C have distinct subcellular distribution kinetics and expression in cancer cell lines. PLoS One. 2015;10(9):e0137675.
412. Kim S, Jung WH, et al. Differences in autophagy-related activity by molecular subtype in triple-negative breast cancer. Tumor Biol. 2012;33:1681-94.
413. Schläfli AM, Adams O, et al. Prognostic value of the autophagy markers LC3 and p62/SQSTM1 in early-stage non-small cell lung cancer. Oncotarget. 2016;7(26):39544.
414. Rosanò L, Cianfrocca R, et al. Acquisition of Chemoresistance and EMT Phenotype Is Linked with Activation of the Endothelin A Receptor Pathway in Ovarian Carcinoma CellsEndothelin Axis Promotes Chemoresistance. Clin Cancer Res. 2011;17(8):2350-60.
415. Sestito R, Cianfrocca R, et al. miR-30a inhibits endothelin A receptor and chemoresistance in ovarian carcinoma. Oncotarget. 2016;7(4):4009.
416. Rosano L, Cianfrocca R, et al. Endothelin A receptor/β-arrestin signaling to the Wnt pathway renders ovarian cancer cells resistant to chemotherapy. Cancer Res. 2014;74(24):7453-64.
417. Bozza WP, Zhang Y, et al. RhoGDI deficiency induces constitutive activation of Rho GTPases and COX-2 pathways in association with breast cancer progression. Oncotarget. 2015;6(32):32723.

418. Marconi GD, Della Rocca Y, et al. C-Myc Expression in Oral Squamous Cell Carcinoma: Molecular Mechanisms in Cell Survival and Cancer Progression. Pharmaceuticals. 2022;15(7):890.
419. Jia X, Zhang Z, et al. TCRP1 transcriptionally regulated by c-Myc confers cancer chemoresistance in tongue and lung cancer. Sci Rep. 2017;7(1):3744.
420. Wang L-H, Xu M, et al. The antihelminthic niclosamide inhibits cancer stemness, extracellular matrix remodeling, and metastasis through dysregulation of the nuclear β-catenin/c-Myc axis in OSCC. Sci Rep. 2018;8(1):12776.
421. Goswami AB, Karadarević D, et al. Immunity-related GTPase IRGM at the intersection of autophagy, inflammation, and tumorigenesis. Inflamm Res. 2022;71(7-8):785-95.
422. Li C, Cai J, et al. TGM2 knockdown reverses cisplatin chemoresistance in osteosarcoma. Int J Mol Med. 2018;42(4):1799-808.
423. Park K-S, Kim H-K, et al. Transglutaminase 2 as a cisplatin resistance marker in non-small cell lung cancer. J Cancer Res Clin Oncol. 2010;136:493-502.
424. Han B, Bhowmick N, et al. FOXC1: an emerging marker and therapeutic target for cancer. Oncogene. 2017;36(28):3957-63.
425. Liu Z, Xu S, et al. Silencing FOXC1 inhibits growth and migration of human oral squamous cell carcinoma cells. Exp Ther Med. 2018;16(4):3369-76.
426. Cao S, Wang Z, et al. FOXC1 induces cancer stem cell-like properties through upregulation of beta-catenin in NSCLC. J Exp Clin Cancer Res. 2018;37:1-12.
427. Nunes T, Hamdan D, et al. Targeting cancer stem cells to overcome chemoresistance. Int J Mol Sci. 2018;19(12):4036.
428. Deng Q-j, Xie L-q, et al. Overexpressed MALAT1 promotes invasion and metastasis of gastric cancer cells via increasing EGFL7 expression. Life Sci. 2016;157:38-44.
429. Luo B-H, Xiong F, et al. Epidermal growth factor-like domain-containing protein 7 (EGFL7) enhances EGF receptor− AKT signaling, epithelial− mesenchymal transition, and metastasis of gastric cancer cells. PLoS One. 2014;9(6):e99922.
430. Lin Y, Cheng K, et al. miR-217 inhibits proliferation, migration, and invasion via targeting AKT3 in thyroid cancer. Biomed Pharmacother. 2017;95:1718-24.
431. You A, Fu L, et al. MicroRNA-203 restrains epithelial–mesenchymal transition, invasion and migration of papillary thyroid cancer by downregulating AKT3. Cell Cycle. 2020;19(10):1105-21.
432. Sui G-Q, Fei D, et al. MicroRNA-338-3p inhibits thyroid cancer progression through targeting AKT3. Am J Cancer Res. 2017;7(5):1177.
433. Gagnon V, Mathieu I, et al. AKT involvement in cisplatin chemoresistance of human uterine cancer cells. Gynecol Oncol. 2004;94(3):785-95.
434. Girouard J, Lafleur M-J, et al. Involvement of Akt isoforms in chemoresistance of endometrial carcinoma cells. Gynecol Oncol. 2013;128(2):335-43.
435. Semenza GL. HIF-1 and tumor progression: pathophysiology and therapeutics. Trends Mol Med. 2002;8(4):S62-S7.
436. Lu H, Samanta D, et al. Chemotherapy triggers HIF-1–dependent glutathione synthesis and copper chelation that induces the breast cancer stem cell phenotype. Proc Natl Acad Sci U S A. 2015;112(33):E4600-E9.
437. Li S, Wei Q, et al. Down-regulating HIF-1α by lentivirus-mediated shRNA for therapy of triple negative breast cancer. Cancer Biol Ther. 2015;16(6):866-75.
438. Ma Q. Role of nrf2 in oxidative stress and toxicity. Annu Rev Pharmacol Toxicol. 2013;53:401-26.

439. Syu J-P, Chi J-T, et al. Nrf2 is the key to chemotherapy resistance in MCF7 breast cancer cells under hypoxia. Oncotarget. 2016;7(12):14659.
440. Tsai K-J, Tsai H-Y, et al. Luteolin inhibits breast cancer stemness and enhances chemosensitivity through the Nrf2-mediated pathway. Molecules. 2021;26(21):6452.
441. He W, Sun Z, et al. Silencing of TGM2 reverses epithelial to mesenchymal transition and modulates the chemosensitivity of breast cancer to docetaxel. Exp Ther Med. 2015;10(4):1413-8.
442. Wang X, Lin Y. Tumor necrosis factor and cancer, buddies or foes? 1. Acta Pharmacol Sin. 2008;29(11):1275-88.
443. Zhang Z, Lin G, et al. Transmembrane TNF-alpha promotes chemoresistance in breast cancer cells. Oncogene. 2018;37(25):3456-70.
444. Simone BA, Palagani A, et al. Caloric restriction counteracts chemotherapy-induced inflammation and increases response to therapy in a triple negative breast cancer model. Cell Cycle. 2018;17(13):1536-44.
445. Hosseini SA, Labilloy A. Genetics, TREX1 Mutations. StatPearls [Internet]: StatPearls Publishing; 2021.
446. Erdal E, Haider S, et al. A prosurvival DNA damage-induced cytoplasmic interferon response is mediated by end resection factors and is limited by Trex1. Genes Dev. 2017;31(4):353-69.
447. Ma Z, Xiong Q, et al. Carboplatin activates the cGAS-STING pathway by upregulating the TREX-1 (three prime repair exonuclease 1) expression in human melanoma. Bioengineered. 2021;12(1):6448-58.
448. Chen Q, Shen H, et al. A nuclear lncRNA Linc00839 as a Myc target to promote breast cancer chemoresistance via PI3K/AKT signaling pathway. Cancer Sci. 2020;111(9):3279-91.
449. Ali A, Shafarin J, et al. SCAMP3 promotes breast cancer progression and metastasis through the c-MYC-β-Catenin-SQSTM1 axis to target growth, stemness and chemoresistance. Cell Signal. 2023:110591.
450. Zhang M, Fan H-Y, et al. Inhibition of c-Myc by 10058-F4 induces growth arrest and chemosensitivity in pancreatic ductal adenocarcinoma. Biomed Pharmacother. 2015;73:123-8.
451. Parasido E, Avetian GS, et al. The Sustained Induction of c-MYC Drives Nab-Paclitaxel Resistance in Primary Pancreatic Ductal Carcinoma Cellsc-MYC Drives Nab-Paclitaxel Resistance in Pancreatic Cancer. Mol Cancer Res. 2019;17(9):1815-27.
452. Sun W, Li J, et al. The c-Myc/miR-27b-3p/ATG10 regulatory axis regulates chemoresistance in colorectal cancer. Theranostics. 2020;10(5):1981.
453. Zhang HL, Wang P, et al. c-Myc maintains the self-renewal and chemoresistance properties of colon cancer stem cells. Oncol Lett. 2019;17(5):4487-93.
454. Folk J. Transglutaminases. Annu Rev Biochem. 1980;49(1):517-31.
455. Yang P, Yu D, et al. TGM2 interference regulates the angiogenesis and apoptosis of colorectal cancer via Wnt/β-catenin pathway. Cell Cycle. 2019;18(10):1122-34.
456. Erdem M, Erdem S, et al., editors. Up-regulation of TGM2 with ITGB1 and SDC4 is important in the development and metastasis of renal cell carcinoma. Urol Oncol; 2014: Elsevier.
457. Zhang H, McCarty N. Tampering with cancer chemoresistance by targeting the TGM2-IL6-autophagy regulatory network. Autophagy. 2017;13(3):627-8.
458. Zheng W, Chen Q, et al. SDC1-dependent TGM2 determines radiosensitivity in glioblastoma by coordinating EPG5-mediated fusion of autophagosomes with lysosomes. Autophagy. 2022:1-19.
459. Yeo SY, Itahana Y, et al. Transglutaminase 2 contributes to a TP53-induced autophagy program to prevent oncogenic transformation. Elife. 2016;5:e07101.

460. Yin J, Oh YT, et al. Transglutaminase 2 Inhibition Reverses Mesenchymal Transdifferentiation of Glioma Stem Cells by Regulating C/EBPβ SignalingTGM2 Regulates Mesenchymal Transdifferentiation of GBM. Cancer Res. 2017;77(18):4973-84.
461. Kang J, Lee J, et al. Renal cell carcinoma escapes death by p53 depletion through transglutaminase 2-chaperoned autophagy. Cell Death Dis. 2016;7(3):e2163-e.
462. Ku BM, Kim S-J, et al. Transglutaminase 2 inhibitor abrogates renal cell carcinoma in xenograft models. J Cancer Res Clin Oncol. 2014;140:757-67.
463. Geleta B, Park KC, et al. Breaking the cycle: targeting of NDRG1 to inhibit bi-directional oncogenic cross-talk between pancreatic cancer and stroma. FASEB J. 2021;35(2):e21347.
464. Yan Y, Chen X, et al. The effects and the mechanisms of autophagy on the cancer-associated fibroblasts in cancer. J Exp Clin Cancer Res. 2019;38:1-12.
465. Yuan M, Tu B, et al. Cancer-associated fibroblasts employ NUFIP1-dependent autophagy to secrete nucleosides and support pancreatic tumor growth. Nat Cancer. 2022;3(8):945-60.
466. Chang Y-H, Kumar VB, et al. Induction of human umbilical mesenchymal stem cell differentiation into retinal pigment epithelial cells using a transwell-based co-culture system. Cell Transplant. 2022;31:09636897221085901.
467. Marshall J. Transwell® invasion assays. Methods Mol Biol. 2011:97-110.
468. Puissant A, Fenouille N, et al. When autophagy meets cancer through p62/SQSTM1. Am J Cancer Res. 2012;2(4):397.